Barrier Island Morphodynamic Insights from Applied Global Sensitivity Analysis and Decadal Exploratory Modeling

Steven W.H. Hoagland

Dissertation submitted to the Faculty of the
Virginia Polytechnic Institute and State University
in partial fulfillment of the requirements for the degree of

Doctor of Philosophy
in
Civil Engineering

Jennifer L. Irish, Chair
Robert Weiss
Kyle B. Strom
Sean Vitousek

September 17, 2024
Blacksburg, Virginia

Keywords: Barrier Island, Modeling, Morphodynamics, Global Sensitivity Analysis,
Coastal Management

Barrier Island Morphodynamic Insights from Applied Global Sensitivity Analysis and Decadal Exploratory Modeling

Steven W.H. Hoagland

ABSTRACT

Barrier islands serve as valuable resources for coastal communities by reducing backbarrier flooding, providing wildlife habitat, and creating local economic activity through opportunities for recreation and tourism. Because the benefits of these islands are linked to their morphology, coastal resource planners must consider what management alternatives will maximize these benefits, considering both short- and long-term goals. Recent advances in long-term computational modeling of barrier island, marsh, and lagoon systems have created opportunities for gaining additional insights into the morphodynamics of these systems, which may help planners make better-informed coastal management decisions. In this series of studies, a recently developed long-term barrier-marsh-lagoon model is evaluated to better understand system morphodynamics and applied to a real barrier island system in the mid-Atlantic to understand its vulnerabilities and the potential impacts of management alternatives. In the first study, a comprehensive review of advances in barrier island morphodynamic modeling was presented. In the second study, a global sensitivity analysis method, the Sobol method, was used to explore the parameter space of the barrier-marsh-lagoon model. The significant influence of initial barrier geometry, the combination of parameters required for short-term drowning to occur, and the significant role of tidal dispersion on backbarrier sediment dynamics were morphodynamic insights drawn from this study. In the third study, five global sensitivity analysis methods were evaluated based on their ability to rank parameters, converge to stable results, and their reliability. Groups of the most significant

parameters were generally identified by all methods; however, the Morris method exceeded all others in terms of performance, especially its ability to converge and its reliability. VARS performed second best, on average, with better convergence and reliability results than the Sobol method, and with lower simulation counts. In the fourth study, the long-term model was applied to a mid-Atlantic barrier island and used to assess the island's vulnerabilities to sea level rise, overwash, and the impact of coastal management alternatives. Thin-layer placement and beach nourishment were found to be effective at sustaining the marsh and minimizing island retreat, respectively.

Barrier Island Morphodynamic Insights from Applied Global Sensitivity Analysis and Decadal Exploratory Modeling

Steven W.H. Hoagland

GENERAL AUDIENCE ABSTRACT

Barrier islands help coastal communities by reducing flooding, providing wildlife habitat, and creating local economic activity through opportunities for recreation and tourism. Because the benefits of these islands are linked to their form, decision-makers must think about how to manage these islands to help the community both now and in the future. Recent advances in computer modeling of barrier islands, and the adjacent marshes and lagoons, over decades to hundreds of years, have created opportunities for us to learn more about how these systems behave over time, which may help planners make better-informed coastal management decisions. In this series of studies, a recently developed computer model of the barrier island, marsh, and lagoon is evaluated to learn how the system changes over time and applied to a real barrier island system in the mid-Atlantic to understand its vulnerabilities and the potential impacts of management alternatives. In the first study, a comprehensive review of advances in computer modeling of barrier island changes over time was presented. In the second study, the impact of the model parameters and their combinations with one another was explored using the Sobol global sensitivity analysis method, which is widely considered to be the standard method in practice. The significant influence of initial barrier geometry, the combination of parameters required for the barrier to be overcome by sea level in the short-term, and the significant role of sediment delivered behind the island through tidal inlets were significant insights into the system behavior that were drawn from this study. In the third study, five global sensitivity analysis methods were evaluated based on

their ability to rank parameters, the number of computer simulations that were required, the ability of a method to arrive at a conclusive answer, and the consistency of a method in providing an answer. Groups of the most significant parameters were generally identified by all methods; however, the Morris method exceeded all others in terms of its ability to find conclusive and consistent answers due to its ability to identify unimportant parameters. VARS performed second best, on average, with better ability to find conclusive and consistent answers with fewer computer simulations than Sobol. In the fourth study, the long-term computer model was applied to a mid-Atlantic barrier island and used to assess the island's vulnerabilities to sea level rise, overwash (when water flows over the dunes), and the impact of coastal management alternatives. Placing thin layers of additional sediment on top of the marsh platforms and extending the shoreline toward the ocean by placing additional sediment on the beach were found to be effective at sustaining the marsh and minimizing movement of the barrier island landward, respectively.

In memory of Bruce "Bubba" Dudley Hoagland.

Acknowledgments

First, I would like to thank Dr. Jennifer Irish for her mentorship, patience, guidance, and encouragement during my years at Virginia Tech. Though I was a non-traditional graduate student in many ways, Dr. Irish was unwavering in her support of me and my family over the last five years. Dr. Irish has also significantly contributed to my growth as a teacher and researcher. She pushed me to become an instructor of record during my fourth year, which gave me invaluable experience and reinforced my desire to teach. She also helped me learn to write proposals and research papers, a skill which I am still improving, but for which I am very grateful and intend to regularly use moving forward.

I would like to thank my committee members, Dr. Robert Weiss, Dr. Kyle Strom, and Dr. Sean Vitousek, who took time to meet with me, discuss my ideas and study approaches, and review manuscript drafts. I also learned much from Dr. Weiss and Dr. Strom in the classroom and intend to pass on what they taught me to future students.

Many fellow graduate students in the research groups of Dr. Irish and Dr. Weiss contributed to my learning and success. I would like to extend a special thanks to Jun-Whan, Anmol, Catherine, Megan, Atefeh, Jad, Harrison, Becca, and Kyutae. I would also like to thank my undergraduate students for their hard work and respectful engagement during my

time as their professor.

I would like to acknowledge and thank the U.S. Coastal Research Program, the Disaster Resilience and Risk Management Program, and Virginia Sea Grant for their financial support of my graduate studies.

My acknowledgement and thanks are extended to Dr. Lindell Ormsbee and Dr. Scott Yost, who invested much time in me as a Master's student and who encouraged me to pursue my doctorate.

I must express my gratitude to my family for their constant support, prayers, and encouragement during my studies. I would like to especially thank my wife, Audrey, who has been right by side through it all, who has worked hard these years with me and with our daughters - I could not have finished this without you. Thank you Amelia and Eleanor for the joy and laughter you've brought into our home these last five years.

Finally, I must acknowledge and give thanks to the sovereign, triune God who created and sustains this amazing universe that we are privileged to learn about, who loved me and redeemed me through the atoning work of Christ, and to whom I owe everything.

Soli Deo gloria.

Contents

List of Figures

List of Tables

Chapter 1

Introduction

1.1 Background and Motivation

Barrier islands are long, narrow landforms that are bounded by tidal inlets and line approximately 10% of the world's coastlines [7]. The islands are separated from the mainland by estuarine bodies of water such as shallow lagoons or coastal bays, which they protect from waves and create opportunities for salt marsh to grow [8]. The barrier island and its backbarrier lagoon and marsh platforms are collectively referred to herein as a "barrier system." Barrier systems provide many important benefits including flood damage mitigation due to a reduction in backbarrier storm surge levels [e.g., 9], socioeconomic benefits such as increases in beach recreation, tourism, and coastal real estate market values [e.g., 10, 11], and ecological benefits such as sediment stabilization, provision of wildlife habitat, and removal of pollutants [12].

Barrier systems are extraordinarily dynamic landforms. Due to both chronic and acute sediment transport processes, the islands are subject to changes in geometry and migration

of the entire island in both the alongshore and cross-shore directions [e.g., 13, 14, 15]. The dynamics of these islands are of particular concern to coastal managers as the benefits that they provide are inherently linked to their morphology. Thus, the ever-changing nature of barrier islands presents a challenge for coastal resource managers who seek to balance competing objectives in order to maximize the usefulness and enjoyment of these islands, both now and in the future.

One useful tool available to coastal resource managers is computational modeling, which has been advancing in the coastal sciences since the 1950s and 60s [e.g., 16]. Recent long-term modeling advancements have coupled marsh-lagoon models with barrier island models, both of which were developed independently, to identify feedbacks between the two systems [e.g., 1, 17]. The latest of these models, developed by Lorenzo-Trueba and Mariotti [1], was created by coupling together the marsh-lagoon model of Mariotti and Carr [18] with the barrier island model of Lorenzo-Trueba and Ashton [19]. Though the model was published with an initial analysis of select parameters, most of the parameter space was left unexplored, and it was anticipated that a more thorough evaluation of the model parameter space could yield some novel insights into the morphodynamics of the barrier system.

Toward this end, it was determined that performing a global sensitivity analysis of the model would be the best way to explore the model's entire parameter space. The Sobol method [20] was selected for implementation given the barrier system model's fast runtime and the Sobol method's general recognition as a comprehensive and robust method [e.g., 21, 22]. However, upon preliminary review of relevant literature, it was discovered that various global sensitivity analysis methods had been developed over the last few decades [23], with new methods continuing to be published [e.g., 24, 25]. In fact, global sensitivity analysis had increasingly turned into its own field of study [26], with method comparison studies seeking an optimal method, or, at a minimum, benefits and drawbacks of using a particular method

[e.g., 27, 28]. It was anticipated that other methods might show some advantage over the Sobol method, if not in robustness of the results, then perhaps in computational expense, reliability, or convergence.

The results of the sensitivity analysis, though interesting in themselves, were ultimately intended for application of the barrier island model to a real-world system, to reduce uncertainty in model parameterization. While much research has been aimed at modeling the long-term evolution of natural barrier systems, relatively few modeling studies have incorporated human impacts or coastal management practices [e.g., 29]. It was anticipated that this long-term barrier island model could be extended to include coastal management alternatives and applied to a real barrier island system to assess its vulnerabilities and response to management scenarios.

1.2 Goals and Objectives

The overarching goals of this dissertation are: (1) to advance the knowledge of long-term barrier island morphodynamics, and (2) to advance the understanding and practice of modeling barrier island morphodynamics. The four manuscripts that comprise Chapters 2 through 5 of this dissertation each contribute their own unique goals and objectives as follows:

- Chapter 2: Present a comprehensive literature review of barrier island modeling advancements from the earliest models of the 1950's to the present day. As the volume of scientific literature expands, this review will help researchers and practitioners identify relevant models for implementation, better understand how physical processes are currently modeled, and place their models within an appropriate historical context.

- Chapter 3: Gain modeling and morphodynamic insights from a recently developed

barrier island evolution model using the Sobol global sensitivity analysis method, which is considered one of the strongest and most comprehensive global sensitivity analysis methods that has been developed.

- Chapter 4: Identify the strengths and weaknesses of various global sensitivity analysis methods in terms of their output, computational burden, convergence, and reliability, as applied to a recently developed barrier island evolution model.

- Chapter 5: Develop long-term projections on the migration and morphological changes of Assateague Island, a mid-Atlantic barrier on the Maryland-Virginia state line, under sea level rise and coastal management scenarios.

1.3 Attribution

Co-authors for each manuscript presented in this dissertation are listed at the beginning of each chapter with the first author. All contributions to the work presented herein are attributed as follows:

- For the manuscript presented in Chapter 2, Steven W.H. Hoagland reviewed the cited literature and drafted the manuscript. Catherine R. Jeffries contributed to manuscript preparation by helping draft the Event-Scale Morphodynamics section. Jennifer L. Irish, Robert Weiss, Kyle Mandli, Sean Vitousek, Catherine M. Johnson, and Mary A. Cialone advised the inclusion of specific literature and datasets, offered suggestions for future research directions, contributed to the manuscript drafting by providing detailed reviews and editing, and provided overall guidance based on their experience and expertise.

- For the manuscripts presented in Chapters 3, 4, and Appendix A, Steven W.H. Hoagland

contributed to the research conceptualization, conducted the investigations and formal analyses, and drafted the manuscripts. Jennifer L. Irish and Robert Weiss contributed to the research conceptualization, provided guidance on the investigations and formal analyses, and contributed to manuscript drafting through detailed reviews and editing.

- For the manuscript presented in Chapter 5, Steven W.H. Hoagland contributed to the research conceptualization, conducted the investigation and formal analysis, and drafted the manuscript. Jennifer L. Irish, Robert Weiss, and Sean Vitousek contributed to the research conceptualization, provided guidance on the investigations and formal analyses, and contributed to manuscript drafting through detailed reviews and editing.

Chapter 2

Advances in Morphodynamic Modeling of Coastal Barriers: A Review

Steven W.H. Hoagland[1], Catherine R. Jeffries[2], Jennifer L. Irish[1], Robert Weiss[2,3], Kyle Mandli[4], Sean Vitousek[5,6], Catherine M. Johnson[7,8], and Mary A. Cialone[9]

[1]Department of Civil and Environmental Engineering, Virginia Tech, Blacksburg, VA

[2]Department of Geosciences, Virginia Tech, Blacksburg, VA

[3]Academy of Integrated Science, Virginia Tech, Blacksburg, VA

[4]Department of Applied Physics and Applied Mathematics, Columbia University, New York City, NY

[5]United States Geological Survey, Pacific Coastal and Marine Science Center, Santa Cruz, CA

[6]Department of Civil and Materials Engineering, University of Illinois at Chicago, Chicago, IL

[7]National Park Service, Region 1, Narragansett, RI

[8]Department of Natural Resources Science, University of Rhode Island, Kingston, RI

[9]Coastal and Hydraulics Laboratory, Engineer Research and Development Center, U.S. Army Corps of Engineers, Vicksburg, MS

Abstract

As scientific understanding of barrier morphodynamics has improved, so has the ability to reproduce observed phenomena and predict future barrier states using mathematical models. In order to use existing models effectively and improve them, it is important to understand the current state of morphodynamic modeling and the progress that has been made in the field. This manuscript offers a review of the literature regarding advancements in morphodynamic modeling of coastal barrier systems and summarizes current modeling abilities and limitations. Broadly, this review covers both event-scale and long-term morphodynamics. Each of these sections begins with an overview of commonly modeled phenomena and processes, followed by a review of modeling developments. After summarizing the advancements toward the stated modeling goals, we identify research gaps and suggestions for future research under the broad categories of improving our abilities to acquire and access data, furthering our scientific understanding of relevant processes, and advancing our modeling frameworks and approaches.

2.1 Introduction

Coastal barriers are narrow landforms that are separated from the continental mainland by a shallow waterbody (see Figure 2.1). These barriers can be book-ended by inlets (i.e., barrier islands) or they can be connected to the mainland at one end (i.e., barrier spits) or both (baymouth barriers). The combination of backbarrier environment, subaerial island, and shoreface are often succinctly referred to as the 'barrier system' or simply 'barrier.' As of 2011, over 20,000 kilometers of the world's coasts were characterized by a barrier system, accounting for approximately 10% of all coastlines [7]. Barriers provide significant benefits

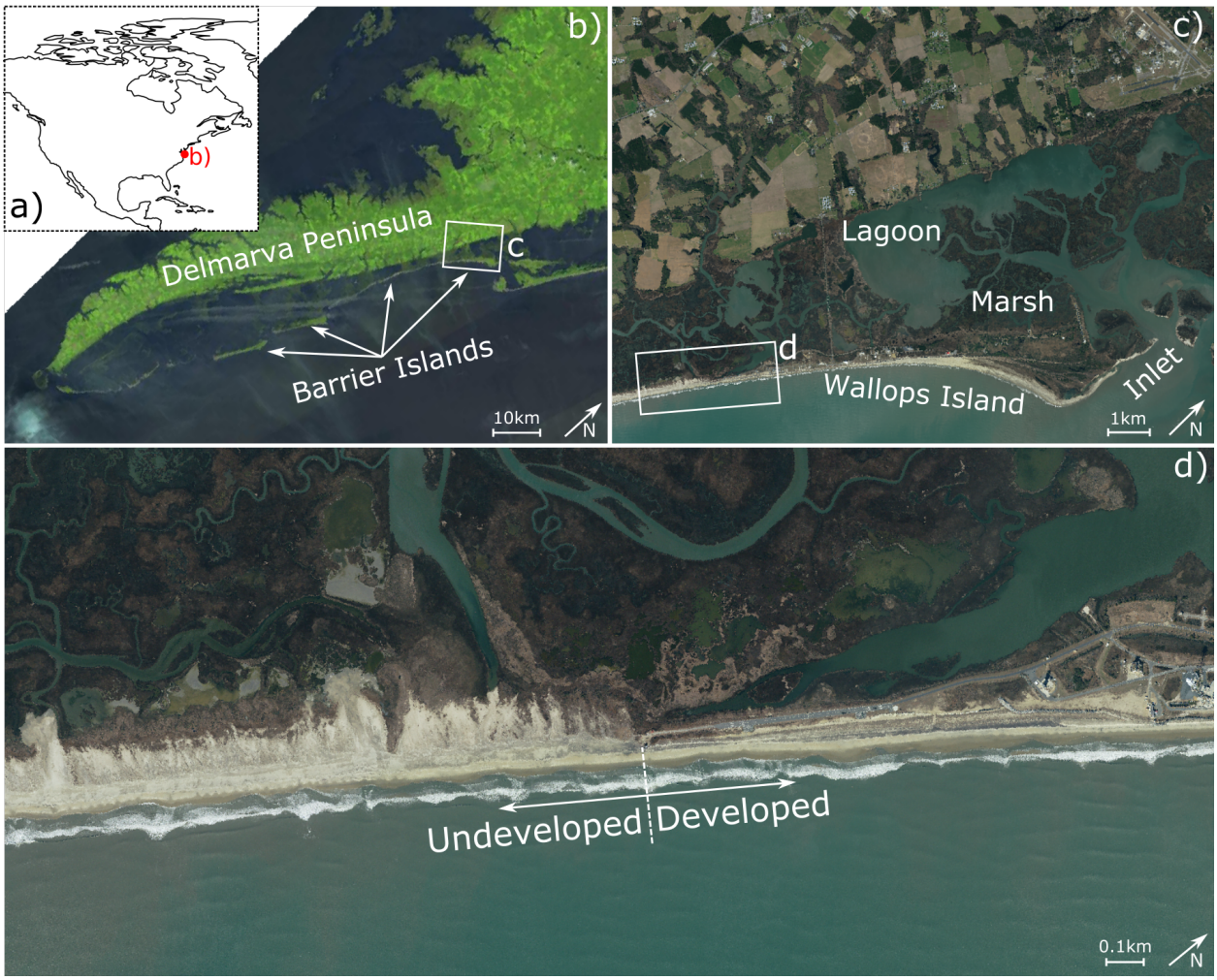

Figure 2.1: Satellite and Aerial Images of a Virginia Barrier Island. *a) Location map. b) Delmarva Peninsula [33]. c) Wallops Island [5]. d) Zoomed Section of Wallops Island [5]*

during coastal storms such as surge volume and wave energy reduction [9], wetland protection [30], sediment stabilization through the presence of subaerial or backbarrier vegetation, and protection of aquatic habitat [31]. Additionally, barrier islands have become popular as both vacation destinations [10] and permanent residential areas, which has led to increases in population density [32].

Although many barriers have undergone rapid urban development since the mid-20th century [34], Stutz and Pilkey [7] described this development boom as being "ironically" timed

due to coastal hazard accelerations associated with current trends in sea level rise (SLR). According to the Intergovernmental Panel on Climate Change, global mean sea level (MSL) is predicted to rise between 0.25 and 1.0 meter by the end of the century [35]. If these predictions hold true, the rates of barrier island morphological change and associated flooding during storms and other events will most certainly increase [e.g., 36]. In addition to exacerbating coastal flooding, SLR also drives the evolution of the barrier system itself, influencing processes that change both the island's shape and location. Thus, on many barrier coastlines, permanent structures have been constructed on land that was and is expected to continue migrating toward the mainland [10]. Changes in the location and geometrical configuration of barrier systems are expected to alter the benefits that they provide to neighboring mainland communities. Therefore, it is critically important for all who are involved in coastal management to understand barrier island morphodynamics to produce the best possible outcomes for coastal communities.

While the earliest literature tended to document observations and initial theories of barrier morphodynamics, research has recently - in the last three or so decades - shifted toward the development and intensified use of computational models. Based on this observation, we note that where modeling often lagged behind or paralleled our advancements in scientific understanding, it has recently been used to validate and advance it. Many models have been developed over the last three to four decades. A review of these models may help new or future researchers survey the field of barrier morphodynamic modeling.

A few notable review papers have recently been published related to barrier morphodynamics. Some of these papers focus on a single, specific component of coastal change such as overwash [e.g., 37] or storm sequencing and recovery [e.g., 38]. Other reviews capture the larger-scale morphological response of barrier systems, but their application is either constrained to a particular location [e.g., 39], focused on a particular driver such as climate change [e.g.,

Table 2.1: Recent Reviews

Citation	Focus
Donnelly et al. [37]	Laboratory work, field studies, and modeling efforts related to coastal overwash.
Rosati and Stone [39]	Barrier evolution concepts from early literature; recent concepts in Northern Gulf of Mexico.
McBride et al. [42]	Observations and conceptual models of barrier morphodynamics for various coastlines and regional locations.
Chardón-Maldonado et al. [43]	Recent advancements on hydrodynamics and sediment transport modeling in the swash zone.
Reeve et al. [44]	Long-term morphodynamic models that employ data-driven and/or hybrid approaches.
Ciavola and Coco [13]	Event-scale processes and their impact on specific coasts (e.g., sandy beaches, barrier islands, tidal flats, etc.).
Moore and Murray [14]	Compilation of recent work and synthesis of current understanding and state of research on barrier morphodynamics.
Eichentopf et al. [38]	Laboratory studies, field work, and modeling exercises related to storm sequencing and beach recovery.
Ranasinghe [45]	Commonly used morphodynamic models for sandy beaches and ideas for future long-term models.
Toimil et al. [40]	Coastal erosion modeling, climate change impacts, and approaches for evaluating uncertainty.
Sherwood et al. [41]	Advances in modeling event-driven morphodynamics on sandy coasts.

40], or focused in-depth on a particular spatiotemporal scale [e.g., 41]. Table 2.1 provides a summary of these reviews and their focus areas. These reviews provide a valuable synthesis of relevant work but are not sufficient to capture the trends and advancements in barrier morphodynamic modeling.

The purpose of this manuscript is to fill that gap by providing a review of the literature regarding advancements in morphodynamic modeling of coastal barrier systems. Our review of modeling advancements is divided in two broad categories: 1) event-scale morphodynamics, and 2) long-term morphodynamics - refer to the *Terminology* section for definitions of "event-scale" and "long-term." These sections begin with a brief description of commonly

modeled phenomena and processes, followed by a review of relevant modeling efforts, which are categorized according to their primary intent. At the conclusion of these sections, we summarize the primary contributions of the modeling developments and their limitations. Finally, we conclude with the identification of research gaps that currently exist and suggest directions for future research.

A few items should be noted regarding this study. First, there are some relevant topics (e.g., anthropogenic impacts, influences of vegetation) which are only briefly discussed due to our focus on morphodynamic modeling. Second, we have intentionally included many models and/or modeling approaches from the early literature so that the current models might be understood in their proper historical context, which requires knowledge of both previous and ongoing efforts. Additionally, this review primarily focuses on models in wide use in the research community. Therefore, some commonly used propriety models have only been briefly mentioned. Lastly, although our review is focused on barrier morphodynamics, many of the relevant processes play an important role for non-barrier coasts. Therefore, in order to fully understand the modeling advancements relevant to barrier systems, we must consider some modeling efforts that are not barrier-specific.

Before starting this review, it may be helpful to orient the unfamiliar reader by defining our modeling goals and our terms. In the next section we have attempted to summarize our modeling goals with one overarching statement or *Grand Challenge*. This is followed by a brief discussion of terminology used in this manuscript.

2.1.1 Grand Challenge

In theory, the ideal morphodynamic model would produce accurate predictions in a reasonable time without significant computational expense. As we consider how these ideals

translate into reality, there are multiple modeling goals that we must work toward and important intermediate steps that we must first achieve. However, rather than outlining each goal, we have attempted to synthesize them into a single overarching goal, or *Grand Challenge*, as follows:

> *To predict barrier system morphodynamics in multiple spatiotemporal dimensions (e.g., short to long time scales, transect to regional evolution) with a high degree of confidence, under reasonable computational resources constraints, and considering relevant factors such as event-driven morphological change, evolution during non-stormy periods, biological processes (and other potential subsystem influences), and anthropogenic impacts.*

We intend the phrase "predicting... with a high degree of confidence" to mean predictions that have at least been partially validated and are useful in planning and decision-making. Throughout this review, the reader is encouraged to consider each development in light of the *Grand Challenge*. At the conclusion of each major section, we summarize the modeling advancements and extant limitations, offering our perspectives on progress toward this overarching goal. To maintain this focus, it should be noted that some relevant topics such as biological processes and anthropogenic impacts are given more of a cursory discussion.

2.1.2 Terminology

There are some inconsistencies in terminology in the body of work on barrier morphodynamics. Thus, for the purpose of this review, our aim here is to define terms that describe what is being modeled (e.g., a phenomenon, a process), the types of mathematical representations that are used (e.g., a model, a formulation), and the spatiotemporal scales used throughout the paper.

When discussing phenomena, we are talking about observable characteristics, behaviors, or events of a system. While the spatiotemporal scales of a system may vary (e.g., initiation of particle movement vs. shoreline behavior), there are phenomena associated with each system that may be mathematically represented via the development of a model. When we discuss processes, we are referring to patterned events that systematically contribute to the observable phenomena of a system. Based on these terms, we also distinguish between models and formulations. Whereas models are developed to represent phenomena, specific formulations are developed to represent processes. Models, therefore, may contain one or more formulations of a process. For example, consider the development and growth of a spit. The spit development and/or growth would be the observed phenomenon that is systematically progressed by the process of longshore sediment transport (LST). Thus, we might develop a model that predicts spit development and growth using a specific LST formulation.

The last terms that need to be defined up front are related to the spatial and temporal scales at which the relevant processes are typically resolved in coastal morphodynamic modeling. Herein, we adopt the temporal scale classification of Rosati and Stone [39], and adopt a slightly modified version of the spatial scale classification of Cowell et al. [46]. These scales are presented in Table 2.2 and are used throughout this paper. Note, we also use the term 'event scale' throughout this manuscript to refer to the combination of small spatial and short temporal scales.

2.2 Event-Scale Morphodynamics

This section provides an overview of commonly modeled phenomena and processes associated with event-scale morphodynamics, a review of relevant modeling efforts, and a summary of

Table 2.2: Spatial and temporal scales of barrier island morphodynamics, respectively modified from Cowell et al. [46] and from Rosati and Stone [39].

Type	Term	Scale
Spatial	Small-scale	$10^0 - 10^2$ meters
Spatial	Moderate-scale	$10^2 - 10^3$ meters
Spatial	Large-scale	$> 10^3$ meters
Temporal	Short-term	hours to days
Temporal	Mid-term	days to decades
Temporal	Long-term	decades to centuries

advancements toward the *Grand Challenge*.

2.2.1 Commonly Modeled Phenomena and Processes

Acute sediment transport processes, which are characterized by a sudden onset and short-term duration, are initiated when a storm approaches the coast. Chronic transport processes, which are characterized by gradual beginnings and mid- to long-term duration, are not initiated during storms but are intensified by them. As these transport processes are initiated or intensified, the barrier responds in the form of morphological adjustment. To frame the discussion on storm response, we use the storm impact scale published by Sallenger [47], wherein acute processes occur within four regime classifications: swash, collision, overwash, and inundation (see Figure 2.2). Each regime has certain morphological responses associated with runup levels.

In the *swash* and *collision* regimes, increased water levels by storm surge and wave runup lead to increased erosion on the beach and dune, depositing the eroded material seaward of the beach. *Collision* differs from *swash* in that the water level exceeds the dune toe, allowing waves to collide with and erode the lower parts of the dune slope, which can lead to avalanching of the upper dune. Sallenger [47] points out that while sediment transported offshore under this regime may return to the beach, this sediment typically does not make it

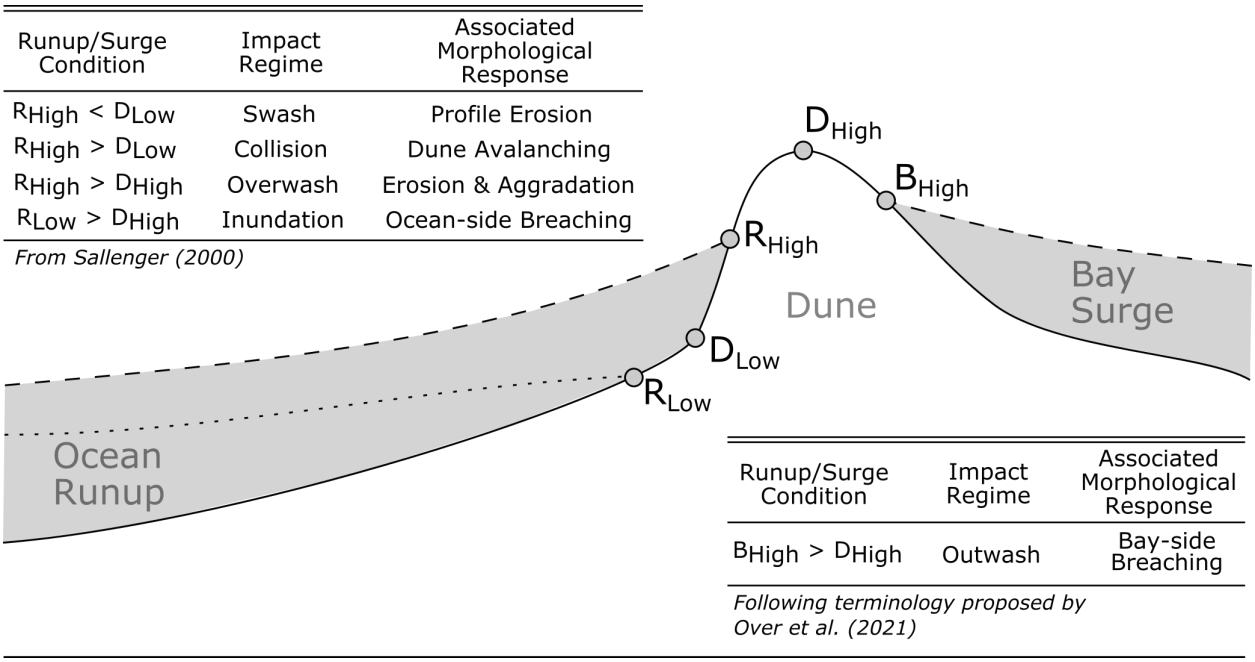

Figure 2.2: Storm Impact Scale. *Figure modified from Sallenger [47] with Outwash regime.*

back to the dune structure, resulting in net erosion of the dunes over time. In the *overwash* regime, water levels are high enough such that incident wave runup intermittently flows over the dune peaks or antecedent low spots, carrying mobilized sediment with it. Lastly, the *inundation* regime involves complete submergence of the barrier which can lead to inlet formation (i.e., breaching) and significant increases in the cross-shore sediment transport (XST) rates [47]. Inundation is associated with extreme levels of erosion that pick up normally dry (subaerial) sediment.

One regime that Sallenger does not include is the *outwash* regime, following the terminology proposed by Over et al. [48], which describes seaward flows and associated offshore sediment transport. Although it is possible to have initial seaward surge depending on the orientation of the islands and the approach angle of the storm, initial surge levels are typically directed onshore. Therefore, seaward flows associated with the *outwash* regime usually occur after storms make landfall or pass by the area of interest, which reverses the predominant wind

direction. Applied to a typical barrier system, this reversed wind field can cause backbarrier water levels to surge above receding ocean-side water levels. In this instance, breaching may be initiated from the backbarrier by outwash flows that scour a new channel through the island, liquefaction of previously-weakened dune structures, or a combination of both. Various studies including Shin [49], McCall et al. [50], Smallegan and Irish [51], Harter and Figlus [52], and Over et al. [48] highlight the importance of considering this regime when modeling storm event morphodynamics.

The following sections offer an introductory discussion on commonly modeled phenomena and processes associated with barrier response to storm events, namely profile erosion and shoreface response, overwash, and breaching. This is followed by a review of relevant modeling efforts.

Beach Profile Erosion and Shoreface Response

While the term 'profile' can be used to describe a wide range of the barrier system, we use the term 'beach profile' herein to describe the morphodynamic response of the barrier's beach-dune complex and upper shoreface, which we loosely define as the morphologically 'active zone' following Stive and de Vriend [53] and Cowell et al. [46]. Generally, there are two primary factors that contribute to erosion of the beach profile under storm conditions: 1) increased offshore-directed currents and 2) increased total runup. As the waves intensify, the beach profile state turns erosional (assuming a prior accretive state) as wave-driven sediment transport becomes dominated by undertow and rip currents which are offshore-directed [54]. Sediment is eroded from the upper portions of the profile and deposited on the shoreface, typically in a subaqueous bar, which is then delivered back to the profile once storm conditions subside [55]. This cycle of erosion and subsequent recovery has been observed over seasonal wave-climate changes [56] and event-scale changes [57]. Secondly,

the total runup, as produced by a combination of storm surge, astronomical tide, and wave runup, may exceed the *swash* regime water level to collide with the dune and cause notching (i.e., erosion and recession of the lower dune), followed by slumping or avalanching [58, 59]. For a more thorough review of sediment transport processes during storms and relevant factors, including the role of infragravity waves and incident wave non-linearity, the reader is referred to Aagaard and Kroon [54] and references therein.

These two primary factors (i.e., increased offshore-directed currents and increased total runup) contribute to barrier morphodynamics in significant ways. For example, in the *collision* regime they lead to a net loss of sediment offshore to the lower (inactive) profile [47]. This net loss effectively limits the ability of the beach and dunes to fully recover to pre-storm conditions without requiring external sediment sources (i.e., from the shelf, erodable profile outcrops, or LST gradients). Moreover, although much of the eroded sediment is brought back to the beach and dunes after the storm, this natural renourishment of the profile is not instantaneous, but can take days or weeks to recover [e.g., 55, 60], leaving the barrier system in a temporarily hyper-vulnerable state. Profile recovery between storm events, although less studied than erosional events, is critically important to understanding barrier vulnerabilities to storm sequences and long-term morphology [38].

Overwash

Overwash occurs when water flows over the dunes. Sediment is carried by the water and deposited behind the dunes as washover. While overwash was associated with intermittent overtopping in Sallenger's *overwash* regime, it should be noted that by definition, overwash also occurs during Sallenger's *inundation* regime and the proposed *outwash* regime, as the landward or seaward directed flows continue to transport sediment across the dunes. Donnelly et al. [37] offered distinct definitions for runup overwash and inundation overwash and

discussed the differences and implications of each process.

Three factors are the primary contributors to increased likelihood of barrier island overwash: 1) antecedent low spots in barrier topography, 2) high water levels driven primarily by storm surge, and 3) large incident waves. Although it can be argued that this is self-evidently true, it is also confirmed in the early literature on barrier island storm response [e.g., 61, 62]. In addition to these three main contributing factors, overwash occurrence has also been associated with other variables including previous overwash activity, barrier island width, and vegetation density [e.g., 62, 63, 64]. However, some of these factors can be indirectly related to antecedent topography. For example, areas that have experienced previous overwash events are also locations where the dunes have been likely been lowered; thus, previous overwash activity can be linked to pre-storm discontinuities in the dune elevation. Similarly, since dune vegetation promotes sediment settling and dune growth, vegetation density could generally be considered a proxy for pre-storm topography. Donnelly et al. [37] identified two other important factors including the direction of storm approach, which influences incident wave heights, and nearshore bathymetry, which impacts wave transformation.

Storms have significant morphological impact on barrier islands, which in turn affect the continued evolution and response to future storms. Observations from the early literature describe both destructive and constructive effects of overwash: destructive in that overwash may lower or destroy the dunes [e.g., 65] and constructive in that overwash may contribute to aggradation of the barrier islands over time [e.g., 66]. Both of these effects directly impact flood risk from future storms. Again, to avoid duplicating work, the reader is referred to the review by Donnelly et al. [37], which covers a variety of topics related to overwash including field and laboratory studies, modeling efforts, and its impact on barrier morphodynamics.

Breaching

Breaching is the creation of an inlet in a barrier that establishes direct hydraulic connectivity between the ocean and backbarrier water body [67]. Breaches have been shown to account for water level increases both during the storm event in the form of bay surge [e.g., 68] and after the storm event in the form of increased tidal range [e.g., 69]. Excess flooding, property damage, habitat loss, and decreased navigability are possible negative outcomes from a breach; however, breaching is also desirable in some cases and may be intentionally performed in order to increase habitat connectivity for certain estuarine wildlife [70] or to prevent undesirable backbarrier conditions including low salinity, poor water quality, and in some cases flooding [71].

From some of the earliest published observations of breaching, we know that multiple breaches, of various widths and depths, may form and expand during a single storm event [e.g., 65]. More recent studies have highlighted the dynamic nature of breaches, which can significantly change dimensions over relatively short time periods and even migrate alongshore [e.g., 71, 72]. Timing of the initial breaching process has received relatively little attention in the literature due to the difficult nature of collecting field data. However, a study by Visser [73] and a related modeling exercise by Roelvink et al. [59] estimated lateral growth rates of breaches between 1 and 2 cm/s during initial formation. During the phases of breach growth, XST is much greater than LST; however, once flow in the breach ceases, LST may cause closure of the breach [74].

In exploring the causes of breaching, researchers have often wanted to know on which side of the barrier breaching is initiated. Multiple theories of breach formation are present in the early literature, as reviewed by Pierce [75], including breaching from the backbarrier side through the escape of impounded water [76] and ocean-side breaching by wave-driven erosion

[77]. Pierce [75] determined that barriers are most likely to breach from the lagoon side but stated that a narrow barrier could also be breached by erosion from the sea. Although this perspective was published as early as 1970, it received little attention until recent years [e.g., 50, 51, 52, 78].

Kraus et al. [74] described two breaching processes and their association with lagoon-side or ocean-side breaching. The two processes are 1) scouring and channelization and 2) seepage and liquefaction. Scouring and channelization most commonly occur from the seaward side of the barrier, when sustained storm surge allows for water to (semi)continuously inundate the island with flow over the barrier; conversely, seepage and liquefaction typically initiate breaching from the landward side of a narrow barrier [74]. However, recent modeling studies [e.g., 49, 50, 51, 78] have also shown that seaward-sloping water level gradients that occur after the ocean-side's peak storm surge have the potential to scour channels across the barrier as well that can lead to seaward sediment transport and breaching.

2.2.2 Modeling Efforts

As stated previously, modeling efforts are classified according to their primary intent. Most event-scale morphodynamic models or formulations were developed to simulate a few key phenomena or processes including: 1) beach and dune erosion, 2) shoreface response, 3) overwash, 4) breaching, and 5) combinations of categories 1 through 4. The following sections review the relevant modeling efforts which are also graphically summarized in Figure 2.3.

Modeling Beach and Dune Erosion

Modeling work on storm-driven response of the beach-dune complex was initiated and significantly advanced by researchers in the Netherlands in the 1960s and 70s. Edelman [58]

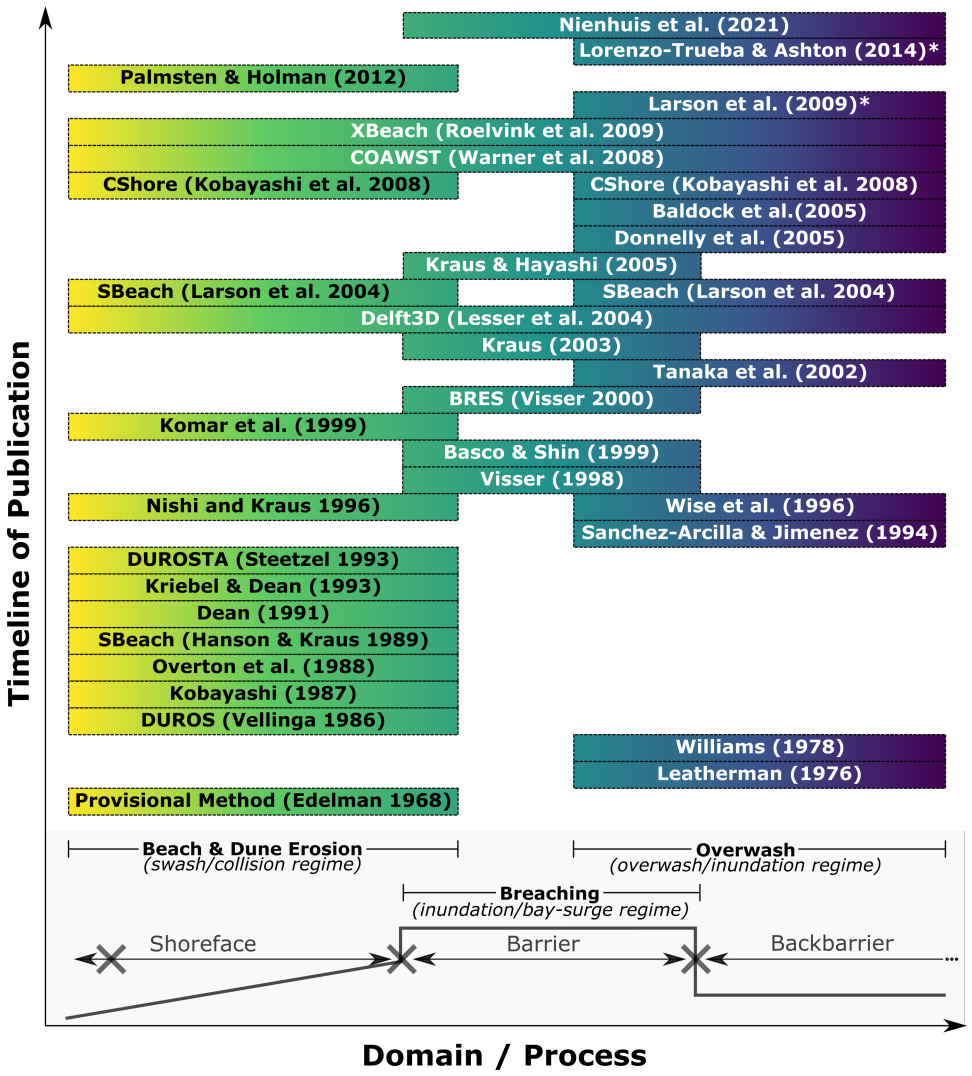

Figure 2.3: Event-Scale Models and Formulations. *Models are shown according to their publication chronology and are aligned with their respective processes, which range from beach and dune erosion, to breaching, to overwash.*

observed that when storm surge levels exceeded the dune toe, the dune would undergo significant erosion and partial avalanching. Based on these observations, Edelman published the first analytical formulation (i.e., method with a closed-form solution) for predicting dune erosion and retreat, later termed the 'Provisional Method.' This method assumed the formation of a new dune toe at the peak storm surge elevation and balanced the volume of sediment eroded from the dunes with deposition in the nearshore zone (see Figure 2.4b) using linear approximations of both the nearshore and dune profiles. Four years later, Edelman used the same principles to publish a similar method which considered more realistic (e.g., non-linear) profile shapes [79]. In addition to sediment conservation and the new dune toe location, Edelman's work was based on other key assumptions including a constant profile shape, rapid (or instantaneous) profile response, and the presence of both storm and pre/post-storm equilibrium profiles.

Other analytical methods were developed to predict beach and dune erosion using similar assumptions; these models included DUROS [82], and those of Kobayashi [83], Dean [84], and Kriebel and Dean [85]. Fundamentally, each of these models is similar in that they are based on balancing eroded and deposited sediment volumes, while the main differences lie in the factors that influence the new profile shape. For example, the profile depth in the non-linear Provisional Method was considered only a function of distance from the shoreline [79], while other methods allowed the depth to adjust based on factors such as wave height and sediment characteristics [e.g., 82, 84]. Komar et al. [86] also developed a simple method to predict dune retreat based on the foreshore slope and the height of the runup above the dune toe; this approach was recommended by FEMA for United States Pacific Coast beaches as of 2005 [87]. Vellinga's DUROS model [82] continues to be used in the Netherlands to assess the health and safety of the coastal dunes [88].

One important limitation with these early models arises from the assumption of instanta-

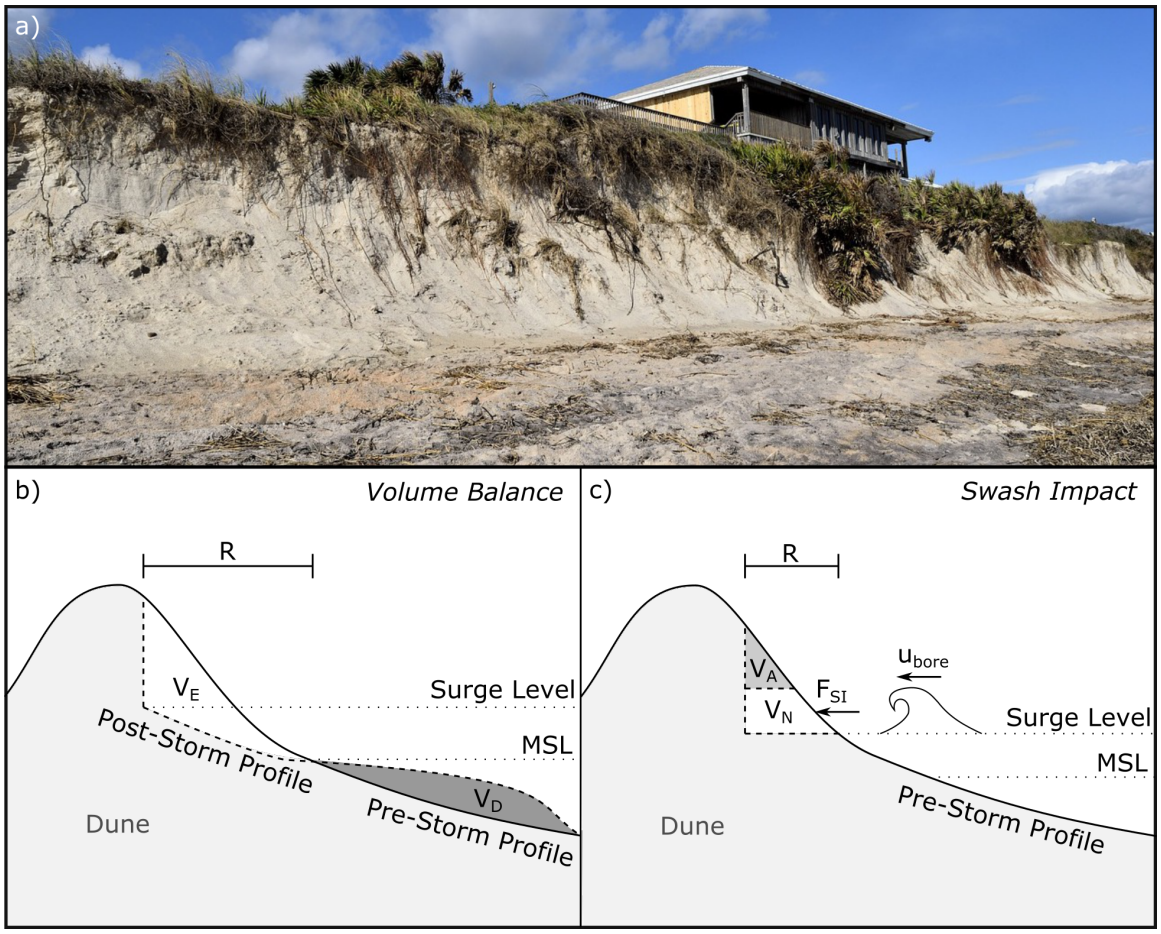

Figure 2.4: Beach and Dune Erosion. *a) Image of beach and dune erosion from Hurricane Matthew [80]. b) Volume balance approach that predicts dune recession (R) by equating the erosion volume (V_E) and deposition volume (V_D), modified from Edelman [79]. c) Swash impact approach that relates wave bore velocity (u_{bore}) to the swash impact force (F_{SI}) which creates notching (V_N) that leads to avalanching (V_A), modified from Nishi and Kraus [81].*

neous response. Because the duration of a storm is often much shorter than the time required for profiles to erode to their new equilibrium states, they rather erode some fractional amount toward equilibrium but never reach it. Komar and Moore [89] put it succinctly, stating that these methods "*should be regarded as an upper limit or an erosion potential that would result if the storm conditions were held constant indefinitely.*" For conservative estimates and design standards, these methods may prove reliable. However, for higher levels of modeling accuracy, it may be necessary to shift toward time-dependent models or the combination of idealized models with a time-dependent function [e.g., 85].

Fisher and Overton [90] proposed another type of modeling approach that focuses on the impact of swash on the dune face. These are appropriately called 'Swash Impact' approaches. The main idea undergirding this approach is that erosion of the dune is proportional to the impact force of colliding waves, which can be related to the waves' bore heights and approach velocities (see Figure 2.4c). Through a series of laboratory experiments, linear relationships were found between the amount of dune erosion and swash impact force, modulated by statistically significant factors such as grain size and dune density [91, 92]. This relationship was also identified in the field through a series of experiments at Duck, North Carolina [93].

Other methods using this approach were developed by Nishi and Kraus [81], Larson et al. [94], and most recently by Palmsten and Holman [95]. Nishi and Kraus [81] calculated the swash impact force by multiplying the mass of water in the approaching wave by its deceleration upon impact. Using large-scale wave tank experiments on compacted and uncompacted dunes, they found linear relationships between the weight of eroded sediment and the impact force. They also found uncompacted sediment to be more susceptible to swash impact erosion and suggested artificially compacted dunes as a possible method of erosion control. Using the linear relationship between erosion and swash impact force as an initial assumption, Larson et al. [94] derived an analytical model that predicted dune recession as a

function of bore speed, initial geometry, empirical transport coefficients, and foreshore slope, which was assumed to linearly continue landward of the dune toe. The authors used four previously published datasets to test their model and to empirically derive an optimal transport coefficient. Lastly, Palmsten and Holman [95] improved on this formulation in two main ways: 1) they used a Gaussian distribution to model variability in wave runup elevations, and 2) they tested various runup exceedance values and found that using a runup exceedance value of 16% led to better dune erosion predictions in the laboratory when compared to the 2% runup exceedance guidance recommended by Sallenger [47].

Modeling Shoreface Response

Paralleling these advancements was the development of more complex sediment transport formulations. While these formulations may vary in approach, they are similar in that they relate hydrodynamic parameters (e.g., velocity) to sediment transport rates. Thus, for the purposes of this discussion, we refer to these more complex formulations as coupled hydrodynamics-sediment transport (HD-ST) formulations. Since a review of each formulation would take considerable space, we offer a cursory description of the HD-ST formulations and refer interested readers to Larson and Kraus [96], Dean and Dalrymple [97], Nielsen [98], Aagaard and Hughes [99], Bosboom and Stive [88], and references therein for additional details.

In highly resolved models, coupled HD-ST formulations use hydrodynamic parameters to predict both bed load and suspended load transport rates. Bed load transport is typically estimated as a function of the bed shear stress, sediment density, and average grain diameter (often using Shields parameter), whereas the suspended sediment transport rate is calculated by integrating the vertical velocity and concentration profiles, the latter of which can be based on functions such as the Rouse profile or advection-diffusion calculations [88].

Depending on the application, not all models can afford the computational burden associated with coupled *HD-ST* formulations. Other approaches with less computational burden have gained popularity, such as the equilibrium-based approach, originally developed by Kriebel and Dean [100], which assumes the existence of an equilibrium shoreface profile that controls how the shoreface responds under specific hydrodynamic conditions. It is founded on the idea that if hydrodynamic conditions remained constant, then the shoreface would respond until constructive (landward) and destructive (seaward) forces along the profile were balanced, leading to a steady profile with a XST rate of zero. Kriebel and Dean [100] developed a formulation that calculates an equilibrium profile based on depth-dependent energy dissipation rates. XST rates are then calculated at a particular shoreface depth based on the difference between the actual energy dissipation rate and the rate associated with the equilibrium profile [97].

Another popular approach is the energetics approach, which was originally developed by Bagnold [101] for fluvial sediment transport. This approach considers the hydrodynamic environment as a machine that performs a certain amount of work (sediment transport) based on the available power input (kinetic energy) modulated by some efficiency factor (resistance to transport) [102]. Bed load and suspended load transport rates are calculated separately based on the available wave power, or the wave energy flux per unit width, which drives the transport [97]. While the energetics approach has been successful in predicting offshore-directed sediment transport rates during storm events, this approach has generally underpredicted onshore sediment transport during recovery periods [99].

Modeling Overwash

Efforts to quantitatively understand and predict overwash have led to the development of various formulations, which generally fall into one of two categories. Those in the first category

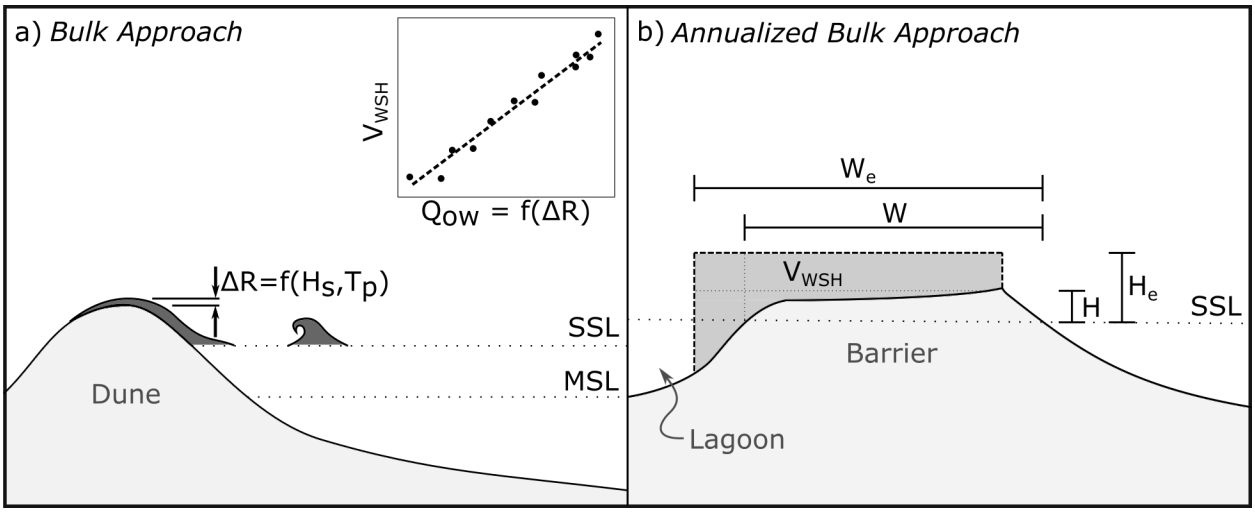

Figure 2.5: Overwash Modeling Approaches. *a) Traditional bulk approach that predicts washover volume (V_{WSH}) based on bulk parameters (e.g., excess runup height ΔR), modified from Donnelly et al. [109]. b) Annualized bulk approach that predicts V_{WSH} based on width (W) and height (H) deviations from equilibrium values (W_e & H_e) based on the storm surge level (SSL), modified from Lorenzo-Trueba and Ashton [19].*

may be described as 'Bulk' approaches, as defined by Donnelly et al. [37], since they relate certain hydrodynamic parameters (e.g., wave height) to bulk washover volumes (see Figure 2.5a). Williams [103] published the earliest bulk formulation, which predicted the washover rate as a function of excess runup (i.e., depth of runup over the dune crest) and wave period. Later bulk formulations [e.g., 104] were based on laboratory experiments by Kobayashi et al. [105], which showed a linear relationship between overwash and washover rates. Formulations in the second category apply coupled *HD-ST* formulations, which were discussed in the previous section. Donnelly et al. [37] reviewed at least three of these formulations and their results including Leatherman [106] who coupled the Einstein transport equation to velocity measurements, Sánchez-Arcilla and Jiménez [107] who combined the Van Rijn formulation with velocities calculated using the Chezy equation, and Baldock et al. [108] who applied a standard sheet flow model based on Shield's parameter to calculated swash velocities.

In the last fifteen years, most overwash modeling efforts have been directed toward developing, improving, and applying the coupled *HD-ST* formulations, which are typically just one component of event-scale morphodynamic models that resolve multiple sediment transport processes at small spatial scales. At the time of Donnelly's 2006 review [37], only one such model (i.e., SBEACH) was able to predict overwash. The original formulation, developed by Wise et al. [110], predicted sediment transport landward of the swash zone boundary based on the estimated wave bore velocity at the dune crest, and interpolated the transport rate to both landward and seaward limits. This formulation was later updated by Larson et al. [111] who modified landward flow dissipation by including a lateral spreading component, and Donnelly et al. [109, 112] who used the Sallenger [47] regimes to model intermittent overwash by wave runup and quasi-steady overwash during barrier inundation, the latter of which used a standard weir equation. Donnelly et al. [109, 112] compared the updated model results to post-Hurricane field data at Assateague Island, Maryland, Folly Beach, South Carolina, and Garden City Beach, South Carolina, showing good agreement with the post-storm profiles. Additionally, Donnelly's model was shown to outperform that of Larson et al. [111] in predicting the post-storm profile at Assateague.

Recent work has also involved the incorporation of bulk overwash formulations into long-term and large-scale barrier evolution models. The long-term model of Jiménez and Sánchez-Arcilla [113] employs a bulk formulation for modeling overwash rates based on empirically derived annual overwash volumes. This formulation uses the critical length concept of Leatherman [114], which posits a theoretical threshold (i.e., critical barrier width and height) at which overwash is prevented. Deviations from these critical thresholds are used to estimate accommodation space (or volume) in the subaerial and backbarrier zones (see Figure 5 2.5b). Thus, event-driven overwash is modeled continuously and quantified by the available accommodation space up to some predetermined maximum annual overwash vol-

ume. More recent models [e.g., 1, 19] also use the critical length concept to model overwash in their long-term models.

Larson et al. [115] followed a different approach, developing an analytical method to simulate the retreat of the barrier (or dune) based on landward (i.e., overwash) and seaward (i.e., profile erosion) sediment fluxes. Using a triangular approximation for the island or dune, these flux values were correlated with the ratio of dune crest to total runup elevations, and validation with field data showed results could provide order-of-magnitude estimations of overwash flux.

Modeling Breaching

In modeling a breach, there are a number of important components that one may wish to consider including the location of breach occurrence, the timing of breach formation, breach dimensions and its progression (i.e., expansion or contraction), and finally its ultimate state (e.g., natural closure, stable inlet). While there has been some quantitative work on predicting systematic breach occurrence [e.g., 116] and long-term inlet stability (see Kraus and Wamsley [71] and references therein), our focus will be limited to models with strong morphodynamic components (i.e., breach formation, initial breach growth, and long-term progression).

Visser [73] developed a conceptual model of breach formation and initial growth. Although the model was originally developed for sand dikes, it can also be applied to barrier islands. The conceptual model described five phases: 1) erosion and steepening of the inner slope of the scour channel, 2) decreasing of the crest width, 3) crest lowering and breach widening, 4) breach widening as flow changes from critical flow to subcritical flow, and 5) breach widening during subcritical flow until the flow ceases. This conceptual model was translated

into BRES, a numerical model that predicts breach formation and initial growth based on discharge (calculated using the broad-crested weir equation) through an initial trapezoidal cross-section [117]. Testing against multiple laboratory and field studies, Visser [117] found good agreement between predicted breach widths over time and measured data.

Basco and Shin [118] published a 1D numerical breaching model based on storm stages, in a similar fashion to Sallenger's regimes [47]. Dune erosion was modeled in the first stage, followed by a diffusion-based approach to overwash in the second stage. The third stage aligns with Sallenger's *inundation* regime, while the fourth stage aligns with the *outwash* regime. In these last two regimes, barrier inundation and breaching were modeled by combining the 1D Saint-Venant equations with the sediment transport formulation of Van Rijn [119]. This approach to breach modeling has been included in more recent event-scale morphodynamic models (e.g., Delft3D, XBeach), which combine hydrodynamic output with specific sediment transport formulations. These models predict breach formation during barrier inundation, when flow velocities across the island scour antecedent low spots into fully-formed channels. Additional details on these models may be found in the following section.

Kraus [120] developed an analytical breaching model that predicts the development of a rectangular breach toward equilibrium dimensions using an exponential time function. The model starts with some initial channel or non-uniformity in the dune or island and proceeds toward a full breach based on flow through the channel which erodes the channel bed and sides. Kraus [120] found the breach response to be sensitive to initial channel dimensions. Kraus and Hayashi [67] later expanded the model to include a coupled *HD-ST* formulation, where breach progression was based on calculated bottom and critical shear stresses. The model was shown to reproduce general trends of an observed breach, yet it tended to underestimate the breach width and overestimate the breach depth [67].

A more recent analytical breaching model was developed by Nienhuis et al. [121] that is

based on the hypothesis that a breach develops when the volume of sediment transport by overwash exceeds the sediment volume stored in the subaerial island. Overwash volume is calculated analytically using a triangular storm surge time series and integrating an overwash flux equation that considers surge height, width and depth of the dune gap, and a friction coefficient to account for vegetation impacts. Nienhuis et al. [121] compared their model results to Delft3D simulations and found that it performed reasonably well, although the Delft3D predictions varied across one additional order of magnitude compared to the analytical model. Results were also compared with observations from Hurricane Sandy which showed that the model performed much better for undeveloped barriers as compared to developed barriers.

Multifaceted Event-Scale Modeling

A variety of morphodynamic models have been developed to simulate more than one event-scale phenomena/process - we refer to these as 'multifaceted' models. Readers familiar with the literature will recognize that many of these multifaceted models are commonly called 'process-based' models, although we have intentionally avoided this term due to its inconsistent and ambiguous usage in the literature, as well as its implication that more abstracted models are not based on processes. Below we present select event-scale models, followed by a brief discussion of multifaceted modeling efforts related to storm sequencing and post-storm recovery, which has received less attention from researchers until recently.

Event Scale Models

While a variety of multifaceted event-scale models exist, herein we focus on models that have been thoroughly cited in the literature and are widely used by the coastal morphodynamics research community. These include models such as SBEACH [96], which rely on equilibrium

concepts, and models such as DUROSTA (also known as Unibest-DE) [122], CShore [123], Delft3D [124], and XBeach [59], which are based on coupled *HD-ST* formulations. Some of the primary differences between these models are shown in Table 2.3, including model dimensionality, included processes, and process formulations. Below we discuss the development of each model and highlight some significant improvements. Readers are referred to the references provided with each model for additional details.

SBEACH [96] was developed in the late 1980s to predict profile response to storm events. The model employed the XST formula of Kriebel and Dean [100], which is based on the difference in energy dissipation between the actual profile and an equilibrium profile. The model was originally calibrated using data from large wave tank experiments, showing its ability to predict foreshore erosion and bar formation, and its inability to predict features landward of the bar such as the trough and berm development during accretionary simulations [96]. The original model (which did not include overwash) was formally updated with the overwash formulations of Wise et al. [110] and again by Larson et al. [111], who showed good agreement between model predictions and measured profile changes for observations at Ocean City and Assateague, Maryland. SBEACH has more recently been incorporated in economic models for evaluating beach nourishment projects [e.g., 130], probabilistic frameworks for predicting erosion [e.g., 131], and model comparison studies, where it produced better morphological predictions than XBeach when using default parameters, but underperformed when calibration data were employed [e.g., 131, 132].

DUROSTA, which is an acronym in Dutch for "dune erosion - time dependent," was developed in the early 1990s as an unsteady, numerical model upgrade to the analytical beach and dune erosion models DUROS [82] and DUROS+ (the '+' representing the addition of wave period to the original model parameterization). The model was initially validated by comparison to laboratory data and various field experiments and showed good prediction capabilities

Table 2.3: Multifaceted Morphodynamic Models

Model Name [Reference]	Dimensions	Process Formulations†				Model Description
		XST	LST	OW	BR	
SBEACH [96]	1D	KD85		WIS96		XST rates estimated through semi-empirical relationships in shoreface regions; considers wave and sediment characteristics, wave shoaling, breaking, setup and setdown, breaker decay and reformation, sediment slumping/avalanching.
DUROSTA/Unibest-DE [122]	1D/Q2D	[...STZL93...]				Only considers suspended load transport (bed load neglected); considers wave set-up, energy dissipation from bed friction after breaking with a turbulence model; employs a bed slope correction factor and extrapolates swash transport rates based on calculated rates at the wet/dry interface.
CShore/C2Shore [125] [126]	1D/2D	[....KBY08....]		KBY10		Hydrodynamic components include the combined action of incident waves and currents, considering wave shoaling, breaking, and roller energy; considers shoreface (or structure) permeability and overtopping using an empirically based, probabilistic runup model.
Delft3D [124]	2D/3D	[.....VRN93.....]				Shallow water equations solved in 2D (depth-averaged) or 3D; allows coupling to HISWA or SWAN wave models which consider breaking, bed friction, and streaming (near-bed currents); includes surface roller and infragravity formulations; includes bed slope correction and morphological acceleration factor.
XBeach [59]	2D	[.....SVR97.....]				Depth-averaged shallow water equations solved in Sallenger (2000) storm impact regimes; includes wave breaking, swash dynamics (modeling wave groups, infragravity waves, surface rollers, and return flows), beach and dune erosion (including avalanching), overwash (using low-frequency wave group forcing), and breaching by channel scouring.

†OW: Overwash; BR: Breaching; KD85: [100]; WIS96: [110]; STZL93: [122]; KBY08: [125]; KBY10: [127]; VRN93: [128]; SVR97: [129]

on the subaqueous profile while underestimating dune retreat [122]. DUROSTA was used by Van Baaren [133], who found that wave period, bed slope, and the location of transition between the wet and dry profile zones were important model parameters. Hoonhout [134] also used the DUROSTA model to study the effects of shoreline curvature on dune erosion and retreat during storm events, finding that consideration of shoreline curvature significantly impacted the model results. Currently, DUROSTA and another cross-shore model Unibest-TC [135] are optional modules that may be employed when using the one-line model Unibest-CL+.

De Goede [136] presented a historical review of the development of Delft3D, from initial 2D shallow water code development in the late 1960s, to coupling of updated wave models (e.g., SWAN), to the addition of turbulence closure models for 3D flows in the 1990s, and finally the incorporation of sediment transport formulations into the hydrodynamic module. Lesser et al. [124] presented details on the latter update, as well as the inclusion of a morphological acceleration factor for long-term simulations and validation studies showing that the results compared well to analytical solutions, laboratory data, and other accepted numerical model solutions. Delft3D is widely used in both practice and research [136], including studies on event-scale flooding [e.g., 68], storm sequence morphodynamics [e.g., 137], breach stability and growth [e.g., 138], and morphodynamic changes between storm events [e.g., 139].

Johnson et al. [140] presented a thorough summary of the historical development of CShore from its initial goals in modeling non-linear wave transformation in the late 1990s, to aiding in coastal structure design, and finally its development toward modeling nearshore morphodynamics in the late 2000s. Johnson et al. [140] also provided results from sensitivity analyses, model calibration, and validation at nine field sites, which showed the model was capable of producing reasonable estimates of event-driven morphological changes, while tending to under-predict dune erosion and retreat. Work and improvement on the model has contin-

ued through at least 2015 [141], and the model has also been extended to two-dimensions (C2Shore), the latter of which was validated through simulations of morphological response to Hurricane Katrina at Ship Island, Louisiana [126]. CShore does not explicitly model sheet flow or ebb currents, reducing its applicability during barrier inundation [52].

XBeach is considered the state-of-the-art event-scale model to predict barrier response to storm events. Lead by Roelvink et al. [59], XBeach was developed as an open source model to predict all of the main morphological responses associated with storm events (i.e., beach and dune erosion, overwash, and breaching) corresponding to the storm impact regimes of Sallenger [47]. Model validation studies showed it was able to predict storm hydrodynamics and morphological responses well [59], although subsequent studies have shown that high simulated velocities in the swash zone consistently led to slight overpredictions of erosion near the dune toe [e.g., 142, 143]. To correct these overpredictions, researchers have attempted to artificially lower sediment mobilization (by modifying the critical Shield's number); however, while this led to more accurate predictions of dune toe erosion, it decreased the accuracy of breaching simulations [143]. Elsayed and Oumeraci [144] found that modifying suspended sediment concentrations based on the local bed slope helped to resolve this issue. Some of the most recent work with XBeach has involved modifying roughness coefficients. Passeri et al. [145] implemented spatially varied roughness coefficients based on land cover, which showed improved morphodynamic predictions over simulations with constant roughness values. Alternatively, van der Lugt et al. [146] implemented dynamic roughness values that vary during the simulation according to erosion and deposition patterns, which showed improved results over simulations with static roughness values.

Many of these event-scale models continue to be tested and applied today. Although XBeach has become the standard for modeling event-scale morphodynamics, recent comparison studies indicate that other models (e.g., CShore, SBEACH, Delft3D) are also being used and

evaluated for their strengths [e.g., 52, 132, 147]. Furthermore, various studies have loosely coupled these event-scale models together to utilize the strengths of each model. For example, Cañizares and Irish [68] used SBEACH to simulate dune erosion and lowering prior to inundation and breaching using Delft3D. XBeach and Delft3D have also been loosely coupled in a recent breaching study by van Ormondt et al. [139], who used XBeach to simulate breach development during the storm and Delft3D to simulate breach development and growth after the storm event.

Model coupling has also been utilized in the development of new modeling systems. The COAWST modeling system, which was developed by coupling a regional ocean model (i.e., ROMS), a nearshore wave model (i.e., SWAN), and an open source sediment transport model (i.e., CSTMS) [148], is appearing more frequently in the coastal morphodynamics literature, including specific application to shoreline change modeling [e.g., 149] and barrier islands [e.g., 150, 151]. Numerous other modeling systems have been developed (see Kaveh et al. [152]), but have yet to gain a literature foothold in this particular field of study.

Storm Sequences and Post-Storm Recovery

Some of these event-scale models have also been applied to the study of storm sequences, which investigates the non-linear impact of sequential storms on beach and dune erosion, where successive smaller storms have a cumulative effect that exceeds the impact of an independent event [153]. Various modeling studies have been conducted to quantify this cumulative impact and to determine the most important driving factors such as antecedent beach states [e.g., 154] and the order of the most severe storms within the sequence [e.g., 155].

Based on a survey of the literature, Eichentopf et al. [38] identified three primary conceptual descriptions to aid in modeling the impact of storm sequences, and discussed evidence from

published studies for each description. The three conceptual descriptions are: 1) initial storm destabilization, where the first storm in the sequence erodes the beach, leaving it more vulnerable to the next storm event, 2) extreme storm impact, where the largest storm event of the sequence is of primary importance regardless of storm order, and 3) benchmark storm impact, where all events in a storm sequence may be combined and modeled as a single large storm event, similar to a benchmark or design storm approach in hydrologic analysis. Various types of models that have been employed and/or developed to study storm sequences including statistical models [e.g., 156], long-term equilibrium-based models such as ShoreFor [157] or PCR [158], and multifaceted event-scale models such as XBeach and Delft3D [e.g., 154, 155].

In addition to reviewing the literature on storm sequencing, Eichentopf et al. [38] also provide a brief section on recovery, which they indicate is much less studied than the impact of storm sequences. They concluded with recommendations for future research, which broadly included additional physical and numerical simulations, improved data collection efforts, and stronger research emphasis on beach recovery processes.

2.2.3 Summary of Advancements and Limitations

The practice of modeling event-scale barrier morphodynamics has followed a natural progression from conceptualizing models based on observations, to the creation of simplified and efficient rule-based models, to the development of more complex sediment transport formulations coupled with hydrodynamic calculations at fine spatiotemporal scales. Reconsidering our *Grand Challenge* statement, it is apparent that significant advancements have been made over the last fifty years. The earliest and most basic models (e.g., analytical dune erosion models) were intuitive, easy to use, and could provide conservative estimates

for dune recession and likelihood of failure. Empirical studies followed, which advanced our ability to quantify the impact of key processes based on hydrodynamic output (e.g., predicting notching/avalanching of the dune face based on swash impact, predicting overwash volumes based on runup exceedance, predicting sediment transport rates based on velocity and concentration profiles, etc.). This improvement in scientific understanding, along with the advancements in computing power, has allowed us to continue reducing the spatiotemporal scales of our morphological predictions while maintaining or increasing accuracy.

However, there are still major limitations to our modeling capabilities. Although the accuracy of simulations has improved, we are still a long way from high confidence predictions. This is partially due to the scarcity of data to evaluate the predictive capability of models mid-storm. Event-scale models are able to capture the general trends of erosion and deposition compared to pre- and post-storm profile (or LiDAR) data; however, the small-scale predictive abilities of our models during storm is largely unknown since there is little to no data to validate those predictions. Our apparent distance from high-confidence predictions can also be attributed to both epistemic uncertainty (i.e., that which arises from our lack of knowledge of the relevant processes) and intrinsic uncertainty (i.e., that which arises from the inherent randomness of natural processes). For example, we know that some factors - such as vegetation and anthropogenic impacts - play an important role in event-scale morphodynamics, yet the modeling of such factors is (for various reasons) still in its infancy. Additionally, the inherent randomness of forcing conditions (e.g., storm characteristics, wave climates) and initial conditions (e.g., bathymetry, sediment characteristics) is difficult to capture at smaller scales.

2.3 Long-Term Morphodynamics

This section provides an overview of commonly modeled phenomena and processes associated with long-term morphodynamics, a review of relevant modeling efforts, and a summary of advancements toward the *Grand Challenge*.

2.3.1 Commonly Modeled Phenomena and Processes

During the periods of time in between storm events, chronic sediment transport processes resume their work that contributes to gradual morphological change. The following sections discuss commonly modeled long-term phenomena (i.e., shoreline change and barrier transgression) and relevant morphodynamic processes.

Shoreline Change

The shoreline can be smoothed or caused to vary in form depending on the angle of the incident waves which drive LST [159]. Thus, shoreline change is observed as the local shoreline is moved either landward or seaward by gradients in LST rates. These gradient-driven changes can also manifest themselves in other ways including island migration, barrier elongation, inlet migration, and island dimensional changes.

Although it is not as common, entire barrier islands can migrate in the direction of LST when sediment is eroded from the updrift end, carried alongshore, and deposited at the downdrift end, assuming no updrift sediment sources. Otvos Jr. [160] noted this phenomenon in the northern Gulf of Mexico by observing that barriers can migrate large distances (i.e., several kilometers) from their location of origin. When the barriers are stable and not prone to migration, newly formed inlets may migrate instead. This phenomenon results from a

LST gradient across the inlet, where sediment is deposited updrift of the inlet and eroded downdrift.

Dimensional changes may also be observed due to LST gradients and the placement of engineering structures. McCann [61] observed that most islands developed greater widths on the downdrift end of the island as compared to the updrift end, which was attributed to a minimal amount of updrift sediment available for transport. If a continuous source of updrift sediment is present, and sediment is not removed from the barrier system, then barrier elongation could be observed as sediment is continually added to the downdrift end. Penland and Boyd [161] described lateral migration of barrier islands and the influence of placing coastal structures at various locations along the islands. For example, structures placed near the updrift end tended to reduce the total island area while structures placed in the middle of the island tended to increase the total area.

Barrier Transgression

In addition to shoreline change, most barrier islands are undergoing transgression (i.e., landward migration) in accordance with SLR. However, this migration did not appear to be widely accepted in some of the earliest literature [e.g., 162, 163]. Nevertheless, once transgression was recognized by the research community, many studies sought to identify the driving mechanisms that were primarily responsible for it. Otvos Jr. [160] indicated that overwash and aeolian processes were primarily responsible for the landward movement, which was supported by others such as Moody [164] and Godfrey [165] [163]. Others found sediment transport through tidal inlets and/or breaches to play a much larger role [e.g., 64, 114, 166, 167, 168].

SLR rate is also considered one of the primary drivers of barrier transgression through its interaction with storm processes such as overwash and breaching. Although not developed

specifically for barriers, the Bruun Rule [169] exemplifies the theorized direct relationship between SLR and shoreline transgression. The interaction between rates of SLR and other transgressive processes was published in an interesting study by Moslow and Heron Jr. [170]. They found that previous high rates of SLR were correlated with dominating overwash processes and high rates of transgression. Conversely, when the rate of SLR slowed, they found that transgression also slowed and inlet dynamics became the dominant method of sediment transport between the ocean and backbarrier environment.

During landward transgression, barrier islands may also maintain their elevation with respect to SLR through the combination of overwash and inlet dynamics/breaching. As SLR effectively reduces barrier island relief, barriers are more prone to overwash and inundation during storm events, which deposit sediment on the island or behind it (i.e., washover deposits). This deposition effectively translates the island landward and increases its elevation. As this process is sustained, the barrier sediment may be conceptualized as 'rolling' over itself, which has led to the description of this cycle as 'barrier rollover' [14]. Lorenzo-Trueba and Ashton [19] referred to this sustainable behavior as dynamic equilibrium.

Similarly, lagoonal washover deposits and flood tidal shoals have been shown to assist the barrier in maintaining its elevation through the reduction of accommodation space for future washover [171]. For example, consider a salt marsh that grows on top of washover deposited in a lagoon during some initial storm event. When a subsequent storm arrives, sediment that would have been deposited in the lagoon is now deposited on top of the new salt marsh. Thus, the salt marsh (and previous washover deposit) acts to reduce the available lagoon space for washover, and elevation is increased in that location as a result. Recent modeling work has suggested that the presence of backbarrier marsh not only increases island elevations, but actually reduces landward transport by encouraging the subaerial deposition of sediments [172]. As the barrier continues its rollover toward the mainland, those previously buried

marsh and lagoonal sediments may show up as shoreface outcrops which can affect the future morphodynamics through changes in the sediment supply (i.e., the source of sediment that feeds the growing barrier).

Although sustained barrier transgression is associated with increases in subaerial elevations with SLR, barriers may also lose elevation due to compaction of the underlying sediment. Hoyt [173] was possibly the first to mention the idea of vertical movement by compaction or isostatic adjustment. He stated that "*compaction or isostatic movement caused by weight of the sediment deposited in the coastal area may result in formation of lakes or lagoons by depression of the chenier plain below water level.*" As the barrier rolls over previous marsh sediment, the marsh sediment compacts under the load of the island, inducing an even higher local rate of SLR.

Barrier island transgression is also considered to be influenced by two other factors: 1) the slope of the shelf over which it is migrating and 2) the sediment supply. If we only consider the geometry of the system and assume that barriers maintain their dimensions, it is apparent that barriers must migrate at higher rates over shallower slopes in order to keep pace with SLR [174]. Numerous studies have concluded that antecedent topography is extremely important to the development and configuration of modern day barrier islands [e.g., 175, 176, 177]. Others have concluded that sediment supply is more important to the rate of migration, with less sediment supply leading to increased migration [e.g., 178, 179, 180, 181]. Dillon [182] commented on the cross-shore migration of barriers through stratigraphy observations and concluded that barriers were not forced to continue landward migration with SLR, but could drown if the sea level advanced too quickly or if there was an insufficient supply of sand.

2.3.2 Modeling Efforts

Perhaps the most challenging question related to barrier morphology is, "What will be the state of a barrier system 10, 100, or even 1000 years from now?" Compared to analyzing and predicting short-term responses, there is considerably less evidence available (that is, evidence or data collected using our current era's level of scientific certainty) to evaluate historical trends and make long-term projections. Stratigraphic observation and analysis may provide a partial glimpse of historical system states; however, it also requires assumptions and a hermeneutic to make the evidence meaningful, thereby reducing the certainty of conclusions that may be drawn. On the other hand, there are also problems when extrapolating small-scale processes to large spatiotemporal scales (i.e., the problem of error propagation). Thus, the problem of long-term morphological analysis and prediction is not a trivial one, especially since it is closely tied to uncertainties surrounding climate change (e.g., future SLR and changes in storminess). Numerous publications from the early 1990s into the early 2000s discuss the philosophy behind long-term morphological prediction. The interested reader is referred to Stive et al. [183], Terwindt and Battjes [184], De Vriend [185], Latteux [186], and Cowell et al. [187] for further details on this topic.

Similar to the previous section, the review of long-term morphodynamic modeling efforts is broken down according to the primary intent of each model. Thus, modeling efforts are categorized by those which model 1) shoreline change, 2) shoreface evolution, 3) barrier transgression, and 4) phenomena that are typically combinations of categories 1-3. To assist the reader in keeping track of the models discussed, Figure 2.6 offers a graphical representation of long-term models, in the chronology of their publication, that simulate some combination of shoreface evolution, shoreline change, dune growth/erosion, or overwash. Table 2.4 is a comprehensive summary of the long-term models discussed in this review, which includes each model's relevant processes.

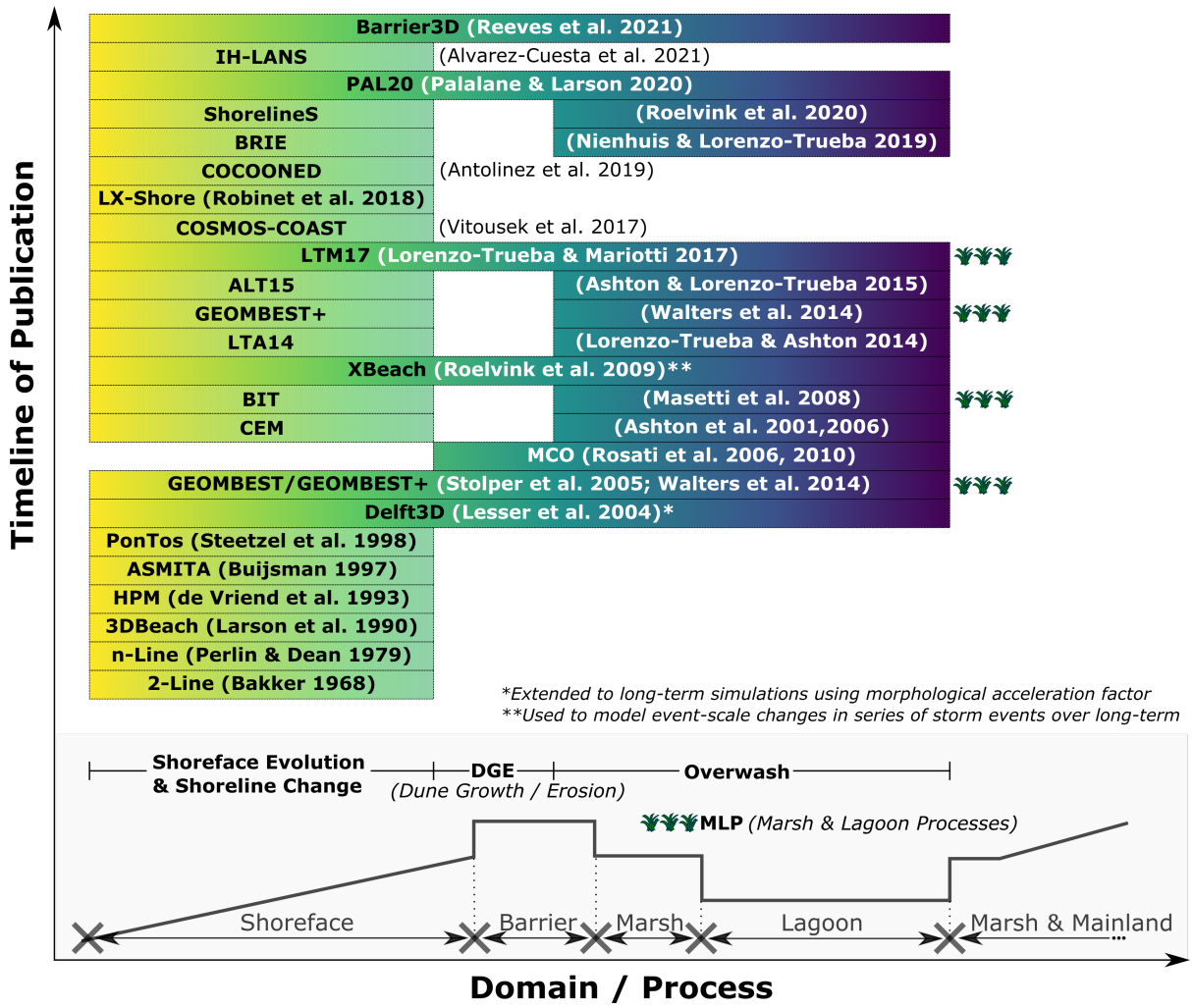

Figure 2.6: Long-term Morphodynamic Models with a Coupled Approach. *Models are shown according to their publication chronology and are aligned with their respective processes, which range from shoreface erosion or shoreline change, to dune growth/erosion, to overwash.*

Table 2.4: Long-Term Morphodynamic Models

Year	Model Name (Reference)	Modeled Phenomena/Processes†							
		SFC	LSC	TRN	ID	DGE	SUB	OW	MLP
1956	PEL56 [16]		X						
1962	Bruun Rule [169]			X					
1968	2-Line [188]	X	X						
1979	n-Line [189]	X	X						
1983	Gen. Bruun Rule [190]			X					
1985	EVR85 [191]			X					
1989	GENESIS [192]		X						
1990	3DBeach [193]	X	X						
1992	STM [194]			X					
1993	HPM [195]	X	X						
1995	ADM [196]	X							
1997	ASMITA [197]	X	X		X				
1998	PonTos [198]	X	X						
2001	CEM [159, 199]		X					X	
2002	Cascade [200]		X		X				
2002	BARSIM [179]			X				X	
2005	GEOMBEST [171]	X		X				X	X
2006	MCO [201, 202]			X		X	X	X	
2008	BIT [203]	X		X				X	X
2009	YAT09 [204]	X							
2012	GenCade [205]		X		X				
2013	ShoreFor [206]	X							
2013	Mod. Bruun Rule [207]			X				X	
2014	LTA14 [19]	X		X				X	
2014	GEOMBEST+ [17]	X		X				X	X
2015	ALT15 [208]	X	X	X				X	
2016	D&H16 [209]			X	X			X	
2017	LTM17 [1]	X		X				X	X
2017	CoSMoS-COAST [210]	X	X	X					
2018	LX-Shore [211]	X	X						
2019	COCOONED [212]	X	X			X			
2019	BRIE [213]	X	X	X	X			X	
2020	ShorelineS [214]		X					X	
2020	PAL20 [215]	X	X	X	X	X		X	
2021	UNIBEST-CL+ [216]	X	X						
2021	ShoreTrans [217]			X		X			
2021	IH-LANS [218]	X	X						
2021	Barrier3D [219]	X		X		X		X	

†SFC: Shoreface Change; LSC: Longshore Shoreline Change; TRN: Transgression; ID: Inlet Dynamics; DGE: Dune Growth or Erosion; SUB: Subsidence; OW: Overwash; MLP: Marsh and Lagoon Processes

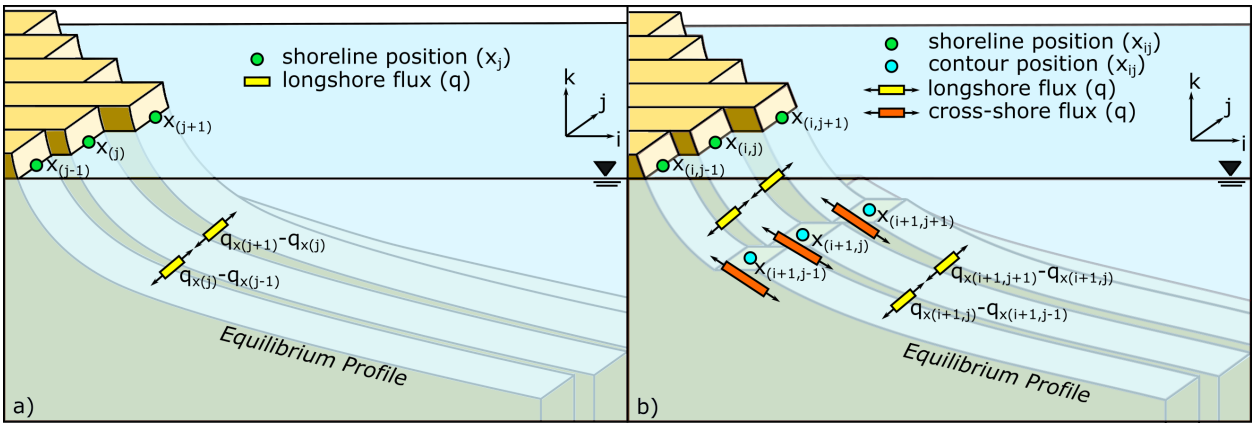

Figure 2.7: One-Line and Two-Line Model Schematics. *a) One-line approach that predicts shoreline changes based on LST gradients* ($q_{x(j+1)} - q_{x(j)}$). *b) Two-line approach that predicts change at the shoreline and an offshore contour, considering LST gradients in each zone and rule-based XST. Figure modified from Perlin and Dean [189].*

Modeling Shoreline Change

Long-term modeling of shoreline change is often referred to as 'shoreline evolution' modeling since the most observable impact of LST gradients is shoreline displacement, either landward or seaward. The first approach to modeling shoreline evolution stemmed from One-line Theory, published by Pelnard-Considere [16]. Models derived from this theory, commonly called 'one-line models,' assume a constant equilibrium profile and calculate position changes in a single contour line - the shoreline - over time considering only the gradients in the LST rate (see Figure 2.7a).

Larson et al. [220] published a review of one-line modeling theory and analytical solutions that had been developed for various coast-specific and structure-specific situations. Two years later, Hanson and Kraus [192] presented the one-line model GENESIS, which would become one of the most widely used one-line models for predicting shoreline evolution in practice, though not without criticism [e.g., 221, 222]. One-line models are still being developed and used today, likely due to their simplicity, intuitiveness, and ease of calculation. The Coastal Evolution Model (CEM) of Ashton et al. [159] is a one-line model that pre-

dicts shoreline response due to high-angle waves, assuming a constant linear shoreface out to an estimated closure depth. From numerical experiments, they found that high-angle waves cause small shoreline perturbations to grow into larger formations, such as cuspates and spits. Additionally, they found that shoreline protrusions can shelter downdrift features from the high-angle waves, affecting the evolution of such features. Thomas and Frey [223] and Kim et al. [224] reviewed other common one-line models including UNIBEST-CL+ [216], GenCade [205], which is a combination of GENESIS and the regional Cascade model [200], and the proprietary LITPACK model. These models include advances such as coupling XST formulations, wave transformation, and wave-current interaction. Notably, GenCade includes advances to model tidal inlet evolution and inlet dynamics such as inlet bypassing and inlet feature (e.g., shoal) sediment balance.

Bakker [188] was unsatisfied with the one-line theory's assumption of parallel bathymetric contour lines near engineered structures due to the apparent discontinuity it produced. In 1968, Bakker published a two-line model whereby XST could be approximated between two profile zones based on the profile's deviation from an equilibrium state (see Figure 2.7b). Perlin and Dean [189] were the first to suggest expanding Bakker's two-line approach to multiple lines, and followed up with publication of their n-line model six years later, which was named for its ability to handle a user-defined 'n' number of contour lines [225]. Although limited in their ability to produce non-monotonically decreasing profiles, these models were the first to add elements of cross-shore change to one-line models, paving the way for later n-line models that would attempt to integrate both XST and LST [e.g., 198].

Buijsman [197] published the ASMITA model, which simulated interaction between the adjacent shoreline and tidal inlets. The model consisted of five nodes that represented the tidal channel, ebb shoal, flood shoal, and the adjacent shorelines. Sediment flux between these nodes was calculated based on equilibrium formulations of each feature. A similar

approach was incorporated into the regional barrier island model called Cascade, presented by Larson et al. [200]. While ASMITA focused on modeling the channel evolution, Cascade focused on modeling the regional shoreline position over long time scales, but accounted for the dynamic inlet features in the form of sediment source and sink terms. Larson et al. [200] applied Cascade to a regional stretch of a U.S. East Coast barrier island and found the model was able to satisfactorily predict the shoreline position updrift and downdrift of two inlets.

Modeling Shoreface Evolution

Although long-term modeling of barrier transgression was well underway by the 1980s, most models assumed a constant profile shape. It wasn't until the mid-1990s that shoreface evolution began to be modeled, with the publication of the Hinged Panel Model (HPM) [195] and the Advection-Diffusion Model (ADM) [196].

A conceptualized model of the shoreface profile by de Vriend et al. [195] discretized the shoreface into 3 sections: 1) the upper shoreface, 2) the lower shoreface, and 3) the middle shoreface, which acted as a transition zone between the upper and lower zones. On the lower shoreface, profile movement was assumed to be negligible compared to the scales of interest, while the upper shoreface was assumed to be highly active out to the depth of closure (i.e., the transition point to the middle shoreface). The sections were considered to be rigid panels, which rotated about hinge points at the panel intersections based on the net sediment transport into or out of the panel zone. This led Cowell et al. [187] to refer to this model as the Hinged-Panel Model (HPM). Stive et al. [226] published a full treatment on HPM, which used Bowen's energetics formulation for XST between the shoreface sections. They found that HPM produced reasonable hindcast simulations, and that the effect of substrate slope on profile evolution was only relevant at geologic timescales.

Niedoroda et al. [196] published a similar model, the main difference being the continuous formulation of XST as compared to the paneled formulation of Stive and de Vriend. The continuous formulation is depth-dependent and breaks down the transport into a bed load (i.e., advective) term and a suspended load (i.e., diffusive) term; thus, it was called the ADM model by Cowell et al. [187]. Although Stive et al. [226] and Niedoroda et al. [196] do not apply their models to barrier coasts specifically, their work signifies advancement in cross-shore shoreface modeling and the increased importance of including cross-shore processes in long-term models.

Another class of models that simulate shoreface evolution are equilibrium shoreline models, which have become increasingly popular for simulating event-based to interannual change. These models combine equilibrium-based formulations of shoreface evolution with shoreline change models (typically one-line models). The two most popular models include Yates et al. [204] and the Shoreline Forecast (ShoreFor) model of Davidson et al. [206]. Both models demonstrate that beaches often respond directly to wave forcing (e.g., as quantified by wave energy or dimensionless fall velocity); however, the equilibrium response time scale (which is often longer than a single storm event) plays an exceedingly important role in the morphological evolution. Further, the extensive observations and developed model of Yates et al. [204] show that beaches become increasingly resistant to erosion while in an eroded state.

Modeling Barrier Transgression

Models of shoreline change and shoreface evolution often produce a landward or seaward shift in the shoreline and/or profile based on gradients in the sediment transport rates. However, these models are not able to account for barrier transgression as an observed phenomenon. Thus, numerous models were developed to simulate long-term transgression based on cross-

shore processes (e.g., overwash, breaching, inlet dynamics) and long-term forcing conditions (e.g., SLR).

Translation Models

Bruun [169] introduced what is perhaps the most popular hypothesis about cross-shore transgression, which states that an equilibrium beach profile translates upward and landward with SLR while conserving sediment volume. Years later this became known as the 'Bruun Rule' [227]. Because the profile is 'translated,' these types of models are often called 'translation models' in the literature, and many them have been developed since publication of the Bruun Rule.

The Bruun Rule [169] predicts profile recession distance based on the amount of SLR and the average beach slope while conserving sediment. In subsequent examination of his theory, Bruun [228] revisited the assumptions behind the model development and cautioned modelers who might attempt to apply the Bruun Rule in coupled alongshore models and progradational scenarios. Upon further review of initial publications by Bruun [169] and Schwartz [227], several researchers have offered criticism of the way that the Bruun Rule (and the underlying equilibrium profile concept) is used in current models [e.g., 229, 230]. Conceding that some of the criticisms of Pilkey et al. [229] were valid, Dubois [231] stated that such models can still be useful in formulating research questions and site-specific equilibrium-based models. A more recent study by Wolinsky and Murray [232] highlighted additional limitations of the Bruun Rule as applied to long-term simulations on the order of millennia.

Rosati et al. [207] offered a review of field studies that attempted to validate the Bruun Rule (or modified forms of it). More recently, the Bruun Rule has been used to model both barred and bermed beach profiles in a laboratory setting [e.g., 233]. D'anna et al. [234] recently presented a reinterpretation of the Bruun Rule that explicitly partitions shoreline

recession into passive flooding of the beach profile and wave-driven reshaping components. Similarly, Troy et al. [235] assessed long-term profile submergence versus Bruunian recession of beaches on the Great Lakes, a model environment to observe the effects of significant water-level variability, which serves as a proxy for future SLR.

The Bruun Rule has also been expanded since its initial publication. Dean and Maurmeyer [190] presented the Generalized Bruun Rule, which expanded the original model to include the recession of barrier coasts specifically, and noted that greater recession rates were predicted due to the additional sand volume being deposited on the subaerial island and in the lagoon. The Bruun Rule was also expanded to include source and sink terms in the models of Everts [191, 236]. Everts proposed that historical rates of SLR and shoreface retreat are preserved in the slope of the seaward profile, assuming that the profile is not significantly reworked by LST or tectonic deformation processes. Everts compared present and past ratios of SLR to shoreface retreat for five U.S. East Coast barrier islands and found that some barriers are in a narrowing state. Everts proposed that these barriers would continue to narrow until a critical width is reached, at which point landward migration of the island would begin. This theory employed the previously mentioned critical length concept, which was first proposed by Leatherman [237] and has since been utilized in other models [e.g., 19]. Further modifications of the Bruun Rule were published by Rosati et al. [207], who included an additional term representing XST in the landward direction by overwash and/or aeolian processes, and Dean and Houston [209], who added a LST term and sediment source/sink terms to Rosati's 2013 formulation.

Cowell et al. [194] developed the Shoreface Translation Model (STM), which allowed modelers to keep track of changes in stratigraphy, and was later used in conjunction with field observations to perform hindcasting simulations [238]. The STM was later expanded using a probabilistic framework to produce distributions of results that could be statistically

evaluated in risk management frameworks [239].

Most recently, McCarroll et al. [217] published the ShoreTrans model, which follows similar profile translation methodology with a couple of distinctions and additions. First, the model uses measured profiles instead of parametric representations. Second, in addition to the profile translation, ShoreTrans has been modified to incorporate dune erosion and accretion, sediment flux between the upper (active) and lower (inactive) shoreface, as well as source and sink terms that can modify the sediment supply.

Other Transgression Models

More recent transgression models can't simply be described as 'translation' models, since they also simulate profile changes. For example, Storms et al. [179] published an evolution model called BARSIM, which was intended to preserve the simulation's erosion and depositional time history for comparison to observed shoreface stratigraphy. They describe BARSIM as a 'process-response' model in which erosional and depositional mechanisms were modeled separately. Storms et al. [179] conducted multiple numerical experiments and found that their model successfully captured several general observations: 1) increased grain sizes led to steeper shoreface slopes, 2) higher sediment supply values decreased retrogradation and increased the likelihood of aggradation or progradation, 3) higher SLR rates increased the likelihood of barrier overstepping, and 4) lower substrate slopes allowed for greater landward rates of migration.

Stolper et al. [171] published the GEOMBEST model, which allows for depth-dependent shoreface adjustment toward a theoretical equilibrium profile, thus allowing the shoreface to temporarily exist in disequilibrium. GEOMBEST is also able to simulate heterogeneous stratigraphic units that can differ in erodability. Using the conceptual model of Cowell et al. [46], GEOMBEST divides each simulated coastal tract into three cross-shore zones

(i.e., shoreface, backbarrier, and estuary). Stolper et al. [171] used this model to estimate possible stratigraphic histories in both steep and gentle sloping environments, showing that quantitative estimates may be useful where historical data may be lost or otherwise unavailable. They also showed that substrate slope plays an important role when non-erodable outcrops are present. Specifically, they found that steep slopes lead to narrowing of the estuary and barrier drowning unless there is an external increase in sediment supply.

Based on sensitivity analyses with GEOMBEST, Moore et al. [180] found that increasing the SLR rate and decreasing sediment supply led to increased barrier migration. Moore et al. [240] also studied the Holocene evolution of U.S. East Coast barrier islands and found that the most vulnerable islands were large with less erodable substrates and gentle slopes. Brenner et al. [241] confirmed these findings and also found that positive and negative feedbacks occur based on the slope of the substrate and island trajectory, and the composition of the substrate and backbarrier deposits; the negative feedback adjusts island trajectory to the substrate slope while the positive feedback leads to barrier width adjustments.

In studying the effects of compaction on barrier island migration, Rosati et al. [201] developed the Migration, Consolidation, and Overwash (MCO) model to predict the response of barrier systems to a series of storm events. The MCO model used the Convolution Method of Kriebel and Dean [85] to predict responses when there was no overwash, and the numerical method of Donnelly et al. [112] to estimate overwash volumes when water levels exceeded the berm height. Rosati et al. [201] found that when consolidation was considered, there were considerable increases in migration distance and reduction of dune elevations. They found that increases in surge heights and deep-water wave heights also led to significant increases in migration and reduction of dune elevations. Rosati et al. [202] updated the 2006 model to include the overwash formulations by Donnelly et al. [109], and found that barriers on top of compressible substrates migrated much faster than barriers on non-compressible substrates,

assuming a sufficient sand supply. They also found lower dune elevations and island volume loss to be more prevalent when compressible substrates were present, the thickness of which was found to be non-linearly related to consolidation rates.

Masetti et al. [203] developed the Barrier Island Translation (BIT) model with separate sediment transport formulations for shoreface evolution, inner shelf reworking, overwash, and backbarrier infilling. They found barrier migration to undergo significant increases and decreases in migration rate according to the substrate slope and sediment availability. Additionally, they found that offshore subaqueous bodies of sediment were most likely due to barrier migration over a non-uniform surface, rather than drowning of previous barrier islands.

Lorenzo-Trueba and Ashton [19] developed a barrier island evolution model (hereafter 'LTA14' model) to evaluate long-term behavior of the system. The model tracked transect boundary changes in the cross-shore direction based on sediment flux calculations. They found that barriers evolved following one of four behaviors: height drowning, width drowning, constant transgression (or dynamic equilibrium), and periodic transgression. Most recently, Reeves et al. [219] expanded the LTA14 model domain to consider dune and subaerial island processes in a model called Barrier3D. The Barrier3D model used the LTA14 equations to simulate shoreline and nearshore profile change, and included additional formulations for dune growth during non-stormy periods, dune reduction by overwash, alongshore dune elevation changes, and sediment transport by overwash and backbarrier overland flow. Barrier3D also used probability distributions to simulate synthetic storm events and barrier recovery between storms [219].

Multifaceted Evolution Models

Whereas most of the previously discussed long-term models were developed to simulate one primary phenomenon (e.g., shoreline change, shoreface evolution, barrier transgression), other recent models have been developed with the intent to simulate multiple long-term phenomena. We discuss four categories of these multifaceted evolution models: 1) coupled barrier-backbarrier models, 2) models that combine shoreline change and transgression, 3) models that combine shoreline change and shoreface evolution (i.e., equilibrium shoreline models), and 4) extended event-scale models.

Coupled Barrier-Backbarrier Models

In the last decade, barrier island evolution models have been coupled with backbarrier models to evaluate interactions or feedbacks between the systems. Walters et al. [17] published GEOMBEST+, which coupled GEOMBEST with a backbarrier model from Mariotti and Fagherazzi [242]. Using this model, they found that overwash played an important role in that it provided a narrow platform for backbarrier marsh growth, which in turn reduced island migration rates by decreasing accommodation space for sediment deposition. Lorenzo-Trueba and Mariotti [1] also developed a coupled model that combined the backbarrier marsh model of Mariotti and Carr [18] and Lorenzo-Trueba and Ashton [19]. They found that including processes such as import/export of fine sediment to the barrier environment significantly impacted the accommodation space for overwashed sediment, which ultimately led to either a sustained island that migrated or one that drowned.

Models that Couple Shoreline Change and Transgression

Noting that most of the previous modeling efforts focused on either shoreline change or transgression, models are increasingly being developed to include both components. In

2006, the CEM model was updated to include a function for barrier overwash [199] and was later coupled with the LTA14 cross-shore barrier model [208]. The authors found that when alongshore coupling was less significant, large alongshore variations persisted longer in the simulation; thus, alongshore coupling was found to act as a dampener on barrier transgression [208].

Nienhuis and Lorenzo-Trueba [213] published the BarrieR Inlet Environment (BRIE) model, which modified and extended the combined model of Ashton and Lorenzo-Trueba [208] to include inlet dynamics. The model simulated inlet formation (i.e., breaching) and cross-sectional area changes, and including alongshore sediment volume balancing between updrift and downdrift sides of the inlet. BRIE also included a stratigraphic model that keeps track of how sediment types (i.e., lagoonal, washover deposits, flood tidal shoals) are re-worked over time [213].

Other models include that of Palalane and Larson [215], ShorelineS [214], and IH-LANS [218]. The Cascade model, which simulates shoreline changes for a region of barrier islands, was updated by Palalane and Larson [215] to include XST components from Larson et al. [243], which included overwash, beach and dune erosion, transport between the beach and offshore bar, and aeolian transport. The ShorelineS model, developed by Roelvink et al. [214], models shoreline change, overwash, and includes the ability to split and merge barrier islands or spits. It is also planned for ShorelineS to be coupled with XBeach or Delft3D to simulate island and inlet migration in future work [214]. Alvarez-Cuesta et al. [218] developed the IH-LANS model which combines LST (using a modified version of CERC based on Hallermeier [244]) and XST (following Toimil et al. [245]), while also including specific formulations for engineering structures such as groins, seawalls, and breakwaters.

Models that Couple Shoreline Change and Shoreface Evolution

Although not limited to barrier island modeling, many long-term models now couple shoreline change and shoreface evolution models. One of the earliest examples of this approach was the 3DBeach model, published by Larson et al. [193], which was a combination of SBEACH and GENESIS, and was capable of simulating dynamic profile features such as offshore bars.

Recently developed models incorporate equilibrium shoreline models as one aspect of their predictive capabilities. These models include CoSMoS-COAST [210], LX-Shore [211], and COCOONED [212]. CoSMoS-COAST combines the one-line model of Vitousek and Barnard [246], the equilibrium model of Yates et al. [204], a translation component similar to Bruun [169], and a long-term residual shoreline trend following Long and Plant [247]. LX-Shore combines the wave model SWAN with LST [e.g., CERC, 248] and XST [e.g., 206] formulations in a 2D horizontal grid, similar to the CEM model setup [211]. Lastly, the COCOONED model [212] couples a one-line approach similar to Vitousek and Barnard [246], a cross-shore equilibrium model similar to Miller and Dean [249], and the analytical dune erosion method of Kriebel and Dean [85].

Notably, data assimilation techniques have been tried with many of these equilibrium shoreline models. Long and Plant [247] were one of the first to use data assimilation for shoreline evolution predictions. They combined a modified version of the Yates et al. [204] model, which predicts long-term and short-term trends of shoreline position, with a joint extended Kalman Filter (eKF) assimilation approach that updates the model predictions based on shoreline position observations. Other models that have used Kalman filtering include CoSMos-COAST [210], ShoreFor [250], and IH-LANS [218].

Extended Event-Scale Models

Another common modeling approach that combines XST and LST is the extension of multifaceted event-scale models for use in long-term simulations. Due to computational con-

straints, event-scale models have primarily been used to simulate short-term changes. However, recently they have also been employed and extended to predict long-term changes where computational burden is reduced through hydrodynamic averaging or lengthening the morphological time step.

Vemulakonda et al. [251] were among the first to utilize this approach with the Coastal Inlet Processes (CIP) Model, which was originally developed to predict tidal inlet shoaling for ingress and egress of U.S. submarines. Wave and circulation models were coupled together with a sediment transport model, the latter of which required a user-defined time step that effectively extended the hydrodynamic conditions. Comparing model results to a year's worth of navigation channel survey data, the model was shown to satisfactorily predict sediment transport rates [251].

A more recent and common approach is that of Lesser et al. [124], who applied a morphological acceleration factor (*morfac*) within Delft3D to effectively lengthen the sediment transport time step for long-term simulations. Lesser et al. [124] showed that using *morfac* in simplified cases did not cause the results to significantly deviate from the full solution. This approach was extended by Roelvink [252], who proposed running multiple accelerated simulations in parallel for different tidal phases and using a weighted average of morphological change to update the bathymetry for the next time step.

Event-scale models are also used to model storm sequences and recovery periods between storms. Ranasinghe et al. [158] developed the Probabilistic Coastline Recession (PCR) model, which generates 100-year sequences of storm events and employs the event-scale swash impact model of Larson et al. [94] (LEH04) to predict dune recession. The model also considered SLR projections and used a constant, empirically derived rate of dune recovery between storm events [158]. Long et al. [253] developed a modeling framework for Breton Island, Louisiana, to assess restoration design alternatives that used XBeach to model the is-

land's response to successive storm events over a 15-year time period. Shoreface and bay-side erosion between storm events were not modeled explicitly, but were accounted for through manual manipulation of the pre-storm profiles [253].

2.3.3 Summary of Advancements and Limitations

The literature indicates that over the last fifty years significant advancements have been made in long-term morphodynamic modeling of barrier systems. Again, model development has followed a rather natural progression - from the simplified to the complex. The intuition behind some of the earliest models (e.g., one-line and translation models) laid a foundation on which subsequent model development has been steadily built. More complex formulations have been developed to predict shoreface shape changes, rather than assuming a constant equilibrium profile. Additional processes have been added (e.g., overwash representations, changes in sediment supply) to more closely capture the underlying mechanics of barrier transgression. Models are also increasingly being developed to incorporate other sub-systems (e.g., the backbarrier marsh-lagoon system) that impact the long-term morphodynamics.

Yet there are still many limitations to be addressed, including (but not limited to) model validation, uncertainty characterization, and the incorporation of relevant processes and important factors. Although there is a wealth of satellite imagery available to coastal researchers, this dataset is limited both in the information it contains (i.e., primarily shoreline and marsh positions) and its temporal coverage for long-term model calibration and validation. This lack of long-term quantitative data is one likely reason why many long-term models have not been thoroughly validated. Other long-term models that were originally created to explore barrier island morphodynamics and develop new hypotheses - what Murray [254] calls 'exploratory models' - have largely remained as such and have not yet shifted

toward the prediction of real systems. Additionally, although testing model sensitivity is common practice, most models are not developed to explicitly consider input parameter uncertainty. Models typically receive averaged or representative input values and produce a single-value output rather than a statistical range of predictions. Another limitation, similar to event-scale modeling, is that most previous efforts have focused on evolution of the natural barrier system and have neglected anthropogenic impacts. Other relevant processes such as barrier subsidence, aeolian transport, backbarrier marsh growth/erosion, and factors that impact erosion and deposition such as vegetation type and density, have mostly been excluded from long-term models with only a few exceptions.

One modeling challenge that has persisted over time is the extrapolation of small-scale sediment transport predictions to large scale coastal behavior (LSCB) - a link which is certainly intuitive. However, the problem of uncertainty or error propagation, where uncertainty or error at the small scale compounds over time resulting in imprecise or inaccurate predictions, has stifled this type of long-term modeling. De Vriend [255] indicates the extraordinary challenge of this unsolved problem saying, "...it must even be doubted whether models formulated at a small scale will ever be able to describe LSCB," and reverently quips that "we may need another Ludwig Prandtl" before we have a good answer.

2.4 Research Gaps and Needs

Based on the advancements that have been made toward our *Grand Challenge*, and the limitations that persist in our modeling efforts, we have identified critical gaps and future research needs that might be addressed moving forward. The gaps and needs highlighted below are those we believe are most critical for making progress toward the *Grand Challenge*. We acknowledge, however, that other gaps and needs exist. The research gaps and needs

may be generally categorized as follows: 1) Observations, data availability and accessibility, 2) Scientific understanding of relevant processes, and 3) Modeling framework and approach. These categories are expounded below.

2.4.1 Observations, Data Availability, and Accessibility

One of major limitations of our current modeling efforts is the availability of data. While technological advancements during the 20th century increased our ability to collect good data, the timing of these advancements means the quantity of long-term data for validation is sparse. On the other hand, event-scale data are not limited by time, but by the complexities and dangers associated with collecting perishable data before, during, and immediately following storm events. However, to improve our scientific understanding of the relevant processes and associated modeling efforts, we must overcome these data limitations so that we can ground truth our theories and formulations in observations. Herein we discuss a few high-level issues regarding data acquisition and accessibility, while assuming that some methodological advancements for data collection and analysis will be required to further our understanding of the relevant processes discussed in the following section.

Long-term observations of coastal morphodynamics generally exist only at a limited number of well-monitored sites (e.g., Duck, NC, [256]; Torrey Pines, CA, [257]; Ocean Beach, CA, [258]; Fire Island, NY, [259]; Narrabeen-collaroy, Australia, [260]; Truc Vert, France, [261]; Hasaki, Japan, [262]; South Holland, Netherlands, [263]), which are maintained by various government agencies and academic institutions. It is vital that these long-term monitoring efforts continue while new avenues of data at higher spatiotemporal resolutions are sought. As such, we must be diligent to make the most of available datasets, develop new ones, and make them broadly accessible. We must develop and promote centralized, open access databases

(e.g., the Community Surface Dynamics Modeling System - CSDMS) that contain both open access models and collected data (e.g., the use of public archival in the National Science Foundation's DesignSafe [264], or post-event field data [265]). Increasing the amount and quality of available data would also be useful for blind model comparisons, data assimilation, and machine learning applications.

One way to push toward increased dataset availability is to continue to capitalize on technologies that exist and are readily available. A perfect example of this is remote sensing data, such as publicly available satellite imagery [e.g., 266, 267, 268]. We also expect that publicly accessible LiDaR datasets will become more widely available with continued advancements in drone technology [269]. It might also require us to creatively enlist the public's help in data collection such as using public photos and photogrammetry [e.g., 270]. A second way to advance this initiative is by developing new data collection methods or technologies. Due to the perishable nature of pre- and post-storm data and the uncertainties surrounding the timing and location of storm events, morphological data before, during, and after storm events is difficult to obtain. Certain efforts are underway to help coordinate, collect, and make available this perishable data, including the National Science Foundation's NHERI RAPID Facility [265, 271] and Nearshore Extreme Events Reconnaissance program [272].

2.4.2 Scientific Understanding of Relevant Processes

Epistemic uncertainty and the exclusion of relevant factors are two important previously mentioned limitations. The epistemological issues discussed herein include both hydrodynamics and sediment transport, and the relevant factors discussed include vegetation dynamics and anthropogenic impacts.

Despite hydrodynamic simulation advancements, increased complexity in sediment transport

formulations has not always translated to increased accuracy. Quoting from a study by Davies et al. [273] in which multiple transport formulations were compared, Bosboom and Stive [88] noted that most sediment transport predictions are only accurate within an order of magnitude, and that empirical calibration of these model formulations is still necessary in many cases. They also remarked that the simpler formulations are still often the best available ones. This indicates an obvious shortcoming in our ability to reproduce realistic hydrodynamic forcing conditions and to model the relationship between forcing and sediment transport. Aagaard and Hughes [99] highlighted some of the latter shortcomings, stating that there is room for improvement in our quantitative understanding of bed load and suspended load transport, as well as our knowledge of which parameters (other than bed shear stress) can lead to better transport rate predictions. Notably, while such improvements would certainly lead to advancements in event-scale modeling efforts, the initial impact on long-term models would be minimal.

One of the greatest advancements in event-scale morphodynamic modeling in recent years was the inclusion of infragravity waves in the hydrodynamic calculations [41]. While we still do not fully understand the mechanics of how these waves impact nearshore sediment transport [54], we now recognize their importance in predicting event-scale morphodynamic response. Other factors such as the non-linearity of incident waves, the interaction of incident and infragravity waves, and swash zone dynamics, including turbulence and boundary layer flows, may also prove to be key missing components in coupled hydrodynamics-sediment transport formulations that have a significant impact on event-scale morphodynamics. While these factors may be key missing components, the small scales needed to resolve some of these hydrodynamic and sediment transport processes would require computational resources that make such modeling practically infeasible at present. Continued computational advancements may help to alleviate such limitations.

In studying and developing formulations for event-scale processes such as overwash and breaching, it is important to consider all of the contributions to total inundation height, including tides, storm surge, and waves. The exclusion of one or more of these contributions can alter the total inundation height and corresponding morphological response. Furthermore, special consideration should be given to the timing of these contributions, as recent work has shown that time differences between the bay peak surge and ocean peak surge can lead to bay-side breaching [e.g., 49, 50, 51, 78].

Since data for event-scale morphodynamic response are sparse, future work should capitalize on previously published studies or available data from historical events [e.g., 139], which may yield additional insights into the nature of overwash and breaching. Moreover, since overwash and breach observations are difficult to obtain in the field, physical modeling that leverages advancements in data collection methods and instrumentation may also help us better understand and quantify these processes. Although these physical modeling studies would require careful consideration of potential scaling issues, we believe that valuable insights into the overwash and breaching processes remain to be gained from this method of study.

Another factor that may be prioritized for future studies is coastal vegetation. Currently, we have a general understanding of how vegetation impacts barrier morphodynamics (e.g., dune stabilization, subaerial accretion, increased flow roughness) and vice versa [e.g., 146]; however, our quantitative understanding, and field-verification of that understanding, is further behind. Moving forward, beneficial research efforts would include the quantification of vegetation impact for parameters such as vegetation type, location, density, and hydrodynamic conditions for implementation in event-scale and long-term models. Recent studies [e.g., 274, 275] indicated that this research is underway, and recent modeling studies [e.g., 145, 146] exemplify the initial stages of incorporating this information into event-scale mor-

phodynamic analysis. Furthermore, with the U.S. Army Corps of Engineers' recent release of international guidelines on the design and implementation of Natural and Nature-Based Features (NNBF) [276], we expect future studies to quantify the performance of NNBF in various coastal environments.

Many coastal barriers are no longer representative of a natural environment as they are either developed or impacted by development and engineering structures on neighboring shorelines. Although many early studies and models sought to quantify the impact of engineering structures on littoral transport (e.g., one-line modeling of shoreline changes near groins), relatively few studies have quantitatively addressed the morphological impact of human development and other large-scale coastal restoration practices. Additionally, we would benefit from better understanding how the coastal management process works holistically, including how policies are developed, how individual restoration decisions are made, and how studies which quantify anthropogenic impacts influence the management process, considering cultural, political, and socioeconomic differences across localities. This type of analysis has largely been absent in the barrier morphodynamics literature, with the exception of a few observational studies on the feedbacks between coastal protection and real estate values [e.g., 277], and modeling studies that consider the coupling of barrier morphodynamics with the incentives of developers and owners [e.g., 278] and individuals in the coastal real estate market [e.g., 279]. Moving forward, beneficial research topics would include understanding the quantitative morphodynamic response between developed and natural barrier systems [e.g., 280]), and the incentives, behavior, and impacts of human agents in what is appropriately called a 'coupled human-landscape' or 'coupled natural-human' system [281, 282].

2.4.3 Modeling Framework and Approach

There are several ways in which our modeling frameworks and overall approach may continue to improve in order to further research and achieve higher-confidence predictions. First, since modeling is inherently tied to the scientific understanding of the processes being studied, advancements in how those processes are understood must be regularly incorporated into the improvement of existing models and the development of new models. As research has naturally become more focused and specialized, many recent studies have been published related to specific components of barrier island morphodynamics (e.g., sediment transport between the inner shelf and active profile, beach-dune interactions, backbarrier marsh dynamics, etc.). Therefore it is critically important that holistic models of barrier morphodynamics incorporate the theory and formulations of more focused models.

Second, although some of the recently published long-term morphodynamic models included sensitivity analyses for various parameters, model results are still largely presented as single simulation output. Modeling efforts would benefit by increasingly employing ensemble approaches (e.g., Monte-Carlo techniques) that consider input parameter uncertainty. Rather than producing a single output, a probabilistic range of results would be produced that can help characterize uncertainty in the model predictions [283]. Such an approach lends itself not only to identifying expected values, but also to identifying extreme scenarios and the input parameter combinations that cause them. Additionally, with the large number of models that have been developed, modelers may consider a multiple-model ensemble approach to evaluate the range of predictions across various models, as has been done with model comparison studies [e.g., 284]. Such an approach would emulate the current practice for forecasting hurricanes and would also naturally facilitate model comparisons and identification of robust and accurate models.

Third, as we focus on expanding data accessibility and collection capabilities, we must be diligent to incorporate the available data. In addition to model validation, data may be used to train and/or reduce error in model predictions using machine learning and data assimilation methods, respectively. There are many ways in which machine learning may be employed in morphodynamic modeling to improve predictions and fine-tune model parameters for a specific site [285]. Machine learning may also be employed to reduce computational burden. As models include relevant processes at smaller scales, the computational burden will naturally increase; however, machine learning techniques can serve to abstract those computationally expensive processes, effectively substituting a recognized or learned pattern for a more complex algorithm. One drawback to these powerful data-driven approaches is that it is possible to 'over-train' a model with limited data, which effectively reduces its predictive capability for conditions that have yet to be observed. Despite the benefits and drawbacks of these methods, there are still relatively few models that explicitly incorporate them, suggesting there is still much room for model improvement.

Fourth, many models still focus only on parts of the barrier system, without considering all relevant processes. Such scientific focus up to this point was likely necessary to better understand specific system components; however, our current knowledge of important processes should lead to more complex, coupled, and fully representative models. For example, recent models [e.g., 1, 17] have shown the importance of coupling the backbarrier marsh-lagoon system to barrier evolution models; however, there are still relatively few models that incorporate these as coupled systems. Barrier subsidence has received relatively little attention in the literature and has been incorporated into a minority of barrier evolution models [e.g., 201, 202]. Yet, from these few studies, we see that consolidation rates can significantly impact the future evolution of the system. The role of aeolian transport has also largely been neglected in barrier island evolution models. Although a large body of work exists regarding

aeolian transport and its role in dune recovery [e.g., 286], few full-scale barrier evolution models have integrated this research. This may be the case, at least in part, because of the relatively recent focus on modeling storm sequences and post-storm beach and dune recovery [38]. However, as various studies have indicated the importance of these morphological components, modeling efforts would be most beneficial by driving toward the incorporation of all relevant processes.

Finally, anthropogenic influences, such as urban development and its associated infrastructure, have changed and will continue to change the way many of the fundamental processes discussed in this review affect barrier island morphology. This also includes coastal engineering infrastructure, which is often intended to reduce inundation and erosion, or to support recreational and commercial navigation. Thus, modeling paradigms shifted toward representing barrier islands as coupled human-natural systems would provide important insights [281]. Modeling frameworks that included anthropogenic impacts such as the effects of human agents [e.g., 278], urban development [e.g., 280], and coastal restoration practices [e.g., 253], would help us explore and evaluate their impacts which would be useful in coastal planning.

2.4.4 Summary

In closing, future research and development in the area of morphodynamic modeling of coastal barrier systems would benefit by leveraging existing and new datasets, advancements in observation technologies, and emerging data science approaches to better characterize morphological response and its uncertainty. Continuing the research community shift toward open access models and data would facilitate more rapid advancement in this area. Scientific advances are most needed in understanding anthropogenic and ecological influ-

ences on barrier morphological change. Also essential is advancing scientific understanding of observed morphological phenomena and the underlying sediment transport processes, including the coupling between a barrier and its sub-systems. Such advancements will bring us closer to achieving the overarching goal of high-confidence predictions of barrier system morphodynamics in multiple spatiotemporal dimensions.

2.5 Data Availability Statement

No data, models, or code were generated or used during the study.

2.6 Acknowledgements and Disclaimers

This material is based upon work that is primarily supported by the U.S. Army Corps of Engineers through the U.S. Coastal Research Program (under Grant No. W912HZ-20-2-0005) and partially supported by the National Science Foundation (under Grant Number 1735139). Any opinions, findings, and conclusions or recommendations expressed in this material are those of the authors and do not necessarily reflect the views of these organizations. This publication was also prepared in part by Steven Hoagland using Federal funds under award NA18OAR4170083, Virginia Sea Grant College Program Project R/72155T, from the National Oceanic and Atmospheric Administration's (NOAA) National Sea Grant College Program, U.S. Department of Commerce. The statements, findings, conclusions, and recommendations are those of the author(s) and do not necessarily reflect the views of Virginia Sea Grant, NOAA, or the U.S. Department of Commerce.

Disclaimer for non-endorsement of commercial products and services: Any use of trade, firm, or product names is for descriptive purposes only and does not imply endorsement

by the U.S. Government.

Chapter 3

Morphodynamic and Modeling Insights from Global Sensitivity Analysis of a Barrier Island Evolution Model

Steven W.H. Hoagland[1], Jennifer L. Irish[1], Robert Weiss[2,3]

[1]Department of Civil and Environmental Engineering, Virginia Tech, Blacksburg, VA

[2]Department of Geosciences, Virginia Tech, Blacksburg, VA

[3]Academy of Integrated Science, Virginia Tech, Blacksburg, VA

Abstract

Recently developed models of coastal barrier morphodynamics include marsh and lagoon processes that have been shown to impact barrier island evolution. To gain additional insights into the simulated barrier-backbarrier system dynamics, this study explores the parameter space of a barrier evolution model using global sensitivity analysis. Influential parameters, their interactions with one another, and regions of sensitivity within the parameter space were identified using Sobol indices and factor mapping techniques for model results through the end of the century. The results of this study highlight an important relationship between initial and critical barrier island geometries and suggest that narrow and low-relief barriers are most vulnerable to be eroded away (width drowning) or overtaken by sea level rise (height drowning), respectively. Width drowning was also strongly associated with other model input parameters such as toe depth, sea level rise rate, and backbarrier critical bed shear stress, which suggests that sub-centennial drowning is dependent on a unique combination of input parameter values and may be averted (or delayed) with a single input parameter change. Barrier dynamics were significantly influenced by the backbarrier marsh platform, which was more impacted by sediment transport parameters such as critical bed shear stress and ocean sediment concentration than maximum annual overwash flux. This suggests that inorganic sediment deposition through tidal inlet dispersion is much more significant to the backbarrier marsh and lagoon system than overwash over sub-centennial timescales and can help to reduce the risk of width drowning.

3.1 Introduction

Barrier islands front an estimated 10% of the world's coastlines [7] and provide a variety of socioeconomic benefits such as flood risk reduction [9], recreation and tourism [12]. One of the most interesting features of barrier islands is that they are dynamic landforms; they change both shape and location in response to storm events and chronic changes in their environment such as sea level rise (SLR) and changes in sediment supply [e.g., 14, 15, 287]. Understanding the processes that drive the evolution of coastal barriers over decades or centuries and accurate prediction of future island states through modeling are two active and interdependent fields of research, both of which are necessary to effectively manage coastal resources.

In the 1980s and 90s, coastal evolution models of various type and formulation began to appear more frequently in the scientific literature [288]. These early models ranged in complexity from one-line models of shoreline change [e.g., 16, 289], to simplified 1D translation models [e.g., 169, 190, 191, 194], to two-dimensional and quasi-two-dimensional approaches [e.g., 188, 189, 193, 195, 196]. Models also varied in their application, some applied to barrier island systems specifically [e.g., 190, 194] and others to shorelines more generally [e.g., 169, 189, 195, 289]. In recent decades, new models have continued to be developed, many of which improve existing formulations and include processes that were not previously captured such as changes in alongshore sediment supply via inlet dynamics [e.g., 197, 200, 205, 209], overwash [e.g., 19, 171, 179, 199, 207], dune growth and erosion [e.g., 202, 212, 215, 217, 219], and substrate consolidation by barrier migration [201, 202].

Sediment transport processes in the backbarrier marsh and lagoon system have also been included in barrier island models of the last two decades. Two notable models that include marsh-lagoon constituents are GEOMBEST+ [17] and the Lorenzo-Trueba and Mariotti

(hereafter 'LTM17') model [1]. These models attempt to capture the inherent complexity in the naturally-coupled barrier and backbarrier systems. The use of these models to explore the coupled system behavior across a variety of scenarios has yielded additional insights into long-term barrier dynamics. For example, Walters et al. [17] found that narrow backbarrier marshes were sustained by barrier island overwash, which slowed the rate of barrier island transgression with sea level rise (SLR). Lorenzo-Trueba and Mariotti [1] arrived at the same conclusion from their modeling study, finding that transgression rates were reduced by the presence of backbarrier marsh, which was impacted by overwash rates, inorganic sediment contributions, and lagoon geometry.

The numerical experiments conducted by Walters et al. [17] and Lorenzo-Trueba and Mariotti [1] were de facto sensitivity analyses in that they measured model output variability in response to changes in model input parameters. These studies also focused on long-term behavior over a 1,000-year simulation time period. While the sensitivity analyses by Walters et al. [17] and Lorenzo-Trueba and Mariotti [1] yielded important insights, we hypothesize that a more thorough exploration of the parameter spaces over a shorter simulation time period may yield additional findings.

To gain additional insights into the simulated barrier-backbarrier system dynamics, our study simulates barrier evolution using the LTM17 model through year 2100, which may be in view at the end of some long-term planning horizons, and explores the model's input parameter space using global sensitivity analysis, which is a tool that can help modelers better understand the impact of their model's input parameters. Twenty of the LTM17 model's input parameters were evaluated in this study. These parameters are related to initial and equilibrium system geometries, external forcing conditions, and inorganic sediment transport, erosion, and deposition. More specifically, this study will focus on answering the following questions:

1. Which parameters significantly influence the model results?

2. Are there significant parameter interactions that influence the model results?

3. Are there regions of higher or lower sensitivity within the parameter space?

A variety of simulations and calculations were performed to address these questions. Input parameter sensitivities were characterized by estimating their contribution to the total model variance using the Sobol method [20]. Factor mapping was also used to explore the association of input parameter values with distinctive simulation categories (e.g., drowning) and regions within the parameter space. This analysis may be used to inform future modeling efforts in terms of understanding which parameters are most important to constrain, which parameters are relatively unimportant and can be fixed at a particular value, and which parameters should always be included as part of uncertainty analysis.

3.2 Lorenzo-Trueba and Mariotti (2017) Model

The LTM17 model was created as a coupled reformulation of two previously published standalone models, namely the Lorenzo-Trueba and Ashton model [19, hereafter 'LTA14'] and the Mariotti and Carr model [18, hereafter 'MAC14']. The LTA14 model focuses on projecting changes in the barrier island itself, while the MAC14 model simulates changes in the backbarrier marsh and lagoon system. For a full description of the LTM17 model, the reader is referred to Lorenzo-Trueba and Mariotti [1] and references therein.

The LTM17 model simulates long-term changes in both the barrier island and backbarrier (marsh and lagoon) subsystems. These subsystems are delineated in the model by six horizontal state variables: the toe position (X_T), shoreface position (X_S), backbarrier position (X_B), backbarrier marsh position (X_{M1}), interior marsh position (X_{M2}), and the main-

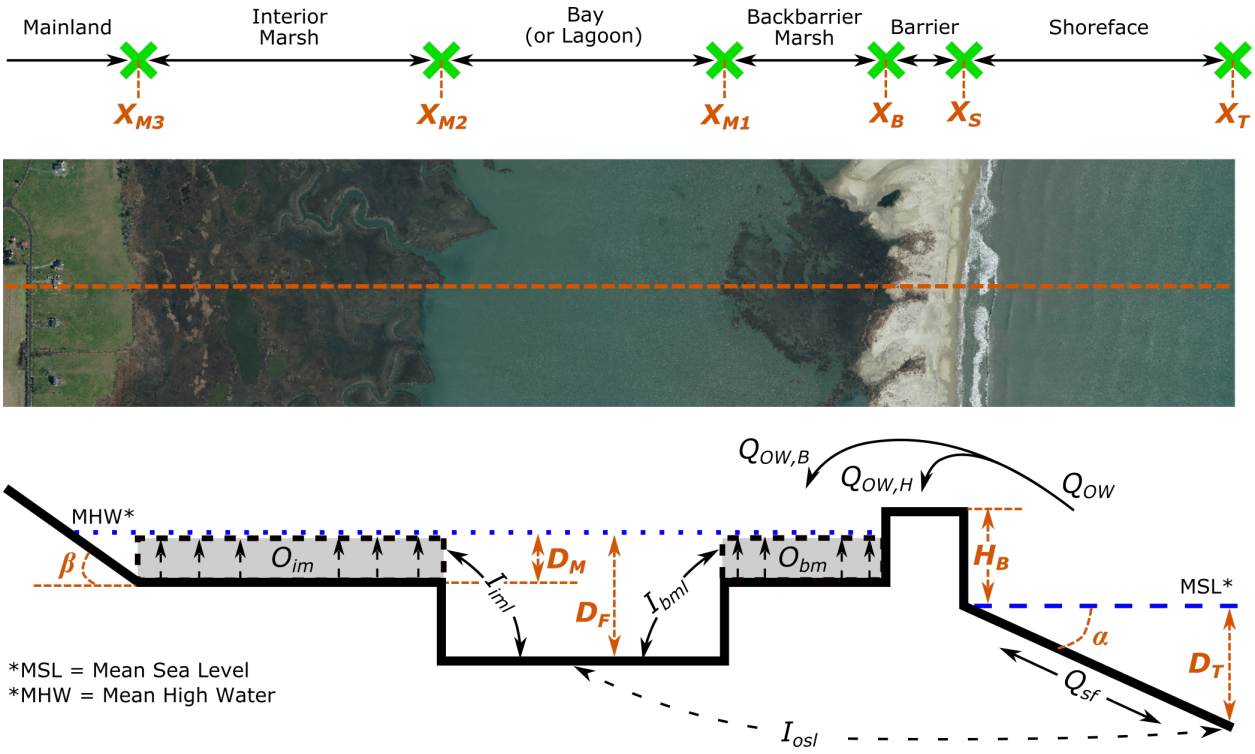

Figure 3.1: Idealized Barrier Profile from *LTM17 Model*. *Figure modified from Lorenzo-Trueba and Mariotti [1]. Aerial image of Assawoman Island section from [5].*

land position (X_{M3}). Four vertical state variables, which include the barrier height (H_B), lagoon depth (D_F), and marsh depths (D_{M1}, D_{M2}), are also used to define the system geometry. Figure 3.1 provides a graphical representation of the barrier subsystems and state variables. Together, simulated changes in these ten state variables are tracked over time through equilibrium-based sediment flux calculations, also shown in Figure 3.1, including shoreface sediment flux (Q_{SF}), overwash flux (Q_{OW}), sediment flux between the shoreface and lagoon (I_{osl}), sediment flux between the lagoon and marshes (I_{bml} and I_{iml}), and biomass production within the marsh platforms (O_{bm} and O_{im}).

Shoreface sediment flux is calculated using the equilibrium profile assumption of Swart [290], who found cross-shore sediment transport on the shoreface to be proportional to its deviation from an estimated equilibrium profile. Overwash flux is driven by the barrier's deficit volume,

which is the volume of sediment required to extend the barrier's height (H_B) to a critical value (H_{cr}) such that overwash could no longer be deposited on the island, plus the volume of sediment required to extend the barrier's width (W_B) to a critical value (W_{cr}) such that overwash could no longer be deposited in the backbarrier system [19]. This idea of a barrier height or width that prevents overwash deposition originated as the 'Critical Length Concept' from Leatherman [114]. The volume deficit indicates the amount of sediment a barrier is able to accommodate before reaching its critical width and height; hence, the volume deficit is also commonly described as 'accommodation space' in the literature. Sediment is exchanged between the shoreface, lagoon, and marshes through tidal dispersion based on the relative concentration of sediments in each zone. Organic creation of marsh sediment and inorganic deposition of sediment in the marshes offset the loss of marsh elevation due to sea level rise and marsh erosion by backbarrier waves.

A number of 'result variables' may be calculated from the state variables shown in Figure 3.1. For example, change in shoreline position (ΔX_S) is a result variable that may be calculated by subtracting the initial shoreline position (X_{S_0}) from the final shoreline position (X_{S_f}). Change in barrier width (ΔW_B) is another result variable that is calculated by subtracting the initial difference between the barrier and shoreline positions ($X_{B_0} - X_{S_0}$) and the final difference between the barrier and shoreline positions ($X_{B_f} - X_{S_f}$). The result variables considered in this study are presented in Table 3.1 with their state variable calculations and associated units. Note that many of the result variables involve calculations between the values at the beginning and end of the simulation to account for variations in the initial system geometry.

The LTM17 model has multiple strengths. One notable strength is its inclusion of marsh-lagoon processes, which relatively few barrier evolution models account for explicitly [288] and which have been shown to significantly impact barrier island evolution dynamics [e.g.,

Table 3.1: LTM17 Model Result Variables

Result Variable	Symbol	Calculation	Units
Change in Shoreline Position	ΔX_S	$(X_{S_f} - X_{S_0})^\dagger$	[m]
Change in Barrier Width	ΔW_B	$(X_{B_f} - X_{S_f}) - (X_{B_0} - X_{S_0})$	[m]
Change in Barrier Height	ΔH_B	$(H_{B_f} - H_{B_0})$	[m]
Change in Backbarrier Marsh Width	ΔB_{M1}	$(X_{M1_f} - X_{B_f}) - (X_{M1_0} - X_{B_0})$	[m]
Change in Lagoon Width	ΔB_F	$(X_{M2_f} - X_{M1_f}) - (X_{M2_0} - X_{M1_0})$	[m]
Marsh Depth	D_M	(D_{M1_f})	[m]
Lagoon Depth	D_F	(D_{F_f})	[m]
Interior Marsh Width	B_{M2}	$(X_{M3_f} - X_{M2_f})$	[m]

†The f and 0 subscripts denote final and initial positions, respectively.

1, 17]. Another strength of the model is its simplicity, from its transect-based setup to its straightforward state equations and Eulerian solution scheme. This simplicity leads to a relatively fast model runtime and gives the model a computational advantage over other, more complex models. This computational advantage allows modelers to evaluate parameter sensitivities toward a more robust understanding of the model and system dynamics, and to perform uncertainty analysis, which accounts for knowledge gaps and inherent parameter randomness in the final model projections.

However, these modeling advantages also come with certain assumptions and limitations which must be considered when interpreting the results. For example, model transects have a perfectly linear shoreface slope and rectangular representations of the subaerial island, marshes, and lagoon. This idealized transect geometry, combined with the equilibrium-based approach to sediment flux calculations, streamlines the model computations but can also lead to some oversimplifications. For example, the linearized shoreface slope is assumed to respond to deviations from the equilibrium value at a single rate, whereas in reality, we would expect the lower shoreface to respond more slowly than the upper shoreface [53, 291, 292]. Another limitation stems from the absence of modeled dunes. The relationship between the water level and dune elevation is typically used to define the storm regime [e.g., 47]

which then has a direct impact on the barrier morphology [e.g., 293, 294]. Additionally, washover is assumed to be deposited uniformly across the rectangular island and backbarrier marsh platform, whereas in reality, washover deposits become increasingly shallow toward the mainland [295].

3.2.1 Distinctive Simulation Categories

As the coupled barrier-backbarrier system evolves in the LTM17 model, there are four types of distinctive simulation categories in which the barrier system undergoes such a substantive change that the simulated processes that drive evolution of the system are no longer applicable. In such simulations the computations are either halted with results at the current timestep taken to be the final results, or significant geometry modifications are introduced. Simulations that do not fall into one of the distinctive categories described above are referred to as 'Normal' simulations, since they experience neither drowning nor lagoon infilling.

The first two distinctive simulation categories are those that result in barrier width drowning, referring to the condition in which the barrier island width reaches zero before the year 2100, and those that result in barrier height drowning for which the barrier height reaches zero before year 2100. The third type of distinctive simulation occurs when the marsh depth exceeds the maximum depth for marsh growth, which is referred to as marsh drowning. The fourth type of distinctive category is lagoon infilling, which occurs when the lagoon depth becomes equal to the marsh depth due to sediment deposition in the lagoon. In this type of simulation, the model's computations are not halted, but the marsh geometries are modified by setting the backbarrier marsh position (X_{M1}) equal to the barrier position (X_B) and the interior marsh position (X_{M2}) equal to the intersection position of interior marsh and the mainland (X_{M3}). This effectively eliminates the marsh widths when the lagoon fills and

should be considered in the interpretation of the results.

3.2.2 Previous Sensitivity Studies

The findings of previous sensitivity studies are briefly highlighted below for comparison with the results of this study. At least four studies have been published that explore the sensitivity of the LTM17 model or its predecessor, the LTA14 model. The four studies were performed by Lorenzo-Trueba and Ashton [19], Ashton and Lorenzo-Trueba [208], Lorenzo-Trueba and Mariotti [1], and Ashton and Lorenzo-Trueba [296].

In the first study of the LTA14 model, Lorenzo-Trueba and Ashton [19] explored how interactions between key parameters such as maximum annual overwash flux ($Q_{OW,*}$), shoreface flux constant (K), SLR rate ($\dot{z}$), and mainland slope (β) influenced long-term behavior patterns. The authors found barrier systems to behave in one of four ways: 1) dynamic equilibrium, 2) periodic retreat, 3) barrier height drowning, and 4) barrier width drowning. Since their study was focused on long-term system behavior out to 1,000 years, the authors evaluated how changes to input parameters affected the model's proclivity toward one of these four behaviors. Thus, parameters that did not impact the long-term oscillatory behavior pattern were considered insensitive.

In the second study, Ashton and Lorenzo-Trueba [208] coupled the longshore model of Ashton and Murray [199] with the LTA14 model to study the effects of sea level rise and longshore coupling over 400 years of barrier evolution. Using an initial shoreline disturbance of decreased width as the catalyst for system change, the authors found that increased sea level rise rates exacerbated the alongshore differences between adjacent island cross-sections. However, they also found that a stronger coupling between adjacent cross-sections could dampen these differences and had a significant impact on producing a smoothed, more uni-

form shoreline.

In the third study, Lorenzo-Trueba and Mariotti [1] explored how larger initial lagoon widths (B_F), smaller ocean sediment concentrations (C_o), and smaller mainland slopes (β) affected system dynamics over 1000 years. They found that each of these parameters increased the accommodation space (either directly or indirectly) and lead to increased likelihood of width drowning.

In the fourth and most recent study, Ashton and Lorenzo-Trueba [296] evaluated the impact of a changing mainland slope, and found that changes to the backbarrier slope directly impacted the accommodation space and associated behavior, similar to previous studies. Results from each of these studies are summarized in Table 3.2.

A common theme across the previous sensitivity analysis studies is a focus on millennial-scale, system-level behavior patterns. While these results shed light on system feedbacks, they do not explicitly consider system sensitivities over the short-term planning horizon, which may be given higher consideration in coastal management decisions. These studies also do not explore the full range of input parameter combinations and thus may not identify all relevant parameter interactions.

3.3 Methodology

For this study, the Sobol method, developed in 1993 by Russian mathematician Ilya M. Sobol [20], was selected due to its widely recognized robustness as a global sensitivity analysis method and its ability to identify parameter interactions. As of 2016, this method was considered to be one of the "most sophisticated [sensitivity analysis] approach[es] developed to-date" [24].

Table 3.2: Results from Previous Sensitivity Studies.

Study*	Parameter**	Impact
LTA14	$\dot{z}(+)$	Increased width drowning; reduced by higher K and Q_{ow}.
LTA14	$K(+)$	Reduced width drowning; increased migration.
LTA14	$Q_{ow}(+)$	Reduced width drowning;*** increased migration.
LTA14	$\beta(-)$	Increased width drowning and decreased migration.
LTA14†	$W_0(+/-)$	Insignificant impact on long-term behavior.
LTA14†	$V_{D,MAX}(+)$	Increased dynamic equilibrium; decreased periodic retreat.
LTA14†	$D_T(+)$	Requires increased Q_{ow} and K to maintain equilibrium.
LTA14†	$W_{cr}(-)$	Increased width drowning.
ALT15	$\dot{z}(+)$	Increased and sustained change between cross-sections.
ALT15	$d_{sh}(-)$††	Increased and sustained change between cross-sections.
LTM17	$B_{F,0}(+)$	Increased marsh erosion and width drowning.
LTM17	$C_0(-)$	Increased width drowning; decreased migration.
LTM17	$\beta(-)$	Increased lagoon depth and width drowning.
ALT18	$d\beta/dx(+)$	Decreased accommodation space; increased migration.
ALT18	$d\beta/dx(-)$	Increased accommodation space and width drowning.

*LTA14: Lorenzo-Trueba and Ashton (2104); ALT15: Ashton and Lorenzo-Trueba (2015); LTM17: Lorenzo-Trueba and Mariotti (2017); ALT18: Ashton and Lorenzo-Trueba (2018)

**Signs following the parameter should be read as an increase or decrease in that parameter leading to the associated impact. E.g., '$\dot{z}(+)$' should be read, 'An increase in $\dot{z}$ leads to... [associated impact].'

***Exception: high Q_{ow} can diminish shoreface sediment and lead to drowning.

†Published in Lorenzo-Trueba and Ashton [19] supporting information.

††Shoreline diffusivity constant (proxy for alongshore coupling).

3.3.1 Sobol Method Overview

The Sobol method involves calculating sensitivity indices for each input parameter that quantifies the percentage of model variance accounted for by that input parameter individually and interactively. Higher index values are associated with more sensitive parameters. In this study, three types of Sobol indices are calculated: (1) first order indices, (2) k-th-order indices, where k is the total number of input parameters being evaluated, and (3) interaction indices.

The first order index for a given input parameter, also commonly referred to as a parameter's 'main effect,' is defined as the variance of the conditional mean associated with fixing said parameter at a given value, divided by the total variance. Mathematically, the first order index (S_i) is as follows:

$$S_i = \frac{V(E(Y|X_i))}{V(Y)} \tag{3.1}$$

where $V(E(Y|X_i))$ is the variance of the expected value, or mean, of the model output (assuming sufficiently many model simulations for stability) given that parameter X_i is fixed at a randomly sampled value in its range, and $V(Y)$ is the total model variance. This calculation produces S_i values between 0 and 1, with higher S_i values indicating greater sensitivity. Because the index calculation involves expected values (means) and variances, the index values will become increasingly stable as more simulations are performed. Conversely, too few simulations increase the likelihood of numerical error in the results.

In many models, input variables often interact with one another so as to amplify or dampen their impact on the results. The Sobol method's k-th order index, more commonly called the 'total effect,' captures a parameter's main effect and all other higher-order or interactive

effects. Mathematically, the calculation is represented by:

$$S_{T_i} = 1 - \frac{V(E(Y|X_{\sim i}))}{V(Y)} \tag{3.2}$$

where $E(Y|X_{\sim i})$ is the conditional mean of the model output associated with fixing the value of all parameters *except* for X_i.

The k-th order Sobol index provides a couple of important insights. First, if the k-th order index is zero or near zero, then it may be concluded that the factor does not significantly contribute to the total model variance and can therefore be fixed at any value in its range. Second, by subtracting the first order index from the k-th order index, the impact of the parameters' interactions is isolated - this metric is referred to herein as an 'interaction index.' Therefore, if there is a significant difference between the first and k-th order indices for a given parameter (i.e., if its interaction index is large), that particular parameter, it may be concluded, significantly contributes to the results through one or more interactions.

3.3.2 Model Parameterization

Twenty input parameters were selected for evaluation in this sensitivity study. Since the Sobol Method requires numerous model simulations and randomly sampled input parameter values, each input parameter was assigned a value range that defined the upper and lower limits of the sampling range. Parameter ranges were selected for this study based on typical ranges or values that have been justified and used in previous studies including Lorenzo-Trueba and Ashton [19], Mariotti and Carr [18], Lorenzo-Trueba and Mariotti [1], and Miselis and Lorenzo-Trueba [297]. A comparison of this study's parameter ranges to those of previous studies is presented in Table B1.1 of the Supplementary Material. The 20 input parameters

Table 3.3: LTM17 Model Input Parameters

Symbol	Input Parameter	Value Range	Units	Category†
β	Mainland Slope	$0.0001 - 0.005$	[m/m]	Geometry
D_T	Toe Depth	$5 - 15$	[m]	Geometry
W_{cr}	Critical Width	$100 - 600$	[m]	Geometry
H_{cr}	Critical Height	$0.5 - 4$	[m]	Geometry
W_0	Initial Width	$100 - 1,000$	[m]	Geometry
H_0	Initial Height	$0.5 - 4$	[m]	Geometry
α_e	Equilibrium Shoreface Slope	$0.005 - 0.025$	[m/m]	Geometry
$B_{M1,cr}$	Critical Backbarrier Marsh Width	$50 - 500$	[m]	Geometry
$B_{M1,0}$	Initial Backbarrier Marsh Width	$50 - 1,000$	[m]	Geometry
$B_{F,0}$	Initial Lagoon Width	$1,000 - 10,000$	[m]	Geometry
$D_{F,0}$	Initial Lagoon Depth	$1 - 3$	[m]	Geometry
$Q_{OW,*}$	Max. Annual Overwash Flux	$1 - 100$	[m^3/m/yr]	Forcing
$\dot{z}$	Sea Level Rise Rate	$3 - 20$	[mm/yr]	Forcing
K	Shoreface Flux Const.	$100 - 10,000$	[m^3/m/yr]	Forcing
U_{ref}	Reference Wind Speed	$5 - 10$	[m/s]	Forcing
r	Tidal Range	$0.7 - 2.8$	[m]	Forcing
ω_s	Sediment Settling Velocity	$0.05 - 0.5$	[mm/s]	Sediment
τ_{cr}	Critical Bed Shear Stress	$0.05 - 0.4$	[Pa]	Sediment
C_o	Ocean Sediment Conc.	$30 - 200$	[mg/l]	Sediment
B_P	Peak Biomass Production	$1.5 - 3.5$	[kg/m^2]	Sediment

†The categories indicate the general nature of the input parameter; some alter the system geometry, others the forcing conditions, and some the sediment transport.

are presented in Table 3.3 with their value range and units. Each parameter was also broadly categorized as influencing the system geometry, forcing conditions, or sediment transport calculations. Initial geometries of the system were also randomized for this sensitivity study to determine the influence of a system's current state on its long-term evolution; some of these initial geometries were also later constrained to evaluate their impact (see Section 3.3.3). The sensitivity of the 20 input parameters was evaluated for each result variable in Table 3.1.

3.3.3 Simulation Sets

Three sets of simulations were performed to answer the proposed research questions. For all of the simulations described below, randomized input parameter values were sampled from a uniform distribution across their value range.

To gain a preliminary understanding of model behavior, we ran 50,000 simulations with fully randomized input parameter values and used factor mapping to associate the parameter values with the distinctive simulation categories described in Section 3.2.1. These simulations required approximately 3.59 CPU-hours and are hereafter referred to as Simulation Set A. Since initial barrier geometries and critical bed shear stress were found to significantly impact the model results toward drowning and lagoon filling (see Section 3.4.1), the geometry parameters were fixed at their average range values and the shear stress parameter was constrained (maximum 0.2 Pa) for the other simulations.

To calculate numerically stable first order and k-th order Sobol indices for input parameters (Table 3.3) and result variables (Table 3.1), 250,000 model simulations were run per input parameter. A total of 5 million simulations were run for conditional variance calculations which required 346 CPU-hours. These simulations are hereafter referred to as Simulation Set B. Input parameter values were randomly generated and index values were calculated following the matrix resampling procedure described in Saltelli et al. [23].

To explore specific parameter interactions and regions of sensitivity within the parameter space, we again ran 50,000 simulations with fully randomized input parameters. This set of simulations required approximately 3.59 CPU-hours and is hereafter referred to as Simulation Set C.

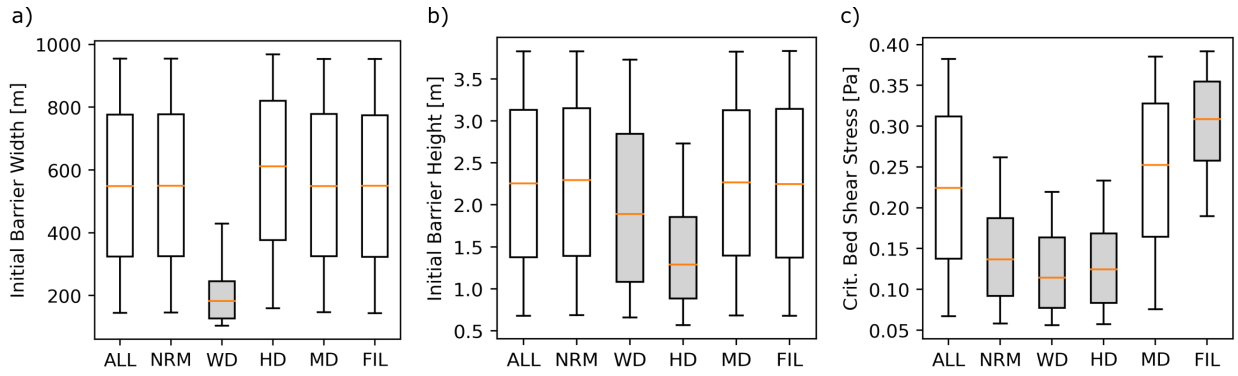

Figure 3.2: Distinctive Simulation Category Boxplots for Simulation Set A by Input Parameter for (a) Initial Barrier Width, (b) Initial Barrier Height, and (c) Critical Bed Shear Stress. *Input parameters are shown on the y-axes. Each boxplot represents the 5^{th}, 25^{th}, 50^{th}, 75^{th}, and 95^{th} percentiles, from bottom to top. Distinctive simulation categories are represented on the x-axes: ALL = all simulations/scenarios; NRM = normal (no drowning/filling); WD = width drowning; HD = height drowning; MD = marsh drowning; FIL = lagoon filling.*

3.4 Results

3.4.1 Preliminary Results

Select results from Simulation Set A are presented in the boxplots in Figure 3.2 (see Figures B2.1 through B2.4 in the Supplementary Material for all results). Comparing these boxplots to one another allows us to see whether an input parameter significantly influences the model toward a drowning and/or filling scenario, which should be taken into consideration in the interpretation of results. Statistically significant differences between each category's median value and the ALL category median value were identified by non-overlapping 95% confidence intervals and are indicated by gray-colored boxplots. Confidence intervals are provided in the Supplementary Material in Tables B2.1-B2.4 and B4.1-B4.3.

The initial and critical barrier geometry parameters (W_0, H_0, W_{cr}, H_{cr}) were found to be most influential on the barrier results. Low values of initial barrier width were strongly associated with width drowning simulations (Fig. 3.2a) while low values of initial barrier height were

strongly associated with height drowning simulations (Fig. 3.2b). Significant interaction indices and heatmap plots of the preliminary results confirm that a significant interaction is present between the initial geometries and critical geometries (see Figure B3.1 in the Supplementary Material). The barrier geometry tends to increase when critical geometry is greater than initial geometry, and the barrier geometry decreases when critical geometry is less than initial geometry.

Preliminary results also show that critical bed shear stress (τ_{cr}) significantly influences the simulation toward lagoon filling and/or drowning, as noted by the statistically significant difference between the ALL and NRM medians in Figure 3.2c. Since the WD and HD boxplots greatly overlap NRM but the FIL boxplot does not, it may be concluded that high τ_{cr} values drive the model toward lagoon filling.

In addition to showing general tendencies or associations, the boxplots in Figure 3.2 also show parameter thresholds. For example, the results suggest that barrier drowning does not typically occur when initial barrier width is above 400 m. Similarly, height drowning does not occur when initial barrier heights are above 3 m, and lagoon filling does not occur when the critical bed shear stress is below 0.2 Pa.

3.4.2 Influential Parameters

From Simulation Set B, the first and k-th order Sobol indices were calculated for each combination of input parameter (Table 3.3) and result variable (Table 3.1). These results are presented graphically in Figure 3.3.

From Figure 3.3a, it may be observed that most input parameters tended to impact a subset of result variables, the exception being SLR rate ($\dot{z}$), which influenced a majority of the results. However, in Figure 3.3b, parameters were more influential over many different result

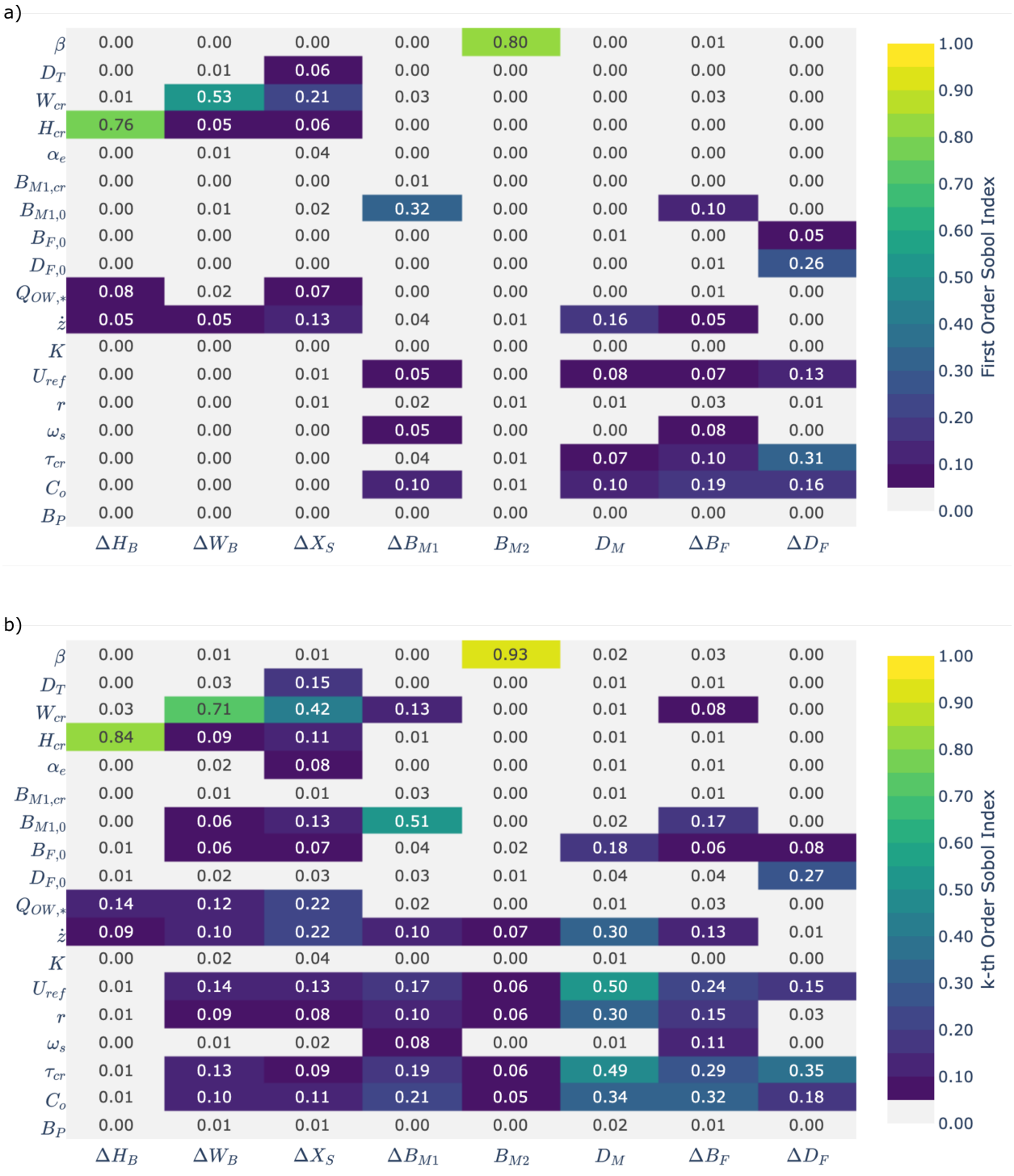

Figure 3.3: Heatmaps of (a) First Order Indices and (b) k-th Order Indices from Simulation Set B. *Result variables are shown on the x-axes according to their symbols, and input parameters are shown on the y-axes according to their symbols.*

variables. In addition to SLR rate ($\dot{z}$), reference wind speed (U_{ref}), tidal range (r), critical bed shear stress (τ_{cr}), and the ocean sediment concentration (C_o) all show at least moderate influence for most result variables. Other parameters such as the shoreface equilibrium slope (α_e), critical backbarrier marsh width ($B_{M1,cr}$), shoreface flux constant (K), sediment settling velocity (ω_s), and peak biomass production (B_P) had zero (or near-zero) Sobol indices for many of the results, suggesting these parameters were relatively non-influential.

Similar to the preliminary results, critical barrier geometries (W_{cr} and H_{cr}) were highly significant for the barrier results. Changes in barrier width and shoreline position were also influenced by the barrier toe depth (D_T). Forcing conditions such as maximum annual overwash flux ($Q_{OW,*}$) and SLR rate ($\dot{z}$) influenced the barrier results individually, while other forcing parameters such as wind speed (U_{ref}) and tidal range (r), and sediment transport parameters such as critical bed shear stress (τ_{cr}) and ocean sediment concentration (C_o), showed low to moderate influence on the barrier results through interactions. The backbarrier results were also consistently influenced by the same forcing conditions and sediment transport parameters. Backbarrier geometry parameters tended to influence one or two related result variables. Mainland slope (β) influenced interior marsh and lagoon widths; the initial backbarrier marsh width ($B_{M1,0}$) influenced the backbarrier marsh and lagoon widths; and the lagoon results were influenced by the initial lagoon width ($B_{F,0}$) and initial lagoon depth ($D_{F,0}$).

The influence of parameters may also be seen in their association with distinctive simulation categories from Section 3.2.1. Boxplots were generated for each input parameter from the 50,000 fully randomized simulations in Simulation Set C. Select results are presented in Figure 3.4 (see Figure B4.1 in the Supplementary Material for all results). Of the 50,000 total simulations, 0.3% resulted in width drowning, 3.2% resulted in marsh drowning, and 4.0% resulted in lagoon filling. There were no height drowning simulations in Simulation Set

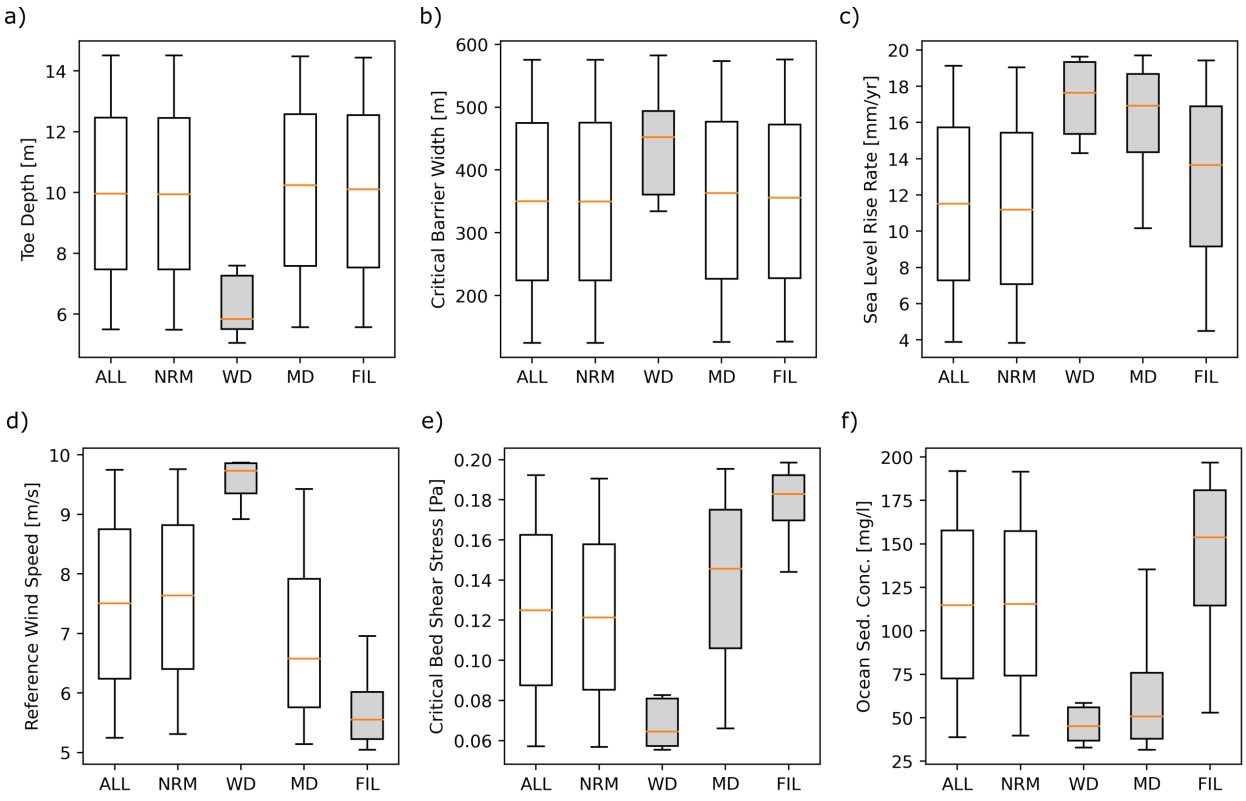

Figure 3.4: Distinctive Simulation Category Boxplots for Simulation Set C by Input Parameter for (a) Toe Depth, (b) Critical Barrier Width, (C) Sea Level Rise Rate, (d) Reference Wind Speed, (e) Critical Bed Shear Stress, and (f) Ocean Sediment Concentration. *Input parameters are shown on the y-axes. Each boxplot represents the 5^{th}, 25^{th}, 50^{th}, 75^{th}, and 95^{th} percentiles, from bottom to top. Distinctive simulation categories are represented on the x-axes: ALL = all simulations/scenarios; NRM = normal (no drowning/filling); WD = width drowning; MD = marsh drowning; FIL = lagoon filling. There were no height drowning simulations in this simulation set.*

C. These drowning scenario numbers exclude cases where lagoon filling lead to drowning. Of the lagoon filling scenarios, 6.0% ended in width drowning and 66% ended in marsh drowning. Thus, only 28.0% of lagoon filling scenarios did not lead to drowning of the marsh or barrier island.

From Figure 3.4, width drowning simulations are associated with low values of toe depth, critical bed shear stress, and ocean sediment concentration, and high values of critical barrier width, SLR rate, and wind speed. Marsh drowning simulations correspond to high SLR rate

Figure 3.5: Heatmap of Interaction Indices ($S_{Ti} - S_i$) from Simulation Set B.

and low ocean sediment concentration, and lagoon filling is associated with low wind speed, high critical bed shear stress, and high ocean sediment concentration.

3.4.3 Interactions and Sensitive Regions

Interaction indices were calculated for each input parameter and result variable combination from Simulation Set B. These indices, presented in the heatmap in Figure 3.5, show that the most interactive parameters are wind speed (U_{ref}), tidal range (r), critical bed shear stress (τ_{cr}), and ocean sediment concentration (C_o), which have very high index values for marsh depth, and relatively high indices across most other result variables. SLR rate ($\dot{z}$) also has moderately high interaction indices across the result variables. Maximum annual overwash flux ($Q_{OW,*}$) is highly interactive for the barrier results, but is not interactive with the backbarrier. Critical barrier geometries (W_{cr} and H_{cr}) are primarily interactive

with the barrier system, with critical barrier width also impacting the backbarrier marsh width. Initial backbarrier marsh width ($B_{M1,0}$) interactions impact both the marsh width and transgression rates, and initial lagoon width ($B_{F,0}$) interactions impact marsh depth and to a lesser extent, barrier width and transgression.

While the relative interactivity of the input parameters and result variables may be known from the interaction indices, it is not always apparent which parameters interact and to what effect. From Figure 3.5, the most interactive parameters for each result variable were identified and used to generate heatmaps using factor mapping from Simulation Set C in Figures 3.6 and 3.7. In Figure 3.6, it should be noted that for each of the results (e.g., barrier height: panes a-c), each pane shows one of the three combinations; thus, all three panes combined give a glimpse of the 3-dimensional parameter space.

Interactions for the barrier results primarily involve critical/initial geometry parameters and forcing conditions. Larger critical geometries are associated with greater barrier heights and widths and greater changes in shoreline position (Fig. 3.6a,b,d,e,g,h). However, this relationship is offset by lower values of overwash flux, SLR rate, and initial marsh width, and by greater values of toe depth. Overwash flux also interacts with SLR rate, initial marsh width, and toe depth to influence the barrier height, width, and transgression results, respectively.

In the backbarrier, initial marsh width controls the change in marsh width results for large critical barrier widths; however, low critical barrier widths significantly reduce the changes in marsh width (Fig. 3.7a). Interior marsh widths are significantly increased by low mainland slopes and high SLR rates (Fig. 3.7b). Larger values of critical bed shear stress tend to increase marsh depth and lagoon width but only for low values of wind speed (Fig. 3.7c,d). Higher critical bed shear stress is also associated with more significant reductions in lagoon depth, particularly for low initial lagoon widths (Fig. 3.7e).

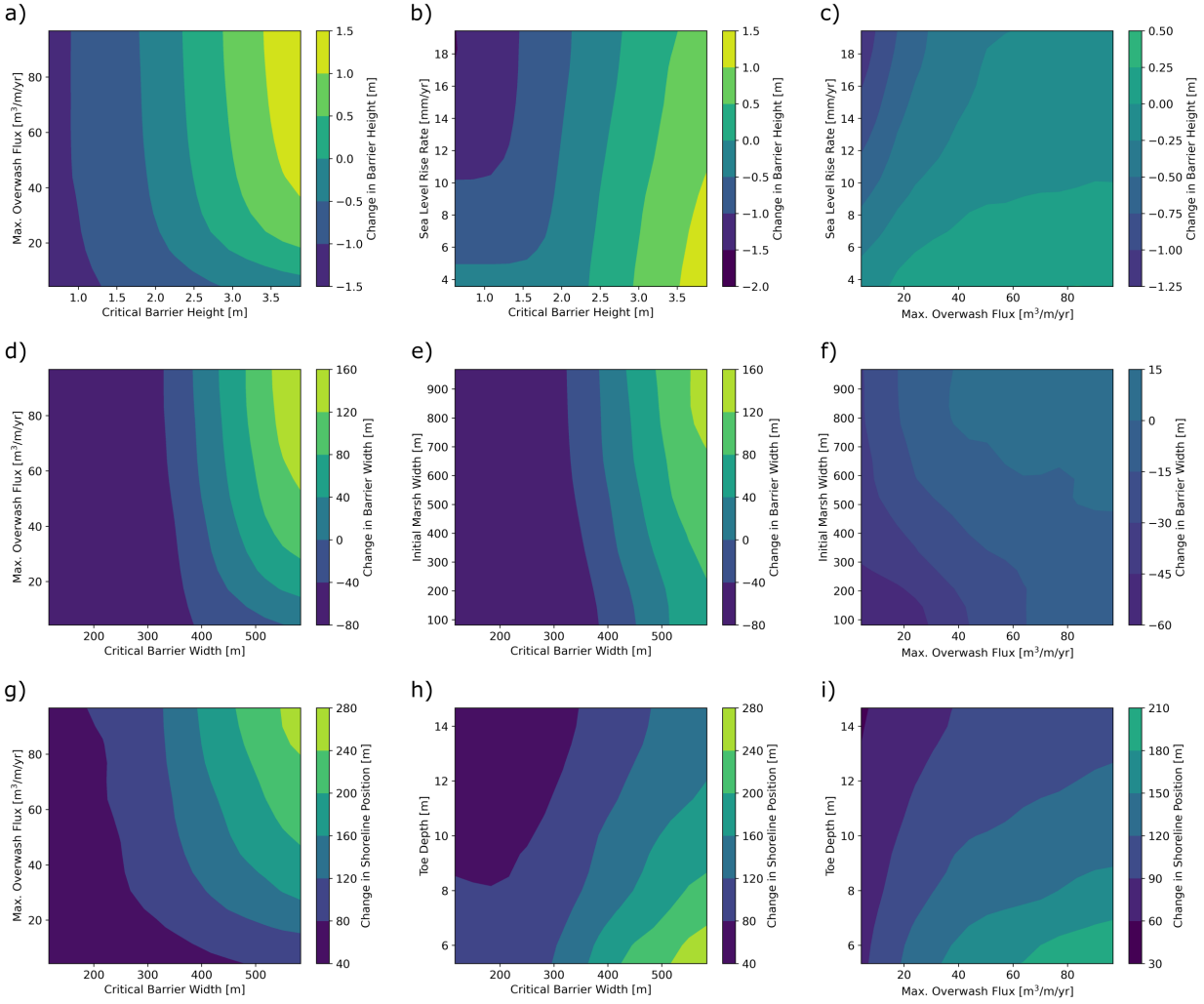

Figure 3.6: Heatmaps of Parameter Interactions for Barrier Results (Simulation Set C).

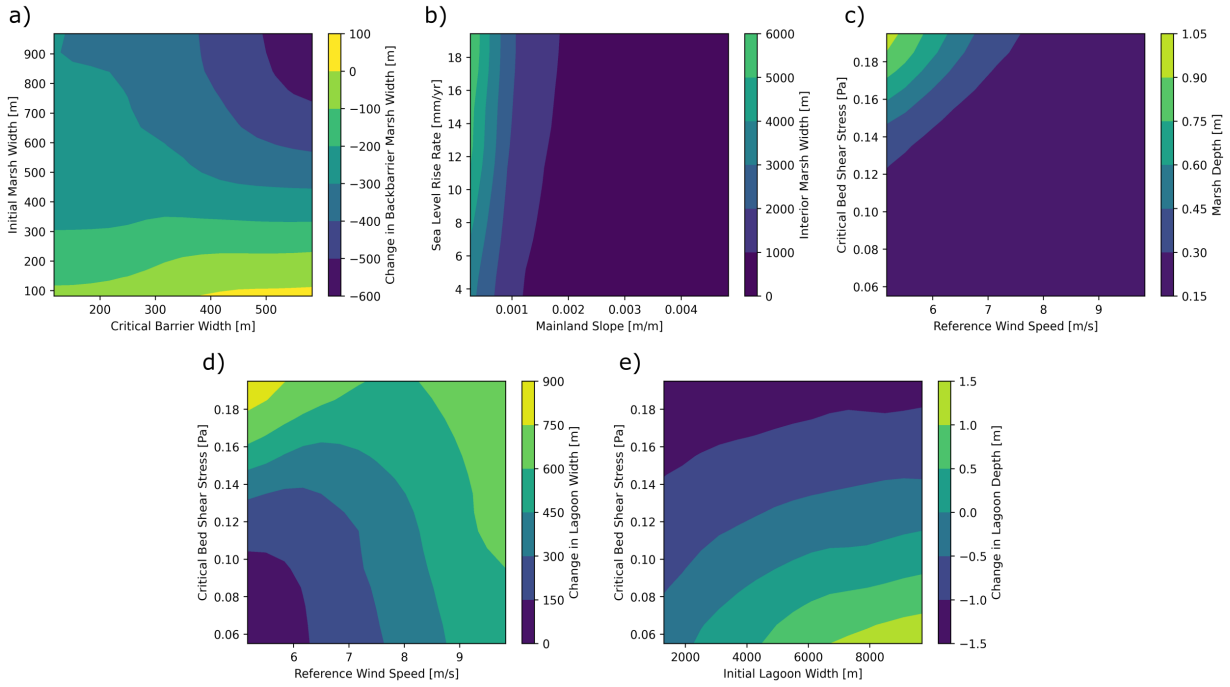

Figure 3.7: Heatmaps of Parameter Interactions for Backbarrier Results (Simulation Set C).

Figures 3.6 and 3.7 also show regions of sensitivity or nonlinearities within the parameter space. For greater critical barrier heights and widths, a significant nonlinearity is observed in the overwash flux parameter between 5 and 10 $m^3/m/yr$ for all of the barrier results. Nonlinearities are also observed for barrier width and transgression results where the critical barrier width nears the initial width. For the backbarrier results, significant nonlinearities are observed for the interior marsh width when mainland slope is lower than 0.001 m/m, and for marsh depth when critical shear stress exceeds 0.15 Pa for lower wind speeds.

3.5 Discussion

Initial and critical island geometry were found to significantly influence the barrier results, both individually and interactively, over the 100-year simulation period. This is because the model was formulated using the critical length concept of Leatherman [114], which acts

as a pseudo-equilibrium formulation that determines where and when overwash flux occurs. The critical length concept was based on Leatherman's observation of a barrier island that narrowed to an observed threshold, or critical width, before experiencing higher rates of transgression, where the overwashed sediment could reach the backbarrier to offset shoreline erosion [114]. This phenomenon was also noted in the subsequent work of Everts [236], who found barrier retreat rates were notably less than preceding rates due to the islands' narrowing states. Robbins et al. [298] have shed additional light on this phenomenon in a more recent study of a U.S. East Coast barrier island chain. Therein, a proposed conceptual model shows eroded sediment from narrowing barriers helps to sustain the width of downdrift neighboring islands, which maintains their low retreat rates. The model results presented herein clearly demonstrate this well-documented behavior, where the change in shoreline position is greatly increased when the initial barrier width is less than or equal to the critical barrier width (Supplementary Material Figure B.3.1c,f), or when the critical barrier width is comparatively large (Fig. 3.6g,h). The interaction plots indicate that critical geometries act as an equilibrium anchoring point to which the system naturally gravitates.

Initial island geometry was also found to have significantly influenced whether or not barriers experienced sub-centennial width drowning or height drowning. From Simulation Set A, barriers that were more than 450 meters wide (the 39th percentile of the barrier width range) rarely experienced width drowning and barriers greater than 3 meters high (the 71st percentile of the barrier height range) rarely experienced height drowning during the multi-decadal simulation period (Fig. 3.2a,b). This expands on and confirms our understanding gained from previous studies, which focused more on the behavioral tendencies of barrier islands toward drowning, periodic retreat, or dynamic equilibrium over centuries. For example, Lorenzo-Trueba and Ashton [19] found that long-term behavior was not significantly influenced by initial geometry parameters as the initial system trajectories would reverse

course toward dynamic equilibrium values over time; however, they did find that width drowning was associated with decreases in critical barrier width. This is likely a result of the phenomenon previously discussed, that a low critical width drives the system toward a sustained low-width equilibrium state that is more likely to drown as ocean-side erosion outpaces backbarrier expansion toward the mainland [e.g., 19, 208].

The results from this study suggest that moving boundaries (i.e., changes in height, width, and shoreline position) of barrier islands through the end of the 21st century will be most significantly influenced by the relationship between the initial and critical geometries and that narrow and low-relief barriers are most vulnerable to width drowning and height drowning, respectively. While barrier drowning is certainly significant, the question remains whether the boundary changes in non-drowning simulations are of any consequence. Wolinsky and Murray [232] concluded that even though initial geometries could influence short term shoreline changes, long-term trends would be independent of such influences and would be controlled primarily by the substrate slope, which was demonstrated in subsequent numerical experiments conducted by Moore et al. [240] and Murray and Moore [299]. For barriers that transgress in a state of periodic retreat, short term changes in barrier geometry could be irrelevant, since the barrier system might shift back toward its dynamic equilibrium state and prograde during the next cycle [19]. However, a more recent modeling study by Ciarletta et al. [300] showed that it is possible for dynamic forcing conditions to interrupt the stability of these cycles. In this study, the authors showed that sudden changes or 'pulses' in SLR could modify depositional patterns and increase a barrier's potential for drowning [300]. Therefore, short term boundary changes from initial and critical geometries may impact the sustainability of barriers, even those which are in a presently stable form of retreat.

Width drowning simulations showed a remarkable association not only with critical and initial widths, but also with multiple other parameters including low toe depth ($\leq 8\ m$), low

initial marsh width ($\leq$ 350 m), high initial lagoon width ($\geq$ 6500 m), high rates of SLR rate ($\geq$ 15 mm/yr), high reference wind speeds ($\geq$ 9 m/s), low critical bed shear stress ($\leq$ 0.08 Pa), and low ocean sediment concentration ($\leq$ 60 mg/l) (Fig. 3.4; Supplementary Material Fig. B4.1). The significance of most of these parameters regarding width drowning confirms the findings of previous studies summarized in Table 3.2, including Lorenzo-Trueba and Ashton [19], Ashton and Lorenzo-Trueba [208], Lorenzo-Trueba and Mariotti [1], and Ashton and Lorenzo-Trueba [296]. However, to the authors' knowledge, these results are the first to show that modeled short-term width drowning is dependent on the unique combination of these parameters. Taken together, the statistically significant parameter associations suggest that all are required for width drowning to occur within the multi-decadal simulation time period. It also indicates that if one or more of these parameters falls outside of the ranges described above, through either natural or anthropogenic changes, then width drowning can be avoided in the short term or at least delayed. Such results may be used to inform localized alternatives analysis of nature-based solutions [301] or other viable coastal restoration practices.

Barrier width and shoreline position were also influenced by the equilibrium shoreface slope and the shoreface toe depth, the latter being more significant (Fig. 3.3). Toe depth was found to influence transgression through interactions with critical barrier width and overwash flux (Fig. 3.5, 3.6h,i), and lower toe depth values were associated with width drowning (Fig. 3.4a). These influences are a result of conservation of mass from the nearshore-shoreface boundary to the barrier-backbarrier marsh boundary. In the model formulation, overwash volume that is deposited on or behind the barrier is eroded from the shoreface and ocean side of the island [1]. Thus, all else being equal, islands with smaller toe depths have less available sediment for transport by overwash than islands with larger toe depths, meaning that islands must migrate larger distances to balance the eroded and deposited sediment

volumes. This finding is consistent with other published studies that found a relationship between decreased sediment supply and increased island transgression [e.g., 180, 240, 241].

Furthermore, because toe depth is defined as the depth of the toe or seaward extent of the active shoreface profile, it can also be connected with the equilibrium profile concept of closure depth, which marks the location at which temporal profile adjustments due to changes in wave climate becomes negligible, effectively separating the active profile from the inactive profile [244, 302]. While this depth threshold of shoreface activity is well-recognized and implemented in various models [e.g., 19, 169, 238], it has been shown that the time frame over which the simulation or study is conducted will impact the threshold, with longer time frames being associated with greater closure depths [187, 303]. It has also been shown that modifying toe depth based on accelerations in SLR rate can also have a significant impact on transgression rates [292].

One surprising result was the relative insignificance of the mainland slope parameter across the barrier and backbarrier results. Numerous studies have demonstrated the importance of antecedent substrate on the morphology of modern barriers [e.g., 176, 177], including more recent studies of U.S. East Coast barriers in which the antecedent substrate was critical to understanding the migrational history of the islands [e.g., 304, 305]. In this study, it was expected that lower mainland slopes would result in larger changes in shoreline position [174] and/or larger lagoon widths as mean sea level rose. However, the lagoon results in Figure 3.3 show only modest index values for SLR rate and insignificant values for mainland slope. Although it is not entirely clear why mainland slope appears insensitive, two hypotheses for these interesting results are: 1) that the LTM17 model's assumption of instantaneous interior marsh growth with SLR increments reduced the mainland slope's impact on lagoon width, and/or 2) the simulation time scale was too short to produce a notable impact on the transgression rates. Additional modeling is suggested to explore this interesting result.

Most of the forcing parameters were found to significantly influence the model results, the exception being shoreface flux (Fig. 3.3), which is associated with how fast the shoreface is driven back toward its equilibrium state by wave climates during recovery periods between storm events. The insignificance of shoreface flux was somewhat surprising, given its demonstrated influence in helping barrier's sustain long-term behaviors such as periodic retreat and dynamic equilibrium [e.g. 19, 300] and its more detailed formulations in other models [e.g., 53, 179]. The results were also surprising given the significance of toe depth, which, in reality, is related to shoreface flux. Taken together, these results suggest that the geometric constraints of the shoreface were more influential than the rates of shoreface response for short term simulations.

Although there were no instances of height drowning in Simulation Set C, the instances of height drowning from the preliminary results (Simulation Set A) help us understand the importance of overwash. Low overwash values ($\leq$ 15 $m^3/m/yr$) were associated with all of the simulations that resulted in height drowning in the preliminary results (Supplementary Material, Fig. B2.4). This highlights the criticality of overwash processes in maintaining the elevation of barrier islands with respect to SLR [e.g., 66, 295, 306]. Based on this understanding, a future increase in the frequency and localized intensity of coastal storms, which is expected among coastal scientists [e.g., 13, 307] and supported by observations and modeling studies [e.g., 308, 309], would naturally lead to increases in overwash flux that would enable barriers to maintain their elevations. However, storm-driven overwash can also have destructive effects on barrier island morphology including beach and dune erosion, channelization of antecedent low spots, and washout [310] that are largely dependent on the storm regime [47, 311, 312]. Higher storm-driven water levels generally increase in the morphological impact on barriers [287], although not in every case [293]. Based on modeling results from Passeri et al. [294], increases in storminess can result in barriers changing from a

narrowing (i.e., decreasing width) to a flattening (decreasing height) state and can increase the likelihood of breaching and drowning when coupled with increases in SLR. Mariotti [313] found that sediment supply played a key role in whether or not barriers gained or lost elevation due to storms, with high sediment supply leading to accretion and low sediment supply leading to barrier flattening. The results of this study also strongly imply that where overwash is artificially reduced, height drowning is possible by the end of the century for low-relief barriers under high rates of SLR. This finding is underscored by other studies which have found anthropogenic impacts to significantly impact overwash and barrier morphology [e.g., 280, 297, 314].

While high overwash values help maintain barrier height, they can also impact the barrier width positively or negatively depending on other geometry parameters such as initial marsh width, toe depth, critical barrier width, and initial barrier width, the latter of which was fixed at 350 m for Simulation Set C. Higher overwash flux values can increase island width when critical width values are high (Fig. 3.6d), and since overwash removes sediment from the shoreface and subaerial island, greater change in the shoreline position is also observed (Fig. 3.6g). The increase in barrier width can be modulated by the initial marsh width, for which lower values offset the changes or lead to decreases in barrier width (Fig. 3.6f). This is because lower backbarrier marsh widths increase accommodation space, requiring additional washover volume to maintain the barrier width [17]. Increases in barrier transgression are also regulated by increasing toe depth, which requires less retreat distance to achieve mass balance of the profile (Fig. 3.6i). In short, under high overwash conditions, barriers with low toe depths and low marsh widths were the least efficient at converting the change in shoreline position to the change in (back)barrier position, which led to reduced barrier widths. Deaton et al. [315] observed this phenomenon in a study of U.S. East Coast barrier islands and estimated that 51% of the observed marsh loss was due to barrier transgression.

The rate of SLR was very influential on the model results, particularly for barrier transgression and marsh depth (Fig. 3.3). Higher rates of SLR created larger accommodation spaces that required liberated sediment from the seaward side of the transgressing barrier to fill. Thus, a direct relationship exists between the rate of SLR and rate of barrier transgression. This is in line with the previous sensitivity results (see Table 3.2) and is supportive of findings from other modeling studies such as Moore et al. [180], who found that significant changes in SLR (based on Intergovernmental Panel on Climate Change projections) could result in a 150% increase in the transgression rate of the studied U.S. East Coast barrier and increase the possibility of drowning.

The results from this study showed that backbarrier marsh and lagoon dynamics were closely aligned with previous modeling studies. Parameters that were associated with the original MAC14 model, such as reference wind speed, tidal range, critical bed shear stress, and ocean sediment concentration, all impacted the backbarrier results in line with the original model [18], while the parameters associated with the original LTA14 model impacted the backbarrier results very little - the exceptions being critical barrier width and mainland slope (Fig. 3.3). SLR rate was a parameter in both original models (LTA14 and MAC14) and was found to be very influential across the board. Backbarrier parameters also influenced the barrier results, specifically the change in barrier width and change in shoreline position. This influence was manifested via reductions in backbarrier marsh width and depth, which increased backbarrier accommodation space and led to increased overwash volumes, decreases in barrier width, and drowning, similar to Lorenzo-Trueba and Mariotti [1].

Critical bed shear stress, which affects the erodability of the lagoon sediment, was found to have significantly influenced the model results. Shear stress was significant both in the original simulations (Simulation Set A) where values greater than 0.2 Pa led to lagoon filling and values lower led to barrier drowning (Fig. 3.2c), and in the modified simulations where

higher values (0.15-2.0 Pa) still led to lagoon filling and lower values (less than 0.08 Pa) were associated with width drowning (Fig. 3.4e). Increasing the critical bed shear stress simulates an increase in the lagoon's erosion resistance. As less lagoonal sediment is eroded, less is exported to the marsh or ocean which causes the lagoon to fill; oppositely, when critical bed shear stress is reduced, the lagoon deepens which increases marsh erosion, accommodation space, and leads to width drowning. Reeves et al. [316] modeled the impact of modified critical bed shear stress by adding seagrass beds to the GEOMBEST+ model of Walters et al. [17] and found very similar results as their seagrass beds act as source and sink terms for inorganic backbarrier sediment. However, they also found that decreases in seagrass beds, corresponding to a decrease in critical bed shear stress, allows the sediment that it had trapped to be exported to the marsh, resulting in marsh progradation [316].

Ocean sediment concentration, which influences the amount of inorganic sediment deposition, was also found to have significantly influenced the model results, as low values corresponded to both width and marsh drowning (Fig. 3.4f). These findings support the conclusions from the original study by Lorenzo-Trueba and Mariotti [1], who found that reduced sediment concentrations led to increased width drowning and decreased migration (see Table 3.2). Low ocean sediment concentrations reduce all inorganic sediment deposition in the back-barrier, thereby increasing accommodation space through reductions in marsh width, marsh depth, and lagoon depth. These results highlight the importance of considering the inorganic sediment transport dynamics in the marsh and lagoon [317, 318] and suggest that tidal inlet dynamics, including the formation of new inlets (i.e., breaching), are critical morphodynamic components of the barrier island system and should be considered in long-term barrier island modeling approaches [e.g., 121, 213]. Considering the influence of these parameters alongside the relative insignificance of overwash for the backbarrier system, these results suggest that inorganic sediment deposition through tidal inlet dispersion is much more significant to the

backbarrier marsh and lagoon system than overwash over sub-centennial timescales.

3.6 Conclusions

The aim of the study was to gain additional insights into multi-decadal barrier-backbarrier system dynamics by exploring the parameter space of the LTM17 model using global sensitivity analysis, specifically the Sobol Method. The influence of each input parameter on the wide range of model results was tested both individually and interactively, and specific regions of sensitivity within the parameter space were identified through heatmaps of parameter interactions and boxplots of parameter values associated with distinctive simulation categories.

Initial and critical barrier geometry parameters were found to significantly influence barrier width, height, and shoreline position through the end of this century, with narrow, low-relief barriers being most vulnerable to drowning. Width drowning was also found to be associated with multiple parameter value ranges, suggesting the risk of sub-centennial width drowning may be averted (or delayed) with a single input parameter change. The barrier profile's toe depth and the shoreface equilibrium slope, which are influenced by average wave climate, were also found to moderately influence barrier width and transgression due to conservation of mass within the barrier profile. The significant influence of critical bed shear stress and ocean sediment concentration on the backbarrier results, especially in contrast to the insignificance of overwash, suggests that inorganic sediment deposition through tidal inlet dispersion is much more significant to the backbarrier marsh and lagoon system than overwash over sub-centennial timescales.

The application of global sensitivity analysis to the LTM17 barrier island morphodynamic model using both the Sobol Method and simple factor mapping techniques has provided

new insights into the modeled system dynamics and has confirmed various elements of our current understanding of barrier evolution. Future modeling studies of barrier evolution should use these sensitivity results to constrain the parameters identified as most significant and to minimize uncertainty.

Acknowledgements

This material is based upon work that is partially supported by the U.S. Army Corps of Engineers through the U.S. Coastal Research Program (under Grant No. W912HZ-20-2-0005), the National Science Foundation (under Grant Numbers 1735139 and 1630099), and Virginia Sea Grant College Program Project R/72155T funded by the National Oceanic and Atmospheric Administration's National Sea Grant College Program, U.S. Department of Commerce (under award NA18OAR4170083). The statements, findings, conclusions, and recommendations are those of the author(s) and do not necessarily reflect the views of the U.S. Army Corps of Engineers, the U.S. Coastal Research Program, the National Science Foundation, Virginia Sea Grant, the National Oceanic and Atmospheric Administration, or the U.S. Department of Commerce. The authors acknowledge Advanced Research Computing at Virginia Tech for providing computational resources and technical support that have contributed to the results reported within this paper. URL: https://arc.vt.edu/.

Chapter 4

Comparability of Global Sensitivity Analysis Methods Applied to a Long-Term Coastal Morphodynamics Model

Steven W.H. Hoagland[1], Jennifer L. Irish[1], Robert Weiss[2,3]

[1]Department of Civil and Environmental Engineering, Virginia Tech, Blacksburg, VA

[2]Department of Geosciences, Virginia Tech, Blacksburg, VA

[3]Academy of Integrated Science, Virginia Tech, Blacksburg, VA

This manuscript is under review.

Abstract

Global sensitivity analysis can help computational modelers understand the dynamics of a complex model and prioritize factors to reduce uncertainty. While many global sensitivity analysis methods exist, it is not always clear which methods are best suited for a particular modeling application. In this study, five sensitivity methods – correlation, factorial, Morris, Sobol, and VARS – were applied to a long-term coastal morphodynamics model and their performance compared for parameter rankings, convergence, and reliability. All of the sensitivity analysis methods evaluated in this study were generally capable of identifying groups of the most sensitive parameters at extremely high simulation counts, with correlation showing some notable exceptions. The Morris method outperformed the other methods in convergence and reliability analysis due to its consistency in identifying the highest and lowest ranked parameters. VARS ranked second in performance, showing better convergence and reliability than the Sobol method, and at lower computational expense.

4.1 Introduction

Computational modeling is a critical component of coastal morphodynamic analysis. Its ability to aid researchers and practitioners both in understanding system dynamics [e.g., 2, 19, 241] and predicting future system states [e.g., 44, 284] has led to its wide adoption and application. Myriad coastal morphodynamic models were developed during the last half century [288]. With this increase in model development and associated model complexity came a need for tools to evaluate and better understand them.

Sensitivity analysis, which Saltelli et al. [319] defined as "The study of how the uncertainty in the output of a model (numerical or otherwise) can be apportioned to different sources of uncertainty in the model input," is perhaps the best available tool to understand the dynamics of a complex model. Because sensitivity analysis often requires many model runs and can impose a significant computational burden, researchers in this field naturally sought to improve the sensitivity analysis procedure to reduce computational burden while maximizing the information gained [26]. This area of research has proved fruitful over the last few decades, while continuous innovations in hardware, software, programming languages, and programming techniques have made sensitivity analysis more practical and economically feasible [23, 26, 320, 321]. Because of these advancements, modelers are able to choose from a variety of sensitivity analysis approaches and methods to best suit their needs.

It is not always clear, however, which approaches or methods of sensitivity analysis are best suited for a particular modeling application since both the models and sensitivity methods can vary widely in their complexity, computational burden, and output [320]. Constrained by project timelines and computational resources, modelers need to understand the benefits and drawbacks of the various sensitivity analysis approaches to determine which methods are most appropriate for their application. Various studies have been published comparing

global sensitivity analysis approaches [e.g., 27, 28]. However, additional comparison studies are needed as global sensitivity analysis is increasingly becoming its own field of study [26], with approaches continuing to be developed and improved [e.g., 24, 25]. Moreover, according to Wang and Solomatine [322], few studies have evaluated the convergence and uncertainty of the sensitivity analysis results themselves.

This study compared the performance of five popular global sensitivity analysis methods - correlation, factorial, Morris, Sobol, and VARS - across evaluation criteria such as factor prioritization (ranking) and fixing (screening), convergence, and reliability. Each of these methods was applied to a long-term coastal morphodynamics model. To the authors' knowledge, this is the first global sensitivity analysis comparison study as applied to long-term coastal models. While this study will be directly relevant for researchers and practitioners using this particular large-scale coastal behavior model or those similar, this study will help researchers and practitioners outside this field who are applying global sensitivity analysis to other models or who are seeking to advance the field of global sensitivity analysis itself.

4.2 Methods

In this study, we applied five global sensitivity analysis approaches to a long-term coastal morphodynamics model by Lorenzo-Trueba and Mariotti [1]. For each global sensitivity approach, the computational burden and model results were evaluated and compared to the other methods. We also analyzed the convergence of the results for each global sensitivity approach by running different numbers of simulations for each method. Details regarding the morphodynamic model and the global sensitivity analysis methods, including implementation particulars, are presented below.

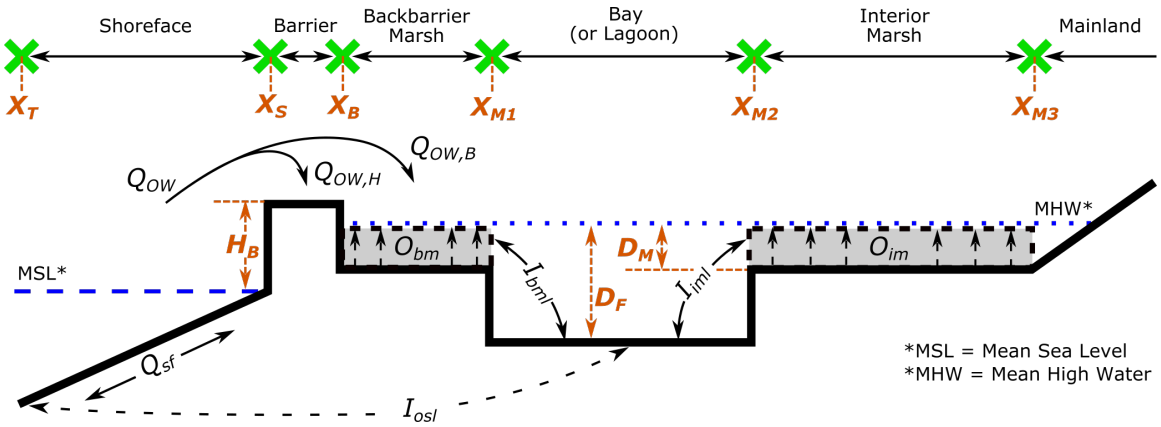

Figure 4.1: Idealized barrier transect based on the LTM17 Model. *Shoreface sediment flux (Q_{sf}), marsh organogenesis (O_{bm} and O_{im}), overwash (Q_{OW}) deposition on the barrier ($Q_{OW,H}$) and marsh ($O_{OW,B}$), and inorganic sediment fluxes between the lagoon and ocean (I_{osl}), and lagoon and marshes (I_{mbl} and I_{iml}) are shown. Figure modified from Lorenzo-Trueba and Mariotti [1] and Hoagland et al. [2].*

4.2.1 Morphodynamics Model

Lorenzo-Trueba and Mariotti [1] published a coastal morphodynamics model (hereafter 'LTM17' model) that simulates the evolution of a barrier-marsh-lagoon system over decades to centuries through equilibrium-based sediment flux calculations. A graphical representation of the modeled barrier-marsh-lagoon transect is shown in Figure 4.1. The transect runs from the seaward extent of the shoreface to the intersection of the mean high water (MHW) elevation with the mainland slope and includes transect subregions such as the shoreface, barrier island, backbarrier marsh, lagoon, and interior marsh.

The model tracks 10 state variables at each timestep, including barrier height (H_B), marsh depths (D_{M1}, D_{M2}), lagoon depth (D_F), and boundaries between the transect subregions (X_T, X_S, X_B, X_{M1}, X_{M2}, X_{M3}), shown in Figure 4.1. Other result variables or metrics may be calculated from these state variables such as change in shoreline position and the widths of the barrier, marshes, and lagoon. These result variables, which are used to evaluate the sensitivity results, are shown in Table 4.1 with their state variable calculations.

Table 4.1: LTM17 Model Result Variables

Result Variable	Symbol	Calculation	Units
Change in Shoreline Position	ΔX_S	$(X_{S_f} - X_{S_0})^\dagger$	[m]
Barrier Width	W_B	$(X_B - X_S)$	[m]
Barrier Height	H_B		[m]
Backbarrier Marsh Width	B_{M1}	$(X_{M1} - X_B)$	[m]
Lagoon Width	B_F	$(X_{M2} - X_{M1})$	[m]
Marsh Depth	D_M		[m]
Lagoon Depth	D_F		[m]
Interior Marsh Width	B_{M2}	$(X_{M3} - X_{M2})$	[m]

†The f and 0 subscripts denote final and initial positions, respectively.
Table modified from Hoagland et al. [2].

Changes to the barrier-marsh-lagoon system are a result of sediment exchanges between the system boundaries including storm-driven overwash, tidal inlet dispersion, and marsh platform erosion and deposition. Boundary changes are also directly impacted by changes in mean sea level (MSL), system geometry, such as shoreface slope and depth, and sediment characteristics that impact its erodability and transport. For additional details on the LTM17 model, the reader is referred to Lorenzo-Trueba and Mariotti [1], and references therein.

The model variables that drive the previously described system changes are user-defined model parameters. Fifteen LTM17 model input parameters were evaluated for this study. These parameters are listed in Table 4.2 with their value ranges and units. The value ranges define the lower and upper bounds of possible values in the sensitivity analysis. Parameter ranges were selected to approximate the value ranges for other modeling studies employing the LTM17 model (or similar models) such as Lorenzo-Trueba and Ashton [19], Mariotti and Carr [18], Lorenzo-Trueba and Mariotti [1], and Miselis and Lorenzo-Trueba [297]. A comparison of these values to previous studies is presented in the supplementary material of Hoagland et al. [2]. For each simulation in the sensitivity analyses, model parameter values were sampled from the value ranges according to a uniform probability distribution.

Table 4.2: LTM17 Model Input Parameters

Symbol	Input Parameter	Value Range	Units
β	Mainland Slope	$0.0001 - 0.005$	[m/m]
D_T	Toe Depth	$5 - 15$	[m]
W_{cr}	Critical Width	$100 - 600$	[m]
H_{cr}	Critical Height	$0.5 - 4$	[m]
α_e	Equilibrium Shoreface Slope	$0.005 - 0.025$	[m/m]
$B_{M1,cr}$	Critical Backbarrier Marsh Width	$50 - 500$	[m]
$Q_{OW,*}$	Max. Annual Overwash Flux	$1 - 100$	[m^3/m/yr]
$\dot{z}$	Sea Level Rise Rate	$3 - 20$	[mm/yr]
K	Shoreface Flux Const.	$100 - 10000$	[m^3/m/yr]
U_{ref}	Wind Speed	$5 - 10$	[m/s]
r	Tidal Range	$0.7 - 2.8$	[m]
ω_s	Sediment Settling Velocity	$0.05 - 0.5$	[mm/s]
τ_{cr}	Critical Bed Shear Stress	$0.05 - 0.2$	[Pa]
C_o	Ocean Sediment Conc.	$30 - 200$	[mg/l]
B_P	Peak Biomass Production	$1.5 - 3.5$	[kg/m^2]

Table modified from Hoagland et al. [2].

All model runs were performed for a 100-year simulation time period at a computational time step of 0.1 years. In addition to the input parameter values defined in Table 4.2, other model-required initial conditions and variables were defined for all simulations using standard or predefined values from the original model publications. These parameters are outlined in Section 1 of Appendix C.

4.2.2 Global Sensitivity Analysis

The five global sensitivity analysis methods evaluated in this study were: (1) correlation method, (2) the two-level full factorial method, (3) the Morris method [323], (4) the Sobol method [20], and (5) the variogram analysis of response surfaces method [24, 25]. A brief overview of each method is provided below. For additional details regarding each method, the reader is referred to Morris [323], Sobol [20], Saltelli et al. [23], Razavi and Gupta [24, 25], and references therein.

Correlation Method

As discussed in Saltelli et al. [23], correlation tests are one of the most simple approaches to global sensitivity analysis. It involves running simulations with a fully randomized set of input parameters and using statistical measures to quantify the relationship between the input and output variables. With independent input parameters, strong correlations between input parameter values and the model output would indicate relatively high parameter sensitivities for those input parameters, while weak correlations would suggest input parameter insensitivities. We refer to this approach hereafter as the 'correlation method.'

Two correlation metrics were used to evaluate parameter sensitivities in this study. The first is the commonly known coefficient of determination, or R^2 value, which was calculated by squaring the Pearson correlation coefficient (R) from a linear least-squares regression model. The R value indicates the linear relationship between the input parameter values and model output, while R^2 indicates how much of the model output variance is explained by the linear regression model. R^2 is calculated by Equation 4.1:

$$R^2 = 1 - \frac{\sum_{i=1}^{n}(y_i - \hat{y}_i)^2}{\sum_{i=1}^{n}(y_i - \overline{y})^2} \tag{4.1}$$

where y is the output, $\overline{y}$ is the average output, and $\hat{y}$ is the output predicted by the linear regression model.

The second correlation metric used is Spearman's rank-order correlation coefficient (ρ), which is calculated by extracting the rank-orders of the input parameter values (RO_{in}) and rank-orders of the model output (RO_{out}), and dividing the covariance of those rank-orders by the standard deviations of the model input (σ_{in}) and output (σ_{out}), as shown by Equation 4.2. Spearman's ρ has an advantage over R^2 in quantifying correlation when a non-linear,

monotonic relationship exists between the model input and output.

$$\rho = \frac{COV(RO_{in}, RO_{out})}{\sigma_{in}\sigma_{out}} \tag{4.2}$$

Implementation of the correlation method was conducted by running a user-defined number of simulations with a fully randomized selection of input parameter values, according to the value ranges presented in Table 4.2, and calculating the R^2 and Spearman's ρ values for each association of input variable and model result variable.

Two-Level Full Factorial Method

The two-level full factorial method (hereafter the "factorial" method) compares the model results at the extremes of the parameter space, often visualized as the corners of a multidimensional hypercube. The method is classified as a derivative-based global sensitivity analysis method in that it calculates the rate of change of model output for a specified step size, or in the case of this method, the entire value range, and it is also classified as a one-at-a-time approach since it calculates these derivatives sequentially [23].

The number of simulations required to calculate parameter sensitivities using the factorial method is 2^k, where k is equal to the number of evaluated input parameters. Since 15 input parameters were evaluated in the study, the factorial method required 32,768 simulations. The parameter space for the model with $k = 15$ is a 15-dimensional hypercube, and each of the 32,768 simulations is located in a unique corner of that hypercube. Derivatives were then calculated from one corner of the input space to another, along the axis of the input parameter of interest.

Each derivative calculation is called an elementary effect (EE) following the terminology of

Morris [323], and is calculated by Equation 4.3:

$$EE_i = \frac{y(x_1, x_2, ..., x_i + \Delta R_i, ..., x_k) - y(x_1, x_2, ..., x_i, ..., x_k)}{\Delta} \tag{4.3}$$

where EE_i is an elementary effect associated with the ith input parameter (x_i), y is the model output, Δ is the derivative step size across the unit value range, and R_i is the range of possible values for parameter x_i. There are 2^{k-1} elementary effects for each input parameter. Thus, for $k = 15$, there are 16,384 possible elementary effects per input parameter, totaling 245,760 possible elementary effects in the parameter space. Final input parameter sensitivities are estimated by calculating the mean of the absolute value of all elementary effects for each input parameter; this is succinctly called the mean absolute elementary effect ($MAEE$).

Implementation of the factorial method involved creating an array of 2^k simulations (i.e., input parameter values), where each simulation was a unique combination of all input parameter extreme values, and systematically calculating all of the elementary effects associated with each input parameter.

Morris Method

The Morris method [323] randomly samples the interior of the multidimensional parameter space using random orientations or trajectories, following the terminology of Saltelli et al. [23]. The number of these trajectories (r_t) are user-specified and each trajectory contains $k+1$ sequential simulations, each of which differs from the previous simulation by modifying a single input parameter value by some specified distance (Δ) across its value range. The appropriate Δ value is determined by the user-specified discretization of the parameter space into $p-1$ intervals along each axis. When there is an odd number of intervals, Morris [323] recommended selecting Δ values equal to $p/[2(p-1)]$ to achieve equal sampling probabilities.

Although the work of Morris [323] involved model input parameters with values between 0 and 1, we apply his method to the LTM17 model, the parameter ranges of which contain various scales, by normalizing each range between the minimum and maximum values, as discussed in Rutjens et al. [324].

Similar to the factorial method, the Morris method estimates parameter sensitivities by calculating all of the elementary effects for each input parameter by Equation 4.3, taking their absolute value, and then calculating $MAEE$ for each input parameter. The Morris method is also classified as a derivative-based, one-at-a-time method for the same reasons as the factorial method. The number of possible elementary effects per input parameter is determined by the following expression, $p^{k-1}[p - \Delta(p-1)]$. For this study, with $p = 4$, $\Delta = 2/3$, and $k = 15$, the maximum number of elementary effects that may be calculated is approximately 537 million. Since each elementary effect calculation requires two simulations, more than 1 billion simulations would be required to compute every elementary effect. However, the Morris method does not compute every elementary effect, but takes random samples of the elementary effects in accordance with the r_t trajectories through the parameter space.

Implementation of the Morris method for this study involved created an array of $k + 1$ simulations for a user-defined number of sample trajectories through the parameter space. The trajectories and simulation arrays were developed following the method originally proposed by Morris [323], and reiterated in detail in Saltelli et al. [23]. Once the simulations were completed, MAEE values were calculated for each input parameter.

Sobol Method

The Sobol method [20] is predicated on the theory of model variance decomposition, which suggests that the total variance of a model's output can be decomposed and assigned to

various model components or inputs. Based on this theory, the total model variance may be considered as a summation of the variances associated with individual input parameters and their combinations. This type of method, which characterizes input parameter sensitivities based on these variances, is called a variance-based method. As described elsewhere, the Sobol method is considered the standard for sensitivity analysis [22] and, along with the Morris method, "one of the most rigorous approaches ... to date" [21].

Variance from the input parameters arises from the fact that each parameter has a range of possible values over which it is sampled. If the total model variance is a summation of variances associated with input parameters and their combinations, then it follows that the total model variance might be reduced if one or more of the input parameters are fixed at a particular value and not allowed to be randomly sampled from their value ranges. This parameter fixing may be visualized as taking slices of the parameter space. Once input parameters are fixed, the reduced model variance that results is called the conditional variance.

The Sobol method uses conditional variance and conditional mean calculations to compute index values for each input parameter. The index values are called Sobol Indices and range from 0 to 1, with larger values indicating greater sensitivity. Although there are multiple types of indices that may be calculated using the Sobol method, this study focuses on the k-th order index, also called the total effect, which represents the fraction of model variance that may be assigned to a particular input parameter and all of the interactions involving that parameter. The total effect of the ith input parameter (S_{T_i}) is calculated by Equation 4.4:

$$S_{T_i} = 1 - \frac{V(E(y|x_{\sim i}))}{V(y)} \tag{4.4}$$

where $V(E(y|x_{\sim i}))$ is the variance of the conditional mean of the output when all parameter values *except* for those of parameter x_i are fixed, and $V(y)$ is the total variance of the model output.

Using brute computational force to calculate the conditional means and variances associated with this Sobol index can be burdensome, requiring thousands of simulations to achieve numerical convergence, which can limit the method to certain modeling applications. To overcome this limitation, various methods have been developed to estimate the conditional variances and associated indices [325]. Saltelli [326] proposed one such method, which involves resampling two independent and randomly generated arrays of simulations that reduced the computational burden by at least 50 percent.

Implementation of the Sobol Method for this study followed the method proposed by Saltelli [326] to estimate the indices for a user-defined number of simulations per input parameter. The equations used to estimate the Sobol indices were optimized for index convergence following the study by Nossent and Bauwens [327].

Variogram Analysis of Response Surfaces Method

The Variogram Analysis of Response Surfaces (VARS) method is the most recently developed global sensitivity analysis method explored in this study and was published by Razavi and Gupta [24, 25]. The method calculates parameter sensitivities using estimated variograms of the response surface.

As Razavi and Gupta [24] discuss, the variogram function was developed in the field of spatial statistics. Estimating these functions involves sampling pairs of points across the parameter space, separated by various distances or perturbation scales ($\mathbf{h}$). Thus, the variogram (γ) is estimated as a function of the perturbation scale and involves calculating the variance (V) of

the differences in the pairs of sampled points separated by the perturbation scale, as shown in Equation 4.5:

$$\gamma(\mathbf{h}) = \frac{V[y(\mathbf{x}+\mathbf{h}) - y(\mathbf{x})]}{2} \tag{4.5}$$

where $y(\mathbf{x}+\mathbf{h})-y(\mathbf{x})$ is the difference in model output (y) for input parameters ($\mathbf{x}$) separated by $\mathbf{h}$, the perturbation scale.

Once the variogram functions for each input parameter are estimated, the sensitivity metrics are calculated by integrating the variogram across a range of scales (iVARS). Three metrics are recommended by Razavi and Gupta [24] including iVARS_{10}, iVARS_{30}, and iVARS_{50}, which are integrations of the variogram across 10%, 30%, and 50% of the input parameter range, respectively. Hereafter these metrics are referred to as i10, i30, and i50.

Implementation of the VARS Method followed Razavi and Gupta [24, 25], using the VARS-TOOL python package made publicly available on github [328]. The VARS analysis was conducted with a latin hypercube sampling scheme, a perturbation scale of 0.1, and a user-defined number of stars, or base sampling points, which is used with the perturbation scale and number of input parameters to determine on the number of simulations performed.

4.2.3 Analysis

It is notable that the sensitivity methods presented herein produce different quantitative ranges of sensitivity metrics. The correlation method produces coefficients between -1 and 1 for Spearman's ρ or between 0 and 1 for R^2; the Morris and factorial methods produce elementary effects, which assume the value range and units of the result variables; the Sobol method produces index values between 0 and 1; and the VARS method produces integrated

values of the variograms, which also vary according to the result variables. This presents a challenge when trying to compare results across methods. To facilitate this comparison, we used the ratio of factor sensitivity (RFS) metric, which divides each parameter's sensitivity value by the sum of all input parameter sensitivities for a particular result variable. This converted the disparate sensitivity results to an index scale between 0 and 1, thereby allowing for the comparison of relative parameter sensitivities across different sensitivity methods and result variables.

Once RFS values were calculated, they were used to rank the input parameters from most sensitive to least sensitive. These parameter rankings were evaluated between sensitivity methods and used to assess the convergence of the each method's sensitivity metrics. For the correlation method, the convergence of Spearman's ρ values were evaluated by the number of simulations spanning five orders of magnitude (i.e., from 10^1 to 10^5 simulations). For the Morris method, the number of user-defined trajectories (each with $k + 1$ simulations) was varied across five orders of magnitude to evaluate convergence of MAEE and associated parameter rankings. For the Sobol method, the number of simulations per input parameter was varied, and for the VARS method, the number of star points was varied, both across five orders of magnitude. For all sensitivity methods and metrics, the results were bootstrapped to produce 90% confidence intervals.

To compare the performance of the methods when constrained by a computational budget, 100 independent trials of each method were performed for computational budgets on the order of 1,000 and 10,000 simulations. In both cases, we calculated the percentage of trials that contained parameter rankings within one position (plus or minus) of each method's "true" ranking, which was determined by the convergence trial with the greatest number of simulations. This analysis provided an estimate of each method's reliability under computational constraints. It may be summarily noted that the methods evaluated herein are

all being compared with one another; thus, a true parameter sensitivity and a true error are not calculable. We may, however, recognize the relative sophistication or robustness of the methods, note areas of agreement and disagreement between them, and discuss where certain methods may be more advantageous than others.

4.3 Results

Before sensitivity analysis is performed, it is a best practice to evaluate the model uncertainty. The results of the uncertainty analysis are presented in Section 4.3.1. This is followed by a comparison of the RFS values and parameter rankings across all sensitivity metrics in Section 4.3.2, analysis of convergence for each method in Section 4.3.3, and method reliability estimates in Section 4.3.4.

4.3.1 Output Uncertainty

Ten thousand model simulations were run to generate the output for the uncertainty analysis. For each of these simulations, input parameter values were sampled from their value range in Table 4.2 according to a uniform probability distribution. The number of model simulations was selected to ensure convergence of the output means and percentiles for all result variables, which are shown in Figure 4.2. Convergence plots of the result variable means and percentile extremes (i.e., 5th and 95th percentiles) are provided in Section 2 of Appendix C.

The overlaid line graphs in Figure 4.2a-c show a wide distribution of final results over the 100-year simulation period, as the change in shoreline position, barrier width, and backbarrier marsh width results at year 2100 all varied on the scale of hundreds of meters. The same is true for lagoon width and interior marsh width, although the latter contained extremely

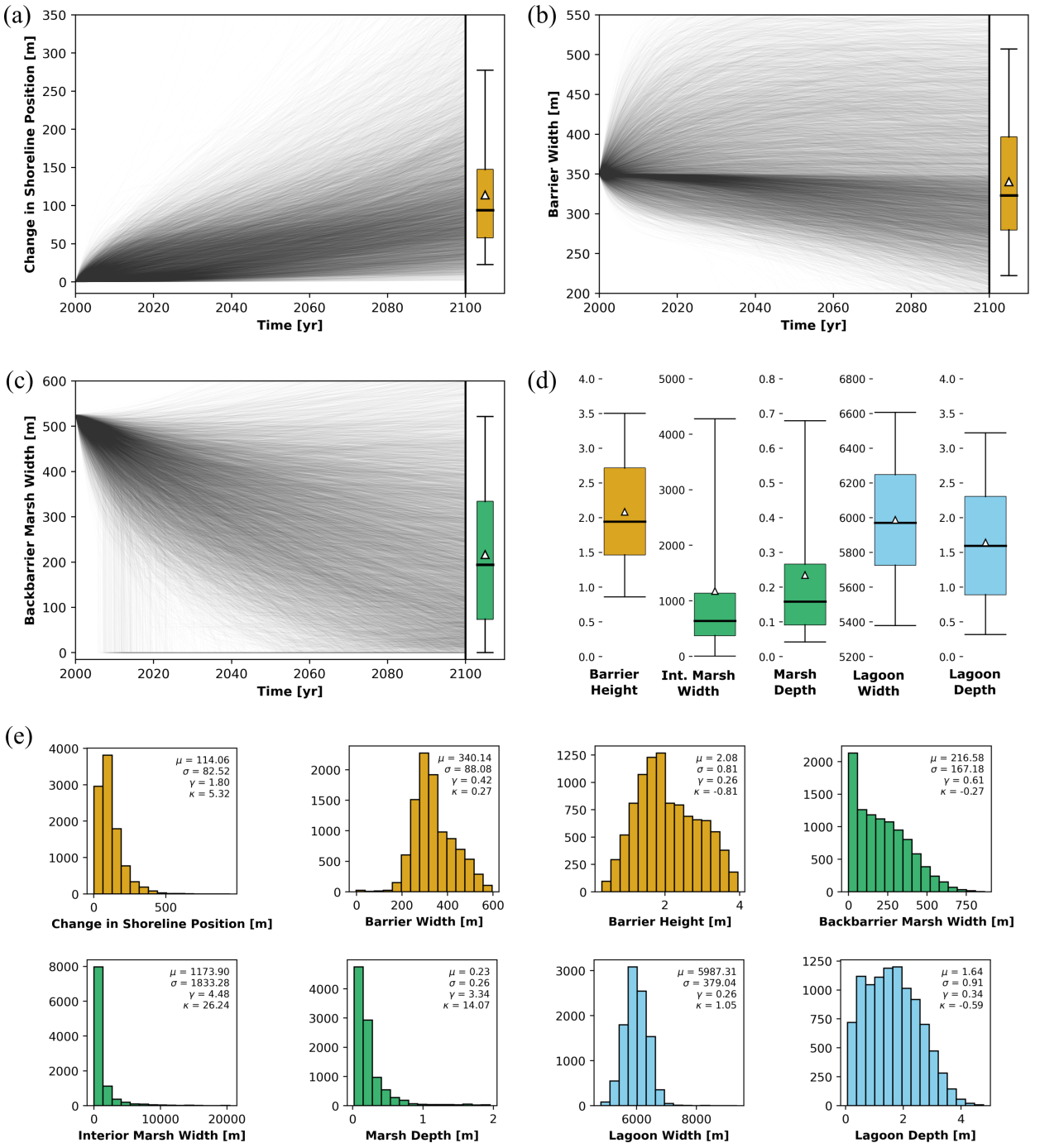

Figure 4.2: Uncertainty analysis for LTM17 model output. *Boxplots in (a)-(d) indicate the mean (triangle) and the following percentiles from bottom to top: p5, p25, p50, p75, p95. Result variable histograms in (e) also show mean (μ), standard deviation (σ), skew (γ), and kurtosis (κ) values.*

Table 4.3: Coefficients of Variation for Model Result Variables

Result Variable [Symbol]	Coefficient of Variation
Change in Shoreline Position [ΔX_S]	0.72
Barrier Width [W_B]	0.26
Barrier Height [H_B]	0.39
Backbarrier Marsh Width [B_{M1}]	0.77
Interior Marsh Width [B_{M2}]	1.56
Marsh Depth [D_M]	1.13
Lagoon Width [B_F]	0.06
Lagoon Depth [D_F]	0.55

high values which increased the variation to thousands of meters (Fig. 4.2d). Barrier height, marsh depth, and lagoon depth results all varied on the meter to sub-meter scale (Fig. 4.2d).

As indicated by the boxplots (Fig. 4.2a-d) and histograms (Fig. 4.2e), all of the results showed a unimodal distribution, most of which also showed a positive skew (γ), with values ranging from 0.26 (lagoon width and barrier height) to 4.48 (interior marsh width). The kurtosis (κ) of the distributions were split. Change in shoreline position, marsh depth, and interior marsh width all displayed high kurtosis values, while the remaining result variables showed low kurtosis. The means and standard deviations are also shown in the histograms for each result variable in Figure 4.2e. To compare standard deviations across the different result variable scales, the coefficient of variation (σ/μ) was calculated for each result variable and presented in Table 4.3. Interior marsh width showed the greatest coefficient of variation at 1.56. In descending order, this was followed by marsh depth (1.13), backbarrier marsh width (0.77), change in shoreline position (0.72), and lagoon depth (0.55). The other three variables all showed coefficients below 0.4, with lagoon width being the lowest at 0.06.

4.3.2 Method Comparison

Eight sensitivity metrics, calculated for each input parameter and result variable combination, were compared with one another via RFS score and parameter ranking. Figure 4.3 displays these results for change in shoreline position and Figure 4.4 presents the parameter rankings for barrier width and backbarrier marsh width. RFS and parameter ranking results for all result variables are presented in Section 3 of Appendix C. Note that all of these results were extracted from the highest number of simulations performed for each method as follows: correlation method = 100,000; factorial method = 32,768; Morris method = 1.6 million; Sobol method = 1.7 million; VARS method = 1.5 million.

Figure 4.3 showed a strong consistency in the highest ranked parameters and the lowest ranked parameters across the sensitivity metrics. RFS values were highest for W_{cr}, $\dot{z}$, and $Q_{OW,*}$, and near zero for β, $B_{M1,cr}$, ω_s, and B_P (Fig. 4.3a). The RFS values for the other parameters generally fell between 0 and 0.15.

The plot of parameter rankings in Figure 4.3b provides a more detailed look at this consistency. The highest ranked parameters were W_{cr} and $\dot{z}$. The top rank was claimed by W_{cr} for all methods except Spearman correlation and factorial, both of which gave W_{cr} a rank of 2 behind $\dot{z}$ and $Q_{OW,*}$, respectively. For the R^2 correlation metric, Sobol index, and VARS metrics, the second rank was assigned to $\dot{z}$, although $\dot{z}$ drops to rank 3 for Morris and rank 4 for factorial. Other consistently top-ranked parameters include $Q_{OW,*}$, which ranked in the top 3 parameters for five of the eight sensitivity metrics, and D_T, which ranked in the top 4 parameters for six of eight metrics. β, $B_{M1,cr}$, ω_s, and B_P ranked in the bottom 5 parameters across all sensitivity metrics with near-zero RFS values.

The other parameters hovered in the middle rankings. For example, U_{ref} varied between rank 5 and 8 across all metrics, τ_{cr} varied between rank 6 and 11 across all metrics, and K varied

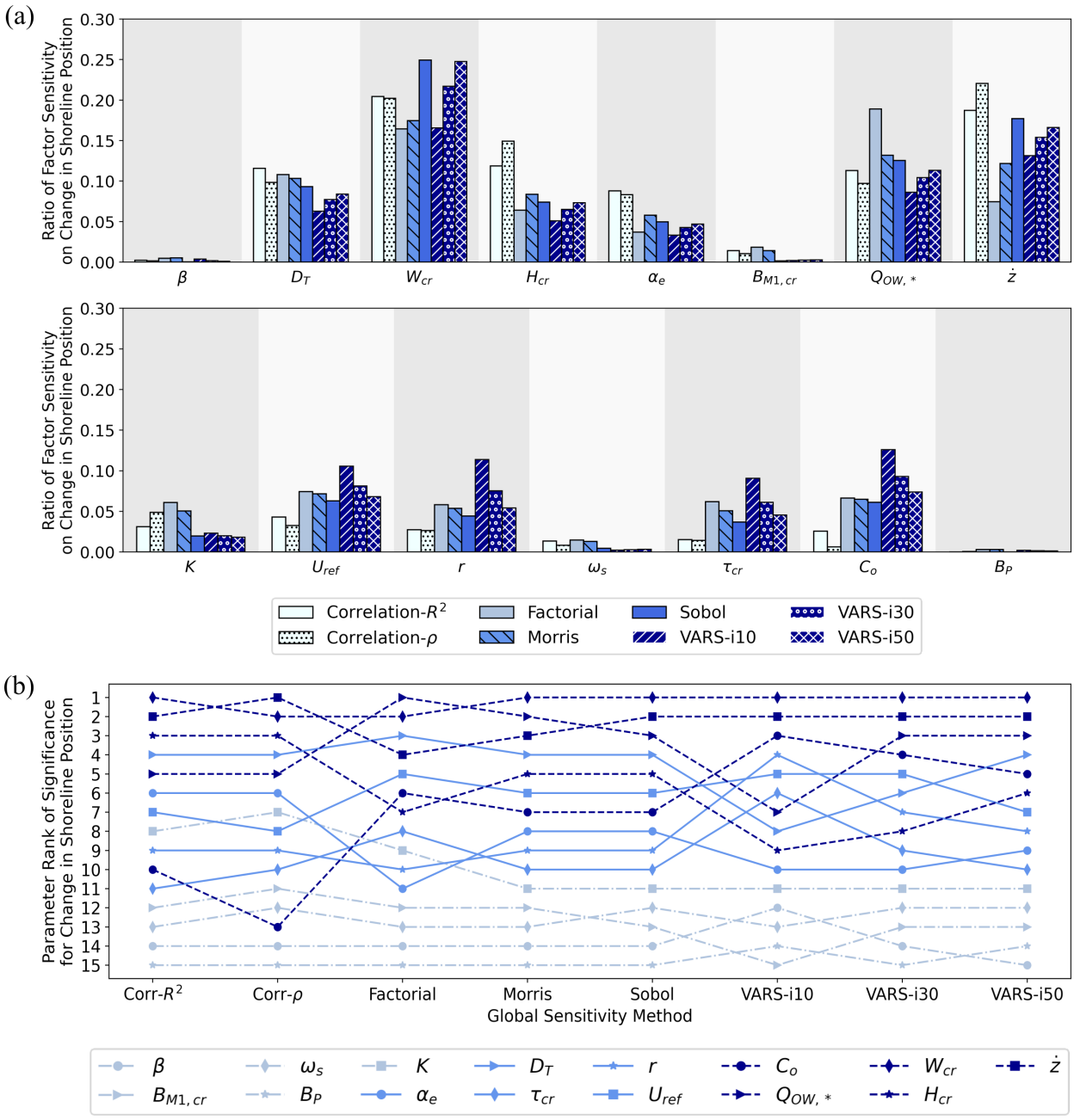

Figure 4.3: Method comparison for change in shoreline position: (a) ratio of factor sensitivity, and (b) parameter rank of significance.

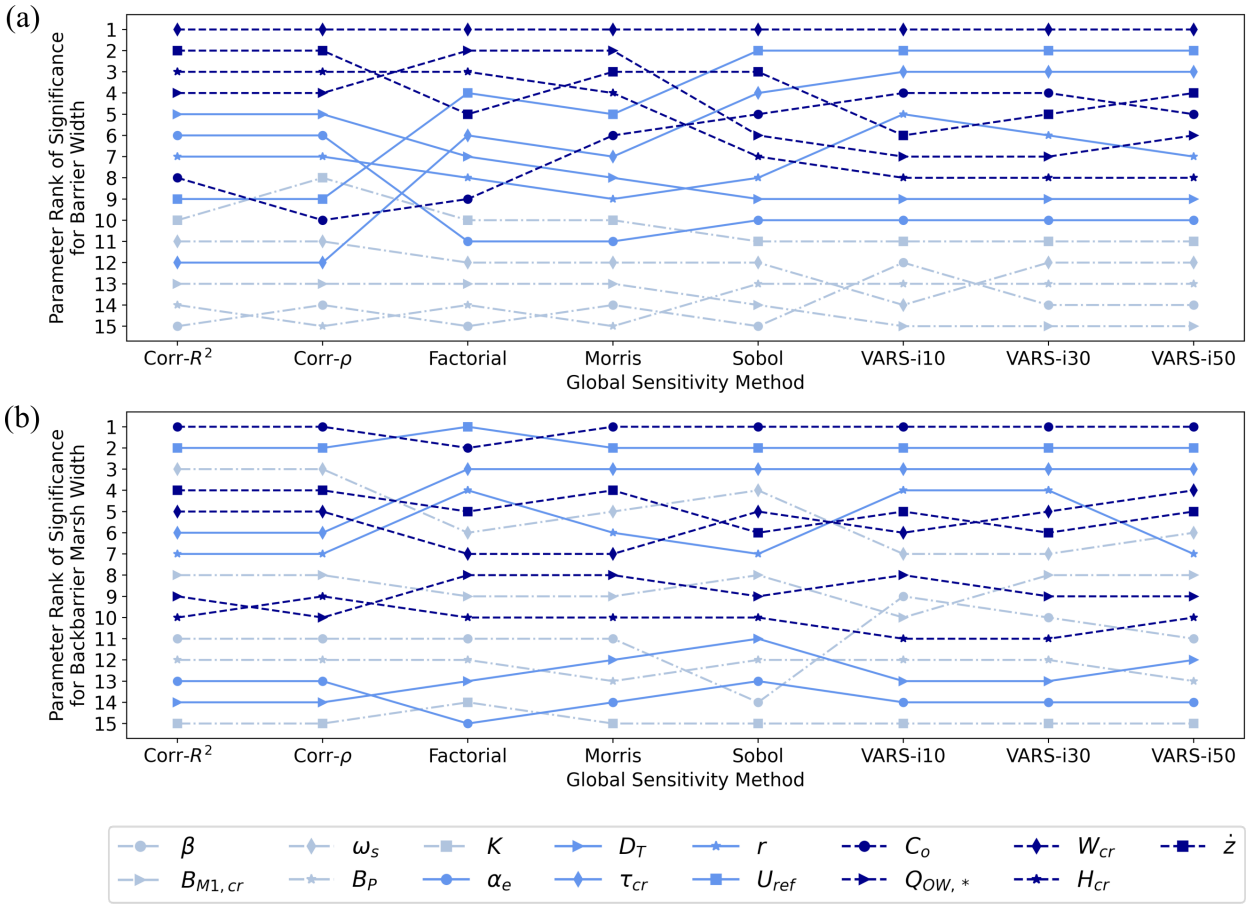

Figure 4.4: Parameter rank of significance for (a) barrier width and (b) backbarrier marsh width.

between rank 7 and 11 consistently. A few parameters showed slightly more variability in rank between sensitivity metrics. C_o, for example, was ranked 10th and 13th for the R^2 and Spearman correlation coefficients, respectively, while ranking 3rd, 4th, and 5th for the i10, i30, and i50 VARS metrics, respectively. The top rank for parameter r was 4 for VARS-i10, while all of the non-VARS metrics showed a 9 or 10 ranking.

This pattern of consistency in the highest and lowest rankings was also demonstrated for the other result variables. For barrier width (Fig. 4.4a), W_{cr} was top ranked for all sensitivity metrics while β, $B_{M1,cr}$, ω_s, and B_P were all consistently ranked in the bottom 5 parameters. For backbarrier marsh width (Fig. 4.4b), all metrics showed C_o as the top rank and U_{ref} as the second rank, except for the factorial method, which reversed these two parameters. The third rank was consistently held by τ_{cr} for all metrics except the R^2 and Spearman coefficients. The lowest ranks included K, α_e, D_T, and B_P, all of which consistently ranked in the bottom 5 parameters. Similar patterns were observed for the result variable plots in Section 3 of Appendix C.

Comparing the correlation metrics (R^2 and Spearman's ρ), there does not appear to be any significant difference between the results. However, there were some significant differences between the rankings of the correlation metrics and the other sensitivity metrics. This is seen, as mentioned previously, in the C_o rankings for change in shoreline position (Fig. 4.3b), which were ranked 10 and 13 in the correlation metrics, and between rank 3 and rank 7 for all other metrics. This was also seen in the barrier width rankings (Fig. 4.4a) for τ_{cr} and U_{ref}. In the correlation metrics, τ_{cr} was ranked 12th, while the other rankings were as follows: factorial (6th), Morris (5th), Sobol (4th), and VARS (3rd). Similarly, U_{ref} was ranked 9th in the correlation metrics, while the other rankings were: factorial (4th), Morris (5th), Sobol (2nd), and VARS (2nd).

There were also notable similarities and dissimilarities between the remaining metrics de-

pending on the input parameter and result variable. For most of the result variables (the only exception being lagoon width), the i10, i30, and i50 VARS metrics showed consistent rankings among the top-ranked parameters. For lower ranked parameters, the VARS metrics showed increasing or decreasing rankings, typically by 1 or 2 positions but at most 3 or 4. The rankings for the factorial, Morris, and Sobol metrics also showed variations in similarity. For the change in shoreline position results (Fig. 4.3b), the rankings were very similar, differing by a maximum of 3 positions between rank 8 and rank 11 across all three metrics. The barrier width results (Fig. 4.4a) showed slightly more variation, with W_{cr} ranging from rank 2 to rank 6, H_{cr} ranging from rank 3 to 7, and C_o ranging from rank 5 to 9.

4.3.3 Convergence

Spearman's ρ was calculated for each input parameter and result variable combination over five simulation sets which spanned five orders of magnitude, from 10 to 100,000 simulations. The absolute value of Spearman's ρ value, 90% confidence intervals, and associated parameter rankings are shown in Figure 4.5 for change in shoreline position. Convergence plots for the other result variables are presented in Section 4 of Appendix C.

The 90% confidence intervals for Spearman's ρ with 10 total simulations (N) were, on average, very large with significant overlap between the highest and lowest ranking parameters (Fig. 4.5a). The average range of ρ values across all result variables at $N = 10^1$ was 0.55. As expected, the confidence interval ranges were substantially reduced as the number of simulations increases. The average ranges were reduced to 0.25 at $N = 10^2$, 0.08 at $N = 10^3$, 0.03 at $N = 10^4$, and 0.01 at $N = 10^5$ simulations (Fig. 4.5a). Most of the confidence intervals at $N = 10^3$ contained the true ρ values, while some parameters showed significant error at $N = 10^1$ and $N = 10^2$ (see Fig. 4.5a, C_o and ω_s).

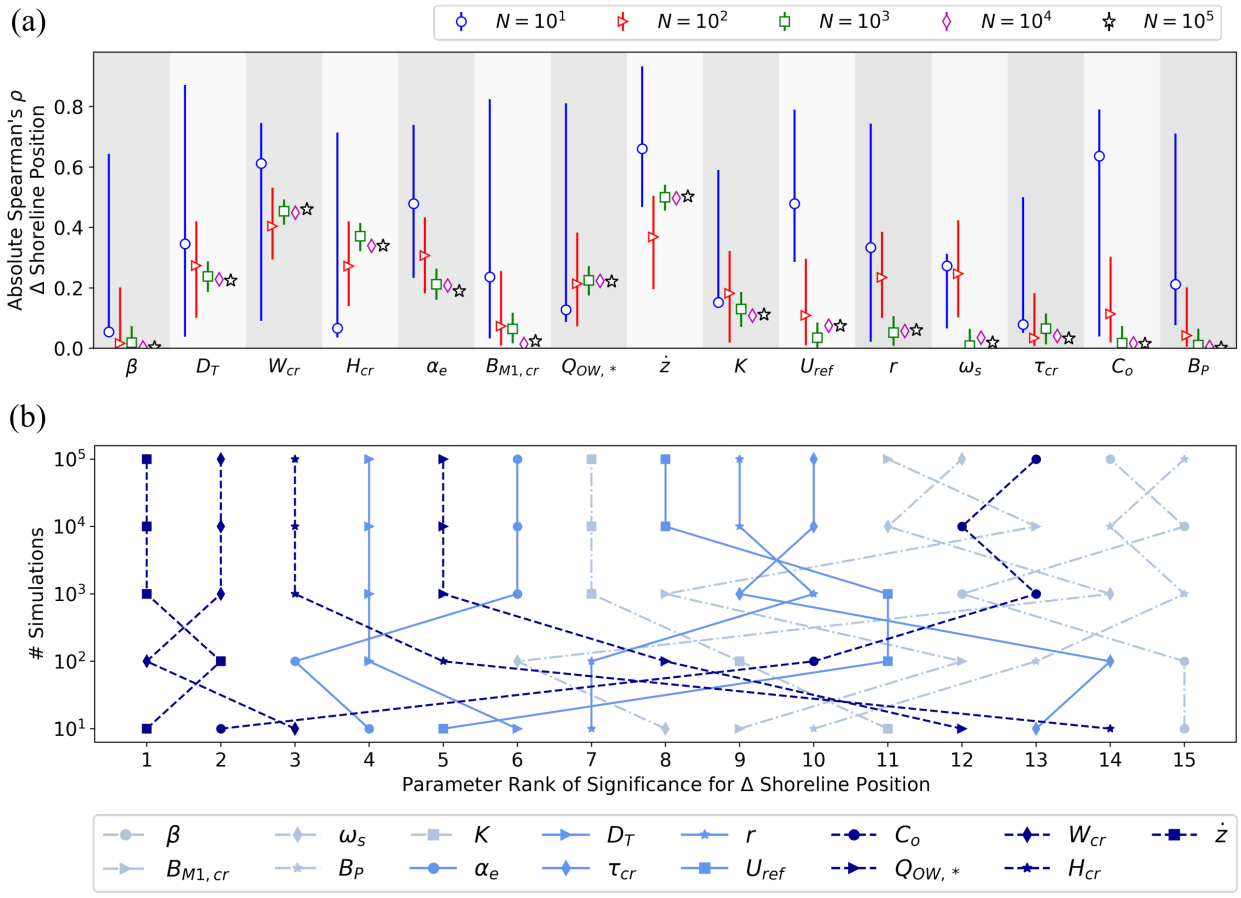

Figure 4.5: Convergence of the Spearman correlation results for change in shoreline position by (a) mean absolute value of Spearman's ρ with 90% confidence intervals and (b) rank of parameter significance.

As the confidence intervals converged, the parameter rankings also stabilized (Fig. 4.5b). If the rankings at $N = 10^5$ are considered "true" rankings, there were many deviations from the true rankings for $N = 10^1$ and $N = 10^2$ simulations. However, at $N = 10^3$ the 7 top-ranked parameters all stabilized to their true ranking. Three more parameters reached their true rankings (8-10) at $N = 10^4$, while the lowest 5 parameter rankings, all of which had ρ values near zero, continued to adjust between $N = 10^4$ and $N = 10^5$. Similar patterns were observable for the other result variables (see Appendix C Section 4).

Convergence of the Morris method results was evaluated by running five simulation sets, varying the number of trajectories of each set by an order of magnitude, from 10 trajectories to 100,000. Since each trajectory required *k+1* simulations, the number of simulations varied from 160 to 1.6 million. Figure 4.6 shows the MAEEs for change in shoreline position with 90% confidence intervals and associated parameter rankings. See Section 5 of Appendix C for Morris convergence plots of the other result variables.

Similar to the convergence results for Spearman correlation, the 90% confidence intervals for the Morris method's MAEEs decreased in range as the number of simulations increased, although there appeared to be substantially less interval overlap. The confidence intervals in Figure 4.6a had relatively large ranges for 10 trajectories ($N = 10^1$) [μ=40m; max=124m] and $N = 10^2$ [μ=28m; max=71], after which the interval ranges dropped considerably for $N = 10^3$ [μ=11m; max=26m], $N = 10^4$ [μ=3m; max=7m], and $N = 10^5$ [μ=1m; max=2m].

It is important to note the accuracy of the MAEE estimates and associated parameter rankings at $N = 10^1$ and $N = 10^2$. At $N = 10^1$, 5 of the 6 most significant parameters were ranked between 1 and 6, and 5 of the 6 most insensitive parameters were ranked between 10 and 15 (Fig. 4.6b). This pattern also holds true for the other result variables (see Appendix C Section 5). However, there was still the potential for significant error at $N = 10^1$. For example, in Figure 4.6b, the 2nd most sensitive parameter ($Q_{OW,*}$) was ranked 7th while the

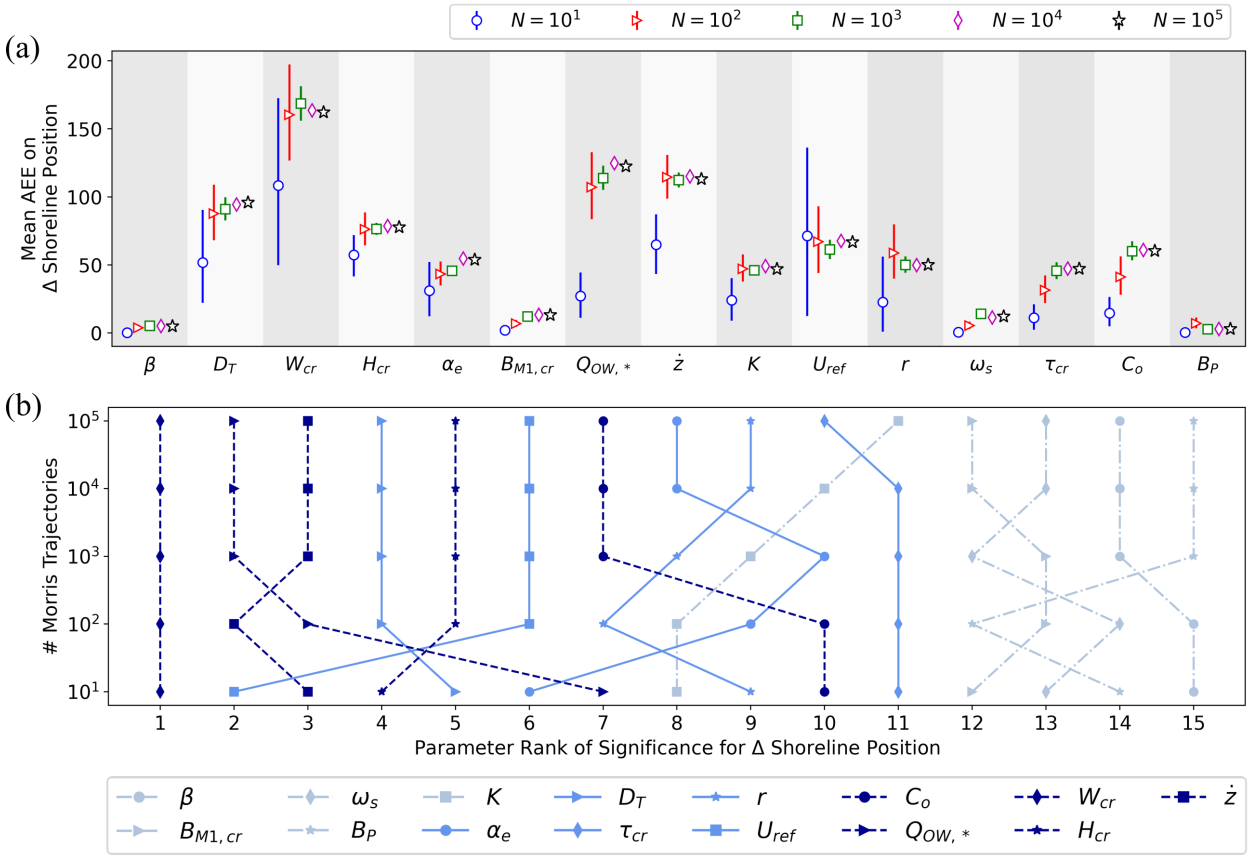

Figure 4.6: Convergence of the Morris method results for change in shoreline position by (a) mean absolute elementary effects with 90% confidence intervals and (b) rank of parameter significance.

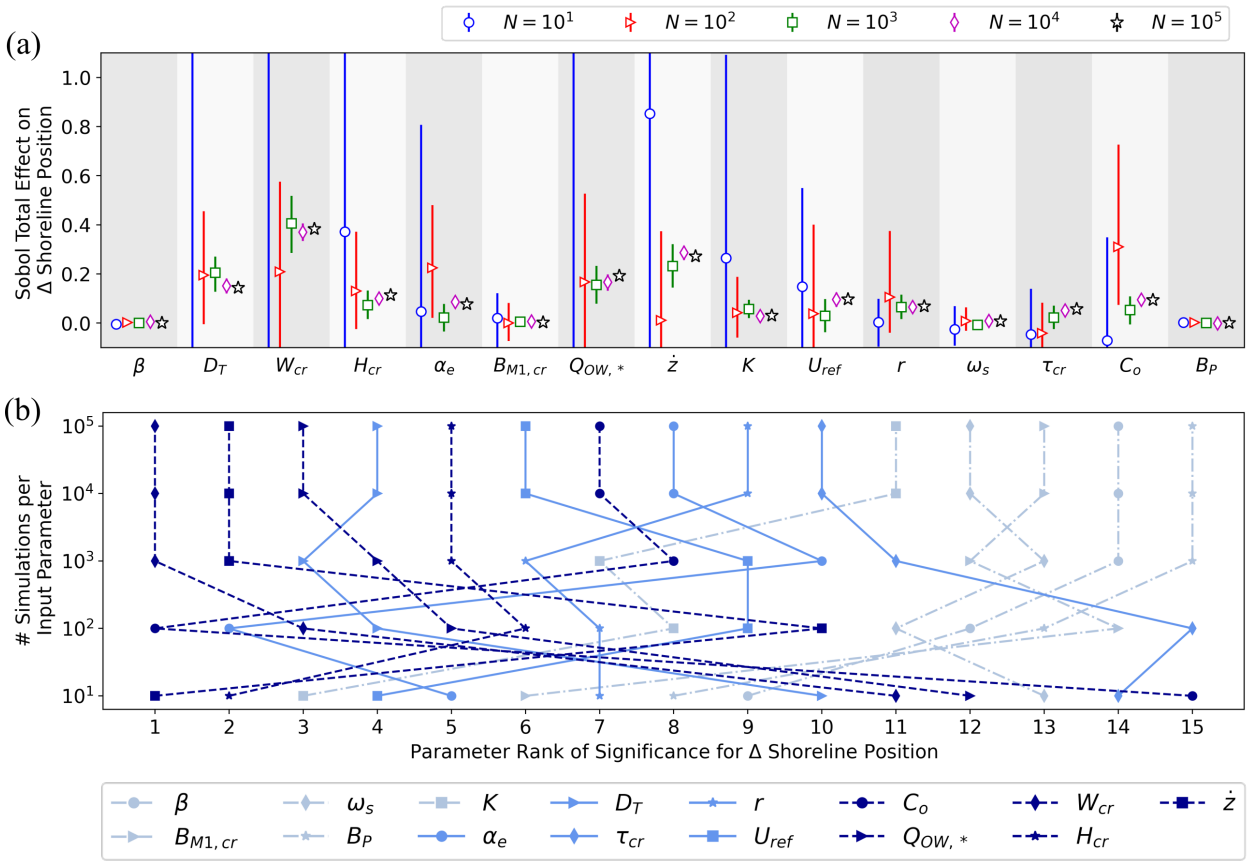

Figure 4.7: Convergence of the Sobol method results for change in shoreline position by (a) total effects with 90% confidence intervals and (b) rank of parameter significance.

6th most sensitive parameter (U_{ref}) was ranked 2nd at $N = 10^1$. This error was rectified at $N = 10^2$. The parameter rankings became mostly stable at $N = 10^3$ with only minor changes in rank for the least sensitive parameters as more simulations were added.

Sobol index convergence was tested over five orders of magnitude of computational effort, as the number of simulations per input parameter was varied from 10 to 100,000. The total effects and 90% confidence intervals are displayed in Figure 4.7a for each input parameter and the change in shoreline position result variable, with associated parameter rankings in Figure 4.7b. Sobol convergence results for all result variables are provided in Section 6 of Appendix C.

The 90% confidence intervals for the S_{T_i} estimates in Figure 4.7a varied widely with the number of simulations per input parameter (N). At $N = 10^1$, 7 of the input parameters had negative S_{T_i} estimates, three of which were well below zero (D_T=-0.38; W_{cr}=-0.8; and $Q_{OW,*}$=-0.1), and the average confidence interval range across all input parameters was 1.84. These numbers indicated a significant amount of numerical error in estimating S_{T_i} since these estimates should have been between 0 and 1. Increasing the number of simulations per input parameter to $N = 10^2$ reduced the confidence interval ranges in Figure 4.7a, but did not completely eliminate the numerical error. Interestingly, the confidence intervals appeared to worsen for some result variables when moving from $N = 10^1$ to $N = 10^2$; see results for barrier width and lagoon width, Figures C.6.1 and C.6.7 in Appendix C. At $N = 10^3$, numerical error in the indices was eliminated and confidence intervals narrowed.

Due to the numerical error in the S_{T_i} estimates and associated confidence intervals, parameter rankings at $N = 10^1$ and $N = 10^2$ were highly erroneous. At $N = 10^3$, the parameter rankings became meaningful, and were quite accurate when compared to the "true" rankings at $N = 10^5$, correctly grouping the top 5 and bottom 4 parameters. At $N = 10^4$, all of the parameter rankings were completely stable and did not change when moving to $N = 10^5$.

Convergence of the VARS i50 metric was also evaluated by increasing the number of star (base) sampling points from 1 to 10,000. With a perturbation scale of 0.1 and 15 input parameters, the number of simulations ranged from 150 to 1.5 million. The i50 results with 90% confidence intervals and associated parameter rankings are presented in Figure 4.8 for change in shoreline position. Similar plots for all result variables are presented in Section 7 of Appendix C.

Because the bootstrapped confidence intervals are generated by resampling the stars (base points) in VARS, there were no confidence intervals generated in the case of a single star ($N = 10^0$). At $N = 10^1$, the extent to which the confidence intervals overlap depended on

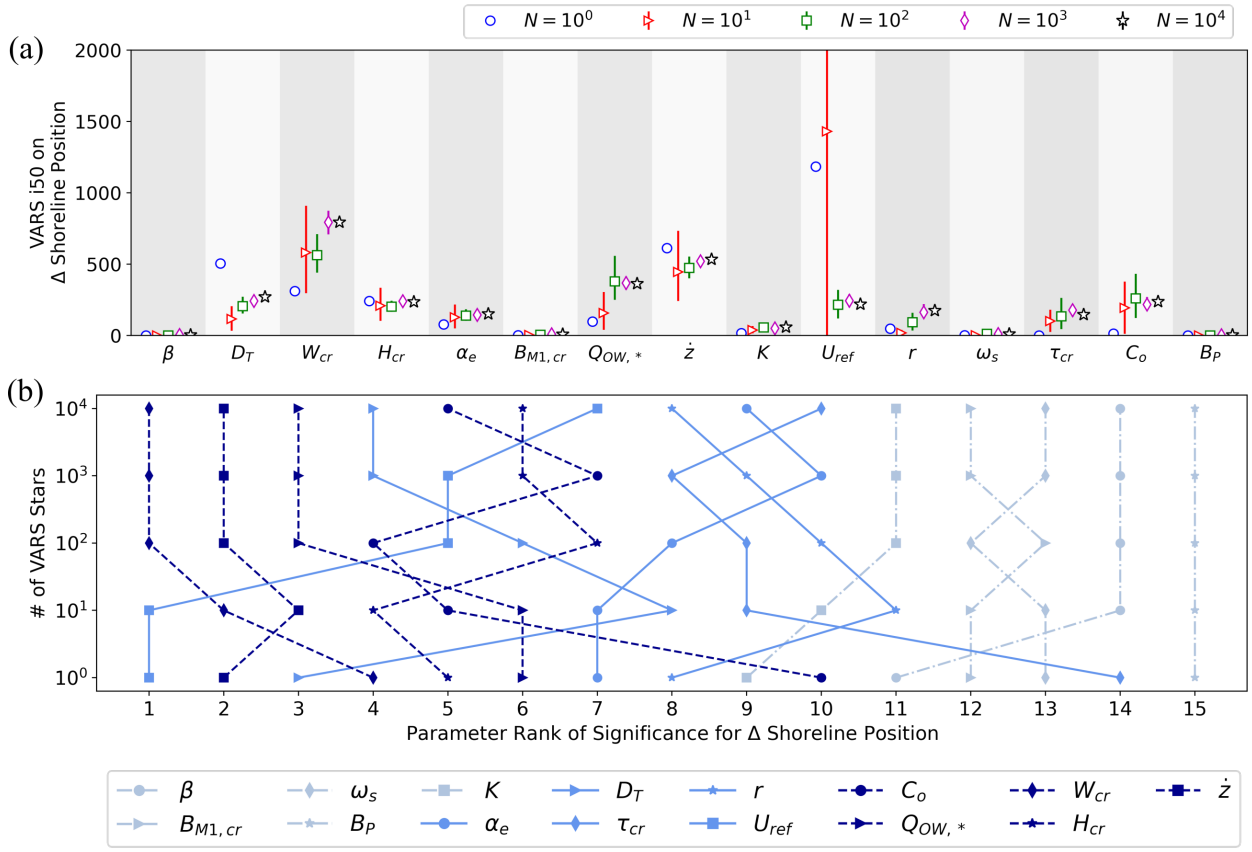

Figure 4.8: Convergence of the VARS method results for change in shoreline position by (a) VARS-i50 with 90% confidence intervals and (b) rank of parameter significance.

both the result variable and the input parameter. From Figure 4.8a, parameters like D_T and H_{cr} had relatively narrow intervals, while the U_{ref} interval was very large. The intervals narrowed as the number of stars increased, similar to the other methods. At $N = 10^3$, the confidence intervals mostly narrowed to provide a good estimate of the true value; however, there were some notable exceptions (e.g., W_{cr} in Figure 4.8a; U_{ref} in C.7.5 and C.7.7; τ_{cr} in C.7.6.).

The stabilization of the parameter rankings based on the i50 metrics also depended on the result variable. In Figure 4.8b, the rankings stabilized in groups at $N = 10^2$ and reached a more complete stabilization between $N = 10^3$ and $N = 10^4$. For example, at $N = 10^2$ the top 3 rankings were identified in the correct order while the other parameters were correctly grouped in ranks 4-7, 8-10, and 11-15. This same pattern was observed for interior marsh width (Fig. C.7.5), marsh depth (Fig. C.7.6) and lagoon width (Fig. C.7.7). Other result variables showed highly accurate rankings at low N values such as lagoon depth (Fig. C.7.8), which had perfect rankings at $N = 10^0$, and backbarrier marsh width (Fig. C.7.4), which showed mostly correct rankings at $N = 10^1$. Across all the result variables, parameter rankings nearly reached stabilization at $N = 10^3$, showing only minor variations in rank between $N = 10^3$ and $N = 10^4$.

4.3.4 Reliability

One hundred independent trials were conducted for all sensitivity methods to test their reliability under computational limitations. The number of simulations performed for each method were as follows: Spearman correlation = 1,000; Morris method = 1,600; Sobol method = 1,700; VARS method = 1,500. Note these values correspond to one of the orders of magnitude in the convergence plots. Parameter rankings were estimated for each trial,

and the percentage of correct rankings (defined as rankings within 1 position of the "true" or converged rank) were calculated for each result variable and input parameter as shown in Figure 4.9. Similar plots for the other result variables are included in Section 8 of Appendix C.

Comparing the top, middle, and bottom heatmaps in Figure 4.9, it is noted again that the result variable selected for analysis impacted the results. For example, the differences between the top rows of each heatmap in Figure 4.9 indicate that the reliability of the parameter rankings by Spearman correlation were considerably different depending on whether change in shoreline position, barrier width, or backbarrier marsh width was evaluated. This can be better visualized by comparing plots showing all of the result variables, which are provided for each sensitivity method in Figures C.8.3-C.8.6 in Appendix C.

The Morris method showed the highest reliability percentages across all result variables in Figure 4.9, followed by Spearman correlation, VARS, and Sobol. The Morris method also showed the highest reliability across all parameters for barrier height and lagoon width, although it was outperformed by VARS for interior marsh width and marsh depth (Fig. C.8.1), and also by lagoon depth, which showed near perfect reliability scores across all parameters (Fig. C.8.2). On average, the Sobol method consistently received the lowest reliability percentages across the result variables.

The same analysis was performed for the second computational constraint, which limited the number of model simulations between 10,000 and 20,000. The number of simulations in each method under this scenario were as follows: Spearman correlation = 10,000; Morris method = 16,000; Sobol method = 17,000; VARS method = 15,000. Figure 4.10 displays the correct ranking percentages for three result variables; the plots for the other result variables are included in Section 9 of Appendix C.

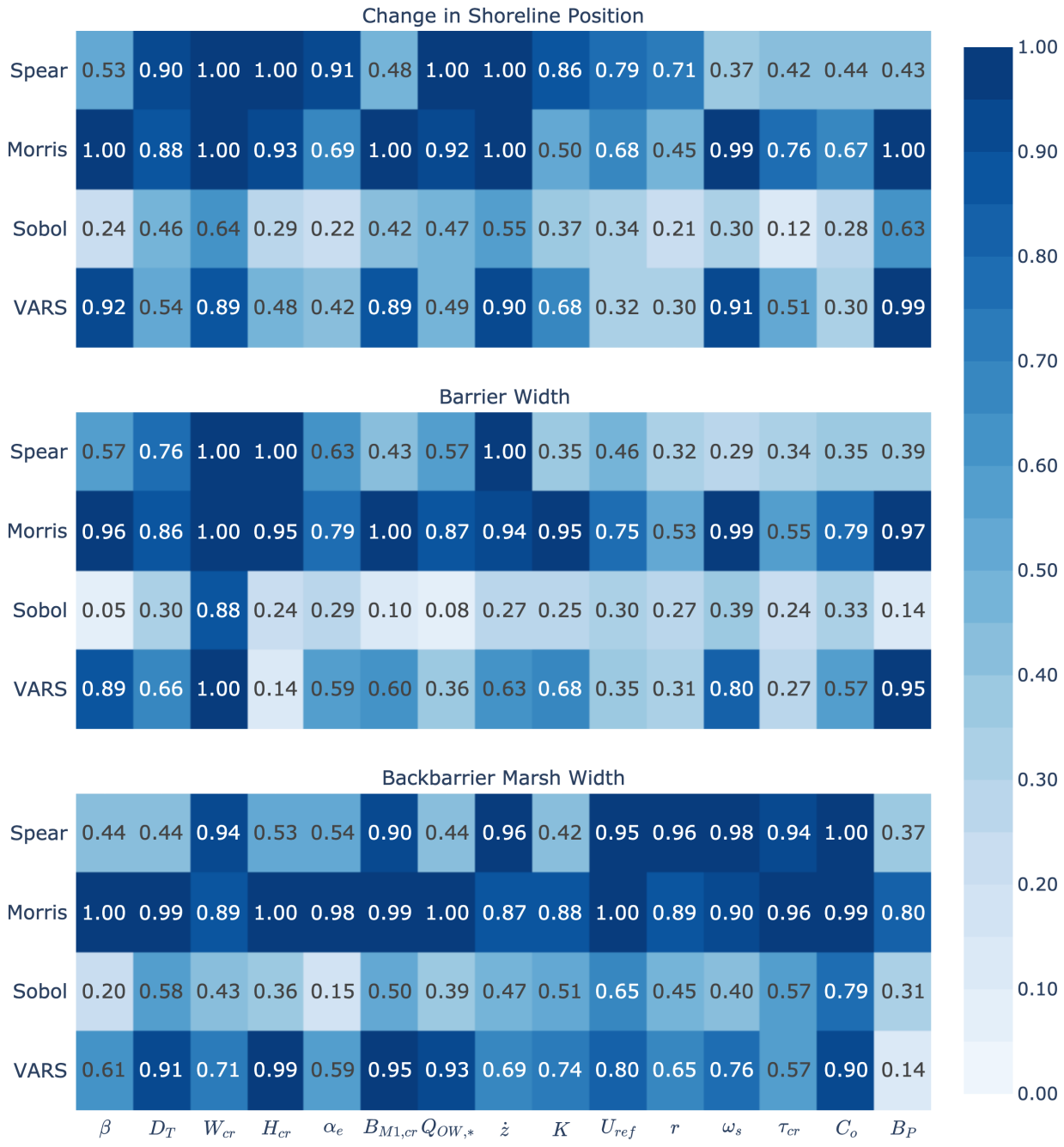

Figure 4.9: Probability of obtaining converged parameter ranking for 100 independent trials with 1-2k simulations. *Results shown by numerical value and color range for (top) change in shoreline position, (middle) barrier width, and (bottom) backbarrier marsh width.*

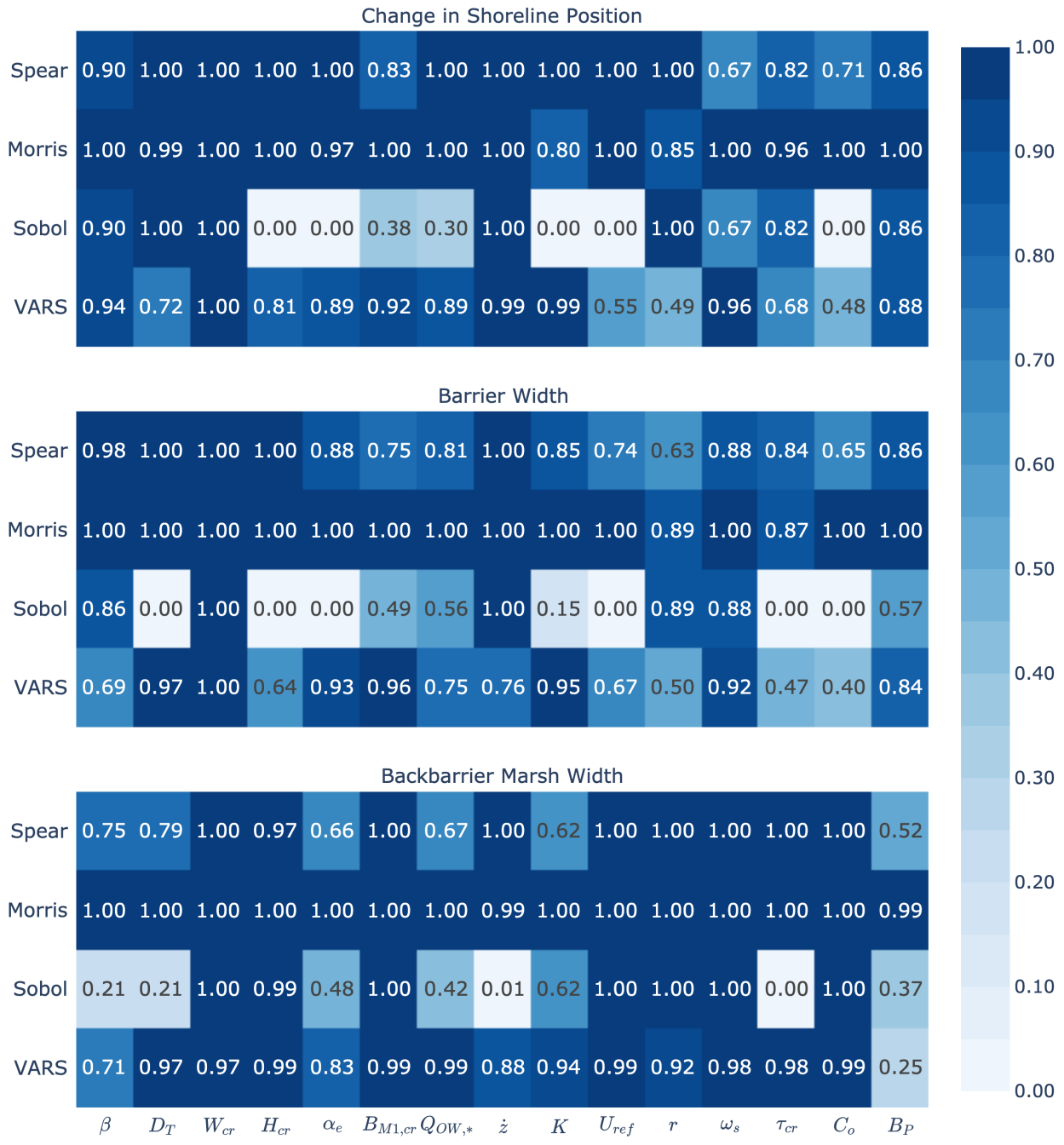

Figure 4.10: Probability of parameter ranking for 100 independent trials with 10-20k simulations. *Results shown by numerical value and color range for (top) change in shoreline position, (middle) barrier width, and (bottom) backbarrier marsh width.*

Again, for the result variables presented in Figure 4.10, the Morris method showed the highest reliability percentages while the Sobol method showed the lowest percentages. The only result variable where the Morris method was clearly outperformed was lagoon depth, for which VARS was again nearly perfect (Fig. C.9.2). On average, VARS was the second most reliable sensitivity method, although it appears that Spearman correlation outperformed VARS for select result variables such as change in shoreline position and barrier width (Fig. 4.10).

4.4 Discussion

One of the benefits of using the LTM17 model to evaluate the performance of global sensitivity analysis methods is the multiple outputs that it generates. Whereas other models are more narrow in their predictive scope, such as hydrologic models predicting streamflow or non-linear functions such as the Ishigami function [329], the latter of which is frequently used in testing sensitivity analysis methods [330], this long-term and large scale barrier island system model produces eight result variables. The results showed that the parameter sensitivities were highly dependent on the result variables, which was consistent with the previous LTM17 sensitivity study by Hoagland et al. [2] and suggests that modelers can and should use global sensitivity analysis to identify the input parameters most important to their results of interest, which echos the recommendation of Alipour et al. [331].

The results also showed that the performance of the global sensitivity methods varied by result variable, both in terms of their RFS values and associated parameter rankings, their convergence, and their reliability. For some result variables like lagoon depth (Fig. C.3.8), RFS values were remarkably consistent across sensitivity metrics, indicating similar distributions of the sensitivity metrics across all parameters. Most other result variables appeared

to show larger discrepancies in RFS, although not all discrepancies corresponded to disparate parameter rankings (e.g., see results for barrier height, Fig. C.3.2). While RFS values are useful in normalizing the various sensitivity metrics, they should be interpreted in conjunction with the parameter rankings for a more clear picture of the differences between methods. Additionally, parameter rankings interpreted in isolation from the RFS values could lead modelers to underestimate the performance of the methods, particularly for near-zero values (e.g., see marsh depth results, Fig. C.3.6).

From the results presented in Figure 4.3 and Section 3 of Appendix C, there is often considerable agreement among the sensitivity metrics as to which parameters are most significant (ranked) and least significant (screened). With some exceptions, the results show that with enough simulations for sensitivity metric convergence, all of the methods in this study were generally capable of ranking and screening groups of parameters. For example, the methods could often identify the top or bottom 'x' number of parameters, while allowing for minor variations in rank within that group. The correlation method sensitivity metrics, R^2 and Spearman's ρ, were the only consistent exceptions, and only for certain result variables (e.g., barrier width, Fig. 4.4a; interior marsh width, Fig. C.3.5; and lagoon depth, Fig. C.3.8).

On average, the results suggest there is no advantage to using R^2 or Spearman's ρ in this context, as these metrics provided similar results across most result variables. For the VARS metrics, the consistency in top-ranked parameters showed the ability of VARS in factor prioritization regardless of which range of scales was chosen for integration. However, more discrepancies appeared between the VARS metrics for the lower rankings (Fig. 4.3b). Comparing the VARS metrics with those from other methods, the i50 rankings seem to be most closely aligned with the Sobol rankings. This is seen in Figure 4.3b for i50 ranks 3 through 10, and for other result variables such as barrier width and backbarrier marsh width (Fig. 4.4a,b). The Morris and factorial results are strongly related, which was expected

given their methodological similarity. However, there are some significant discrepancies between these metrics and others, such as the correlation method differences mentioned above and differences with the Sobol and VARS metrics as seen in Figure 4.4a, where, for example, $Q_{OW,*}$ is ranked 2nd by factorial and Morris, but 6th and 7th by Sobol and VARS. Interpretation of these discrepancies should involve the recognition of differences in method, where factorial and Morris involve first-order derivative calculations across the large portions of the parameter space, while Sobol and VARS consider more of the interior of the parameter space. Thus, the combined results in Figure 4.4a may suggest that $Q_{OW,*}$ is more sensitive at one or both ends of the parameter range, which the interaction plots from Hoagland et al. [2] confirm.

Convergence and reliability of sensitivity results are two other considerations that modelers should take into account. The sensitivity metrics, 90% confidence intervals, and associated rankplots in Figures 4.5-4.8 show how these methods performed for computational limits across five orders of magnitude. Large and overlapping confidence intervals for Spearman's ρ values at 10 and 100 simulations indicate that even though parameter rankings may seem accurate for the highest parameters, very few conclusions may be drawn with a high degree of confidence. The same is true for the Sobol method at 10 and 100 simulations per input parameter and some of the VARS results, depending on the result variable. The Morris method, however, showed excellent performance, even at the two lowest computational levels. At 10 trajectories, the confidence intervals are still relatively large, compared to the converged results; however, there is significantly less overlap between them, in comparison to the Spearman and Sobol results, allowing conclusions to be drawn for ranking and screening with minimal simulations, a finding consistent with Sarrazin et al. [332] and references therein. Similar to the Morris method results, VARS showed an ability to rank and screen groups of parameters for low simulation counts, albeit with more variability between result

variables.

The final part of the analysis demonstrated reliability by illustrating how the convergence of each method impacted sensitivity results for 100 independent trials under computational constraints. The Morris method proved to be the most reliable method for all parameters under both constraint scenarios, followed by VARS, Spearman correlation, and then Sobol. Although Spearman was able to consistently identify top-ranked parameters, its inabilities to consistently identify the lowest-ranked parameters decreased overall reliability. The Sobol method, though it offers a robust exploration of the parameter space, requires a large number of simulations to avoid numerical error. Thus, for the lower computational constraint, the Sobol results proved to be very unreliable. The reliability of the Sobol method improved at the higher computational constraint, particularly for the most sensitive parameters, although it still underperformed Morris and VARS.

Aside from method performance, modelers also likely consider, either explicitly or implicitly, the complexity of the approach and the intuitiveness of the results when selecting their sensitivity analysis method. From our own perspectives, correlation is the simplest of the methods to implement and requires no additional learning beyond what is taught in introductory statistics courses. The remaining methods, ranked in complexity from least to greatest, are factorial, Morris, Sobol, and VARS. We believe that the intuitiveness of the sensitivity results follows a reverse order, with correlation results being most intuitive and VARS results the least intuitive - the latter is discussed at length by Puy et al. [22]. However, as seen with these methods, the robustness of the method tends to increase with complexity, echoing Wang and Solomatine [322]. Correlation coefficients are easy to calculate but provide very little information about the model, relatively speaking. The factorial and Morris methods are more complex, averaging first-order derivatives across the full parameter space and randomly sampled interior of the parameter space, respectively. The Sobol method is even more

complex, with conditional mean and variance calculations, though it provides a wealth of information, including both main and total effects, which offer quantitative measures of the variance explained by parameters and their interactions across the entire parameters space. The main and total effects may also be used to estimate the contribution of parameter interactions to the total variance. Although VARS is the most complex and least intuitive method, it provides a nice variety of variogram-based metrics, accounting for different ranges of perturbation scales, and also can provide estimates of the Morris and Sobol sensitivity metrics without running additional simulations.

4.5 Conclusions

In this study, five global sensitivity analysis methods were applied to a long-term coastal morphodynamics model to compare their results, computational burden, convergence, and reliability. Across all of the evaluation criteria, the Morris method achieved top performance, particularly for the convergence and reliability analyses through excellent ranking and screening at low simulation counts. VARS followed Morris in terms of performance, but was still successful in identifying the high and low ranking parameter groups. VARS outperformed the Sobol method, both in terms of convergence and reliability, and at lower computational expense. Although the correlation method was able to identify groups of the most sensitive parameters, significant discrepancies were found between its results and the other methods for certain results variables.

The most appropriate sensitivity analysis method for a given modeling application will be one that balances the computational expense and quality of results. For models like the coastal morphodynamics model presented herein, modelers should consider using the Morris, Sobol, or VARS method, or some combination of the approaches. The correlation and

factorial methods, while generally capable of identifying groups of the highest-ranking parameters, are not preferred over the other methods due to their lower performance across many of the evaluation criteria and ranking discrepancies with the more robust methods. For models with fast runtimes, like the LTM17 model, and with sufficient availability of computational resources, Sobol and VARS are excellent options for factor prioritization and can provide additional insights about the model and its parameters, as discussed above. Where computational constraints exist, VARS can provide an alternative to the expensive Sobol method, while the Morris method proved to quite reliable for low simulation counts due to its strength in both factor ranking and screening.

Acknowledgements

This material is based upon work that is partially supported by the U.S. Army Corps of Engineers through the U.S. Coastal Research Program (under Grant No. W912HZ-20-2-0005), the National Science Foundation (under Grant Numbers 1735139 and 1630099), and Virginia Sea Grant College Program Project R/72155T funded by the National Oceanic and Atmospheric Administration's National Sea Grant College Program, U.S. Department of Commerce (under award NA18OAR4170083). The statements, findings, conclusions, and recommendations are those of the author(s) and do not necessarily reflect the views of the U.S. Army Corps of Engineers, the U.S. Coastal Research Program, the National Science Foundation, Virginia Sea Grant, the National Oceanic and Atmospheric Administration, or the U.S. Department of Commerce. The authors acknowledge Advanced Research Computing at Virginia Tech for providing computational resources and technical support that have contributed to the results reported within this paper. URL: https://arc.vt.edu/.

Chapter 5

Modeling Decadal Evolution of a Mid-Atlantic Barrier Island Under Sea Level Rise and Management Scenarios

Steven W.H. Hoagland[1], Jennifer L. Irish[1], Robert Weiss[2,3], Sean Vitousek[4,5]

[1]Department of Civil and Environmental Engineering, Virginia Tech, Blacksburg, VA

[2]Department of Geosciences, Virginia Tech, Blacksburg, VA

[3]Academy of Integrated Science, Virginia Tech, Blacksburg, VA

[4]United States Geological Survey, Pacific Coastal and Marine Science Center, Santa Cruz, CA

[5]Department of Civil & Materials Engineering, University of Illinois at Chicago, Chicago, IL

Abstract

This study provides an evaluation of long-term projected changes to Assateague Island, a mid-Atlantic barrier island, under sea level rise, overwash, and coastal management scenarios. Low elevation backbarrier marsh platforms were found to be extremely vulnerable to moderate and high SLR rates ($\geq$ 5 mm/yr), but were sustained by thin-layer placement at average rates greater than or equal to SLR. Sustaining the marsh using thin-layer placement did not contribute to the long-term sustainability of Assateague Island, which is more susceptible to height drowning under low overwash scenarios. High sea level rise and overwash rates increased shoreline retreat rates and reduced island width for most of Assateague Island, although regular beach nourishment proved to alleviate these conditions, even for the highest SLR rate. Reductions and increases in dune elevation altered shoreline retreat, island width, and island height as expected; however, they did not appear to alter the long-term sustainability of the island.

5.1 Introduction

Barrier islands are found along ten percent of continental shorelines across the world [7]. Generally speaking, these islands are long and narrow, and shelter their landward waterbodies from incident waves, allowing for the development and sustainability of salt marsh on their backbarrier shorelines [8]. These islands are prevalent along the United States (U.S.) Atlantic and Gulf Coasts, and provide a variety of benefits to coastal communities such as reduced flood levels from (extra)tropical storm surge and protected ecosystems for fish, shorebirds, and other wildlife [e.g., 9, 12, 333]. These islands also attract tourists and vacationers, which increase local economic activity [334].

The benefits provided by these barrier-marsh-lagoon systems are closely linked with their morphology, which are subject to changes by erosion and deposition of sediment. Longshore sediment transport, driven by oblique currents and waves [335], plays a significant role in barrier morphodynamics, including spit development, inlet migration, and even the longshore migration of entire islands [e.g., 160, 336]. Cross-shore sediment transport is also significant, altering the barrier profile along the shoreface [337, 338] and moving sediment between the shoreface and lagoon through tidal inlets [e.g,. 64, 114, 339, 340]. Punctuated transport of sediment to the subaerial island and lagoon occurs during storm events through both overwash and breaching processes [e.g., 71, 295]. These processes and morphodynamic changes are all impacted by rises in mean sea level (MSL), projections of which range between 0.6 and 2.2 meters for the contiguous U.S. in the 21st century [341].

In the interest of protecting and preserving the benefits of barrier islands, coastal scientists, engineers, and planners have considered myriad protection and restoration alternatives [e.g., 342]. Coastal protection received relatively little attention in the U.S. prior to 1930, when the first federal advisory board on beach erosion was created to assist state and local governments with carrying out scientific studies on erosion and possible solutions; however, interest quickly expanded with the increasing role of the U.S. federal government through the U.S. Army Corps of Engineers (USACE) [343, 344]. Throughout the 20th century, coastal protection was geared toward "hard" engineered structures, such as seawalls and breakwaters, and artificial beach nourishment, the latter of which was viewed as a "soft" or low-impact alternative to hard structures, though its implementation was found to be costly and its benefits temporary [343, 345, 346, 347, 348].

In recent decades, coastal scientists and planners have continued to shift away from hard structures, mainly due to their negative environmental impacts and unintended downdrift consequences [348], toward softer or hybrid coastal restoration approaches that offer similar

protection to traditional hard structures while meeting environmental goals. The "functional restoration" concept proposed by Rosati [349] exemplifies this balance, considering the geometry of a restored barrier island, geologic constraints such as availability of local sediment, and environmental concerns such as habitat development and protection. Many soft restoration approaches encourage the growth or development of natural coastal features, or are designed to mimic them and provide similar ecosystem benefits; thus, these types of restorations are called Natural and Nature-Based Features, or "NNBF" [31]. Though the potential environmental benefits of NNBF were well known, it was recognized that further quantification of their performance was needed [31, 350, 351]. Cunniff and Schwartz [352] brought together 19 experts from industry, government, and academia to discuss the then-current knowledge of NNBF performance, and produced a summary document that highlighted published studies and completed projects. Figlus et al. [353] highlight a more recent collection of 16 publications on NNBF performance, including case studies and engineering designs.

Although there has been a focus on NNBF implementation and performance, there has been relatively few studies on predicting the long-term impacts of these measures, especially for particular islands. Rosati et al. [354] tested nourishment alternatives on their Migration, Consolidation, and Overwash (MCO) model for a typical Louisiana barrier island, and found that a single, large nourishment project, prevented island migration, while the smaller, successive nourishment projects allowed significant migration. Modeling studies by McNamara and Werner [278], Lazarus et al. [355], Brad Murray et al. [356], and Gopalakrishnan et al. [357] couple predictions of shoreline erosion with nourishment decisions by socioeconomic agents and highlight system complexities and consequences that can arise from parochial decisions, suggesting the need for a broader view of coastal management decisions, both spatially and temporally. Using observations from Hurricane Sandy, Rogers et al. [280] modeled overwash reduction by dune creation and found that artificial reductions in overwash could

lead to long-term drowning. Miselis and Lorenzo-Trueba [297] modeled a similar scenario for a New Jersey barrier island, also finding that implementation of coastal protection measures that minimized or eliminated overwash resulted in faster island drownings. Tenebruso et al. [314] simulated nourishment and development-based reductions in overwash in a hindcast modeling study of Long Beach Island, New Jersey. Most recently, Anarde et al. [358] developed the CASCADE modeling framework, which couples Barrier3D [219] with BRIE [213], to simulate the influence of management decisions, such as roadway protection or removal, dune building, and nourishment, for the managing coastal communities and those adjacent.

In this study, we use a long-term barrier island morphodynamics model developed by Lorenzo-Trueba and Mariotti [1] to simulate the evolution of a mid-Atlantic barrier island under recently updated sea level rise (SLR) projections and coastal management scenarios. This modeling study highlights island vulnerabilities to SLR and provides insights as to which management strategies may lead to the best long-term impacts. Such insights may be helpful for coastal resource managers and planners in deciding which management strategies to pursue.

5.2 Study Site

This study is focused on Assateague Island, which is the northernmost barrier island in Virginia and also Maryland's southernmost island, as the majority of it extends north into Maryland (Fig. 5.1). Assateague is separated from Fenwick Island to the north by Ocean City Inlet and Wallops/Assawoman Island to the south by Chincoteague Inlet. Just northeast of Chincoteague Inlet is Chincoteague Island, which lies in the southern part of Chincoteague Bay, landward of Assateague. Wallops/Assawoman, Chincoteague, and the southern portion of Assateague Island reside in Accomack County, VA, which covers approximately 450 square

miles and has a population of approximately 33,400.[1] The Maryland portion of Assateague is in Worcester County, which covers approximately 470 square miles and is home to about 52,500 people.[2]

5.2.1 Jurisdiction and Use

Three separate jurisdictions cover Assateague Island, including the Assateague Island National Seashore (ASIS), which is managed by the National Park Service (NPS), Assateague State Park, managed by the state of Maryland's Department of Natural Resources, and the Chincoteague National Wildlife Refuge (NWR), managed by the U.S. Fish and Wildlife Service (USFWS); see Figure 5.1 for approximate jurisdictional zones. Each authority has their own mission and goals, though they overlap in their concern for protection of natural resources, wildlife conservation, and provision of recreational activities such as beach-going, wildlife viewing, hiking, hunting, and camping.

5.2.2 Morphology

Assateague Island is approximately 60 km in length, bounded by Ocean City Inlet at its northern end and Chincoteague Inlet at the south. Although no other inlets currently exist between Ocean City and Chincoteague, there is strong evidence that at least 11 inlets existed along the coast of Assateague Island over the last 300 years [359]. Following the classification scheme of Hayes [360], Assateague Island is a microtidal (<= 1 m), wave-dominated barrier, as shown by its long, narrow form and widely spaced inlets. The island's width varies from 260 m to 2,000 m and its height averages 2 m [361]. Dune heights average 3.6 m across the island and range from 0.9 to 8.0 m [362], with distinct zones of dune type and height. For

[1] U.S. Census Bureau, https://data.census.gov/profile/Accomack_County,_Virginia?g=050XX00US51001
[2] U.S. Census Bureau, https://data.census.gov/profile/Worcester_County,_Maryland?g=050XX00US24047

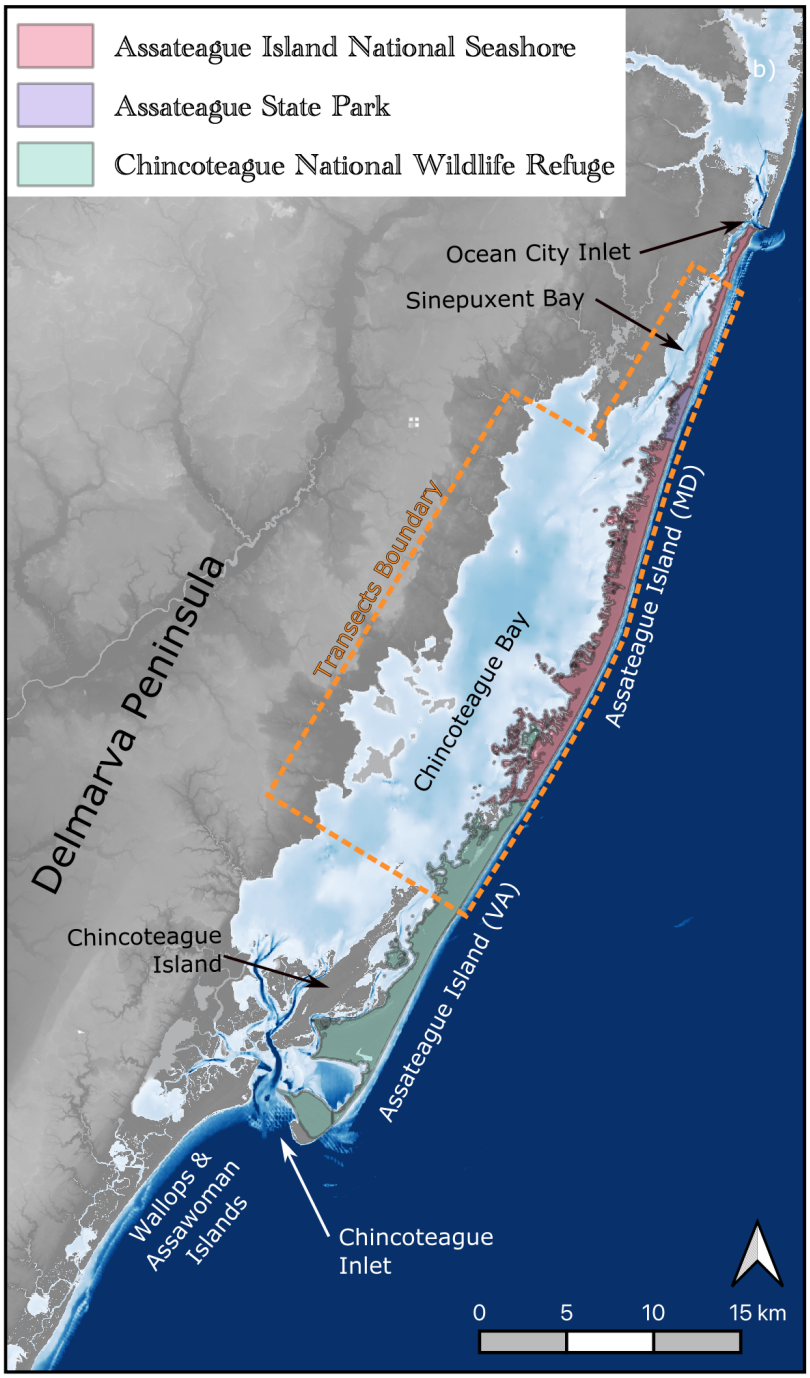

Figure 5.1: Study Site: Assateague Island. *Background from NCEI 2014 Digital Elevation Model [3]. Assateague jurisdictions from Assateague Island National Seashore [4].*

example, dunes on the the northern end are not managed and are characterized by lower elevation and varied spacing, while the dunes fronting Assateague State Park are linear and managed to a higher elevation. A narrow band of salt marsh lines the backbarrier shoreline, with the largest marsh platforms appearing near the middle of Chincoteague Bay [363]. The backbarrier tidal range varies between 0.07 and 1.1 m, with the largest ranges occurring near Chincoteague Inlet (∼1 m) and Ocean City Inlet (∼0.8 m), and the smallest ranges occurring in the middle of Chincoteague Bay (∼0.14 m) and Sinepuxent Bay (∼0.07 m) [6]. Chincoteague Bay is 10 km wide and has an average depth of 1.4 m, with a 2-3 m deep channel that runs through the west-central part of the bay [364].

5.2.3 Morphodynamics and Management Efforts

Net longshore sediment transport is to the south along Assateague Island, estimated between 115,000 and 220,000 m^3/yr [365]. Ocean City Inlet, which was originally planned as a joint construction project between Worcester County, Ocean City, and USACE, but ultimately postponed due to the start of the Great Depression in 1929, developed naturally as a result a large offshore hurricane in 1933 [366]. USACE stabilized Ocean City Inlet in 1935, which led to trapping of longshore transport updrift of the inlet and significant increases in erosion at the northern end of Assateague Island [114]. The northern shoreline moved landward between 6 and 8 m/yr, on average, as a result of inlet stabilization efforts [365]. However, since the start of the North End Restoration Project in the early 2000s, semiannual dredging of Ocean City Inlet and its tidal deltas and subsequent placement in Assateague's nearshore region has led to accretionary trends between 2005 and 2020 [367]. The middle of the island is largely stable [361], while the southern portion, managed by Chincoteague NWR, has experienced net erosion since 2005 and lengthening of the recurved spit (Fishing Point) further south at an average rate of about 30 m/yr [367].

As a wave-driven barrier, Assateague morphology is significantly impacted by storm events, especially the northern end with low, spatially varied dunes. As of 1977, the northern end was experiencing overwash approximately 5 times per year [368]. Leatherman [114] noted that these overwash events primarily contributed to vertical aggradation of the island and would only reach the lagoon when the barrier width was below a critical width threshold. It has been estimated that most ($\sim$ 75%) of the sediment entering Chincoteague and Sinepuxent Bays comes from overwash or aeolian transport, with the remaining amount coming from erosion of the backbarrier shoreline [363, 369].

Assateague has also been historically impacted by breaching events. Seminack and Mcbride [359] identified 11 sites of historical inlets along the modern coast of Assateague that occurred since the mid-1700s. This underscores the argument by Charles E. Bartberger [339], that sedimentation rates in Chincoteague Bay are far lower than previous centuries due to the closing of historical tidal inlets. Recent breaches have been observed on Assateague at Swan Pool during Hurricane Irene (2011) and Sandy (2012), although both of these breaches closed naturally within 2 weeks [365]. To reduce the occurrence and impacts of overwash and breaching, artificial dunes have been constructed in various locations since 1950, as documented by Schupp [361]. The ongoing management approach for ASIS by the NPS is detailed in their updated 2021 General Management Plan, which includes maintaining existing artificial dunes and continuing to place dredged material from Ocean City Inlet at the northern end [370].

5.3 Methods

The long-term barrier-marsh-lagoon model developed by Lorenzo-Trueba and Mariotti [1], hereafter 'LTM17' model, was extended to simulate the evolution of Assateague Island under

SLR and coastal management scenarios. Due to model limitations, the southern portion of Assateague was excluded from the simulations. A brief description of the model and an overview of this study's simulated scenarios are presented below.

5.3.1 Barrier Island Model

The LTM17 model is an idealistic 1D barrier system transect model that simulates geometric changes to the coupled barrier-marsh-lagoon system on the order of decades to centuries. System geometry is tracked by 10 state variables including both horizontal positions of the shoreface toe (X_T), shoreline (X_S), backbarrier (X_B), backbarrier marsh (X_{M1}), interior marsh (X_{M2}), mainland-marsh intersection (X_{M3}), and mainland (X_L), and vertical positions defined by barrier height (H_B), marsh depth (D_M), and lagoon depth (D_F). These state variables change in response to sediment fluxes between subsystems, including shoreface flux (Q_{SF}), overwash flux (Q_{OW}), tidal inlet dispersion (I_{osl}), and sediment exchange between the lagoon and marsh platforms (I_{bml} and I_{iml}). The marsh platforms also generate organic sediment (O_{bm} and O_{im}), which increases marsh platform elevation over time. An example LTM17 model transect is displayed in Figure 5.2 with state variables and sediment flux terms.

SLR rate and overwash flux are the two primary drivers of system changes in the LTM17 model. Because the model assumes an equilibrium shoreface profile with a specific depth of closure, SLR causes the profile to increase in elevation and, to preserve mass, shift landward, following a Bruunian response [169]. These changes also remove the island from island height and island width equilibria, engendering overwash based on the volume deficit concept from Leatherman [114]. The modeled overwash process removes sediment from the shoreface and seaward part of the island, and divides the deposition into three zones: 1) the top of island,

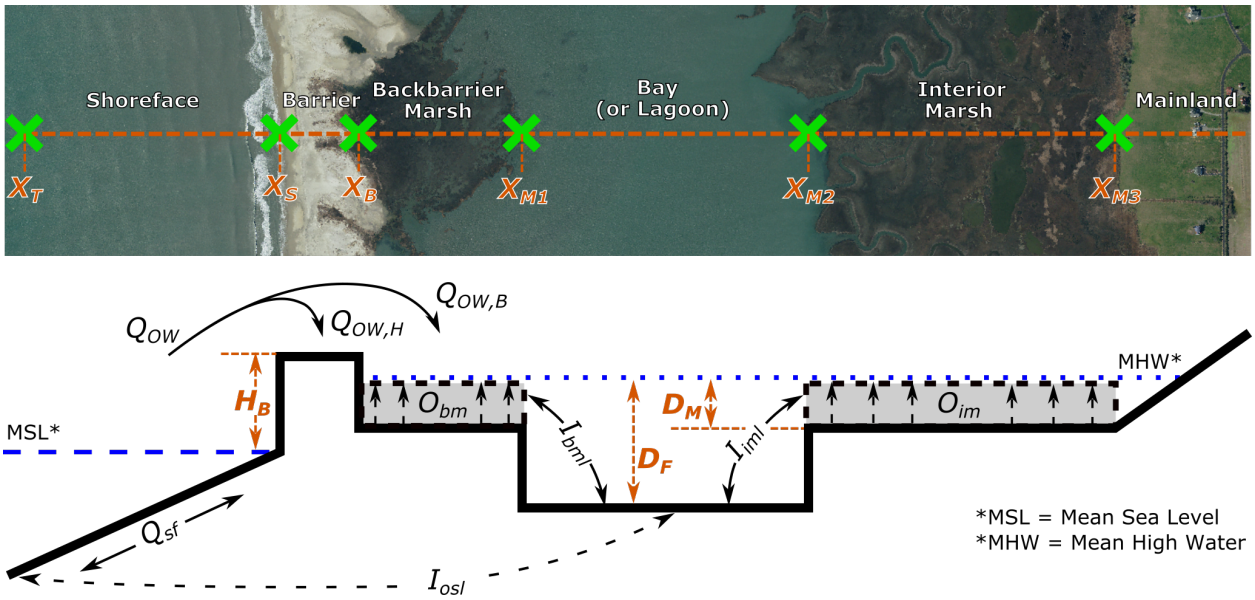

Figure 5.2: LTM17 Model Transect and State Variables. *Modified from Lorenzo-Trueba and Mariotti [1] and Hoagland et al. [2]. Aerial image of Assawoman Island section from [5].*

increasing its height; 2) the backbarrier marsh, increasing island width; and 3) the lagoon, extending the backbarrier marsh boundary landward. For a full description of these and other processes in the LTM17 model, see Lorenzo-Trueba and Mariotti [1] and references therein.

Transect Parameterization

The LTM17 model simulates the long-term evolution of independent transects, each of which must be parameterized with initial system geometry, forcing conditions, and sediment transport-related factors associated with the marsh and lagoon. Some parameters, like SLR rate, are the same for all transects; the values for these parameters are presented in the supplementary material (Table D.1, Appendix D). Table 5.1 provides a list of the parameters that were assigned transect-specific values, along with average, maximum, and minimum values for the island and their associated data source(s).

Table 5.1: Transect Parameterization Data and Sources

Parameter	Mean	Min	Max	Data Source(s)
Initial Lagoon Width [B_F]	6,000	770	10,700	[3, 6]
Initial Lagoon Depth [D_F]	1.6	0.7	2.3	[3]
Initial Backbarrier Marsh Width [B_{M1}]	870	0	2,800	[3, 6]
Initial Interior Marsh Width [B_{M2}]	750	0	5,000	[3, 6]
Initial Marsh Depth [D_M]	-0.2	-0.6	0	[6]
Tidal Range [r]	0.15	0.07	0.5	[6]
Initial Barrier Width [W_B]	510	50	1,630	[3, 6]
Initial Barrier Height [H_B]	1.6	0.8	2.5	[3]
Overwash Multiplier [$Q_{OW,X}$]	0.6	0	1	[362]
Critical Bed Shear Stress [τ_{cr}]	0.19	0.16	0.2	[361]

Many of the parameters listed in Table 5.1 are initial geometries, which were extracted for each transect from a 3 m resolution topography/bathymetry digital elevation model [3], and a shapefile of salt marsh boundaries from Defne and Ganju [6]. Two hundred (200) shore-perpendicular transects were generated at 100 m spacing along Assateague Island and numbered sequentially from south to north. These transects were then subdivided by shoreline, marsh, and lagoon boundaries, as determined by the data sources in Table 5.1. Lengths and average DEM elevations were then calculated for each subdivided transect segment. Select transect segments and associated data are shown in Figure 5.3.

Spatially varied backbarrier marsh depth and tidal range values were extracted exclusively from the Defne and Ganju [6] dataset. Dune crest elevations, although not explicitly accounted for in the LTM17 model, were extracted from Sturdivant et al. [362] and averaged for each transect. These dune crest elevations were then converted to an overwash multiplier ($Q_{OW,X}$) between 0 and 1; the highest dune elevation was assigned an $Q_{OW,X}$ value of 0 and the lowest a value of 1, with all other dune elevations receiving a linearly interpolated $Q_{OW,X}$ value between 0 and 1. The critical bed shear stress (τ_{cr}) parameter was also spatially varied between 0.16 and 0.2 across the transects based on data from Schupp [361], which showed

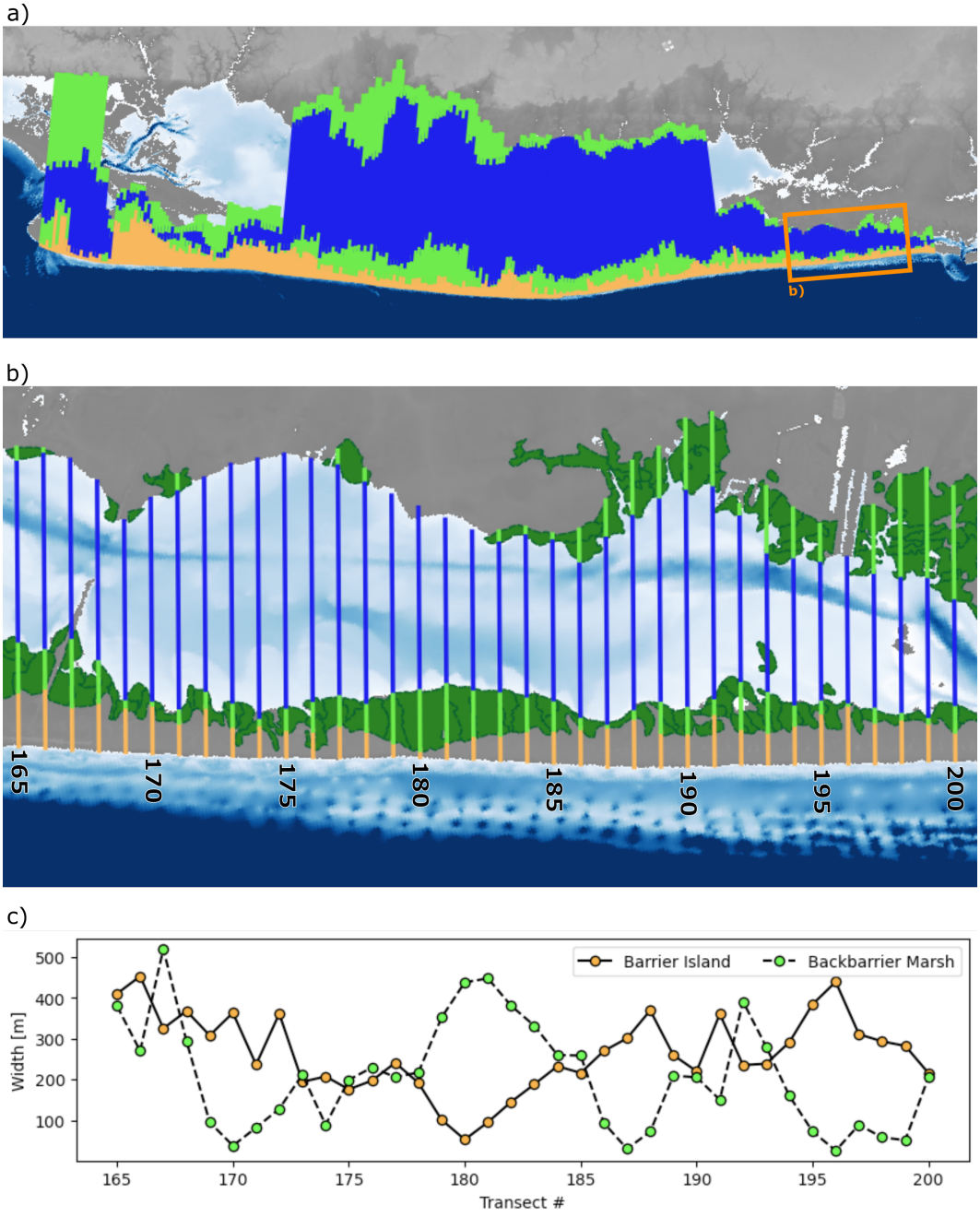

Figure 5.3: Example of Transect Segmentation and Parameterization. *a) Transects colored by subaerial island (orange), marsh (green), and lagoon (blue) zones. Note: more transects are shown here than were included in the modeling study. b) Zoomed in image of transects 165-200, overlaid on NCEI 2014 Digital Elevation Model [3] and marsh dataset from Defne and Ganju [6]. c) Extracted barrier island and backbarrier marsh widths from transects 165-200.*

Table 5.2: Shoreline Change Calibration Data

Shoreline Region†	Model Transects	Obs. Change Rate [m/yr]	Obs. 15-yr Change [m]	Modeled 15-yr Change [m]
N-ASIS	168-200	-2.01	-30.2	-30.5
ASP	152-167	-0.64	-9.6	-7.4
S-ASIS	36-151	-0.87	-13.1	-11.5
N-CNWR	1-35	-0.72	-10.8††	-5.5

†Abbreviations: North Assateague Island National Seashore (N-ASIS); Assateague State Park (ASP); South Assateague Island National Seashore (S-ASIS); North Chincoteague National Wildlife Refuge (N-CNWR)

††This value is skewed by the high retreat rates in the southern portion of N. Chincoteague.

percentage of sand within zones of Chincoteague and Sinepuxent Bays. Transects with higher average sand percentages were assigned larger shear stress values. Initial conditions for all spatially varied parameters are shown in Figure 5.4.

Calibration

One of the most significant limitations of applying these long-term models is the lack of data that can be used in model calibration, particularly given the various types of model output. In this study, three groups of data were used to, in a limited sense, calibrate the model: 1) shoreline change rates from 2005-2020; 2) horizontal marsh retreat rates from 1942-1989; and 3) vertical marsh accretion rates from 2000-2015.

Shoreline change rates are spatially varied along Assateague. Table 5.2 lists the regions, associated model transects, and observed change rates and distances, following categorization by Psuty et al. [367]. These data, along with the observed SLR rate of 8.27 mm/yr [371] were used to calibrate the following model parameters which influence shoreline change rates: equilibrium/critical barrier width (W_{cr} = 400 m) and height (H_{cr} = initial width), and maximum annual overwash flux ($Q_{OW,*}$= 37 m^3/m/yr).

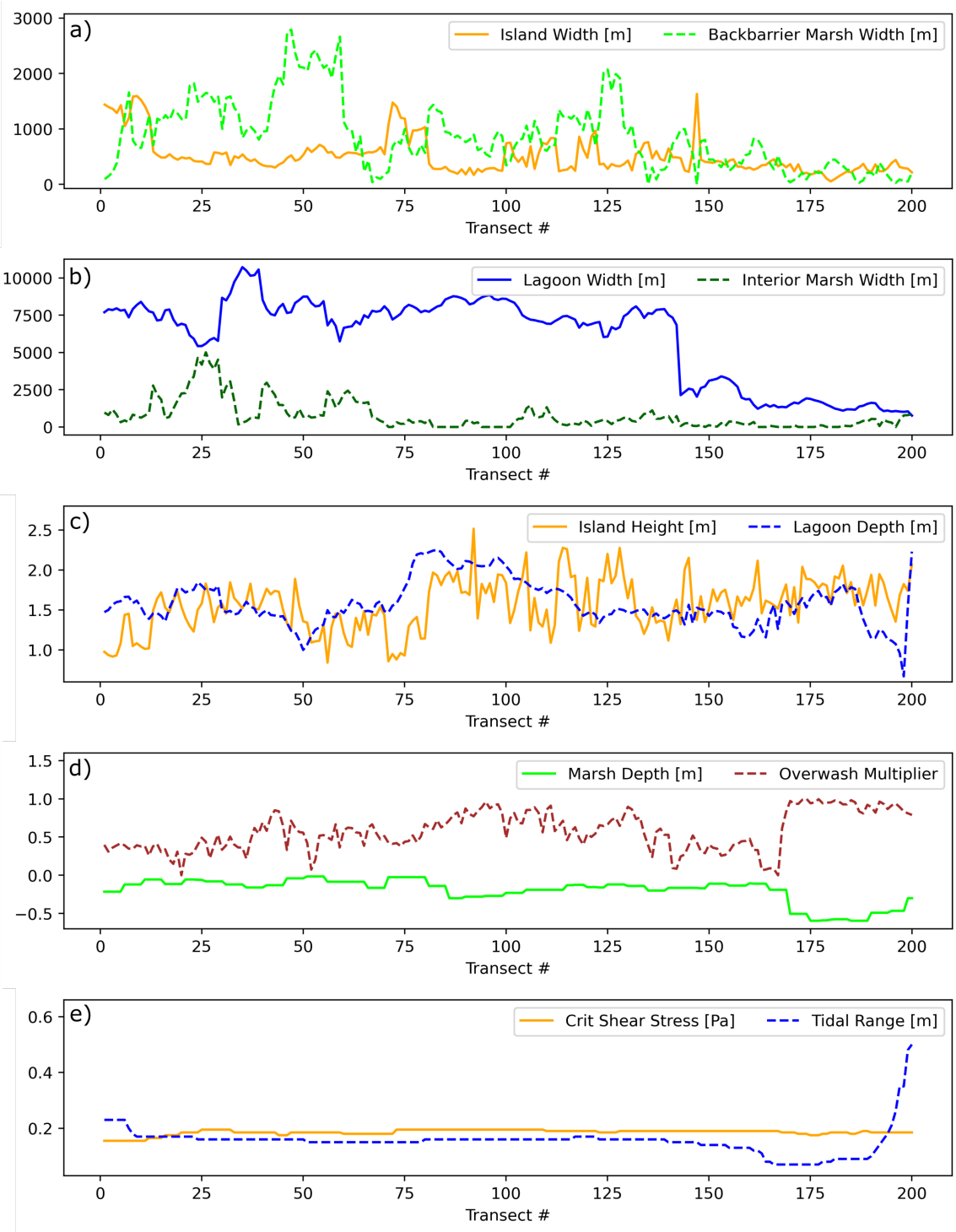

Figure 5.4: Initial Conditions for Spatially Varied Parameters.

The average marsh horizontal retreat rate, as reported by Wells et al. [369] and Carruthers et al. [363], was observed to be 0.2 (+/- 0.04) m/yr between 1942 and 1989. The average marsh vertical accretion rates, as reported by Morris et al. [372], was observed to be approximately 0.51 (+/- 0.21) cm/yr from 2000-2015, and 0.34 (+/- 0.12) cm/yr since Hurricane Sandy in 2012. Using the observed SLR rate of 3.1 mm/yr at Ocean City Inlet from 1975-1989 [371], calibration of the marsh progradation coefficient ($K_a = 1$), erosion coefficient ($K_e = 0.01$), and ocean sediment concentration ($C_o = 25$ mg/l) parameters was completed, resulting in a modeled average marsh retreat rate of 0.22 m/yr across all transects. Also, using the observed SLR rate of 8.3 mm/yr at Ocean City Inlet since 2002 [371], calibration of the fraction of refractory carbon ($\chi_{ref} = 0.21$) parameter was completed, resulting in modeled maximum vertical marsh accretion rates of approximately 0.34 cm/yr.

Coastal Management Alternatives

The LTM17 model was extended to include three coastal management alternatives: 1) regular beach nourishment, 2) dune elevation adjustments, and 3) thin-layer placement. Beach nourishment involves taking dredged sand, typically from offshore borrow sites, and placing this material on the beach to expand its area and extend the shoreline seaward [97]. Dunes may be created and adjusted by various methods, including scraping sand from the beach, importing sand from external sources, or capturing wind-blown sand via sand fences and dune vegetation [373]. Thin-layer placement involves the depositing a slurry of dredged sediment in thin layers on top of existing marsh platforms to aid vertical marsh growth with respect to rising sea levels [374].

These management practices were integrated into the LTM17 by modifying system geometry and sediment flux parameters. To model thin-layer placement, backbarrier marsh platform elevations were increased 5 cm for a single time step at 5 year intervals. Regular beach

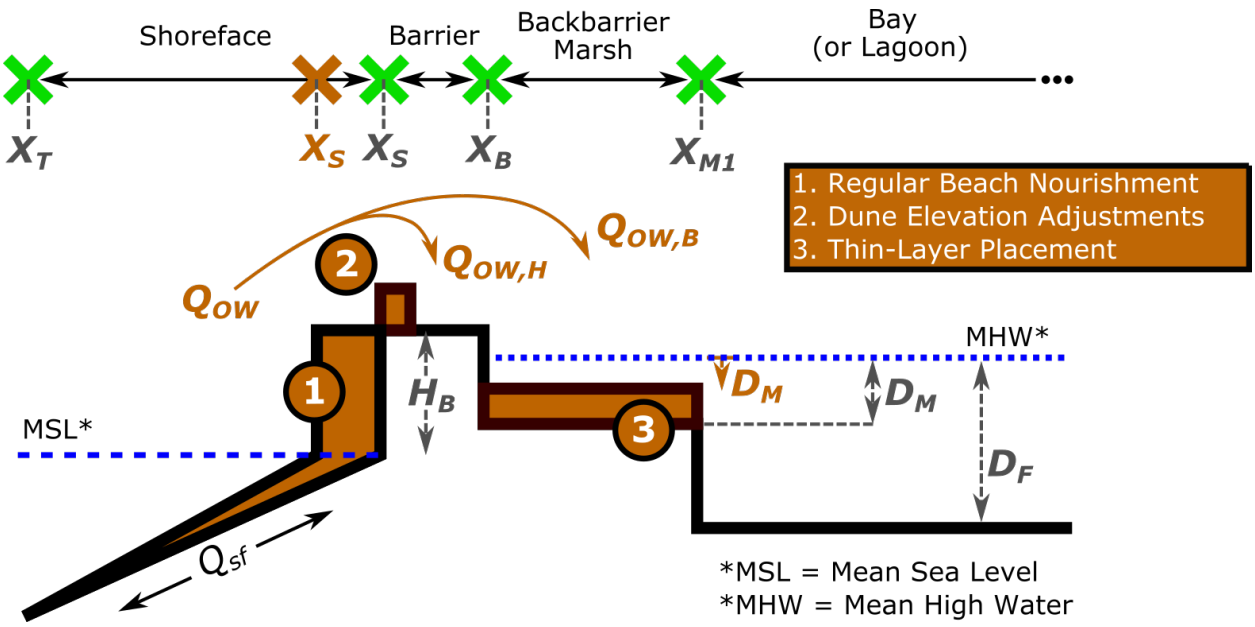

Figure 5.5: Management Alternatives for the LTM17 Model.

nourishment was also modeled with geometry modifications, by extending the shoreline back to its original position once it had retreated by 30 m; this simulated a "hold the line" approach. Dune modification was modeled by adjusting the overwash multiplier, a parameter that modulates the percentage of maximum annual overwash flux that is applied to the system based on the dune crest height. For the dune reduction scenario, the overwash multipliers were linearly increased from their starting values to 1 over 50 years, simulating a natural reduction over time. By contrast, dune increases were implemented at the first simulation time step and overwash multipliers were set equal to 0.2. These management alternatives are illustrated graphically in Figure 5.5.

5.3.2 Scenarios

Sixteen scenarios were simulated in this study. Table 5.3 provides a summary of these scenarios, each of which was assigned a unique ID and combination of SLR rate, annual

Table 5.3: Simulated Scenarios

Scenario ID	SLR Rate	Overwash Rate†	Management††	Assessment
E1	3.3 mm/yr	37 m^3/m/yr	...	SLR Vulnerability
E2	5.4 mm/yr	37 m^3/m/yr	...	SLR Vulnerability
E3	8.3 mm/yr	37 m^3/m/yr	...	SLR Vulnerability
P1	7.7 mm/yr	37 m^3/m/yr	...	SLR Vulnerability
P2	9.9 mm/yr	37 m^3/m/yr	...	SLR Vulnerability
P3	13.0 mm/yr	37 m^3/m/yr	...	SLR Vulnerability
P4	16.3 mm/yr	37 m^3/m/yr	...	SLR Vulnerability
O1	varies	0 m^3/m/yr	...	Overwash Impact
O2	varies	2 m^3/m/yr	...	Overwash Impact
O3	varies	10 m^3/m/yr	...	Overwash Impact
O4	varies	37 m^3/m/yr	...	Overwash Impact
O5	varies	100 m^3/m/yr	...	Overwash Impact
M1	varies	varies	TLP	Management
M2	varies	varies	RBN	Management
M3	varies	varies	RDE	Management
M4	varies	varies	IDE	Management

†This is the maximum annual overwash flux parameter ($Q_{OW,*}$) in the LTM17 model.

††Management Abbreviations: Thin-Layer Placement (TLP); Regular Beach Nourishment (RBN); Reduced Dune Elevation (RDE); Increased Dune Elevation (IDE)

overwash rate, and management alternatives. Seven scenarios (E1-P4) evaluated the vulnerability of Assateague to SLR; five scenarios (O1-O5) evaluated the impact of annual overwash rates; and four scenarios (M1-M4) evaluated the impact of management alternatives on Assateague's morphology.

Scenarios E1-E3 contain extrapolated SLR rates based on different periods of historical data at Ocean City Inlet [371]. The E1 SLR rate of 3.3 mm/yr is an extrapolation of the SLR rate observed at Ocean City between 1975 and 1991, while the E2 rate of 5.4 mm/yr and the E3 rate of 8.3 mm/yr are based on data from the periods 1975-2024 and 2002-2024, respectively. Scenarios P1-P4 are projected SLR rates for Ocean City, MD, from the 6th Assessment Report (AR6) from the International Panel on Climate Change (IPCC) [375, 376, 377]. The P1 SLR rate of 7.7 mm/yr is the average projected rate of SLR between 2025 and 2125

from the 50th percentile of the medium-confidence Shared Socioeconomic Pathway (SSP) 1-2.6 scenario. The other projected rates are calculated similarly, where P2 and P3 use the medium-confidence SSP2-4.5 and SSP5-8.5 scenarios, respectively, and the P4 rate uses the low-confidence SSP5-8.5 scenario, which accounts for potential ice-sheet contributions.

Scenarios O1-O5 are designed to evaluate the impact of a wide range of overwash values. Each overwash scenario is simulated for representative SLR scenarios (E2 and P4) to assess potential interactions between overwash and SLR rates. The last four scenarios, M1-M4, are designed to evaluate the management alternatives presented in the previous section. The management scenarios are evaluated for the combinations of selected SLR scenarios (E2 and P4) and overwash scenarios (O2 and O4). All scenarios were run for a simulation time of 100 years or until barrier drowning occurs.

5.4 Results

Results for the simulated SLR scenarios, including time to marsh drowning, change in barrier width, and shoreline retreat, are presented in Figure 5.6 for all model transects. Higher rates of SLR are associated with the marshes drowning earlier in the simulations (Fig. 5.6a). The average, maximum, and minimum times to marsh drowning are also summarized in Table 5.4 by groups of model transects.

The results in Table 5.4 show that for a SLR rate of 3.3 mm/yr (E1), the marshes are able to keep pace with SLR during the simulation, while for a SLR rate of 5.4 mm/yr (E2), the marshes drown, on average, after 56 years. The results also show considerable spatial variation in time to marsh drowning across the island transects, particularly at lower rates of SLR. North Assateague (NAS) marsh platforms drowned, on average, after 95 years, while the marsh platforms just south at Assateague State Park (ASP) drowned, on average, after 37

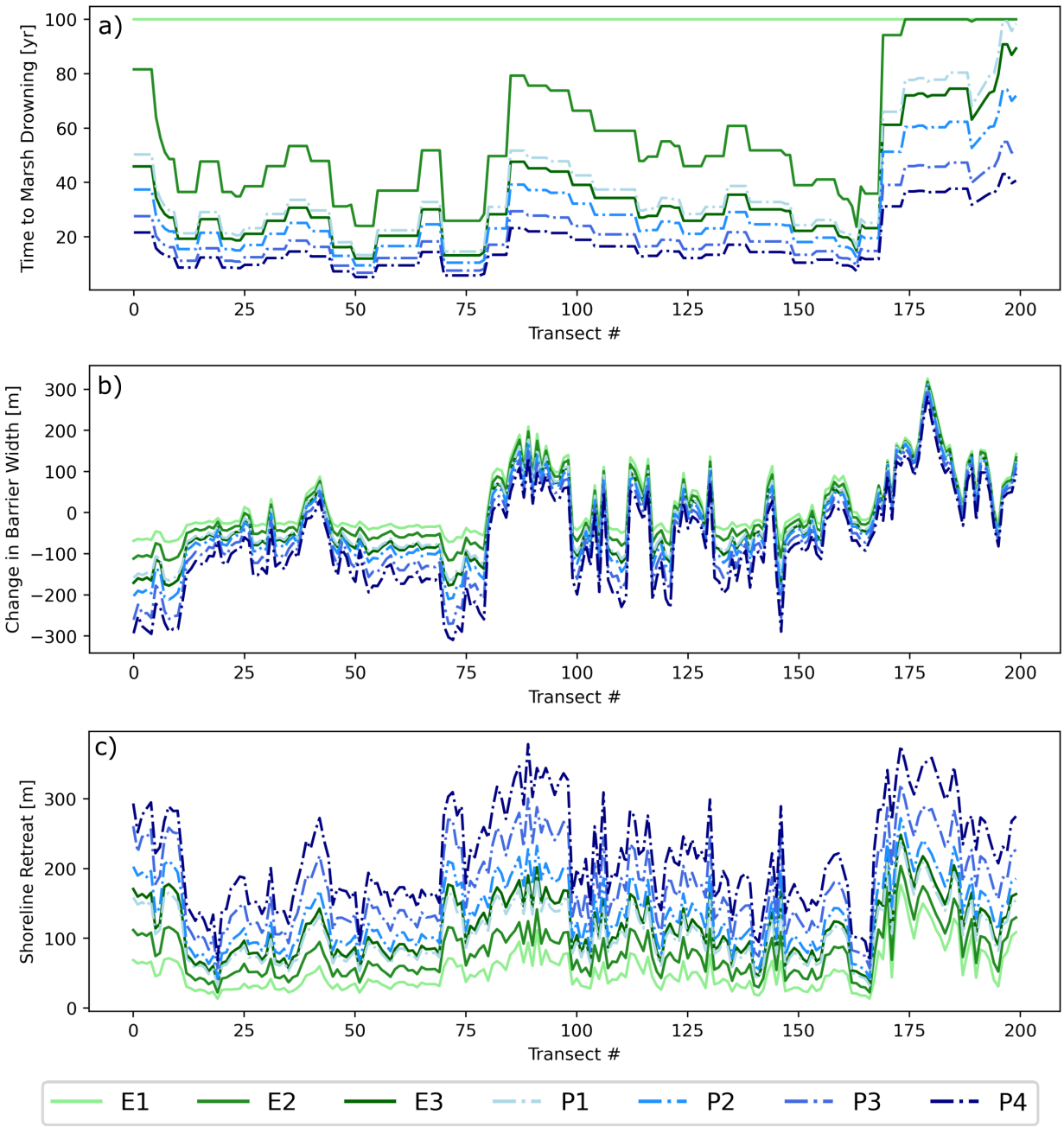

Figure 5.6: SLR Scenario Results. *(a) Time to Simulated Marsh Drowning; (b) Change in Barrier Width; (c) Shoreline Retreat. Marsh drowning times displayed at 100 yrs represent marshes that did not drown during the simulation time frame.*

Table 5.4: Average, Minimum, and Maximum Times to Simulated Marsh Drowning by Region. *Times shown are average values, with minimum and maximum values in brackets.*

Scenario	SLR Rate	All (1-200)	NAS (168-200)	ASP (152-167)	SAS (36-151)	NCR (1-35)
E1	3.3 mm/yr	...	...	...	...	...
E2	5.4 mm/yr	56 [24-]	95 [36-]	37 [24-41]	50 [24-79]	49 [35-82]
E3	8.3 mm/yr	34 [12-91]	69 [23-91]	22 [15-24]	29 [12-48]	27 [19-46]
P1	7.7 mm/yr	37 [13-99]	75 [25-99]	24 [16-26]	31 [13-52]	29 [21-50]
P2	9.9 mm/yr	28 [10-74]	57 [20-74]	18 [12-20]	23 [10-39]	22 [15-37]
P3	13.0 mm/yr	21 [7-55]	43 [15-55]	13 [9-16]	17 [7-29]	16 [11-28]
P4	16.3 mm/yr	17 [5-43]	34 [12-43]	11 [7-12]	14 [5-23]	12 [8-22]

years. The South Assateague (SAS) and North Chincoteague Wildlife Reserve (NCR) results showed marsh drowning times around 50 years, between these two extremes. Increasing the rate of SLR reduces time to simulated marsh drowning across all transects and also the variability in drowning time.

Higher rates of SLR are also associated with larger reductions in barrier width and shoreline retreat, modulated again by island transect as shown in Figure 5.6b,c. Mean shoreline retreat rates ranged between 52 m (min 37m, max 176m) for E1 and 218 m (min 67m, max 378m) for P4. Groups of model transects in the north (170-200), middle (70-100), and south (1-10) showed more significant retreat rates than other parts of the island. Higher rates of SLR were associated with greater reductions in island width for transects that were reducing in width. However, some transects (e.g., 80-100, 170-185) showed increases in island width over the simulation period, in which cases, increases in SLR rate were associated with decreases in island accretion. Mean changes in island width ranged from +22 m (min -71m, max 326m) for E1 to -77 m (min -310m, max 281m) for P4.

Results for the overwash scenarios, including time to barrier height drowning, change in barrier width, and shoreline retreat, are presented in Figure 5.7 for SLR scenarios E2 and P4, which were selected as representative low and high SLR scenarios, respectively. Height

drowning, which occurs in the model when MSL exceeds the barrier height, was only observed for SLR scenario P4; the island was able to maintain elevation above MSL for all transects during the simulation period in SLR scenario E2. Figure 5.7a shows that, on average, height drowning was most pronounced for scenarios with no overwash (01) or low overwash (O2-O3). Times to height drowning in these simulations ranged between 50 and 100 years. The results were also spatially varied, with transect groups to the south (1-10, 45-80) showing lower drowning times.

From Figures 5.7b,c, we see that greater changes in barrier width and shoreline position are associated with the larger overwash scenarios. This relationship is observed for both the E2 and P4 scenarios. For E2, average changes in width range from -22 m (min -25m, max -19m) for the no overwash scenario (O1) to -64 m (min -72m, max -37m) for the highest overwash scenario (O5). For P4, average changes in width range from 11 m (min -135m, max 338m) for O1 to -65 m (min -388m, max 322m) for O5. For E2, average shoreline retreat values range from 22 m (min 19m, max 25m) for O1 to 93 m (min 22m, max 249m) for O5. For P4, average shoreline retreat values range from 64 m (min 37m, max 72m) for O1 to 273 m (min 67m, max 463m) for O5. Spatial variability in results was observed to be similar to that of Figure 5.6.

Results for management scenario 1 (M1), which simulated thin-layer placement (TLP) of sediment on the marsh platforms, are presented in Figure 5.8, including time to marsh drowning and change in shoreline retreat. The results are presented for the same representative SLR scenarios, E2 and P4, and for overwash scenarios O2 and O4, which represent low and high overwash scenarios, respectively.

Times to marsh drowning in Figure 5.8a without management mirror the results from Figure 5.6a. When TLP is applied, marsh drowning is avoided for all transects for SLR scenario E2, increasing simulated times to marsh drowning by 50+ years, on average. For SLR scenario

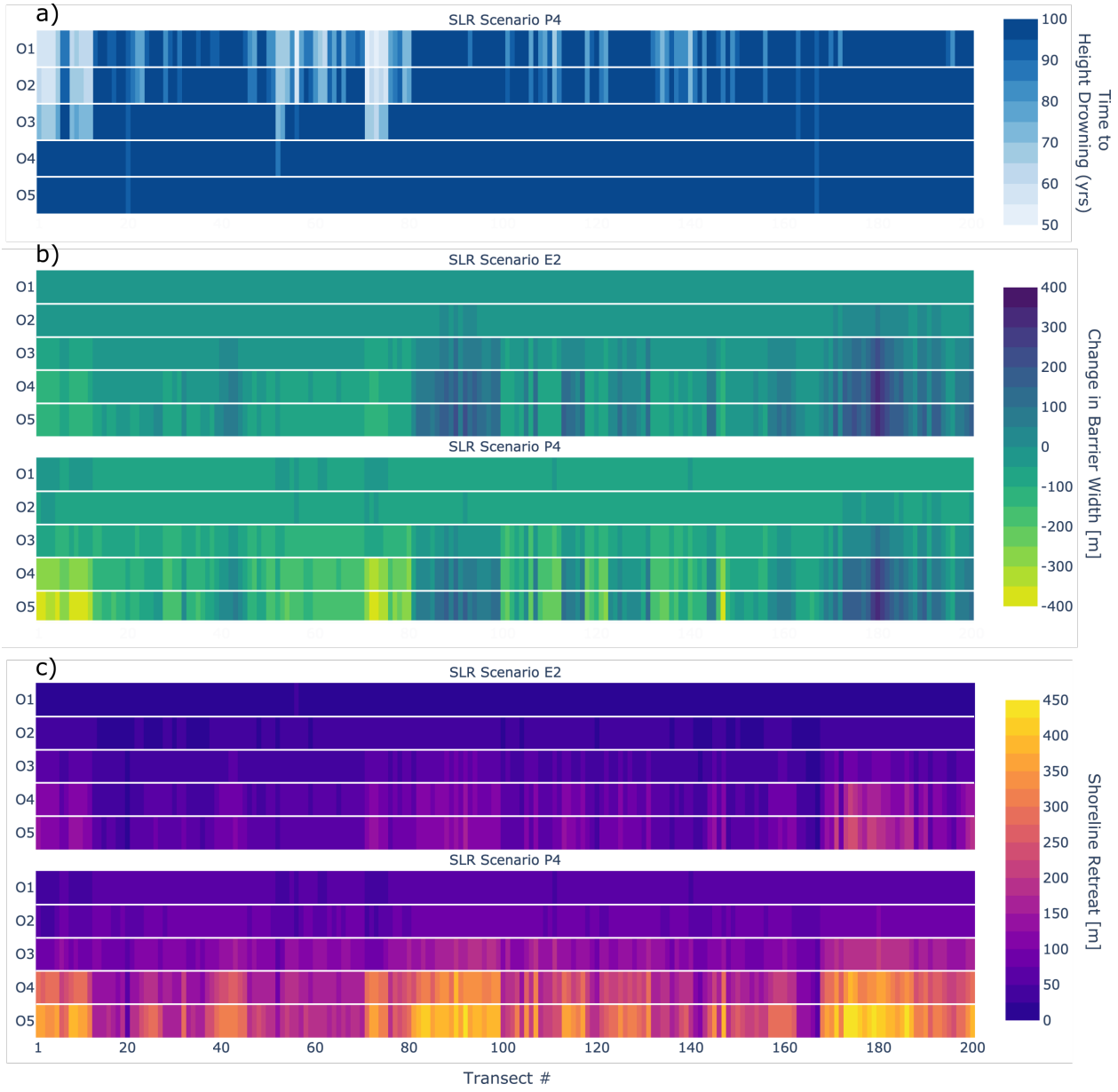

Figure 5.7: Results for Overwash and SLR Scenarios. *a) Time to Height Drowning; b) Change in Barrier Width; c) Shoreline Retreat.*

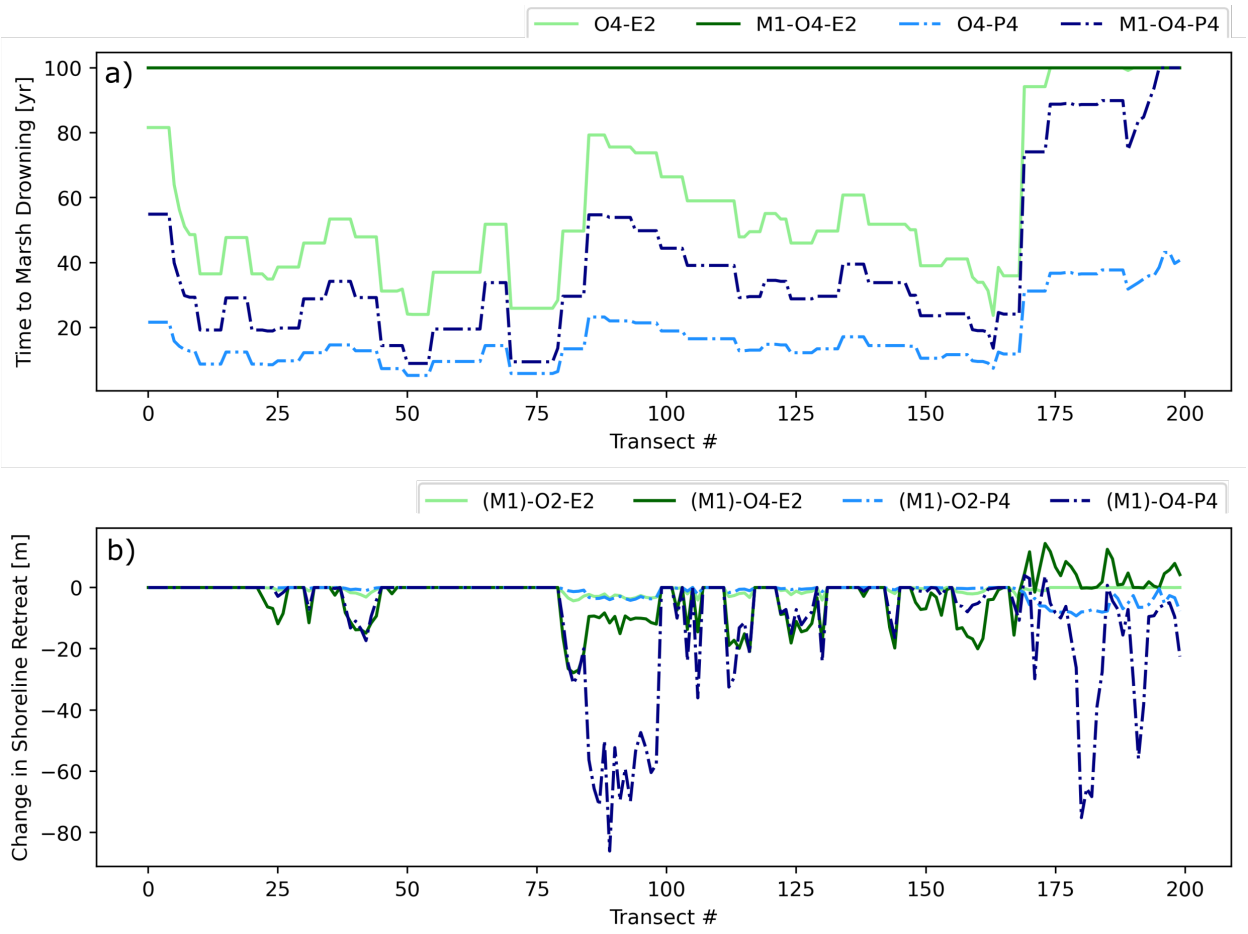

Figure 5.8: Results for Management Scenario 1: Thin-Layer Placement. *(a) Time to Simulated Marsh Drowning; (b) Change in Shoreline Retreat. Line labels are identified by their SLR, Overwash, and Management Scenario IDs from Table 5.3. Marsh drowning times displayed at 100 yrs represent marshes that did not drown during the simulation time frame.*

P4, TLP increased marsh drowning times by 22 years (min 4yrs, max 62yrs), on average. The O2 and O4 scenario results were identical for these simulations.

The results in Figure 5.8b show that TLP generally reduces shoreline retreat for the high overwash scenario (O4), while having minimal impact for the low overwash scenario (O2). As with the other results, we observed significant spatial variability between transects; some shoreline retreat rates were not modified at all while others were reduced by up to 80 m. SLR also modified the impact of TLP across the transects. The low SLR scenario (E2) showed modest increases in shoreline retreat for North Assateague (transects 170-200) and reductions in shoreline retreat for the other transects to the south. The high SLR scenario (P4) showed the most significant reductions in shoreline retreat, particularly at North Assateague and in the middle of the island (transects 80-100).

Results for M2, regular beach nourishment (RBN), including change in barrier width and the number of required nourishments, are presented in Figure 5.9. The change in barrier width results, shown for the high SLR scenario and both overwash scenarios, show that the modeled "hold the line" approach eliminates reductions in barrier width while allowing for backbarrier width accretions, particularly for island segments with low initial widths, as shown in Figure 5.9a. For scenario O2-P4, barrier widths were reduced by 66 m, on average. However, when RBN was applied (M2-O2-P4), the barrier width reduction was decreased to 7 m, on average, across all transects, with width increases for some transects. The same pattern of results was observed for the O4-P4 scenario, where pre-management width reduction was averaged to be 76 m and over 300 m at some transects. When RBN was applied (M2-O4-P4), the change in barrier width became +41m, on average.

The number of nourishments required to hold the shoreline position varied by SLR and overwash scenario as shown in Figure 5.9b. M2-O2-E2 required the least number of nourishments. Sixty percent of the island transects never required nourishment, while the remaining forty

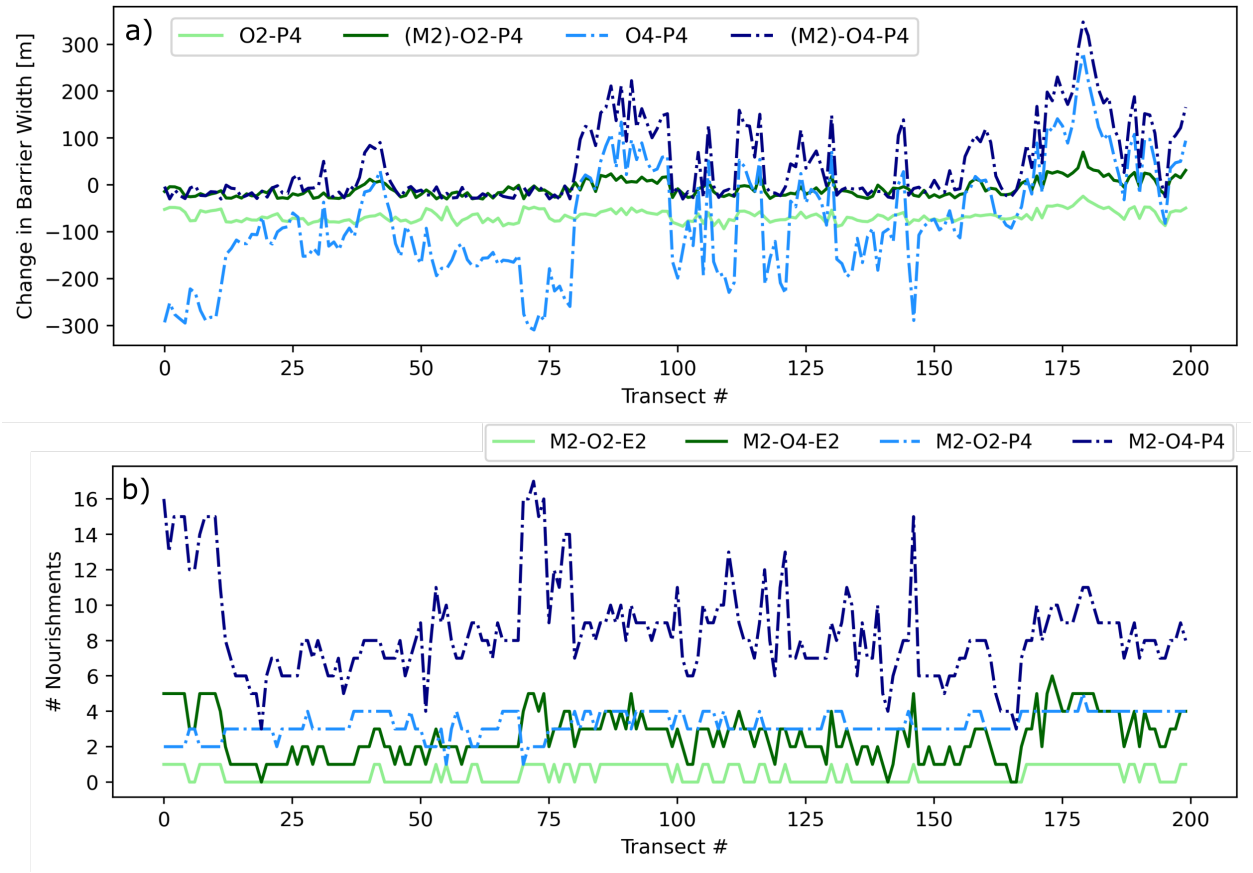

Figure 5.9: Results for Management Scenario 2: Regular Beach Nourishment. *(a) Change in Barrier Width, and (b) Number of Nourishments. Line labels are identified by their SLR, Overwash, and Management Scenario IDs from Table 5.3.*

percent required only one nourishment over the simulation time period. The M2-O2-P4 and M2-O4-E2 scenarios were comparable, each requiring an average of 3 nourishments across all transects. The M2-O4-P4 scenario required an average of 9 nourishments, or about one every 11 years.

Results for M3, reduced dune elevations (RDE), and M4, increased dune elevations (IDE), are presented in Figures 5.10 and 5.11, respectively. Height drowning was minimally impacted by RDE and IDE as shown in Figure 5.10a and 5.11a. Only a few transects showed height drowning for the high overwash scenario (O4-P4); however, for those that did, RDE alleviated the height drowning. Surprisingly, IDE also alleviated height drowning for these transects, although it created additional height drowning for others. Drowning was observed for many more transects for the low overwash scenario (O2-P4), with some drowning times between 55 and 60 years. RDE reduced drowning times, but only by 5 years, on average. IDE had the opposite effect, increasing drowning times by about 3 years, on average.

RDE showed substantial increases in shoreline retreat for the high SLR and high overwash scenario (M3-O4-P4), averaging 41 m (min 0m, max 226m) across all transects, as shown in Figure 5.10b. The other scenarios showed significantly less impact from RDE, averaging between 4 m and 10 m of change. Oppositely, IDE reduced shoreline retreat for M4-O4-P4 by 74 m (max 216m), on average, while averaging between 4 m and 24 m reductions for the other scenarios (Fig. 5.11b).

The average changes in barrier island width and height from RDE were minimal for all scenarios except M3-O4-P4, which showed an average height increase of 0.26 m (max 1.27m), and width changes that varied dramatically by transect, ranging from -121 m to +84 m (Fig. 5.10c,d). Similar but opposite patterns were observed for the IDE results, which showed an average height decrease of 0.44 m (max 0.83m), and width changes that ranged from -197 m to +162 m for the M4-O4-P4 scenario. IDE also showed significant width changes for

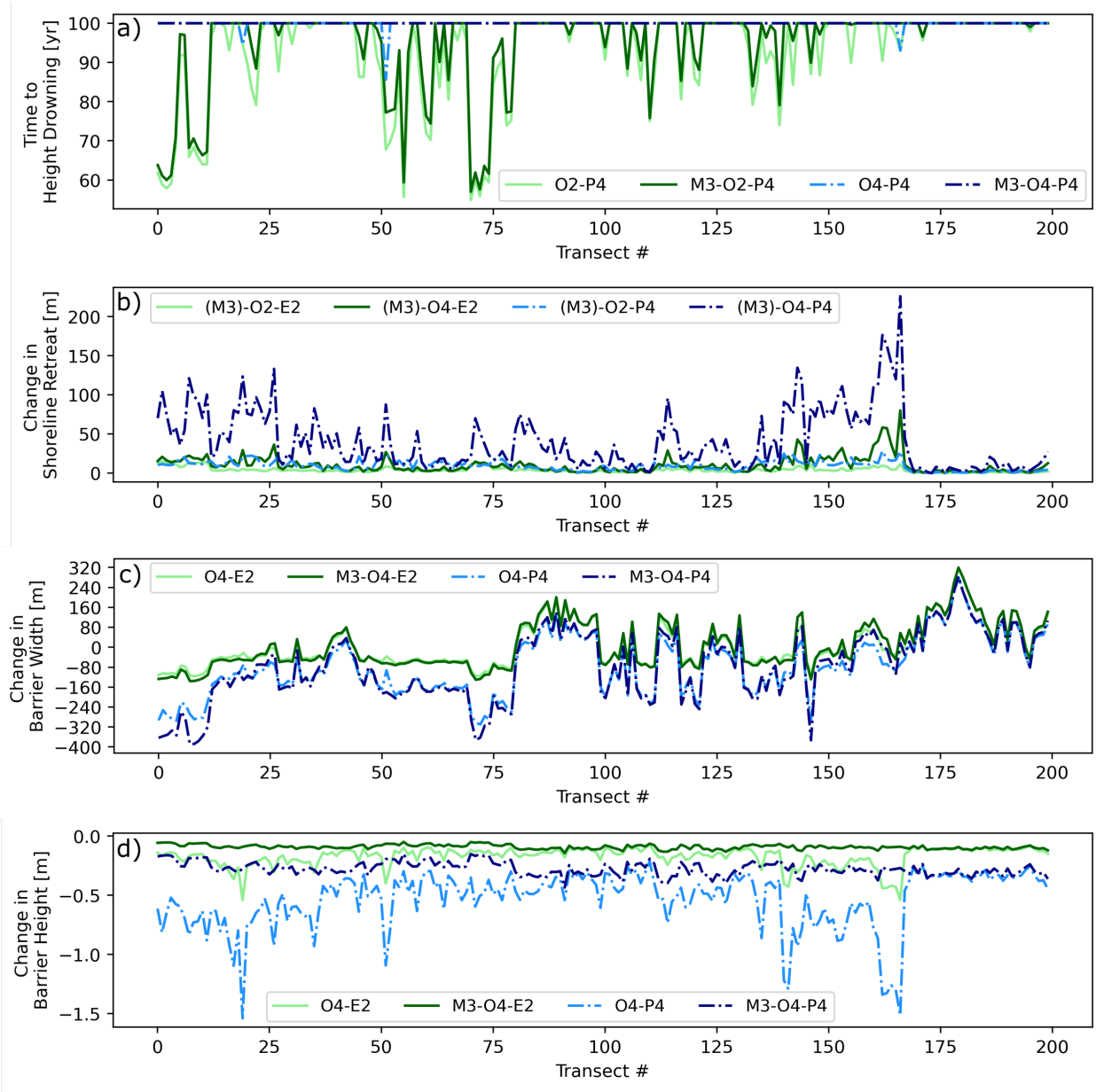

Figure 5.10: Results for Management Scenario 3: Reduce Dune Elevations. *(a) Time to Height Drowning, (b) Change in Shoreline Retreat, (c) Change in Barrier Width, and (d) Change in Barrier Height. Line labels are identified by their SLR, Overwash, and Management Scenario IDs from Table 5.3.*

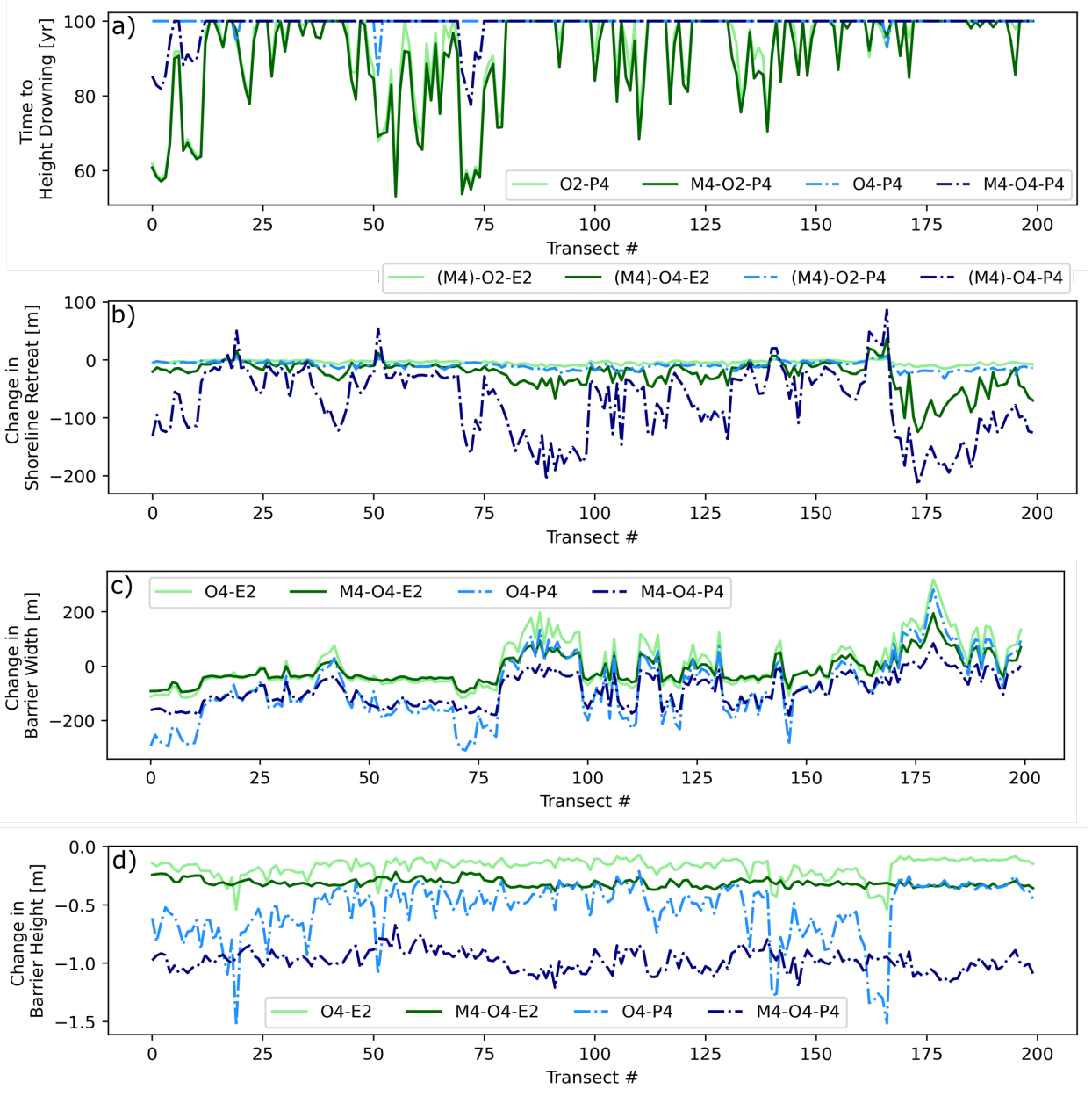

Figure 5.11: Results for Management Scenario 4: Increase Dune Elevations. *(a) Time to Height Drowning, (b) Change in Shoreline Retreat, (c) Change in Barrier Width, and (d) Change in Barrier Height. Line labels are identified by their SLR, Overwash, and Management Scenario IDs from Table 5.3.*

specific transects in the M4-O4-E2 scenario, ranging from -140 m to +39 m.

5.5 Discussion

The results in Figure 5.6 provide an assessment of the vulnerability of Assateague Island for seven SLR scenarios. Because only the rate of SLR was modified for these scenarios, they assume that the calibrated maximum annual overwash rate of 37 m^3/m/yr, which averages to about 21 m^3/m/yr after accounting for the variations in dune elevation (i.e., overwash multiplier), is held constant, with no changes due to management. These scenarios highlight a couple of significant vulnerabilities due to SLR.

First, many of the backbarrier marsh platforms are likely to experience drowning within the next 40 years, even for some of the lowest, extrapolated SLR rates (between 5 and 9 mm/yr). For SLR rates of 13 mm/yr and 16.3 mm/yr, which correspond to the highest SLR projections evaluated herein, the model suggests that marshes will drown in the next 21 years, on average. These estimates are consistent with previous studies that discuss the high vulnerability of Assateague marshes due to its low backbarrier tidal range [e.g., 372] and low lifespan estimates for lower elevation marshes from Defne and Ganju [6] and Ganju et al. [378]. Current marsh depth primarily accounts for the spatial variations in the results, as lower elevation marshes drown first, with tidal range differences playing a minor role, particularly near Ocean City Inlet. Marsh drowning did not, however, impact the barrier's ability to maintain its elevation with respect to SLR over the simulation period with the calibrated overwash rate.

Second, higher rates of SLR will increase rates of shoreline retreat across all of Assateague, but especially those portions of the island with lower initial widths and lower dune elevations, such as the northern end, which has been in an erosional state in recent decades [367].

Reductions in barrier width will also increase with SLR, in accordance with current island widths. Island segments with smaller initial widths reach their critical values much sooner, at which point overwash will offset shoreline losses with backbarrier shoreline expansions, while island segments with large initial widths remain purely erosional. Some island transects are currently below the modeled critical width, such as the northern end, which is why their results indicate the island width is in an accretive state, even while the shoreline is retreating. For such island segments, increased SLR rates actually reduce the accretive changes in barrier width.

These vulnerabilities due to SLR can be both exacerbated and mitigated by storm-driven overwash that is too much or too little. From the model results, low overwash scenarios minimize changes in barrier width and shoreline retreat across the island; however, they were also associated with island height drowning for certain transects in 50 to 100 years, particularly in the southern half of the study area, where the initial barrier heights were lowest, on average. Scenarios with greater overwash had the opposite effect, reducing the potential for drowning but increasing rates of shoreline retreat and changes in barrier width. It will be important for Assateague to find a balance in its management strategies that account for both the constructive and destructive impact of overwash.

Each of the management alternatives explored herein had different impacts on the evolving system. TLP, as modeled in this study (5 cm applied every 5 years), helped extend the life of the marsh for both high and low rates of SLR. The annualized rate of TLP was 10 mm/yr, which exceeds the rate of SLR in all but the highest SLR scenarios (P3 and P4). Due to Assateague's small backbarrier tidal range and low rates of marsh accretion, the rate of TLP needed to sustain the marsh approaches the rate of SLR. Variations in the time to marsh drowning suggest, as expected, that marsh platforms at the lowest elevation are most susceptible to drowning and should be prioritized for TLP. However, given Assateague's

susceptibility to height drowning, as opposed to width drowning, sustaining the marshes through TLP has little impact on sustaining the island itself over time.

RBN, modeled as a "hold the line" approach, proved to be effective at maintaining the current barrier width in addition to holding the shoreline position. Whereas the overwash and SLR scenarios showed the potential for reductions in barrier width, RBN eliminated these reductions while also allowing overwash to extend the backbarrier shoreline landward for island segments with low initial widths. The number of nourishments required in this management scenario ranged between 1 and 9 over the 100-yr simulation period, when averaged across all island transects. For the highest rates of SLR, about one nourishment every 11 years was sufficient to sustain the island width and hold the shoreline position.

RDE and IDE were the final management scenarios evaluated herein and these, as expected, had opposite impacts from one another. Where RDE tended to increase shoreline retreat, reduce barrier width, and increase barrier height, IDE had the opposite effect. However, these modifications had little impact on reducing height drowning, which primarily occurred during low overwash scenarios. Given that increases in storm frequency and intensity are expected [e.g., 13, 309], low overwash scenarios coupled with high SLR rates may be out of the question. In this case, maintaining protective dunes that minimize overwash for a time may not have long-term detrimental impacts for island sustainability. Future studies may consider adjusting the timing and location of RDE and IDE as temporary management alternatives that control sediment flux to the backbarrier island.

5.5.1 Limitations and Future Work

The primary limitation of this study is available data for model calibration and validation, particularly for model output that has not been historically tracked such as barrier height and

width, and marsh elevation and boundary changes. Future modeling efforts would benefit from research and data collection that quantifies these changes over time via remote sensing technologies and field studies.

Other study limitations arise out of the way that certain processes are modeled or excluded from modeling. For example, longshore sediment transport (LST) is not included in the LTM17 model, though it is known to impact shoreline retreat at the north end and accretion at Fishing Point [e.g., 365, 367]. The model is also unable to account for marshes at various depths along the same transect, which can lead to over- or underestimations of marsh drowning due to SLR. Future modeling efforts should account for both of these important factors to more accurately project changes to the barrier island system.

Further changes to the LTM17 model framework should be considered to more accurately reflect the system morphodynamics. One such change is the theoretical basis of modeled overwash, which is summarized in the volume deficit concept from Leatherman [114]. In the current model, overwash is distributed between the barrier height and barrier or marsh widths based on calculated deficit volumes; however, in reality, dune heights and storm size are going to primarily control the amount and extent of overwash. Additionally, the model is currently limited to modeling traditional barrier systems, which have a narrow backbarrier marsh, wide lagoon, and interior marsh platform abutting the mainland. However, some barrier systems, such as south Assateague and Wallops Islands, do not fit this idealized morphology. Future model developments should consider possible improvements in this area to expand model applicability.

5.6 Conclusions

This study modeled the evolution of Assateague Island, a mid-Atlantic barrier island, under combinations of SLR, overwash, and coastal management scenarios for a simulation period of 100 years. Backbarrier marsh platforms were found to be extremely vulnerable to SLR rates above 5 mm/yr, particularly low elevation marshes, with projected drowning times less than 40 years. Thin-layer placement of dredged sediment was found to alleviate the risk of marsh drowning, although it did not contribute to the long-term sustainability of Assateague Island, which is more susceptible to height drowning than width drowning. Higher rates of SLR and overwash contributed to increases in shoreline retreat and reduced island widths, except for island segments with low initial widths, such as Assateague's northern end, which increased in width due to overwash-driven progradation of the backbarrier shoreline. Modeled beach nourishment scenarios helped maintain both the barrier width and shoreline position, with one nourishment required per decade for the highest SLR scenario. Reductions and increases in dune elevation impacted shoreline retreat, island width, and island height while having little long-term impact on height drowning.

Acknowledgements and Disclaimers

This material is based upon work that is partially supported by the U.S. Army Corps of Engineers through the U.S. Coastal Research Program (under Grant No. W912HZ-20-2-0005), the National Science Foundation (under Grant Numbers 1735139 and 1630099), and Virginia Sea Grant College Program Project R/72155T funded by the National Oceanic and Atmospheric Administration's National Sea Grant College Program, U.S. Department of Commerce (under award NA18OAR4170083). The statements, findings, conclusions, and

recommendations are those of the author(s) and do not necessarily reflect the views of the U.S. Army Corps of Engineers, the U.S. Coastal Research Program, the National Science Foundation, Virginia Sea Grant, the National Oceanic and Atmospheric Administration, or the U.S. Department of Commerce. The authors acknowledge Advanced Research Computing at Virginia Tech for providing computational resources and technical support that have contributed to the results reported within this paper. URL: https://arc.vt.edu/. We also thank the projection authors for developing and making the sea-level rise projections available, multiple funding agencies for supporting the development of the projections, and the NASA Sea-Level Change Team for developing and hosting the IPCC AR6 Sea-Level Projection Tool.

Chapter 6

Conclusions

6.1 Summary

Four studies were presented herein, each of which was intended to advance the knowledge of long-term barrier island morphodynamics and/or to advance the understanding and practice of modeling barrier island morphodynamics.

In Chapter 2, a comprehensive review of advances in modeling barrier island morphodynamics was presented, including summaries of commonly modeled phenomena and modeling efforts for both event-scale and long-term morphodynamics. Five popular event-scale models and thirty eight long-term models were presented from the literature with their associated processes. Research gaps and needs were also identified, such as expanding access and availability of data, improving our understanding of relevant processes, and adjusting our modeling framework and approach.

In Chapter 3, global sensitivity analysis was used to explore the parameter space of a long-term barrier island evolution model. The Sobol method was used in addition to factor

mapping. Each input parameter's influence on the model results was tested both individually and interactively using the first-order and kth-order Sobol indices. Parameter interactions were identified using interaction indices and heatmaps, which were also used to idenifty regions of sensitivity. Boxplots were also generated for parameter values that fell into a distinctive simulation categories, such as width drowning, height drowning, and lagoon filling.

In Chapter 4, the Correlation, Factorial, Morris, Sobol, and VARS global sensitivity analysis methods were compared to one another after being applied to a long-term barrier system model. Evaluation criteria included parameter rankings, convergence of parameter rankings, and reliability of results. The ratio of factor prioritization was used to convert disparate sensitivity metrics to ratios between 0 and 1 for comparison. Convergence was evaluated for each method across five orders of magnitude of simulations. To assess reliability, results from 100 independent trials of each method were compared for two computational budget scenarios.

In Chapter 5, a long-term barrier system model was applied to Assateague Island, a mid-Atlantic barrier, and used to assess the island's vulnerabilities to sea level rise, overwash and the impact of coastal management alternatives. The island was evaluated for three extrapolated sea level rise rates from historical data recorded at a nearby inlet, and four sea level rise rates based on the latest projections, while overwash scenarios ranged from no overwash to relatively high values. Thin-layer placement, regular beach nourishment, reductions in dune elevation, and increases in dune elevation were all modeled as management alternatives through geometry modifications and sediment flux alterations.

6.2 Contributions and Significance

From the studies presented herein, the main contributions and their significance are as follows:

- (Chapter 3) Islands that were found to be most prone to width and height drowning within the 100-year simulation period were those with low initial geometries. This finding can help coastal managers to easily identify which parts of their islands are most vulnerable and should be prioritized for restoration efforts. It also highlights the need to reexamine and possibly improve the theoretical foundations of critical barrier geometry, which underlies some equilibrium-based models. A specific combination of input parameters, including critical barrier width, initial width, toe depth, initial marsh and lagoon width, sea level rise rate, wind speed, critical shear stress, and ocean sediment concentration, was required for short-term width drowning to occur. This finding is also significant for coastal managers, as it suggests that the risk of barrier drowning could be alleviated by modifying one of those parameters. Tidal dispersion was more influential on the backbarrier marsh and lagoon than overwash for the simulation period. This finding supports the theory that marsh platforms are primarily associated with flood shoals from historical tidal inlets. This finding can also help coastal managers plan for management alternatives that will likely be required for marsh platforms in microtidal bays with limited access to sediment from tidal inlets.

- (Chapter 4) The global sensitivity methods evaluated were generally able to identify groups of the most important parameters; however, the Correlation method had some notable deviations. This suggests that while the Correlation method is the easiest sensitivity method to implement, and may often be able to identify groups of the most sensitive parameters, the method showed some significant deviations in param-

eter ranking from the more robust methods. In evaluating method convergence and reliability, the Morris method outperformed all the others due to its factor fixing ability at low simulation counts. This finding suggests that modelers should use the Morris method for models with longer run times or when there are computational constraints. The VARS method performed better than Sobol when compared by convergence and reliability, and it had lower simulation counts than Sobol; however, it did not perform better than Morris. This finding suggest that VARS is a viable alternative to the computationally expensive Sobol method, with better convergence and reliability of results.

- (Chapter 5) Assateague's backbarrier marsh platforms, particularly those at low elevation, were found to be very vulnerable to rates of sea level rise above 5 mm/yr, with estimated marsh drowning times below 40 years. The marsh life was extended by thin-layer placement of dredged sediment; however, this restoration did not help the island sustain its elevation with respect to sea level rise in the short-term. Higher rates of sea level rise and overwash increased island retreat and reduced island width, on average, though regular beach nourishment was able to minimize these impacts. Dune modifications also impacted shoreline retreat and width changes, although they had minimal impact on alleviating or exacerbating drowning. These findings may be helpful for the coastal resource managers at Assateague who are actively implementing some of these scenarios and who will continue to be faced with management decisions in years to come.

6.3 Future Work

Suggestions for future work based on the findings presented herein are as follows:

- Future studies planning to use the long-term barrier island model employed herein should consider re-examining the theoretical underpinnings of the model to see if it may be improved. The critical length concept of Leatherman [114] is a solid, evidence-based concept; however, the formulation may be improved by considering how island characteristics, such as dune elevations, or storm characteristics, such as intensity or frequency, impact the possible extent of overwash.

- Future modeling studies should consider simulating additional management alternatives at Assateague or other sites. Even using the three management alternatives from this study, additional management scenarios might be created by applying two or more alternatives simultaneously. Other scenarios might consider the impact of spatially varied or temporally varied management scenarios on long-term changes to the island geometry.

- Lastly, future modeling studies should consider applying this framework with management alternatives to other barrier island systems to evaluate their impact on systems with differing morphology and/or forcing conditions. For example, since Assateague is a microtidal barrier island, it would be good to apply these management scenarios to a meso or macrotidal barrier to evaluate the differences.

Bibliography

[1] Jorge Lorenzo-Trueba and Giulio Mariotti. Chasing boundaries and cascade effects in a coupled barrier-marsh-lagoon system. *Geomorphology*, 290:153–163, 2017. doi: 10.1016/j.geomorph.2017.04.019. URL http://dx.doi.org/10.1016/j.geomorph.2017.04.019.

[2] Steven W.H. Hoagland, Jennifer L. Irish, and Robert Weiss. Morphodynamic and modeling insights from global sensitivity analysis of a barrier island evolution model. *Geomorphology*, 451(September 2023):109087, 4 2024. ISSN 0169555X. doi: 10.1016/j.geomorph.2024.109087. URL https://doi.org/10.1016/j.geomorph.2024.109087https://linkinghub.elsevier.com/retrieve/pii/S0169555X24000370.

[3] CIRES. Continuously Updated Digital Elevation Model (CUDEM) - 1/9 Arc-Second Resolution Bathymetric-Topographic Tiles., 2014. URL doi:10.25921/ds9v-ky35.

[4] Assateague Island National Seashore. Assateague Island National Seashore Jurisdictional Boundary 2003-2005, 2006.

[5] VGIN. Virginia Base Mapping Program (VBMP) Orthoimagery, 2021. URL https://vgin.vdem.virginia.gov/pages/base-mapping.

[6] Z. Defne and N.K. Ganju. Mean tidal range in marsh units of Assateague Island

National Seashore and Chincoteague Bay, Maryland and Virginia: U.S. Geological Survey data release, 2018.

[7] Matthew L. Stutz and Orrin H. Pilkey. Open-Ocean Barrier Islands: Global Influence of Climatic, Oceanographic, and Depositional Settings. *Journal of Coastal Research*, 272:207–222, 2011. ISSN 0749-0208. doi: 10.2112/09-1190.1.

[8] Chris Mcowen, Lauren Weatherdon, Jan-Willem Bochove, Emma Sullivan, Simon Blyth, Christoph Zockler, Damon Stanwell-Smith, Naomi Kingston, Corinne Martin, Mark Spalding, and Steven Fletcher. A global map of saltmarshes. *Biodiversity Data Journal*, 5:e11764, 3 2017. ISSN 1314-2828. doi: 10.3897/BDJ.5.e11764. URL http://bdj.pensoft.net/articles.php?id=11764.

[9] Alison Sleath Grzegorzewski, Mary A. Cialone, and Ty V. Wamsley. Interaction of Barrier Islands and Storms: Implications for Flood Risk Reduction in Louisiana and Mississippi. *Journal of Coastal Research*, 59:156–164, 2011. ISSN 0749-0208. doi: 10.2112/si59-016.1.

[10] Orrin H. Pilkey, William J. Neal, Joseph T. Kelley, and J. Andrew G. Cooper. *The World's Beaches: A Global Guide to the Science of the Shoreline*. University of California Press, 2011. ISBN 9780520268715.

[11] Sathya Gopalakrishnan, Craig E Landry, Martin D Smith, and John C Whitehead. Economics of Coastal Erosion and Adaptation to Sea Level Rise. *Annual Review of Resource Economics*, 8, 2016. doi: 10.1146/annurev-resource-100815-095416.

[12] E.B. Barbier, S.D. Hacker, C. Kennedy, E.W. Koch, A.C. Stier, and B.R. Silliman. The value of estuarine and coastal ecosystem services. *Ecological Monographs*, 81(2)(2):169–193, 2011.

[13] Paolo Ciavola and Giovanni Coco, editors. *Coastal Storms*. John Wiley & Sons, Ltd, Chichester, UK, 5 2017. ISBN 9781118937099. doi: 10.1002/9781118937099.

[14] Laura J. Moore and A. Brad Murray, editors. *Barrier Dynamics and Response to Changing Climate*. Springer International Publishing, Cham, Switzerland, 2018. ISBN 978-3-319-68084-2. doi: 10.1007/978-3-319-68086-6. URL http://link.springer.com/10.1007/978-3-319-68086-6.

[15] R. A. McBride, J. B. Anderson, I. V. Buynevich, M. R. Byrnes, W. Cleary, M. S. Fenster, D. M. FitzGerald, C. J. Hapke, M. S. Harris, C. J. Hein, C. L. Johnson, A. H.F. Klein, B. Liu, J. T. De Menezes, J. S. Mulhern, T. S.N. Oliver, M. Pejrup, S. R. Riggs, H. H. Roberts, A. B. Rodriguez, C. T. Seminack, A. D. Short, G. W. Stone, T. Tamura, D. J. Wallace, and P. Wang. *Morphodynamics of Modern and Ancient Barrier Systems: An Updated and Expanded Synthesis*, volume 8. Elsevier, second edi edition, 2022. ISBN 9780128182352. doi: 10.1016/B978-0-12-818234-5.00153-X. URL http://dx.doi.org/10.1016/B978-0-12-818234-5.00153-X.

[16] R. Pelnard-Considere. Essai de theorie de l'evolution des formes de rivage en plages de sable et de galets. *Journees de L'hydraulique*, pages 289–298, 1956.

[17] David Walters, Laura J. Moore, Orencio D. Vinent, Sergio Fagherazzi, and Giulio Mariotti. Interactions between barrier islands and backbarrier marshes affect island system response to sea level rise: Insights from a coupled model. *Journal of Geophysical Research: Earth Surface*, pages 2013–2031, 2014. doi: 10.1002/2014JF003091.

[18] Giulio Mariotti and J. Carr. Dual role of salt marsh retreat: Long-term and short-term resilience. *Water Resources Research*, 50(4):2963–2974, 2014. doi: 10.1002/2013WR014676.

[19] Jorge Lorenzo-Trueba and Andrew D. Ashton. Rollover, drowning, and discontinuous retreat: Distrinct modes of barrier response to sea-level rise arising from a simple morphodynamic model. *Journal of Geophysical Research: Earth Surface*, pages 779–801, 2014. doi: 10.1002/2013JF002871.Received.

[20] I.M. Sobol. Sensitivity estimates for nonlinear mathematical models. *Mathematical Modelling and Computational Experiment*, 1(4):407–414, 1993.

[21] Saman Razavi and Hoshin V. Gupta. What do we mean by sensitivity analysis? The need for comprehensive characterization of "global" sensitivity in Earth and Environmental systems models. *Water Resources Research*, 51(5):3070–3092, 5 2015. ISSN 00431397. doi: 10.1002/2014WR016527. URL http://doi.wiley.com/10.1002/2014WR016527.

[22] Arnald Puy, Samuele Lo Piano, and Andrea Saltelli. Is VARS more intuitive and efficient than Sobol' indices? *Environmental Modelling and Software*, 137(December 2020):104960, 2021. ISSN 13648152. doi: 10.1016/j.envsoft.2021.104960. URL https://doi.org/10.1016/j.envsoft.2021.104960.

[23] Andrea Saltelli, Marco Ratto, Terry Andres, Francesca Campolongo, Jessica Cariboni, Debora Gatelli, Michaela Saisana, and Stefano Tarantola. *Global Sensitivity Analysis. The Primer*. Wiley, Chichester, UK, 12 2008. ISBN 9780470059975. doi: 10.1002/9780470725184. URL http://doi.wiley.com/10.1002/9780470725184.

[24] Saman Razavi and Hoshin V. Gupta. A new framework for comprehensive, robust, and efficient global sensitivity analysis: 1. Theory. *Water Resources Research*, 52 (1):423–439, 1 2016. ISSN 0043-1397. doi: 10.1002/2015WR017558. URL https://onlinelibrary.wiley.com/doi/abs/10.1002/2015WR017558.

[25] Saman Razavi and Hoshin V. Gupta. A new framework for comprehensive, robust, and efficient global sensitivity analysis: 2. Application. *Water Resources Research*, 52(1):440–455, 1 2016. ISSN 0043-1397. doi: 10.1002/2015WR017559. URL https://onlinelibrary.wiley.com/doi/10.1111/j.1752-1688.1969.tb04897.xhttps://onlinelibrary.wiley.com/doi/abs/10.1002/2015WR017559.

[26] Stefano Tarantola, Federico Ferretti, Samuele Lo Piano, Mariia Kozlova, Alessio Lachi, Rossana Rosati, Arnald Puy, Pamphile Roy, Giulia Vannucci, Marta Kuc-Czarnecka, and Andrea Saltelli. An annotated timeline of sensitivity analysis. *Environmental Modelling and Software*, 174(December 2023):105977, 2024. ISSN 13648152. doi: 10.1016/j.envsoft.2024.105977. URL https://doi.org/10.1016/j.envsoft.2024.105977.

[27] Florian Pappenberger, Keith J. Beven, Marco Ratto, and Patrick Matgen. Multi-method global sensitivity analysis of flood inundation models. *Advances in Water Resources*, 31(1):1–14, 2008. ISSN 03091708. doi: 10.1016/j.advwatres.2007.04.009.

[28] Yanjun Gan, Qingyun Duan, Wei Gong, Charles Tong, Yunwei Sun, Wei Chu, Aizhong Ye, Chiyuan Miao, and Zhenhua Di. A comprehensive evaluation of various sensitivity analysis methods: A case study with a hydrological model. *Environmental Modelling and Software*, 51:269–285, 2014. ISSN 13648152. doi: 10.1016/j.envsoft.2013.09.031. URL http://dx.doi.org/10.1016/j.envsoft.2013.09.031.

[29] Eli D. Lazarus, Michael A. Ellis, A. Brad Murray, and Damon M. Hall. An evolving research agenda for human-coastal systems. *Geomorphology*, 256:81–90, 2016. ISSN 0169555X. doi: 10.1016/j.geomorph.2015.07.043. URL http://dx.doi.org/10.1016/j.geomorph.2015.07.043.

[30] Ty V. Wamsley, Mary A. Cialone, Jane M. Smith, Bruce A. Ebersole, and Alison S. Grzegorzewski. Influence of landscape restoration and degradation on storm surge and

waves in southern Louisiana. *Natural Hazards*, 51(1):207–224, 2009. ISSN 0921030X. doi: 10.1007/s11069-009-9378-z.

[31] Todd S. Bridges, Roselle Henn, Shawn Komlos, Debby Scerno, Ty Wamsley, and Kate White. Coastal Risk Reduction and Resilience. Technical Report July, United States Army Corps of Engineers, Civil Works Directorate, Washington, D.C., 2013. URL http://www.swg.usace.army.mil/Portals/26/docs/PAO/Coastal.pdf.

[32] Keqi Zhang and Stephen Leatherman. Barrier Island Population along the U.S. Atlantic and Gulf Coasts. *Journal of Coastal Research*, 27(2):356, 2011. ISSN 1551-5036. doi: 10.2112/jcoastres-d-10-00126.1.

[33] ESA. Sentinel-2 satellite imagery (courtesy of the U.S. Geological Survey), 2021. URL https://sentinel.esa.int/web/sentinel/missions/sentinel-2.

[34] Robert Dolan and Harry F. Lins. *The Outer Banks of North Carolina*. U.S. Geological Survey, 1986.

[35] Michael Oppenheimer, Bruce Glavovic, Jochen Hinkel, Roderik van de Wal, Alexandre K. Magnan, Amro Abd-Elgawad, Rongshuo Cai, Miguel Cifuentes-Jara, Robert M. Deconto, Tuhin Ghosh, John Hay, Federico Isla, Ben Marzeion, Benoit Meyssignac, and Zita Sebesvari. Sea Level Rise and Implications for Low Lying Islands, Coasts and Communities Coordinating. In H.-O. Portner, D.C. Roberts, V. Masson-Delmotte, P. Zhai, M. Tignor, E. Poloczanska, K. Mintenbeck, A. Alegria, M. Nicolai, A. Okem, J. Petzold, B. Rama, and N.M. Weye, editors, *IPCC SR Ocean and Cryosphere*. In press., 2019. ISBN 1095-9203 (Electronic) 0036-8075 (Linking).

[36] Benjamin T. Gutierrez, S. Jeffress Williams, and E. Robert Thieler. Potential for shoreline changes due to sea-level rise along the US mid-Atlantic region. Technical report, U.S. Geological Survey, Reston, VA, 2007.

[37] Chantal Donnelly, Nicholas Kraus, and Magnus Larson. State of Knowledge on Measurement and Modeling of Coastal Overwash. *Journal of Coastal Research*, 22(4): 965–991, 2006. ISSN 0749-0208. doi: 10.2112/04-0431.1.

[38] Sonja Eichentopf, Harshinie Karunarathna, and José M. Alsina. Morphodynamics of sandy beaches under the influence of storm sequences: Current research status and future needs. *Water Science and Engineering*, 12(3):221–234, 2019. ISSN 24058106. doi: 10.1016/j.wse.2019.09.007.

[39] Julie D. Rosati and Gregory W. Stone. Geomorphologic Evolution of Barrier Islands along the Northern U.S. Gulf of Mexico and Implications for Engineering Design in Barrier Restoration. *Journal of Coastal Research*, 251:8–22, 2009. ISSN 0749-0208. doi: 10.2112/07-0934.1.

[40] A. Toimil, P. Camus, I. J. Losada, G. Le Cozannet, R. J. Nicholls, D. Idier, and A. Maspataud. Climate change-driven coastal erosion modelling in temperate sandy beaches: Methods and uncertainty treatment. *Earth-Science Reviews*, 202(January): 103110, 2020. ISSN 00128252. doi: 10.1016/j.earscirev.2020.103110.

[41] Christopher R. Sherwood, Ap van Dongeren, James Doyle, Christie A. Hegermiller, Tian-Jian Hsu, Tarandeep S. Kalra, Maitane Olabarrieta, Allison M. Penko, Yashar Rafati, Dano Roelvink, Marlies van der Lugt, Jay Veeramony, and John C. Warner. Modeling the Morphodynamics of Coastal Responses to Extreme Events: What Shape Are We In? *Annual Review of Marine Science*, 14(1):1–36, 1 2022. ISSN 1941-1405. doi: 10.1146/annurev-marine-032221-090215. URL https://www.annualreviews.org/doi/10.1146/annurev-marine-032221-090215.

[42] R. A. McBride, J. B. Anderson, I. V. Buynevich, W. Cleary, M. S. Fenster, D. M. FitzGerald, M. S. Harris, C. J. Hein, A. H.F. Klein, B. Liu, J. T. de Menezes, M. Pe-

jrup, S. R. Riggs, A. D. Short, G. W. Stone, D. J. Wallace, and P. Wang. Morphodynamics of Barrier Systems: A Synthesis. In John F. Shroder, editor, *Treatise on Geomorphology*, volume 10, pages 166–244. Elsevier, 2013. ISBN 9780080885223. doi: 10.1016/B978-0-12-374739-6.00279-7.

[43] Patricia Chardón-Maldonado, José Carlos Pintado-Patiño, and Jack A. Puleo. Advances in swash-zone research: Small-scale hydrodynamic and sediment transport processes. *Coastal Engineering*, 115:8–25, 2016. ISSN 03783839. doi: 10.1016/j.coastaleng.2015.10.008.

[44] Dominic E. Reeve, Harshinie Karunarathna, Shunqi Pan, Jose M. Horrillo-Caraballo, Grzegorz Różyński, and Roshanka Ranasinghe. Data-driven and hybrid coastal morphological prediction methods for mesoscale forecasting. *Geomorphology*, 256:49–67, 2016. ISSN 0169555X. doi: 10.1016/j.geomorph.2015.10.016.

[45] Roshanka Ranasinghe. On the need for a new generation of coastal change models for the 21st century. *Scientific Reports*, 10(1):1–6, 2020. ISSN 20452322. doi: 10.1038/s41598-020-58376-x.

[46] Peter J. Cowell, Marcel J.F. Stive, Alan W. Niedoroda, Huib J. De Vriend, Donald J.P. Swift, George M. Kaminsky, and Michele Capobianco. The Coastal-Tract (Part 1): A Conceptual Approach to Aggregated Modeling of Low-Order Coastal Change. *Journal of Coastal Research*, 19(4):812–827, 2003. ISSN 07490208.

[47] Asbury H. Sallenger. Storm impact scale for barrier islands. *Journal of Coastal Research*, 16(3):890–895, 2000. ISSN 0749-0208.

[48] Jin-Si Over, Jenna Brown, Christopher Sherwood, Christie Hegermiller, Phillipe Wernette, Andrew Ritchie, and Jonathan Warrick. A survey of storm-induced seaward-

transport features observed during the 2019 and 2020 hurricane seasons. *Shore & Beach*, 89(2):31–40, 2021. ISSN 0037-4237. doi: 10.34237/1008924.

[49] Cheol Shik Shin. *A One-Dimensional Model for Storm Breaching of Barrier Islands*. PhD thesis, Old Dominion University, 1996.

[50] R. T. McCall, J. S.M. Van Thiel de Vries, N. G. Plant, A. R. Van Dongeren, J. A. Roelvink, D. M. Thompson, and A. J.H.M. Reniers. Two-dimensional time dependent hurricane overwash and erosion modeling at Santa Rosa Island. *Coastal Engineering*, 57(7):668–683, 2010. ISSN 03783839. doi: 10.1016/j.coastaleng.2010.02.006. URL http://dx.doi.org/10.1016/j.coastaleng.2010.02.006.

[51] Stephanie M. Smallegan and Jennifer L. Irish. Barrier Island Morphological Change by Bay-Side Storm Surge. *Journal of Waterway, Port, Coastal, and Ocean Engineering*, 143(5):04017025, 2017. ISSN 0733-950X. doi: 10.1061/(asce)ww.1943-5460.0000413.

[52] Craig Harter and Jens Figlus. Numerical modeling of the morphodynamic response of a low-lying barrier island beach and foredune system inundated during Hurricane Ike using XBeach and CSHORE. *Coastal Engineering*, 120(April 2016):64–74, 2017. ISSN 03783839. doi: 10.1016/j.coastaleng.2016.11.005. URL http://dx.doi.org/10.1016/j.coastaleng.2016.11.005.

[53] Marcel J.F. Stive and Huib J. de Vriend. Modelling shoreface profile evolution. *Marine Geology*, 126:235–248, 1995. ISSN 00253227. doi: 10.1016/0025-3227(95)00080-I. URL http://dx.doi.org/10.1016/0025-3227(95)00080-I.

[54] Troels Aagaard and Aart Kroon. Sediment Transport Under Storm Conditions on Sandy Beaches. In Paolo Ciavola and Giovanni Coco, editors, *Coastal Storms: Processes and Impacts*, chapter 3, pages 44–63. John Wiley & Sons Ltd., 2017.

[55] S. Quartel, B. G. Ruessink, and A. Kroon. Daily to seasonal cross-shore behaviour of quasi-persistent intertidal beach morphology. *Earth Surface Processes and Landforms*, 32:1293–1307, 8 2007. doi: 10.1002/esp.1477.

[56] Francis P. Shephard. Beach cycles in southern california. Technical report, United States Army Corps of Engineers, 1950.

[57] Roshanka Ranasinghe, Rob Holman, Matthieu De Schipper, Tom Lippmann, Jennifer Wehof, Trang Minh Duong, Dano Roelvink, and Marcel Stive. Quantifying nearshore morphological recovery time scales using argus video imaging: Palm Beach, Sydney and Duck, North Carolina. *Proceedings of the Coastal Engineering Conference*, pages 1–7, 2012. ISSN 0589-087X. doi: 10.9753/icce.v33.sediment.24.

[58] T. Edelman. Dune erosion during storm conditions. In *Proc. 11th ICCE*, pages 719–722, Reston, VA, 1968. American Society of Civil Engineers.

[59] Dano Roelvink, Ad Reniers, Ap van Dongeren, Jaap van Thiel de Vries, Robert McCall, and Jamie Lescinski. Modelling storm impacts on beaches, dunes and barrier islands. *Coastal Engineering*, 56(11-12):1133–1152, 2009. ISSN 03783839. doi: 10.1016/j.coastaleng.2009.08.006.

[60] Jeffrey H. List, Amy S. Farris, and Charlene Sullivan. Reversing storm hotspots on sandy beaches: Spatial and temporal characteristics. *Marine Geology*, 226:261–279, 2006. doi: 10.1016/j.margeo.2005.10.003.

[61] S.B. McCann. Barrier Islands in the Southern Gulf of St. Lawrence, Canada. In Stephen P. Leatherman, editor, *Barrier Islands: From the Gulf of St. Lawrence to the Gulf of Mexico*. Academic Press, 1979.

[62] William J. Cleary and Paul E. Hosier. Geomorphology, Washover History, and Inlet

Zonation: Cape Lookout, North Carolina to Bird Island, North Carolina. In Stephen P. Leatherman, editor, *Barrier Islands: From the Gulf of St. Lawrence to the Gulf of Mexico*. Academic Press, 1979.

[63] S.B. McCann. Reconnaissance Survey of Hog Island, Prince Edward Island. *Maritime Sediments*, 0(3):107–113, 1972. ISSN 1098-6596.

[64] John J. Fisher and Elizabeth J. Simpson. Washover and Tidal Sedimentation Rates as Environmental Fators in Development of a Transgressive Barrier Shoreline. In Stephen P. Leatherman, editor, *Barrier Islands: From the Gulf of St. Lawrence to the Gulf of Mexico*, pages 127–148. Academic Press, 1979.

[65] R.L. Nichols and A.F. Marston. Shoreline changes in Rhode Island produced by hurricane of September 21, 1938. *Geological Society of America Bulletin*, 50, 1939.

[66] Peter S. Rosen. Aeolian Dynamics of a Barrier Island System. In Stephen P. Leatherman, editor, *Barrier Islands: From the Gulf of St. Lawrence to the Gulf of Mexico*, pages 81–98. Academic Press, 1979.

[67] Nicholas C. Kraus and Kentaro Hayashi. Numerical Morphologic Model of Barrier Island Breaching. In *Proc. 29th ICCE*, pages 2120–2132. World Scientific Press, 2005.

[68] Rafael Cañizares and Jennifer L. Irish. Simulation of storm-induced barrier island morphodynamics and flooding. *Coastal Engineering*, 55(12):1089–1101, 2008. ISSN 03783839. doi: 10.1016/j.coastaleng.2008.04.006. URL http://dx.doi.org/10.1016/j.coastaleng.2008.04.006.

[69] Daniel C. Conley. Observations on the impact of a developing inlet in a bar built estuary. *Continental Shelf Research*, 19(13):1733–1754, 1999. ISSN 02784343. doi: 10.1016/S0278-4343(99)00035-7.

[70] Travis G. Gerwing, Elmar Plate, Jess Kidd, Jesse Sinclair, Christopher W. Burns, Shane Johnson, Steven Roias, Cameron McCulloch, and Robert C. Bocking. Immediate response of fish communities and water chemistry to causeway breaching and bridge installation in the Kaouk River estuary, British Columbia, Canada. *Restoration Ecology*, 28(3):623–631, 2020. ISSN 1526100X. doi: 10.1111/rec.13110.

[71] Nicholas C. Kraus and Ty V Wamsley. Coastal Barrier Breaching, Part 1: Overview of Breaching Processes. *US Army Corps of Engineers*, pages 1–14, 2003.

[72] Ty V Wamsley and Nicholas C. Kraus. Coastal Barrier Island Breaching, Part 2: Mechanical Breaching and Breach Closure. *Erdc/Chl Chetn-Iv-65*, page 21, 2005.

[73] Paul J. Visser. Breach erosion in sand-dikes. *Proceedings of the Coastal Engineering Conference*, 3:3516–3528, 1998. ISSN 08938717. doi: 10.9753/icce.v26.

[74] N.C. Kraus, A. Militello, and G. Todoroff. Barrier Beaching Processes and Barrier Spit Breach, Stone Lagoon, California. *Shore and Beach*, 70(4):21–28, 2002. ISSN 0037-4237.

[75] J.W. Pierce. Tidal Inlets and Washover Fans. *J. Geol.*, 78, 1970.

[76] N.S. Shaler. *Beaches and Tidal Marshes of the Atlantic Coast*. American Book Company, 1895.

[77] Douglas W. Johnson. *Shore Processes and Shoreline Development*. John Wiley & Sons, Inc., 1919. ISBN 3663537137.

[78] Christopher R Sherwood, Joseph W Long, Patrick J Dickhudt, P Soupy Dalyander, David M Thompson, and Nathaniel G Plant. Inundation of a barrier island (Chandeleur Islands, Louisiana, USA) during a hurricane: Observed water-level gradients

and modeled seaward sand transport. *Journal of Geophysical Research: Earth Surface*, 119(7):1498–1515, 7 2014. ISSN 2169-9003. doi: 10.1002/2013JF003069. URL https://onlinelibrary.wiley.com/doi/10.1002/2013JF003069.

[79] T. Edelman. Dune erosion during storm conditions. In *Proc. 13th ICCE*, pages 1305–1311, Reston, VA, 1972. American Society of Civil Engineers. doi: 10.1525/9780520948068-073.

[80] Paul Brennan. Image of Beach Erosion from Hurricane Matthew, 2016. URL https://pixabay.com/users/paulbr75-2938186/.

[81] R. Nishi and N.C. Kraus. Mechanism and Calculation of Sand Dune Erosion by Storms. In *Proc. 26th ICCE*, pages 3034–3047, Reston, VA, 1996. American Society of Civil Engineers.

[82] P. Vellinga. *Beach and dune erosion during storm surges*. PhD thesis, Delft University of Technology, Delft, Netherlands, 1986.

[83] Nobuhisa Kobayashi. Analytical Solution for Dune Erosion by Storms. *Journal of Waterway, Port, Coastal, and Ocean Engineering*, 113(4):401–418, 1987. ISSN 0733-950X. doi: 10.1061/(asce)0733-950x(1987)113:4(401).

[84] Robert G. Dean. Equilibrium beach profiles: characteristics and applications. *Journal of Coastal Research*, 7(1):53–84, 1991. ISSN 0749-0208.

[85] David L. Kriebel and Robert G. Dean. Convolution Method for Time-Dependent Beach-Profile Response. *J. Waterway, Port, Coastal, Ocean Eng.*, 119(2):204–226, 1993.

[86] Paul D. Komar, W.G. McDougal, J.J. Marra, and Peter Ruggiero. The rational analysis of setback distances: Applications to the Oregon Coast. *Shore & Beach*, 67, 1999.

[87] Jeremy Mull and Peter Ruggiero. Estimating Storm-Induced Dune Erosion and Overtopping along U.S. West Coast Beaches. *Journal of Coastal Research*, 298(6):1173–1187, 2014. ISSN 0749-0208. doi: 10.2112/jcoastres-d-13-00178.1.

[88] Judith Bosboom and Marcel J F Stive. *Coastal Dynamics*. Delft University of Technology, Delft, The Netherlands, 2021. ISBN 9789463663700. doi: 10.5074/T.2021.001.

[89] Paul D. Komar and J. Robert Moore. *Handbook of Coastal Processes and Erosion*. CRC Press, Taylor and Francis Group, 2018 (orig edition, 1983. ISBN 9781315893808. doi: 10.1201/9781351072908.

[90] J.S. Fisher and M.F. Overton. Numerical Model for Dune Erosion Due to Wave Uprush. In Billy L. Edge, editor, *Proc. 19th ICCE*, pages 1553–1558, Reston, VA, 1984. American Society of Civil Engineers.

[91] M. F. Overton, J. S. Fisher, and M. A. Young. Laboratory Investigation of Dune Erosion. *Journal of Waterway, Port, Coastal, and Ocean Engineering*, 114 (3):367–373, 5 1988. ISSN 0733-950X. doi: 10.1061/(ASCE)0733-950X(1988) 114:3(367). URL http://ascelibrary.org/doi/10.1061/%28ASCE%290733-950X%281988%29114%3A3%28367%29.

[92] M. F. Overton, W. A. Pratikto, J. C. Lu, and J. S. Fisher. Laboratory investigation of dune erosion as a function of sand grain size and dune density. *Coastal Engineering*, 23(1-2):151–165, 1994. ISSN 03783839. doi: 10.1016/0378-3839(94)90020-5.

[93] J. S. Fisher, M. F. Overton, and T. Chisholm. Field Measurements of Dune Erosion. *Proceedings of the Coastal Engineering Conference*, 2(1984):1107–1115, 1987. doi: 10.1061/9780872626003.082.

[94] Magnus Larson, Li Erikson, and Hans Hanson. An analytical model to predict dune erosion due to wave impact. *Coastal Engineering*, 51(8-9):675–696, 2004. ISSN 03783839. doi: 10.1016/j.coastaleng.2004.07.003.

[95] Margaret L. Palmsten and Robert A. Holman. Laboratory investigation of dune erosion using stereo video. *Coastal Engineering*, 60(1):123–135, 2012. ISSN 03783839. doi: 10.1016/j.coastaleng.2011.09.003. URL http://dx.doi.org/10.1016/j.coastaleng.2011.09.003.

[96] Magnus Larson and Nicholas Kraus. SBEACH : Numerical Model for Simulating Storm-Induced Beach Change. *Technical Report CERC-89-9*, 1989.

[97] Robert G. Dean and Robert A. Dalrymple. *Coastal Processes with Engineering Applications*. Cambridge University Press, 2002. ISBN 0521495350.

[98] Peter Nielsen. *Coastal And Estuarine Processes*. World Scientific Publishing Company, 2009.

[99] Troels Aagaard and Michael Hughes. Sediment Transport. In J. Shroder and D.J. Sherman, editors, *Treatise on Geomorphology*, chapter 10.4, pages 74–105. Academic Press, San Diego, CA, vol. 10 edition, 2013.

[100] David L. Kriebel and Robert G. Dean. Numerical Simulation of Time-Dependent Beach and Dune Erosion. *Coastal Engineering*, 9:221–245, 1985.

[101] R. A. Bagnold. Mechanics of Marine Sedimentation. In M.N. Hill, editor, *The Sea: Ideas and Observations of Progress in the Study of the Seas, Vol. 3, The Earth Beneath the Sea; History.*, pages 507–528. John Wiley & Sons, Inc., New York, New York, 1963.

[102] R. A. Bagnold. An Approach to the Sediment Transport Problem from General Physics. Technical report, United States Government Printing Office, Washington, D.C., 1966.

[103] P.J. Williams. *Laboratory development of a predictive relationship for washover volume on barrier island coastlines*. PhD thesis, University of Delaware, Newark, Delaware, 1978.

[104] Hitoshi Tanaka, Suntoyo, and Tsuyoshi Nagasawa. Sediment Intrusion Into Gamo Lagoon by Wave Overtopping. In *Coastal Engineering 2002*, pages 823–835. World Scientific Publishing Company, 3 2002. ISBN 978-981-238-238-2. doi: 10.1142/9789812791306{_}0070.

[105] Nobuhisa Kobayashi, Yukiko Tega, and Mark W. Hancock. Wave Reflection and Overwash of Dunes. *Journal of Waterway, Port, Coastal, and Ocean Engineering*, 122(3):150–153, 5 1996. ISSN 0733-950X. doi: 10.1061/(ASCE)0733-950X(1996)122:3(150). URL http://ascelibrary.org/doi/10.1061/%28ASCE%290733-950X%281996%29122%3A3%28150%29.

[106] Stephen P. Leatherman. *Quantification of Overwash Processes*. PhD thesis, University of Virginia, Charlottesville, Virginia, 1976.

[107] Agustín Sánchez-Arcilla and José A. Jiménez. Breaching in a wave-dominated barrier spit: The trabucador bar (north-eastern spanish coast). *Earth Surface Processes and Landforms*, 19(6):483–498, 1994. ISSN 10969837. doi: 10.1002/esp.3290190602.

[108] T. E. Baldock, M. G. Hughes, K. Day, and J. Louys. Swash overtopping and sediment overwash on a truncated beach. *Coastal Engineering*, 52(7):633–645, 2005. ISSN 03783839. doi: 10.1016/j.coastaleng.2005.04.002.

[109] Chantal Donnelly, Magnus Larson, and Hans Hanson. A numerical model of coastal overwash. *Proceedings of the Institution of Civil Engineers - Maritime Engineering*, 162(3):105–114, 9 2009. doi: 10.1680/maen.2009.162.3.105. URL http://www.icevirtuallibrary.com/doi/10.1680/maen.2009.162.3.105.

[110] Randall A Wise, Jarrell Smith, and Magnus Larson. SBEACH: Numerical Model for Simulating Storm-Induced Beach Change; Report 4 - Cross-Shore Transport Under Random Waves and Model Validation with SUPERTANK and Field Data. Technical report, US Army Corps of Engineers, Coastal Research Program, 1996.

[111] M. Larson, R.A. Wise, and N. C. Kraus. Coastal Overwash, Part 2: Upgrade to SBEACH. *Coastal and Hydraulics Engineering Technical Note ERDC/CHL CHETN-XIV-14. Vicksburg, MS: US Army Engineer Research and Development Center, Coastal and Hydraulics Laboratory*, Coastal an(September):21, 2004. URL http://scholar.google.com/scholar?hl=en&btnG=Search&q=intitle:Coastal+Overwash+:+Part+2+,+Upgrade+to+SBEACH#0%5Cnhttp://scholar.google.com/scholar?hl=en&btnG=Search&q=intitle:Coastal+Overwash,+Part+2:+Upgrade+to+SBEACH#0.

[112] Chantal Donnelly, Roshanka Ranasinghe, and Magnus Larson. Numerical modeling of beach profile change caused by overwash. *Coastal Dynamics 2005 - Proceedings of the Fifth Coastal Dynamics International Conference*, pages 1–15, 2005. doi: 10.1061/40855(214)56.

[113] José A. Jiménez and Agustín Sánchez-Arcilla. A long-term (decadal scale) evolution model for microtidal barrier systems. *Coastal Engineering*, 51(8-9):749–764, 2004. ISSN 03783839. doi: 10.1016/j.coastaleng.2004.07.007.

[114] Stephen P. Leatherman. Migration of Assateague Island, Maryland, by inlet and overwash processes. *Geology*, 7:104–107, 1979.

[115] M. Larson, C. Donnelly, J. A. Jiménez, and H. Hanson. Analytical model of beach erosion and overwash during storms. *Proceedings of the Institution of Civil Engineers*

- *Maritime Engineering*, 162(3):115–125, 9 2009. doi: 10.1680/maen.2009.162.3.115. URL http://www.icevirtuallibrary.com/doi/10.1680/maen.2009.162.3.115.

[116] Nicholas C. Kraus, Kiki Patsch, and Sophie Munger. Barrier beach breaching from the lagoon side, with reference to Northern California. *Shore and Beach*, 76(2):33–43, 2008.

[117] Paul J. Visser. A model for breach erosion in sand-dikes. *Coastal Engineering 2000 - Proceedings of the 27th International Conference on Coastal Engineering, ICCE 2000*, 276(March 2001):3829–3842, 2000. doi: 10.1061/40549(276)299.

[118] David R. Basco and Cheol S. Shin. A one-dimensional numerical model for storm-breaching of barrier islands. *Journal of Coastal Research*, 15(1):241–260, 1999. ISSN 07490208.

[119] L. C. Van Rijn. Sediment transport: bed load transport. *Journal of Hydraulic Engineering - ASCE*, 110(10):1431–1456, 1984.

[120] Nicholas C. Kraus. Analytical model of incipient breaching of coastal barriers. *Coastal Engineering Journal*, 45(4):511–531, 2003. ISSN 17936292. doi: 10.1142/S057856340300097X.

[121] Jaap H. Nienhuis, Leoni G.H. Heijkers, and Gerben Ruessink. Barrier Breaching Versus Overwash Deposition: Predicting the Morphologic Impact of Storms on Coastal Barriers. *Journal of Geophysical Research: Earth Surface*, 126(6):1–17, 2021. ISSN 21699011. doi: 10.1029/2021JF006066.

[122] Hendrik J. Steetzel. *Cross-Shore Transport during Storm Surges*. PhD thesis, Technische Universiteit Delft, 1993.

[123] Nobuhisa Kobayashi, Andres Payo, and Lauren Schmied. Cross-shore suspended sand and bed load transport on beaches. *Journal of Geophysical Research: Oceans*, 113(7): 1–17, 2008. ISSN 21699291. doi: 10.1029/2007JC004203.

[124] Giles R. Lesser, J. A. Roelvink, J. A.T.M. van Kester, and G. S. Stelling. Development and validation of a three-dimensional morphological model. *Coastal Engineering*, 51 (8-9):883–915, 2004. ISSN 03783839. doi: 10.1016/j.coastaleng.2004.07.014.

[125] Nobuhisa Kobayashi and Ali Farhadzadeh. Cross-Shore Numerical Model Cshore for Waves, Currents, Sediment Transport and Beach Profile Evolution. Technical report, Center for Applied Coastal Research, Ocean Engineering Laboratory, Univ. of Delaware, Newark, Delaware, 2008.

[126] Alison Sleath Grzegorzewski, Bradley D Johnson, Ty V. Wamsley, and Julie Dean Rosati. Sediment Transport and Morphology Modeling of Ship Island, Mississippi, USA, During Storm Events. In *Coastal Dynamics 2013*, pages 1505–1516, Arcachon, France, 2013.

[127] Nobuhisa Kobayashi, Ali Farhadzadeh, Jeffrey Melby, Bradley D Johnson, and Mark B Gravens. Wave Overtopping of Levees and Overwash of Dunes. *Journal of Coastal Research*, 26(5):888–900, 2010. ISSN 0749-0208. doi: 10.2112/JCOASTRES-D-09-00034. 1.

[128] L van Rijn. *Principles of Sediment Transport in Rivers, Estuaries and Coastal Seas*. Aqua Publications, Amsterdam, 1993. ISBN 9080035629.

[129] R. L. Soulsby. *Dynamics of Marine Sands*. Thomas Telford, London, 1997.

[130] M. B. Gravens, R. M. Males, and D. A. Moser. Beach-fx: Monte Carlo life-cycle

simulation model for estimating shore protection project evolution and cost benefit analyses. *Shore and Beach*, 75(1):12–19, 2007.

[131] David P. Callaghan, Roshanka Ranasinghe, and Dano Roelvink. Probabilistic estimation of storm erosion using analytical, semi-empirical, and process based storm erosion models. *Coastal Engineering*, 82:64–75, 2013. ISSN 03783839. doi: 10.1016/j.coastaleng.2013.08.007. URL http://dx.doi.org/10.1016/j.coastaleng.2013.08.007.

[132] Joshua A. Simmons, Kristen D. Splinter, Mitchell D. Harley, and Ian L. Turner. Calibration data requirements for modelling subaerial beach storm erosion. *Coastal Engineering*, 152(November 2018):103507, 2019. ISSN 03783839. doi: 10.1016/j.coastaleng.2019.103507. URL https://doi.org/10.1016/j.coastaleng.2019.103507.

[133] Paula F.J. Van Baaren. *Influence of the wave period in the dune erosion model DUROSTA*. PhD thesis, Delft University of Technology, 2007.

[134] Bas Hoonhout. *Dune erosion along curved coastlines*. PhD thesis, Delft University of Technology, 2009.

[135] B. G. Ruessink, Y. Kuriyama, A. J.H.M. Reniers, J. A. Roelvink, and Dirk Jan R. Walstra. Modeling cross-shore sandbar behavior on the timescale of weeks. *Journal of Geophysical Research: Earth Surface*, 112(3):1–15, 2007. ISSN 21699011. doi: 10.1029/2006JF000730.

[136] Erik D. De Goede. Historical overview of 2D and 3D hydrodynamic modelling of shallow water flows in the Netherlands. *Ocean Dynamics*, 70(4):521–539, 2020. ISSN 16167228. doi: 10.1007/s10236-019-01336-5.

[137] Santiago Alfageme and Rafael Cañizares. Process-Based Morphological Modeling of a

Restored Barrier Island: Whiskey Island, Louisiana, USA. In *Coastal Dynamics 2005*, pages 1–11, Reston, VA, 9 2005. American Society of Civil Engineers.

[138] Santiago R. Alfageme, Masood Khondker, and Rafael Canizares. Breach Stability and Growth Analysis Using a Morphological Model. In *Coastal Sediments '07*, pages 2025–2036, Reston, VA, 5 2007. American Society of Civil Engineers. ISBN 978-0-7844-0926-8. doi: 10.1061/40926(239)159. URL http://ascelibrary.org/doi/10.1061/40926%28239%29159.

[139] Maarten van Ormondt, Timothy R. Nelson, Cheryl J. Hapke, and Dano Roelvink. Morphodynamic modelling of the wilderness breach, Fire Island, New York. Part I: Model set-up and validation. *Coastal Engineering*, 157(December 2019):103621, 2020. ISSN 03783839. doi: 10.1016/j.coastaleng.2019.103621. URL https://doi.org/10.1016/j.coastaleng.2019.103621.

[140] Bradley D Johnson, Nobuhisa Kobayashi, and Mark B Gravens. Cross-Shore Numerical Model CSHORE for Waves , Currents , Sediment Transport and Beach Profile Evolution. Technical report, US Army Corps of Engineers, Engineer Research and Development Center, 2012.

[141] Nobuhisa Kobayashi. Coastal Sediment Transport Modeling for Engineering Applications. *Journal of Waterway, Port, Coastal, and Ocean Engineering*, 142(6):03116001, 2016. ISSN 0733-950X. doi: 10.1061/(asce)ww.1943-5460.0000347.

[142] Ap Van Dongeren, Annelies Bolle, Michalis I. Vousdoukas, Theocharis Plomaritis, Petya Eftimova, Jon Williams, Clara Armaroli, Deborah Idier, Pieter Van Geer, Jaap Van Thiel de Vries, Piet Haerens, Rui Taborda, Javier Benavente, Ekaterina Trifonova, Paolo Ciavola, Yann Balouin, and Dano Roelvink. MICORE: DUNE EROSION AND OVERWASH MODEL VALIDATION WITH DATA FROM NINE EUROPEAN

FIELD SITES. In *Proceedings of Coastal Dynamics 2009*, pages 1–15. WORLD SCIENTIFIC, 8 2009. ISBN 978-981-4282-46-8. doi: 10.1142/9789814282475{_}0084. URL http://www.worldscientific.com/doi/abs/10.1142/9789814282475_0084.

[143] P.L.M. De Vet. *Modelling sediment transport and morphology during overwash and breaching events*. PhD thesis, Delft University of Technology, 2014.

[144] Saber M. Elsayed and Hocine Oumeraci. Effect of beach slope and grain-stabilization on coastal sediment transport: An attempt to overcome the erosion overestimation by XBeach. *Coastal Engineering*, 121(June 2016):179–196, 2017. ISSN 03783839. doi: 10.1016/j.coastaleng.2016.12.009. URL http://dx.doi.org/10.1016/j.coastaleng.2016.12.009.

[145] Davina L. Passeri, Joseph W. Long, Nathaniel G. Plant, Matthew V. Bilskie, and Scott C. Hagen. The influence of bed friction variability due to land cover on storm-driven barrier island morphodynamics. *Coastal Engineering*, 132(November 2017): 82–94, 2018. ISSN 03783839. doi: 10.1016/j.coastaleng.2017.11.005. URL https://doi.org/10.1016/j.coastaleng.2017.11.005.

[146] Marlies A. van der Lugt, Ellen Quataert, Ap van Dongeren, Maarten van Ormondt, and Christopher R. Sherwood. Morphodynamic modeling of the response of two barrier islands to Atlantic hurricane forcing. *Estuarine, Coastal and Shelf Science*, 229(May): 106404, 2019. ISSN 02727714. doi: 10.1016/j.ecss.2019.106404. URL https://doi.org/10.1016/j.ecss.2019.106404.

[147] Minsang Cho, Hyun-Doug Yoon, Kidoek Do, Sangyoung Son, and In-Ho Kim. Comparative Study on the Numerical Simulation of Bathymetric Changes under Storm Condition. *Journal of Coastal Research*, 91(sp1):106, 8 2019. ISSN 0749-0208. doi: 10.2112/SI91-022.1. URL https://bioone.org/

journals/journal-of-coastal-research/volume-91/issue-sp1/SI91-022.1/Comparative-Study-on-the-Numerical-Simulation-of-Bathymetric-Changes-under/10.2112/SI91-022.1.full.

[148] John C. Warner, Brandy Armstrong, Ruoying He, and Joseph B. Zambon. Development of a Coupled Ocean-Atmosphere-Wave-Sediment Transport (COAWST) Modeling System. *Ocean Modelling*, 35(3):230–244, 2010. ISSN 14635003. doi: 10.1016/j.ocemod.2010.07.010.

[149] Ilgar Safak, Jeffrey H. List, John C. Warner, and William C. Schwab. Persistent Shoreline Shape Induced From Offshore Geologic Framework: Effects of Shoreface Connected Ridges. *Journal of Geophysical Research: Oceans*, 122(11):8721–8738, 2017. ISSN 21699291. doi: 10.1002/2017JC012808.

[150] Ilgar Safak, John C. Warner, and Jeffrey H. List. Barrier island breach evolution: Alongshore transport and bay-ocean pressure gradient interactions. *Journal of Geophysical Research: Oceans*, 121:8720–8730, 12 2016. doi: 10.1002/2016JC012029.

[151] John C Warner, Maitane Olabarrieta, Christopher R Sherwood, Christie Hegermiller, and Tarandeep Singh Kalra. Investigations of Morphological Changes During Hurricane Sandy Using a Coupled Modeling System. In *AGU Fall Meeting Abstracts*, Washington, D.C., 2018. American Geophysical Union.

[152] Keivan Kaveh, Markus Reisenbüchler, Sandip Lamichhane, Tobias Liepert, Ngoc Dung Nguyen, Minh Duc Bui, and Peter Rutschmann. A Comparative Study of Comprehensive Modeling Systems for Sediment Transport in a Curved Open Channel. *Water*, 11, 8 2019. ISSN 2073-4441. doi: 10.3390/w11091779.

[153] Nadia Senechal, Bruno Castelle, and Karin R. Bryan. Storm Clustering and Beach

Response. In Paolo Ciavola and Giovanni Coco, editors, *Coastal Storms: Processes and Impacts*, chapter 8. John Wiley & Sons Ltd., 2017.

[154] Kristen D. Splinter, James T. Carley, Aliasghar Golshani, and Rodger Tomlinson. A relationship to describe the cumulative impact of storm clusters on beach erosion. *Coastal Engineering*, 83:49–55, 2014. ISSN 03783839. doi: 10.1016/j.coastaleng.2013.10.001. URL http://dx.doi.org/10.1016/j.coastaleng.2013.10.001.

[155] Pushpa Dissanayake, J. Brown, and H. Karunarathna. Impacts of storm chronology on the morphological changes of the Formby beach and dune system, UK. *Natural Hazards and Earth System Sciences*, 15(7):1533–1543, 2015. ISSN 16849981. doi: 10.5194/nhess-15-1533-2015.

[156] Doug Pender and Harshinie Karunarathna. A statistical-process based approach for modelling beach profile variability. *Coastal Engineering*, 81:19–29, 11 2013. ISSN 03783839. doi: 10.1016/j.coastaleng.2013.06.006. URL https://linkinghub.elsevier.com/retrieve/pii/S0378383913001142.

[157] Mark A. Davidson, Ian L. Turner, Kristen D. Splinter, and Mitchel D. Harley. Annual prediction of shoreline erosion and subsequent recovery. *Coastal Engineering*, 130 (October):14–25, 2017. ISSN 03783839. doi: 10.1016/j.coastaleng.2017.09.008. URL https://doi.org/10.1016/j.coastaleng.2017.09.008.

[158] Roshanka Ranasinghe, David Callaghan, and Marcel J.F. Stive. Estimating coastal recession due to sea level rise: Beyond the Bruun rule. *Climatic Change*, 110(3-4): 561–574, 2012. ISSN 01650009. doi: 10.1007/s10584-011-0107-8.

[159] Andrew D. Ashton, A. Brad Murray, and Olivier Arnoult. Formation of coastline features by large-scale instabilities induced by high-angle waves. *Nature*, 414:296–300, 2001. ISSN 00280836. doi: 10.1038/415666a.

[160] E.G. Otvos Jr. Development and Migration of Barrier Islands, Northern Gulf of Mexico. *Geol. Soc. Amer. Bull.*, 81, 1970.

[161] Shea Penland and Ron Boyd. Shoreline Changes on the Louisiana Barrier Coast. *Oceans*, 1981. ISSN 1098-6596. doi: 10.1017/CBO9781107415324.004.

[162] Maurice L. Schwartz. Barrier Islands. In *Benchmark Papers in Geology*. Dowden, Hutchinson & Ross, Inc., 1973.

[163] Stephen P. Leatherman. Annotated Chronological Bibliography of Barrier Island Migration. *Journal of Coastal Research*, 3(1):1–14, 1987.

[164] D.W. Moody. *Coastal morphology and processes in relation to the development of submarine sand ridges off Bethany Beach, Delaware*. PhD thesis, Johns Hopkins University, Baltimore, Maryland, 1964.

[165] Paul J. Godfrey. Oceanic overwash and its ecological implications on the Outer Banks of North Carolina. Technical report, Office of Natural Science Studies, National Parks Service, Washington, D.C., 1970.

[166] J.W. Pierce. Sediment budget along a barrier island chain. *Sedimentary Geology*, 3: 5–16, 1969.

[167] J. W. Armon and S. B. McCann. Morphology and landward sediment transfer in a transgressive barrier island system, southern Gulf of St. Lawrence, Canada. *Marine Geology*, 31(3-4):333–344, 1979. ISSN 00253227. doi: 10.1016/0025-3227(79)90041-0.

[168] USACE. *Shore Protection Manual: Vol. I*, volume I. US Army Corps of Engineers, Coastal Engineering Research Center, Vicksburg, MS, 1984.

[169] Per Bruun. Sea Level Rise as a Cause of Shore Erosion. *Proc. ASCE Journal Waterways Harbors Div.*, 88:117–130, 1962.

[170] Thomas F. Moslow and S. Duncan Heron Jr. Quaternary Evolution of Core Banks, North Carolina: Cape Lookout to New Drum Inlet. In Stephen P. Leatherman, editor, *Barrier Islands: From the Gulf of St. Lawrence to the Gulf of Mexico*. Academic Press, 1979.

[171] David Stolper, Jeffrey H. List, and E. Robert Thieler. Simulating the evolution of coastal morphology and stratigraphy with a new morphological-behaviour model (GEOMBEST). *Marine Geology*, 218:17–36, 2005. ISSN 00253227. doi: 10.1016/j.margeo.2005.02.019.

[172] Cody L. Johnson, Qin Chen, Celalettin E. Ozdemir, Kehui Xu, Robert McCall, and Kees Nederhoff. Morphodynamic modeling of a low-lying barrier subject to hurricane forcing: The role of backbarrier wetlands. *Coastal Engineering*, 167(April):103886, 2021. ISSN 03783839. doi: 10.1016/j.coastaleng.2021.103886. URL https://doi.org/10.1016/j.coastaleng.2021.103886.

[173] J.H. Hoyt. Chenier Versus Barrier, Genetic and Stratigraphic Distinction. *Amer. Assn. Petroleum Geologists Bull.*, 53, 1969.

[174] Orrin H. Pilkey and T. W. Davis. An analysis of coastal recession models: North Carolina coast. In *Sea-level fluctuation and coastal evolution*, pages 59–68. SEPM (Society for Sedimentary Geology), 1987. ISBN 9781565760950.

[175] Susan D. Halsey. Nexus: New Model of Barrier Island Development. In Stephen P. Leatherman, editor, *Barrier Islands: From the Gulf of St. Lawrence to the Gulf of Mexico*. Academic Press, 1979.

[176] George F. Oertel. Barrier Island Development during the Holocene Recession, Southeastern United States. In Stephen P. Leatherman, editor, *Barrier Islands: From the Gulf of St. Lawrence to the Gulf of Mexico*, pages 273–290. Academic Press, 1979.

[177] Daniel F. Belknap and John C. Kraft. Influence of antecedent geology on stratigraphic preservation potential and evolution of Delaware's barrier systems. *Marine Geology*, 63(1-4):235–262, 1985. ISSN 00253227. doi: 10.1016/0025-3227(85)90085-4.

[178] Donald J.P. Swift. Barrier-island genesis: evidence from the central atlantic shelf, eastern U.S.A. *Sedimentary Geology*, 14(1):1–43, 1975. ISSN 00370738. doi: 10.1016/0037-0738(75)90015-9.

[179] J. E.A. Storms, G.J. Weltje, J.J. van Dijke, C.R. Geel, and S.B. Kroonenberg. Process-Response Modeling of Wave-Dominated Coastal Systems: Simulating Evolution and Stratigraphy on Geological Timescales. *Journal of Sedimentary Research*, 72(2):226–239, 2002. ISSN 1527-1404. doi: 10.1306/052501720226.

[180] Laura J. Moore, Jeffrey H. List, S. Jeffress Williams, and David Stolper. Modeling Barrier Island Response to Sea-Level Rise in the Outer Banks, North Carolina. In *Coastal Sediments '07*, pages 1153–1164, Reston, VA, 2007. American Society of Civil Engineers.

[181] Peter Ruggiero, Maarten Buijsman, George M. Kaminsky, and Guy Gelfenbaum. Modeling the effects of wave climate and sediment supply variability on large-scale shoreline change. *Marine Geology*, 273(1-4):127–140, 2010. ISSN 00253227. doi: 10.1016/j.margeo.2010.02.008. URL http://dx.doi.org/10.1016/j.margeo.2010.02.008.

[182] W.P. Dillon. Submergence Effects on a Rhode Island Barrier and Lagoon and Inferences on Migration of Barriers. *J. Geol.*, 78, 1970.

[183] Marcel J.F. Stive, Dano J.A. Roelvink, and H.J. de Vriend. Large-Scale Coastal Evolution Concept. In *Proc. 22nd ICCE*, pages 1962–1974, 1990.

[184] J.H.J. Terwindt and J.A. Battjes. Research on Large-Scale Coastal Behavior. In *Proc.*

22nd ICCE, pages 1975–1983, 1990. URL http://0-ovidsp.tx.ovid.com.library.lausys.georgetown.edu/sp-3.2.1/ovidweb.cgi.

[185] Huib J. De Vriend. Mathematical modelling and large-scale coastal behaviour - Part 1: Physical Processes. *Journal of Hydraulic Research*, 29(6):727–740, 1991. ISSN 00221686. doi: 10.1080/00221689109498955.

[186] B. Latteux. Techniques for long-term morphological simulation under tidal action. *Marine Geology*, 126(1-4):129–141, 1995. ISSN 00253227. doi: 10.1016/0025-3227(95)00069-B. URL http://dx.doi.org/10.1016/0025-3227(95)00069-B.

[187] Peter J. Cowell, Marcel J.F. Stive, Alan W. Niedoroda, Don J.P. Swift, Huib J. De Vriend, Maarten C. Buijsman, Robert J. Nicholls, Peter S. Roy, George M. Kaminsky, Jelmer Cleveringa, Chris W. Reed, and Poppe L. De Boer. The Coastal-Tract (Part 2): Applications of Aggregated Modeling of Lower-order Coastal Change. *Journal of Coastal Research*, 19(4):828–848, 2003. ISSN 07490208.

[188] W.T. Bakker. The Dynamics of a Coast with a Groyne System. In *Proc. 11th ICCE*, pages 492–517, Reston, VA, 1968. American Society of Civil Engineers. doi: 10.31826/9781463212209-031.

[189] Marc Perlin and R. G. Dean. Prediction of Beach Planforms With Littoral Controls. *Proceedings of the Coastal Engineering Conference*, 2(1):1818–1838, 1979. ISSN 08938717. doi: 10.9753/icce.v16.110.

[190] Robert G. Dean and E.M. Maurmeyer. Models for Beach Profile Response. In Paul D. Komar, editor, *Handbook of Coastal Processes and Erosion*, chapter 7, pages 151–166. CRC Press, Taylor and Francis Group, 1983.

[191] Craig H. Everts. Sea Level Rise Effects on Shoreline Position. *J. Waterway, Port, Coastal, Ocean Eng.*, 111(6):985–999, 1985.

[192] Hans Hanson and NIcholas C. Kraus. GENESIS: Generalized Model for Simulating Shoreline Change. Technical Report CERC-89-19. Technical report, US Army Corps of Engineers, 1989.

[193] Magnus Larson, Nicholas C. Kraus, and Hans Hanson. Decoupled Numerical Model of Three-Dimensional Beach Change. In *Proc. 22nd ICCE*, pages 2173–2185, Delft, The Netherlands, 1990. American Society of Civil Engineers.

[194] P.J. Cowell, P.S. Roy, and R.A. Jones. Shoreface Translation Model: Computer Simulation of Coastal-Sandbody Response to Sea Level Rise. *Mathematics and Computers in Simulation*, 33:603–608, 1992.

[195] H. J. de Vriend, M. Capobianco, T. Chesher, H. E. de Swart, B. Latteux, and M. J.F. Stive. Approaches to long-term modelling of coastal morphology: A review. *Coastal Engineering*, 21(1-3):225–269, 1993. ISSN 03783839. doi: 10.1016/0378-3839(93)90051-9.

[196] Alan W. Niedoroda, Christopher W. Reed, Donald J.P. Swift, Hiroyuki Arato, and Koichi Hoyanagi. Modeling shore-normal large-scale coastal evolution. *Marine Geology*, 126:181–199, 1995. ISSN 00253227. doi: 10.1016/0025-3227(95)98961-7. URL http://dx.doi.org/10.1016/0025-3227(95)98961-7.

[197] Maarten C. Buijsman. The impact of gas extraction and sea level rise on the morphology of the Wadden Sea: Extension and Application of the model ASMITA. Technical report, Netherlands Center for Coastal Research, 1997.

[198] Henk J. Steetzel, Hans de Vroeg, Leo C. van Rijn, and Jean Marie Stam. Morphological

modelling using a modified multi-layer approach. *Proceedings of the Coastal Engineering Conference*, 2:2368–2381, 1998. ISSN 08938717. doi: 10.1061/9780784404119.178.

[199] Andrew D. Ashton and A. Brad Murray. High-angle wave instability and emergent shoreline shapes: 1. Modeling of sand waves, flying spits, and capes. *Journal of Geophysical Research: Earth Surface*, 111(4):1–19, 2006. ISSN 21699011. doi: 10.1029/2005JF000422.

[200] Magnus Larson, Nicholas C. Kraus, and Hans Hanson. Simulation of Regional Longshore Sediment Transport and Coastal Evolution - The "Cascade" Model. In *Coastal Engineering 2002*, pages 2612–2624. World Scientific Publishing Company, 2002. ISBN 978-981-238-238-2. doi: 10.1142/9789812791306{_}0218. URL http://www.worldscientific.com/doi/abs/10.1142/9789812791306_0218.

[201] Julie Dean Rosati, Robert G. Dean, Nicholas C. Kraus, and Gregory W. Stone. Morphologic Evolution of Subsiding Barrier Island Systems. In *Coastal Engineering 2006*, pages 3963–3975, San Diego, California, 4 2006. World Scientific Publishing Company. ISBN 978-981-270-636-2. doi: 10.1142/9789812709554{_}0333. URL http://www.worldscientific.com/doi/abs/10.1142/9789812709554_0333.

[202] Julie D. Rosati, Robert G. Dean, and Gregory W. Stone. A cross-shore model of barrier island migration over a compressible substrate. *Marine Geology*, 271(1-2):1–16, 2010. ISSN 00253227. doi: 10.1016/j.margeo.2010.01.005. URL http://dx.doi.org/10.1016/j.margeo.2010.01.005.

[203] Riccardo Masetti, Sergio Fagherazzi, and Alberto Montanari. Application of a barrier island translation model to the millennial-scale evolution of Sand Key, Florida. *Continental Shelf Research*, 28(9):1116–1126, 2008. ISSN 02784343. doi: 10.1016/j.csr.2008.02.021.

[204] M. L. Yates, R. T. Guza, and W. C. O'Reilly. Equilibrium shoreline response: Observations and modeling. *Journal of Geophysical Research: Oceans*, 114(9):1–16, 2009. ISSN 21699291. doi: 10.1029/2009JC005359.

[205] Ashley E Frey, Kenneth J Connell, Hans Hanson, Magnus Larson, Robert C Thomas, Sophie Munger, and Alan Zundel. GenCade Version 1 Model Theory and User's Guide. Technical Report December, US Army Corps of Engineers, Coastal and Hydraulics Laboratory, 2012.

[206] M. A. Davidson, K. D. Splinter, and I. L. Turner. A simple equilibrium model for predicting shoreline change. *Coastal Engineering*, 73:191–202, 2013. ISSN 03783839. doi: 10.1016/j.coastaleng.2012.11.002. URL http://dx.doi.org/10.1016/j.coastaleng.2012.11.002.

[207] Julie D. Rosati, Robert G. Dean, and T. L. Walton. The modified Bruun Rule extended for landward transport. *Marine Geology*, 340:71–81, 2013. ISSN 00253227. doi: 10.1016/j.margeo.2013.04.018. URL http://dx.doi.org/10.1016/j.margeo.2013.04.018.

[208] Andrew D. Ashton and Jorge Lorenzo-Trueba. Complex Responses of Barriers to Sea-Level Rise Emerging from a Model of Alongshore-Coupled Dynamic Profile Evolution. In *The Proceedings of the Coastal Sediments 2015*, pages 1–7. World Scientific, 7 2015. ISBN 978-981-4689-96-0. doi: 10.1142/9789814689977{_}0003.

[209] Robert G. Dean and J. R. Houston. Determining shoreline response to sea level rise. *Coastal Engineering*, 114:1–8, 2016. ISSN 03783839. doi: 10.1016/j.coastaleng.2016.03.009. URL http://dx.doi.org/10.1016/j.coastaleng.2016.03.009.

[210] Sean Vitousek, Patrick L. Barnard, Patrick Limber, Li Erikson, and Blake Cole. A model integrating longshore and cross-shore processes for predicting long-term shore-

line response to climate change. *Journal of Geophysical Research: Earth Surface*, pages 782–806, 2017. doi: 10.1002/2016JF004065.

[211] Arthur Robinet, Déborah Idier, Bruno Castelle, and Vincent Marieu. A reduced-complexity shoreline change model combining longshore and cross-shore processes: The LX-Shore model. *Environmental Modelling and Software*, 109(August):1–16, 2018. ISSN 13648152. doi: 10.1016/j.envsoft.2018.08.010. URL https://doi.org/10.1016/j.envsoft.2018.08.010.

[212] José A.A. Antolínez, Fernando J. Méndez, Dylan Anderson, Peter Ruggiero, and George M. Kaminsky. Predicting Climate-Driven Coastlines With a Simple and Efficient Multiscale Model. *Journal of Geophysical Research: Earth Surface*, 124(6): 1596–1624, 2019. ISSN 21699011. doi: 10.1029/2018JF004790.

[213] Jaap H. Nienhuis and Jorge Lorenzo-Trueba. Simulating barrier island response to sea level rise with the barrier island and inlet environment (BRIE) model v1.0. *Geoscientific Model Development*, 12(9):4013–4030, 2019. ISSN 19919603. doi: 10.5194/gmd-12-4013-2019.

[214] Dano Roelvink, Bas Huisman, Ahmed Elghandour, Mohamed Ghonim, and Johan Reyns. Efficient Modeling of Complex Sandy Coastal Evolution at Monthly to Century Time Scales. *Frontiers in Marine Science*, 7(July):1–20, 2020. ISSN 22967745. doi: 10.3389/fmars.2020.00535.

[215] Jaime Palalane and Magnus Larson. A Long-Term Coastal Evolution Model with Longshore and Cross-Shore Transport. *Journal of Coastal Research*, 36(2):411–423, 2020. ISSN 15515036. doi: 10.2112/JCOASTRES-D-17-00020.1.

[216] Deltares. UNIBEST-CL+, 2021. URL https://www.deltares.nl/en/software/unibest-cl/#technical-specifications.

[217] R. Jak McCarroll, Gerd Masselink, Nieves G. Valiente, Timothy Scott, Mark Wiggins, Josie Alice Kirby, and Mark A. Davidson. A rules-based shoreface translation and sediment budgeting tool for estimating coastal change: ShoreTrans. *Marine Geology*, 435:106466, 2021. ISSN 00253227. doi: 10.1016/j.margeo.2021.106466. URL https://doi.org/10.1016/j.margeo.2021.106466.

[218] M. Alvarez-Cuesta, A. Toimil, and I. J. Losada. Modelling long-term shoreline evolution in highly anthropized coastal areas. Part 1: Model description and validation. *Coastal Engineering*, 169, 2021. ISSN 03783839. doi: 10.1016/j.coastaleng.2021.103960. URL https://doi.org/10.1016/j.coastaleng.2021.103960.

[219] I. R.B. Reeves, L. J. Moore, A. B. Murray, K. A. Anarde, and E. B. Goldstein. Dune Dynamics Drive Discontinuous Barrier Retreat. *Geophysical Research Letters*, 48(13): 1–11, 2021. ISSN 19448007. doi: 10.1029/2021GL092958.

[220] Magnus Larson, Hans Hanson, and Nicholas C. Kraus. Analytical Solutions of the One-Line Model of Shoreline Change. *Technical Report CERC-87-15*, 1987.

[221] R.S. Young, Orrin H. Pilkey, D.M. Bush, and E.R. Thieler. A discussion of the generalized model for simulating shoreline change (GENESIS). *Journal of Coastal Research*, 11(3):875–886, 1995. ISSN 0749-0208.

[222] James R. Houston. Discussion of: Young, R.S.; Pilkey, O.H.; Bush, D.M.; and Thieler, E.R. A discussion of the generalized model for simulating shoreline change (GENESIS), Journal of Coastal Research 11(3), 875-886. *Journal of Coastal Research*, 12(4):1038–1043, 1996. ISSN 0749-0208.

[223] Robert C Thomas and Ashley E Frey. Shoreline change modeling using one-line models: General model comparison and literature review. *ERDC/CHL CHETN-II-55. Vicks-*

burg, MS: US Army Engineer Research and Development Center, 1956(December), 2013. doi: ERDC/CHLCHETN-II-55.

[224] Sung-chan Kim, Richard Styles, Julie Rosati, Yan Ding, and Rusty Permenter. A Comparison of GenCade, Pelnard-Considere, and LITPACK. Technical Report April, United States Army Corps of Engineers, 2020.

[225] Marc Perlin and Robert G. Dean. 3-D Model of Bathymetric Response to Structures. *J. Waterway, Port, Coastal, Ocean Eng.*, 111(2):153–170, 1985.

[226] Marcel J. Stive, Huib J. De Vriend, Peter J. Cowell, and Alan Wm Niedoroda. Behaviour-oriented models of shoreface evolution. In *Coastal Dynamics - Proceedings of the International Conference*, pages 998–1005. ASCE, 1995.

[227] Maurice L. Schwartz. The Bruun Theory of Sea-Level Rise as a Cause of Shore Erosion. *The Journal of Geology*, 75(1):76–92, 1967.

[228] Per Bruun. Review of conditions for uses of the Bruun rule of erosion. *Coastal Engineering*, 7(1):77–89, 1983. ISSN 03783839. doi: 10.1016/0378-3839(83)90028-5.

[229] Orrin H. Pilkey, R. S. Young, S. R. Riggs, A. W.S. Smith, and W. D. Pilkey. The concept of shoreface profile of equilibrium: a critical review. *Journal of Coastal Research*, 9(1):255–278, 1993. ISSN 0749-0208.

[230] E. Robert Thieler, Orrin H. Pilkey, Robert S. Young, David M. Bush, and Fei Chai. The use of mathematical models to predict beach behavior for U.S. coastal engineering: A critical review. *Journal of Coastal Research*, 16(1):48–70, 2000. ISSN 0749-0208.

[231] Roger N. Dubois. Discussion of Orrin Pilkey, Robert S. Young, Stanley R. Riggs, A. W. Sam Smith, Huiyan Wu and Walter D. Pilkey, 1993. The concept of shoreface profile

of equilibrium: A critical review. *Journal of Coastal Research*, 9(4):28–31, 1993. ISSN 0749-0208.

[232] Matthew A. Wolinsky and A. Brad Murray. A unifying framework for shoreline migration: 2. Application to wave-dominated coasts. *Journal of Geophysical Research: Earth Surface*, 114(1):1–13, 2009. ISSN 21699011. doi: 10.1029/2007JF000856.

[233] Alexander L. Atkinson, Tom E. Baldock, Florent Birrien, David P. Callaghan, Peter Nielsen, Tomas Beuzen, Ian L. Turner, Chris E. Blenkinsopp, and Roshanka Ranasinghe. Laboratory investigation of the Bruun Rule and beach response to sea level rise. *Coastal Engineering*, 136(December 2017):183–202, 2018. ISSN 03783839. doi: 10.1016/j.coastaleng.2018.03.003. URL https://doi.org/10.1016/j.coastaleng.2018.03.003.

[234] Maurizio D'anna, Deborah Idier, Bruno Castelle, Sean Vitousek, and Goneri Le Cozannet. Reinterpreting the bruun rule in the context of equilibrium shoreline models. *Journal of Marine Science and Engineering*, 9(9), 2021. ISSN 20771312. doi: 10.3390/jmse9090974.

[235] Cary D. Troy, Yi Ting Cheng, Yi Chun Lin, and Ayman Habib. Rapid lake Michigan shoreline changes revealed by UAV LiDAR surveys. *Coastal Engineering*, 170(March): 104008, 2021. ISSN 03783839. doi: 10.1016/j.coastaleng.2021.104008. URL https://doi.org/10.1016/j.coastaleng.2021.104008.

[236] Craig H. Everts. Continental Shelf Evolution in Response to a Rise in Sea Level. In *Sea-Level Fluctuations and Coastal Evolution*, pages 49–57. SEPM (Society for Sedimentary Geology), 1987. doi: 10.2110/pec.87.41.0049. URL https://pubs.geoscienceworld.org/books/book/1045/chapter/10534595/.

[237] Stephen P. Leatherman. Barrier dynamics and landward migration with Holocene sea-level rise. *Nature*, 301(3):415–417, 1983. ISSN 1098-6596.

[238] P.J. Cowell, P. S. Roy, and R. A. Jones. Simulation of large-scale coastal change using a morphological behaviour model. *Marine Geology*, 126:45–61, 1995. ISSN 00253227. doi: 10.1016/0025-3227(95)00065-7. URL http://dx.doi.org/10.1016/0025-3227(95)00065-7.

[239] Peter J. Cowell, Bruce G. Thom, Robert A. Jones, Craig H. Everts, and Denis Simanovic. Management of uncertainty in predicting climate-change impacts on beaches. *Journal of Coastal Research*, 22(1):232–245, 2006. ISSN 07490208. doi: 10.2112/05A-0018.1.

[240] Laura J. Moore, Jeffrey H. List, S. Jeffress Williams, and David Stolper. Complexities in barrier island response to sea level rise: Insights from numerical model experiments, North Carolina Outer Banks. *Journal of Geophysical Research*, 115:F03004, 2010. ISSN 0148-0227. doi: 10.1029/2009jf001299.

[241] Owen T. Brenner, Laura J. Moore, and A. Brad Murray. The complex influences of back-barrier deposition, substrate slope and underlying stratigraphy in barrier island response to sea-level rise: Insights from the Virginia Barrier Islands, Mid-Atlantic Bight, U.S.A. *Geomorphology*, 246:334–350, 2015. ISSN 0169555X. doi: 10.1016/j.geomorph.2015.06.014. URL http://dx.doi.org/10.1016/j.geomorph.2015.06.014.

[242] Giulio Mariotti and Sergio Fagherazzi. A numerical model for the coupled long-term evolution of salt marshes and tidal flats. *Journal of Geophysical Research*, 115:F01004, 1 2010. ISSN 0148-0227. doi: 10.1029/2009JF001326. URL http://doi.wiley.com/10.1029/2009JF001326.

[243] Magnus Larson, Jaime Palalane, Caroline Fredriksson, and Hans Hanson. Simulating cross-shore material exchange at decadal scale. Theory and model component validation. *Coastal Engineering*, 116:57–66, 2016. ISSN 03783839. doi: 10.1016/j.coastaleng.2016.05.009. URL http://dx.doi.org/10.1016/j.coastaleng.2016.05.009.

[244] Robert J. Hallermeier. A profile zonation for seasonal sand beaches from wave climate. *Coastal Engineering*, 4(C):253–277, 1980. ISSN 03783839. doi: 10.1016/0378-3839(80)90022-8.

[245] Alexandra Toimil, Inigo J. Losada, Paula Camus, and Pedro Díaz-Simal. Managing coastal erosion under climate change at the regional scale. *Coastal Engineering*, 128 (August):106–122, 2017. ISSN 03783839. doi: 10.1016/j.coastaleng.2017.08.004. URL http://dx.doi.org/10.1016/j.coastaleng.2017.08.004.

[246] Sean Vitousek and Patrick L. Barnard. A Nonlinear, Implicit, One-Line Model to Predict Long-Term Shoreline Change. In *The Proceedings of the Coastal Sediments 2015*, pages 1–14. WORLD SCIENTIFIC, 7 2015. ISBN 978-981-4689-96-0. doi: 10.1142/9789814689977{_}0215. URL http://www.worldscientific.com/doi/abs/10.1142/9789814689977_0215.

[247] Joseph W. Long and Nathaniel G. Plant. Extended Kalman Filter framework for forecasting shoreline evolution. *Geophysical Research Letters*, 39(13):1–6, 2012. ISSN 00948276. doi: 10.1029/2012GL052180.

[248] J. W. Kamphuis. Alongshore sediment transport rate distribution. *Coastal Sediments '91*, 117(6):170–183, 1991.

[249] Jon K. Miller and Robert G. Dean. A simple new shoreline change model. *Coastal Engineering*, 51(7):531–556, 2004. ISSN 03783839. doi: 10.1016/j.coastaleng.2004.05.006.

[250] Raimundo Ibaceta, Kristen D. Splinter, Mitchell D. Harley, and Ian L. Turner. Enhanced Coastal Shoreline Modeling Using an Ensemble Kalman Filter to Include Nonstationarity in Future Wave Climates. *Geophysical Research Letters*, 47:1–12, 2020. ISSN 19448007. doi: 10.1029/2020GL090724.

[251] S. Rao Vemulakonda, N. W. Scheffner, J. A. Earickson, and L. W. Chou. Kings Bay Coastal Processes Numerical Model. *Technical Report - US Army Coastal Engineering Research Center*, 88-3, 1988.

[252] J. A. Roelvink. Coastal morphodynamic evolution techniques. *Coastal Engineering*, 53(2-3):277–287, 2006. ISSN 03783839. doi: 10.1016/j.coastaleng.2005.10.015.

[253] Joseph Long, P. Soupy Dalyander, Michael Poff, Brian Spears, Brett Borne, David Thompson, Rangley Mickey, Steve Dartez, and Gregory Grandy. Event and decadal-scale modeling of barrier island restoration designs for decision support. *Shore & Beach*, 88(1):49–57, 2020. ISSN 0037-4237. doi: 10.34237/1008816.

[254] A Brad Murray. Contrasting the Goals, Strategies, and Predictions Associated with Simplified Numerical Models and Detailed Simulations. In Peter R. Wilcock and Richard M. Iverson, editors, *Prediction in Geomorphology, Geophysical Monograph 135*, pages 151–165. American Geophysical Union, Washington, D.C., 3 2003. doi: 10.1029/135GM11. URL https://onlinelibrary.wiley.com/doi/10.1029/135GM11.

[255] Huib J. De Vriend. Mathematical modelling and large-scale coastal behavior - Part 2: Predictive Models. *Journal of Hydraulic Research*, 29(6):741–753, 1991. ISSN 00221686. doi: 10.1080/00221689109498956.

[256] Magnus Larson and Nicholas C. Kraus. Temporal and spatial scales of beach profile change, Duck, North Carolina. *Marine Geology*, 117(1-4):75–94, 1994. ISSN 00253227. doi: 10.1016/0025-3227(94)90007-8.

[257] B. C. Ludka, R. T. Guza, W. C. O'Reilly, M. A. Merrifield, R. E. Flick, A. S. Bak, T. Hesser, R. Bucciarelli, C. Olfe, B. Woodward, W. Boyd, K. Smith, M. Okihiro, R. Grenzeback, L. Parry, and G. Boyd. Sixteen years of bathymetry and waves at San Diego beaches. *Scientific Data*, 6(1):1–13, 2019. ISSN 20524463. doi: 10.1038/s41597-019-0167-6.

[258] Patrick L. Barnard, Jeff E. Hansen, and Li H. Erikson. Synthesis study of an erosion hot spot, Ocean Beach, California. *Journal of Coastal Research*, 28(4):903–922, 2012. ISSN 07490208. doi: 10.2112/JCOASTRES-D-11-00212.1.

[259] Erika E. Lentz and Cheryl J. Hapke. Geologic framework influences on the geomorphology of an anthropogenically modified barrier island: Assessment of dune/beach changes at Fire Island, New York. *Geomorphology*, 126(1-2):82–96, 3 2011. ISSN 0169555X. doi: 10.1016/j.geomorph.2010.10.032. URL https://linkinghub.elsevier.com/retrieve/pii/S0169555X10004708.

[260] Ian L. Turner, Mitchell D. Harley, Andrew D. Short, Joshua A. Simmons, Melissa A. Bracs, Matthew S. Phillips, and Kristen D. Splinter. A multi-decade dataset of monthly beach profile surveys and inshore wave forcing at Narrabeen, Australia. *Scientific Data*, 3:1–13, 2016. ISSN 20524463. doi: 10.1038/sdata.2016.24.

[261] Bruno Castelle, Stéphane Bujan, Vincent Marieu, and Sophie Ferreira. 16 Years of Topographic Surveys of Rip-Channelled High-Energy Meso-Macrotidal Sandy Beach. *Scientific Data*, 7(1):1–9, 2020. ISSN 20524463. doi: 10.1038/s41597-020-00750-5.

[262] Masayuki Banno, Satoshi Nakamura, Taichi Kosako, Yasuyuki Nakagawa, Shin Ichi Yanagishima, and Yoshiaki Kuriyama. Long-term observations of beach variability at Hasaki, Japan. *Journal of Marine Science and Engineering*, 8(11):1–17, 2020. ISSN 20771312. doi: 10.3390/jmse8110871.

[263] Matthieu A. de Schipper, Sierd de Vries, Gerben Ruessink, Roeland C. de Zeeuw, Jantien Rutten, Carola van Gelder-Maas, and Marcel J.F. Stive. Initial spreading of a mega feeder nourishment: Observations of the Sand Engine pilot project. *Coastal Engineering*, 111:23–38, 2016. ISSN 03783839. doi: 10.1016/j.coastaleng.2015.10.011. URL http://dx.doi.org/10.1016/j.coastaleng.2015.10.011.

[264] Ellen M. Rathje, Clint Dawson, Jamie E. Padgett, Jean-Paul Pinelli, Dan Stanzione, Ashley Adair, Pedro Arduino, Scott J. Brandenberg, Tim Cockerill, Charlie Dey, Maria Esteva, Fred L. Haan, Matthew Hanlon, Ahsan Kareem, Laura Lowes, Stephen Mock, and Gilberto Mosqueda. DesignSafe: New Cyberinfrastructure for Natural Hazards Engineering. *Natural Hazards Review*, 18(3):06017001, 2017. ISSN 1527-6988. doi: 10.1061/(asce)nh.1527-6996.0000246.

[265] Jeffrey W. Berman, Joseph Wartman, Michael Olsen, Jennifer L. Irish, Scott B. Miles, Troy Tanner, Kurtis Gurley, Laura Lowes, Ann Bostrom, Jacob Dafni, Michael Grilliot, Andrew Lyda, and Jaqueline Peltier. Natural Hazards Reconnaissance With the NHERI RAPID Facility. *Frontiers in Built Environment*, 6(November):1–16, 2020. ISSN 22973362. doi: 10.3389/fbuil.2020.573067.

[266] Arjen Luijendijk, Gerben Hagenaars, Roshanka Ranasinghe, Fedor Baart, Gennadii Donchyts, and Stefan Aarninkhof. The State of the World's Beaches. *Scientific Reports*, 8(1):6641, 12 2018. ISSN 2045-2322. doi: 10.1038/s41598-018-24630-6.

[267] Kilian Vos, Mitchell D. Harley, Kristen D. Splinter, Joshua A. Simmons, and Ian L. Turner. Sub-annual to multi-decadal shoreline variability from publicly available satellite imagery. *Coastal Engineering*, 150(April):160–174, 2019. ISSN 03783839. doi: 10.1016/j.coastaleng.2019.04.004. URL https://doi.org/10.1016/j.coastaleng.2019.04.004.

[268] Ian L. Turner, Mitchell D. Harley, Rafael Almar, and Erwin W.J. Bergsma. Satellite optical imagery in Coastal Engineering. *Coastal Engineering*, 167:103919, 2021. ISSN 03783839. doi: 10.1016/j.coastaleng.2021.103919. URL https://doi.org/10.1016/j.coastaleng.2021.103919.

[269] L. Shaw, P. Helmholz, D. Belton, and N. Addy. Comparison of uav lidar and imagery for beach monitoring. *International Archives of the Photogrammetry, Remote Sensing and Spatial Information Sciences - ISPRS Archives*, 42(2/W13):589–596, 2019. ISSN 16821750. doi: 10.5194/isprs-archives-XLII-2-W13-589-2019.

[270] Mitchell D. Harley, Michael A. Kinsela, Elena Sánchez-García, and Kilian Vos. Shoreline change mapping using crowd-sourced smartphone images. *Coastal Engineering*, 150:175–189, 2019. ISSN 03783839. doi: 10.1016/j.coastaleng.2019.04.003.

[271] Joseph Wartman, Jeffrey W. Berman, Ann Bostrom, Scott Miles, Michael Olsen, Kurtis Gurley, Jennifer Irish, Laura Lowes, Troy Tanner, Jake Dafni, Michael Grilliot, Andrew Lyda, and Jaqueline Peltier. Research Needs, Challenges, and Strategic Approaches for Natural Hazards and Disaster Reconnaissance. *Frontiers in Built Environment*, 6(November):1–17, 2020. ISSN 22973362. doi: 10.3389/fbuil.2020.573068.

[272] Britt Raubenheimer. DEVELOPMENT OF A NEARSHORE EXTREME EVENTS RECONNAISSANCE COMMUNITY. *Coastal Engineering Proceedings*, 12 2020. ISSN 2156-1028. doi: 10.9753/icce.v36v.keynote.12.

[273] A. G. Davies, L. C. Van Rijn, J. S. Damgaard, J. Van De Graaff, and J. S. Ribberink. Intercomparison of research and practical sand transport models. *Coastal Engineering*, 46(1):1–23, 2002. ISSN 03783839. doi: 10.1016/S0378-3839(02)00042-X.

[274] Berna Ayat and Nobuhisa Kobayashi. Vertical Cylinder Density and Toppling Effects on Dune Erosion and Overwash. *Journal of Waterway, Port, Coastal, and Ocean En-*

gineering, 141(1):04014026, 2015. ISSN 0733-950X. doi: 10.1061/(asce)ww.1943-5460.0000264.

[275] Julie C. Zinnert, Stephen M. Via, Benjamin P. Nettleton, Philip A. Tuley, Laura J. Moore, and Jon Anthony Stallins. Connectivity in coastal systems: Barrier island vegetation influences upland migration in a changing climate. *Global Change Biology*, 25(7):2419–2430, 2019. ISSN 13652486. doi: 10.1111/gcb.14635.

[276] Todd Bridges, Jeffrey King, Johnathan Simm, Michael Beck, Georganna Collins, Quirijn Lodder, and Ram Mohan. International Guidelines on Natural and Nature-Based Features for Flood Risk Management. Technical report, U.S. Army Corps of Engineers, Washington, D.C., 9 2021.

[277] A. G. Keeler, Dylan E. McNamara, and Jennifer L. Irish. Responding to Sea Level Rise: Does Short-Term Risk Reduction Inhibit Successful Long-Term Adaptation? *Earth's Future*, 6(4):618–621, 2018. ISSN 23284277. doi: 10.1002/2018EF000828.

[278] Dylan E. McNamara and B. T. Werner. Coupled barrier island-resort model: 1. Emergent instabilities induced by strong human-landscape interactions. *Journal of Geophysical Research: Earth Surface*, 113(1):1–10, 2008. ISSN 21699011. doi: 10.1029/2007JF000840.

[279] Dylan E. McNamara and Andrew Keeler. A coupled physical and economic model of the response of coastal real estate to climate risk. *Nature Climate Change*, 3(6): 559–562, 2013. ISSN 1758678X. doi: 10.1038/nclimate1826.

[280] Laura J. Rogers, Laura J. Moore, Evan B. Goldstein, Christopher J. Hein, Jorge Lorenzo-trueba, and Andrew D. Ashton. Anthropogenic controls on overwash deposition: Evidence and consequences. *Journal of Geophysical Research: Earth Surface*, pages 2609–2624, 2015. doi: 10.1002/2015JF003634.

[281] Dylan E. McNamara and Eli D. Lazarus. Barrier Islands as Coupled Human-Lanscape Systems. In Laura J. Moore and A. Brad Murray, editors, *Barrier Dynamics and Response to Changing Climate*, pages 363–383. Springer, New York, 2018.

[282] NASEM. *Understanding the Long-Term Evolution of the Coupled Natural-Human Coastal System*. The National Academies Press, 2018. ISBN 9780309475846. doi: 10.17226/25108.

[283] Sean Vitousek, Laura Cagigal, Jennifer Montaño, and Ana Rueda. The Application of Ensemble Wave Forcing to Quantify Uncertainty of Shoreline Change Predictions Journal of Geophysical Research : Earth Surface. *Journal of Geophysical Research: Earth Surface*, pages 1–43, 2021.

[284] Jennifer Montaño, Giovanni Coco, Jose A.A. Antolínez, Tomas Beuzen, Karin R. Bryan, Laura Cagigal, Bruno Castelle, Mark A. Davidson, Evan B. Goldstein, Raimundo Ibaceta, Déborah Idier, Bonnie C. Ludka, Sina Masoud-Ansari, Fernando J. Méndez, A. Brad Murray, Nathaniel G. Plant, Katherine M. Ratliff, Arthur Robinet, Ana Rueda, Nadia Sénéchal, Joshua A. Simmons, Kristen D. Splinter, Scott Stephens, Ian Townend, Sean Vitousek, and Kilian Vos. Blind testing of shoreline evolution models. *Scientific Reports*, 10(1):1–10, 2020. ISSN 20452322. doi: 10.1038/s41598-020-59018-y.

[285] Evan B. Goldstein, Giovanni Coco, and Nathaniel G. Plant. A review of machine learning applications to coastal sediment transport and morphodynamics. *Earth-Science Reviews*, 194(April):97–108, 2019. ISSN 00128252. doi: 10.1016/j.earscirev.2019.04.022. URL https://doi.org/10.1016/j.earscirev.2019.04.022.

[286] Katherine L. Brodie, Margaret L. Palmsten, and Nicholas J Spore. Coastal Foredune

Evolution, Part 1: Environmental Factors & Forcing Processes Affecting Morphological Evolution. Technical report, US Army Corps of Engineers, 2017.

[287] Nathaniel Plant, Kara Doran, and Hilary Stockdon. Examples of Storm Impacts on Barrier Islands. In *Coastal Storms*, pages 65–79. Wiley, 5 2017. ISBN 9781118937099. doi: 10.1002/9781118937099.ch4. URL https://onlinelibrary.wiley.com/doi/10.1002/9781118937099.ch4.

[288] Steven W.H. Hoagland, Catherine R. Jeffries, Jennifer L. Irish, Robert Weiss, Kyle Mandli, Sean Vitousek, Catherine M. Johnson, and Mary A. Cialone. Advances in Morphodynamic Modeling of Coastal Barriers: A Review. *Journal of Waterway, Port, Coastal, and Ocean Engineering*, 149(5), 9 2023. ISSN 0733-950X. doi: 10.1061/JWPED5.WWENG-1825. URL https://ascelibrary.org/doi/10.1061/JWPED5.WWENG-1825.

[289] H. Hanson. GENESIS - a generalized shoreline change numerical model. *Journal of Coastal Research*, 5(1):1–27, 1989. ISSN 0749-0208.

[290] D. H. Swart. *Offshore Sediment Transport and Equilibrium Beach Profiles*. PhD thesis, Bibliotheek Technische Universiteit, 1974.

[291] Alejandra C. Ortiz and Andrew D. Ashton. Exploring shoreface dynamics and a mechanistic explanation for a morphodynamic depth of closure. *Journal of Geophysical Research: Earth Surface*, 2016. doi: 10.1002/2013JF002871.Received.

[292] Peter J. Cowell and Michael A. Kinsela. Shoreface Controls on Barrier Evolution and Shoreline Change. In Laura J. Moore and Brad A. Murray, editors, *Barrier Dynamics and Response to Changing Climate*, pages 243–275. Springer International Publishing, 2018.

[293] Joseph W. Long, Anouk T.M. de Bakker, and Nathaniel G. Plant. Scaling coastal dune elevation changes across storm-impact regimes. *Geophysical Research Letters*, 41 (8):2899–2906, 2014. ISSN 19448007. doi: 10.1002/2014GL059616.

[294] Davina L. Passeri, P. Soupy Dalyander, Joseph W. Long, Rangley C. Mickey, Robert L. Jenkins, David M. Thompson, Nathaniel G. Plant, Elizabeth S. Godsey, and Victor M. Gonzalez. The Roles of Storminess and Sea Level Rise in Decadal Barrier Island Evolution. *Geophysical Research Letters*, 47(18):1–8, 2020. ISSN 19448007. doi: 10.1029/2020GL089370.

[295] Emily A. Carruthers, D. Philip Lane, Rob L. Evans, Jeffrey P. Donnelly, and Andrew D. Ashton. Quantifying overwash flux in barrier systems: An example from Martha's Vineyard, Massachusetts, USA. *Marine Geology*, 343:15–28, 2013. ISSN 00253227. doi: 10.1016/j.margeo.2013.05.013. URL http://dx.doi.org/10.1016/j.margeo.2013.05.013.

[296] Andrew D. Ashton and Jorge Lorenzo-Trueba. Morphodynamics of Barrier Response to Sea-Level Rise. In Laura J. Moore and Brad A. Murray, editors, *Barrier Dynamics and Response to Changing Climate*, pages 277–304. Springer International Publishing, 2018.

[297] Jennifer L. Miselis and Jorge Lorenzo-Trueba. Natural and Human-Induced Variability in Barrier-Island Response to Sea Level Rise. *Geophysical Research Letters*, 44(23): 922–11, 2017. ISSN 19448007. doi: 10.1002/2017GL074811.

[298] Mahinaokalani G. Robbins, Justin L. Shawler, and Christopher J. Hein. Contribution of longshore sand exchanges to mesoscale barrier-island behavior: Insights from the Virginia Barrier Islands, U.S. East Coast. *Geomorphology*, 403(September

2021):108163, 2022. ISSN 0169555X. doi: 10.1016/j.geomorph.2022.108163. URL https://doi.org/10.1016/j.geomorph.2022.108163.

[299] Brad A. Murray and Laura J. Moore. Geometric Constraints on Long-Term Barrier Migration: From Simple to Surprising. In Laura J. Moore and Brad A. Murray, editors, *Barrier Dynamics and Response to Changing Climate*, pages 211–242. Springer International Publishing, 2018.

[300] Daniel J. Ciarletta, Jorge Lorenzo-Trueba, and Andrew D. Ashton. Interaction of Sea-Level Pulses With Periodically Retreating Barrier Islands. *Frontiers in Earth Science*, 7(October):1–14, 2019. ISSN 22966463. doi: 10.3389/feart.2019.00279.

[301] Todd S. Bridges, Paul W. Wagner, Kelly A. Burks-copes, Matthew E. Bates, Zachary A. Collier, Craig J. Fischenich, Joe Z. Gailani, Lauren D. Leuck, Candice D. Piercy, Julie D. Rosati, Edmond J. Russo, Deborah J. Shafer, Burton C. Suedel, Emily A. Vuxton, and Ty V. Wamsley. Use of Natural and Nature-Based Features (NNBF) for Coastal Resilience. Technical report, US Army Corps of Engineers, Engineer Research and Development Center, 2015.

[302] Robert J. Hallermeier. Calculating a yearly limit depth to the active beach profile. Technical report, U.S. Army Corps of Engineers, Coastal Engineering Research Center, 1977.

[303] Robert J. Nicholls, William A. Birkemeier, and Guan-hong Lee. Evaluation of depth of closure using data from Duck, NC, USA. *Marine Geology*, 148:179–201, 1998. ISSN 13652427. doi: 10.1111/j.1365-2427.2008.02031.x.

[304] Jessica L. Raff, Justin L. Shawler, Daniel J. Ciarletta, Emily A. Hein, Jorge Lorenzo-Trueba, and Christopher J. Hein. Insights into barrier-island stability derived from

transgressive/regressive state changes of Parramore Island, Virginia. *Marine Geology*, 403(April):1–19, 2018. ISSN 00253227. doi: 10.1016/j.margeo.2018.04.007.

[305] Justin L. Shawler, Daniel J. Ciarletta, Jennifer E. Connell, Bianca Q. Boggs, Jorge Lorenzo-Trueba, and Christopher J. Hein. Relative influence of antecedent topography and sea-level rise on barrier-island migration. *Sedimentology*, 68(2):639–669, 2021. ISSN 13653091. doi: 10.1111/sed.12798.

[306] Andrew D. Ashton and Alejandra C. Ortiz. Overwash Controls Coastal Barrier Response to Sea-Level Rise. In *The Proceedings of the Coastal Sediments 2011*, pages 230–243. World Scientific Publishing Company, 4 2011. ISBN 978-981-4355-52-0. doi: 10.1142/9789814355537{_}0018. URL http://www.worldscientific.com/doi/abs/10.1142/9789814355537_0018.

[307] Sathya Gopalakrishnan, Craig E. Landry, and Martin D. Smith. Climate change adaptation in coastal environments: Modeling challenges for resource and environmental economists. *Review of Environmental Economics and Policy*, 12(1):48–68, 2018. ISSN 17506824. doi: 10.1093/reep/rex020.

[308] Morris A. Bender, Thomas R. Knutson, Robert E. Tuleya, Joseph J. Sirutis, Gabriel A. Vecchi, Stephen T. Garner, and Isaac M. Held. Modeled Impact of Anthropogenic Warming on the Frequency of Intense Atlantic Hurricanes. *Science*, 327(5964):454–458, 1 2010. ISSN 0036-8075. doi: 10.1126/science.1180568. URL https://www.science.org/doi/10.1126/science.1180568.

[309] S.I. Seneviratne, X. Zhang, M. Adnan, W. Badi, C. Dereczynski, A. Di Luca, S. Ghosh, I. Iskandar, J. Kossin, S. Lewis, F. Otto, I. Pinto, M. Satoh, S.M. Vicente-Serrano, M. Wehner, and B. Zhou. Weather and Climate Extreme Events in a Changing Climate. In *Climate Change 2021 – The Physi-*

cal Science Basis, pages 1513–1766. Cambridge University Press, 7 2023. doi: 10.1017/9781009157896.013. URL https://www.cambridge.org/core/product/identifier/9781009157896%23c11/type/book_part.

[310] Robert A. Morton and Asbury H. Sallenger. Morphological impacts of extreme storms on sandy beaches and barriers. *Journal of Coastal Research*, 19(3):560–573, 2003. ISSN 07490208.

[311] Hilary F. Stockdon, Asbury H. Sallenger, Rob A. Holman, and Peter A. Howd. A simple model for the spatially-variable coastal response to hurricanes. *Marine Geology*, 238 (1-4):1–20, 2007. ISSN 00253227. doi: 10.1016/j.margeo.2006.11.004.

[312] Nathaniel G. Plant and Hilary F. Stockdon. Probabilistic prediction of barrier-island response to hurricanes. *Journal of Geophysical Research: Earth Surface*, 117(3):1–17, 2012. ISSN 21699011. doi: 10.1029/2011JF002326.

[313] G. Mariotti. Self-Organization of Coastal Barrier Systems During the Holocene. *Journal of Geophysical Research: Earth Surface*, 126(5):1–23, 2021. ISSN 21699011. doi: 10.1029/2020JF005867.

[314] Christopher Tenebruso, Shane Nichols-O'Neill, Jorge Lorenzo-Trueba, Daniel J. Ciarletta, and Jennifer L. Miselis. Undeveloped and developed phases in the centennial evolution of a barrier-marsh-lagoon system: The case of Long Beach Island, New Jersey. *Frontiers in Marine Science*, 9(October):1–15, 2022. ISSN 22967745. doi: 10.3389/fmars.2022.958573.

[315] Charles D. Deaton, Christopher J. Hein, and Matthew L. Kirwan. Barrier island migration dominates ecogeomorphic feedbacks and drives salt marsh loss along the Virginia Atlantic Coast, USA. *Geology*, 45(2):123–126, 2017. ISSN 19432682. doi: 10.1130/G38459.1.

[316] I. R.B. Reeves, L. J. Moore, E. B. Goldstein, A. B. Murray, J. A. Carr, and M. L. Kirwan. Impacts of Seagrass Dynamics on the Coupled Long-Term Evolution of Barrier-Marsh-Bay Systems. *Journal of Geophysical Research: Biogeosciences*, 125(2):1–19, 2020. ISSN 21698961. doi: 10.1029/2019JG005416.

[317] Sergio Fagherazzi, Giuilio Mariotti, and Patricia L. Wiberg. Marsh collapse does not require sea level rise. *Oceanography*, 26(3):70–77, 2013. ISSN 10428275. doi: 10.5670/oceanog.2013.47.

[318] Giulio Mariotti and Sergio Fagherazzi. Critical width of tidal flats triggers marsh collapse in the absence of sea-level rise. *Proceedings of the National Academy of Sciences of the United States of America*, 110(14):5353–5356, 2013. ISSN 00278424. doi: 10.1073/pnas.1219600110.

[319] Andrea Saltelli, Stefano Tarantola, Francesca Campolongo, and Marco Ratto. *Sensitivity Analysis in Practice*. John Wiley & Sons Ltd., 2004. ISBN 9780470870952. doi: 10.1002/0470870958. URL https://onlinelibrary.wiley.com/doi/book/10.1002/0470870958.

[320] Francesca Pianosi, Keith Beven, Jim Freer, Jim W. Hall, Jonathan Rougier, David B. Stephenson, and Thorsten Wagener. Sensitivity analysis of environmental models: A systematic review with practical workflow. *Environmental Modelling and Software*, 79:214–232, 2016. ISSN 13648152. doi: 10.1016/j.envsoft.2016.02.008. URL http://dx.doi.org/10.1016/j.envsoft.2016.02.008.

[321] Sébastien Da Veiga, Fabrice Gamboa, Bertrand Iooss, and Clémentine Prieur. *Basics and Trends in Sensitivity Analysis*. Society for Industrial and Applied Mathematics, Philadelphia, PA, 1 2021. ISBN 978-1-61197-668-7. doi: 10.1137/1.9781611976694. URL https://epubs.siam.org/doi/book/10.1137/1.9781611976694.

[322] Anqi Wang and Dimitri P. Solomatine. Practical Experience of Sensitivity Analysis: Comparing Six Methods, on Three Hydrological Models, with Three Performance Criteria. *Water*, 11(5):1062, 5 2019. ISSN 2073-4441. doi: 10.3390/w11051062. URL https://www.mdpi.com/2073-4441/11/5/1062.

[323] Max D. Morris. Factorial Sampling Plans for Preliminary Computational Experiments. *Technometrics*, 33(2):161, 5 1991. ISSN 00401706. doi: 10.2307/1269043. URL https://www.jstor.org/stable/1269043?origin=crossref.

[324] Rik J. L. Rutjens, Leah R. Band, Matthew D. Jones, and Markus R. Owen. Elementary effects for models with dimensional inputs of arbitrary type and range: Scaling and trajectory generation. *PLOS ONE*, 18(10):e0293344, 10 2023. ISSN 1932-6203. doi: 10.1371/journal.pone.0293344. URL https://dx.plos.org/10.1371/journal.pone.0293344.

[325] Arnald Puy, William Becker, Samuele Lo Piano, and Andrea Saltelli. A COMPREHENSIVE COMPARISON OF TOTAL-ORDER ESTIMATORS FOR GLOBAL SENSITIVITY ANALYSIS. *International Journal for Uncertainty Quantification*, 12(2):1–18, 2022. ISSN 2152-5080. doi: 10.1615/Int.J.UncertaintyQuantification.2021038133. URL http://www.dl.begellhouse.com/journals/52034eb04b657aea,221f21d635d3d68f,6de6348a17770dba.html.

[326] Andrea Saltelli. Making best use of model evaluations to compute sensitivity indices. *Computer Physics Communications*, 145(2):280–297, 2002. ISSN 00104655. doi: 10.1016/S0010-4655(02)00280-1.

[327] Jiri Nossent and Willy Bauwens. Optimising the convergence of a Sobol' sensitivity analysis for an environmental model: Application of an appropriate estimate for the square of the expectation value and the total variance. In R. Seppelt, A.A.

Voinov, S. Lange, and D. Bankamp, editors, *iEMSs 2012 - Managing Resources of a Limited Planet: Proceedings of the 6th Biennial Meeting of the International Environmental Modelling and Software Society*, pages 1080–1087. International Environmental Modelling and Software Society, 2012. ISBN 9788890357428. URL http://www.iemss.org/society/index.php/iemss-2012-proceedings%0A.

[328] Saman Razavi, Razi Sheikholeslami, Hoshin V. Gupta, and Amin Haghnegahdar. VARS-TOOL: A toolbox for comprehensive, efficient, and robust sensitivity and uncertainty analysis. *Environmental Modelling and Software*, 112(October 2018): 95–107, 2019. ISSN 13648152. doi: 10.1016/j.envsoft.2018.10.005. URL https://doi.org/10.1016/j.envsoft.2018.10.005.

[329] T. Ishigami and T. Homma. An importance quantification technique in uncertainty analysis for computer models. In *[1990] Proceedings. First International Symposium on Uncertainty Modeling and Analysis*, pages 398–403. IEEE Comput. Soc. Press, 1990. ISBN 0-8186-2107-9. doi: 10.1109/ISUMA.1990.151285. URL http://ieeexplore.ieee.org/document/151285/.

[330] S. Kucherenko, S. Tarantola, and P. Annoni. Estimation of global sensitivity indices for models with dependent variables. *Computer Physics Communications*, 183(4):937–946, 2012. ISSN 00104655. doi: 10.1016/j.cpc.2011.12.020. URL http://dx.doi.org/10.1016/j.cpc.2011.12.020.

[331] Atieh Alipour, Keighobad Jafarzadegan, and Hamid Moradkhani. Global sensitivity analysis in hydrodynamic modeling and flood inundation mapping. *Environmental Modelling and Software*, 152(April):105398, 2022. ISSN 13648152. doi: 10.1016/j.envsoft.2022.105398. URL https://doi.org/10.1016/j.envsoft.2022.105398.

[332] Fanny Sarrazin, Francesca Pianosi, and Thorsten Wagener. Global Sensitivity Analysis

of environmental models: Convergence and validation. *Environmental Modelling and Software*, 79:135–152, 2016. ISSN 13648152. doi: 10.1016/j.envsoft.2016.02.005. URL http://dx.doi.org/10.1016/j.envsoft.2016.02.005.

[333] Sara L. Zeigler, Benjamin T. Gutierrez, Anne Hecht, Nathaniel G. Plant, and Emily J. Sturdivant. Piping plovers demonstrate regional differences in nesting habitat selection patterns along the U.S. Atlantic coast. *Ecosphere*, 12(3), 3 2021. ISSN 2150-8925. doi: 10.1002/ecs2.3418. URL https://esajournals.onlinelibrary.wiley.com/doi/10.1002/ecs2.3418.

[334] J. R. Houston. The economic value of America's beaches - a 2018 update. *Shore & Beach*, 86(2):3–13, 2018.

[335] J. A.G. Cooper and O. H. Pilkey. Longshore drift: Trapped in an expected universe. *Journal of Sedimentary Research*, 74(5):599–606, 2004. ISSN 15271404. doi: 10.1306/022204740599.

[336] Jaap H. Nienhuis and Andrew D. Ashton. Mechanics and rates of tidal inlet migration: Modeling and application to natural examples. *Journal of Geophysical Research: Earth Surface*, 121(11):2118–2139, 11 2016. ISSN 2169-9003. doi: 10.1002/2016JF004035. URL https://agupubs.onlinelibrary.wiley.com/doi/10.1002/2016JF004035.

[337] Donald J.P. Swift, Alan W. Niedoroda, Chistopher E. Vincent, and Tom Sawyer Hopkins. Barrier island evolution, middle Atlantic shelf, U.S.A. Part I: Shoreface dynamics. *Marine Geology*, 63(1-4):331–361, 1985. ISSN 00253227. doi: 10.1016/0025-3227(85)90089-1.

[338] L. D. Wright, J. D. Boon, S. C. Kim, and J. H. List. Modes of cross-shore sediment transport on the shoreface of the Middle Atlantic Bight. *Marine Geology*, 96(1-2):19–51, 1991. ISSN 00253227. doi: 10.1016/0025-3227(91)90200-N.

[339] Charles E. Bartberger. Sediment Sources and Sedimentation Rates, Chincoteague Bay, Maryland and Virginia. *SEPM Journal of Sedimentary Research*, Vol. 46(2):326–336, 1976. ISSN 1527-1404. doi: 10.1306/212f6f50-2b24-11d7-8648000102c1865d.

[340] Jaap H. Nienhuis and Jorge Lorenzo-Trueba. Can Barrier Islands Survive Sea-Level Rise? Quantifying the Relative Role of Tidal Inlets and Overwash Deposition. *Geophysical Research Letters*, 46(24):14613–14621, 2019. ISSN 19448007. doi: 10.1029/2019GL085524.

[341] W.V. Sweet, B.D. Hamlington, R.E. Kopp, C.P. Weaver, P.L. Barnard, D. Bekaert, W. Brooks, M. Craghan, G. Dusek, T. Frederikse, G. Garner, A.S. Genz, J.P. Krasting, E. Larou, D. Marcy, J.J. Marra, J. Obeysekera, M. Osler, M. Pendleton, D. Roman, L. Schmied, W. Veatch, K.D. White, and C. Zuzak. Global and Regional Sea Level Rise Scenarios for the United States: Updated Mean Projections and Extreme Water Level Probabilities Along U.S. Coastlines. Technical report, National Oceanic and Atmospheric Administration, National Ocean Service, Silver Spring, MD, 2022. URL https://oceanservice.noaa.gov/hazards/sealevelrise/noaa-nos-.

[342] Virginia DCR. Virginia Coastal Resilience Master Plan: Phase I. Technical report, Virginia Department of Conservation and Recreation, Richmond, VA, 2021.

[343] Per Bruun. The History and Philosophy of Coastal Protection. *Coastal Engineering*, 1972. ISSN 1098-6596.

[344] Hugo R. Valverde, Arthur C. Trembanis, and Orrin H. Pilkey. Summary of beach nourishment episodes on the U.S. East Coast barrier islands. *Journal of Coastal Research*, 15(4):1100–1118, 1999. ISSN 07490208.

[345] Megan E McQuarrie and Orrin H Pilkey. Evaluation of alternative or non-traditional shoreline stabilization devices; Proceedings of the international coastal symposium

(ICS98). *Journal of Coastal Research - Special Issue 26*, pages 269–272, 1998. ISSN 0749-0208.

[346] L. Leonard, T. Clayton, and O. Pilkey. An analysis of replenished beach design parameters on US east coast barrier islands. *Journal of Coastal Research*, 6(1):15–36, 1990. ISSN 07490208.

[347] Arthur C. Trembanis, Orrin H. Pilkey, and Hugo R. Valverde. Comparison of beach nourishment along the u.S. Atlantic, great lakes, gulf of mexico, and new england shorelines. *Coastal Management*, 27(4):329–340, 1999. ISSN 15210421. doi: 10.1080/089207599263730.

[348] Roger H. Charlier, Marie Claire P. Chaineux, and Selim Morcos. Panorama of the history of coastal protection. *Journal of Coastal Research*, 21(1):79–111, 2005. ISSN 07490208. doi: 10.2112/03561.1.

[349] Julie D. Rosati. Concepts for Functional Restoration of Barrier Islands. Technical Report September 2009, ERDC/CHL US Army Corps of Engineers, 2009.

[350] National Research Council. *Reducing Coastal Risk on the East and Gulf Coasts*. The National Academies Press, Washington, D.C., 2014. ISBN 0309305861. doi: 10.17226/18811.

[351] Ariana E. Sutton-Grier, Rachel K. Gittman, Katie K. Arkema, Richard O. Bennett, Jeff Benoit, Seth Blitch, Kelly A. Burks-Copes, Allison Colden, Alyssa Dausman, Bryan M. DeAngelis, A. Randall Hughes, Steven B. Scyphers, and Jonathan H. Grabowski. Investing in natural and nature-based infrastructure: Building better along our coasts. *Sustainability (Switzerland)*, 10(2):1–11, 2018. ISSN 20711050. doi: 10.3390/su10020523.

[352] Shannon Cunniff and Aaron Schwartz. Performance of Natural Infrastructure and Nature-based Measures as Coastal Risk Reduction Features. Technical report, Environmental Defense Fund, 2015.

[353] J. Figlus, J. M. Smith, T. Tomiczek, and B. C. McFall. Editorial: Natural and nature-based features for flood risk management. *Frontiers in Built Environment*, 8, 1 2023. ISSN 2297-3362. doi: 10.3389/fbuil.2022.1128508. URL https://www.frontiersin.org/articles/10.3389/fbuil.2022.1128508/full.

[354] J.D. Rosati, G.W. Stone, R.G. Dean, and N.C. Kraus. Restoration of barrier islands overlying poorly-consolidated sediments, South-Central Louisiana. *Gulf Coast Association of Geological Societies Transactions*, 56(May):727–740, 2006. URL http://scholar.google.com/scholar?hl=en&btnG=Search&q=intitle:Restoration+of+Barrier+Islands+Overlying+Poorly-Consolidated+Sediments,+South-Central+Louisiana#0.

[355] E. D. Lazarus, D. E. McNamara, M. D. Smith, S. Gopalakrishnan, and A. B. Murray. Emergent behavior in a coupled economic and coastline model for beach nourishment. *Nonlinear Processes in Geophysics*, 18(6):989–999, 2011. ISSN 10235809. doi: 10.5194/npg-18-989-2011.

[356] A. Brad Murray, Sathya Gopalakrishnan, Dylan E. McNamara, and Martin D. Smith. Progress in coupling models of human and coastal landscape change. *Computers and Geosciences*, 53:30–38, 2013. ISSN 00983004. doi: 10.1016/j.cageo.2011.10.010. URL http://dx.doi.org/10.1016/j.cageo.2011.10.010.

[357] Sathya Gopalakrishnan, Dylan McNamara, Martin D. Smith, and A. Brad Murray. Decentralized Management Hinders Coastal Climate Adaptation: The Spatial-dynamics

of Beach Nourishment. *Environmental and Resource Economics*, 67(4):761–787, 2017. ISSN 15731502. doi: 10.1007/s10640-016-0004-8.

[358] K. A. Anarde, L. J. Moore, A. B. Murray, and I. R.B. Reeves. The Future of Developed Barrier Systems: 1. Pathways Toward Uninhabitability, Drowning, and Rebound. *Earth's Future*, 12(4), 2024. ISSN 23284277. doi: 10.1029/2023EF003672.

[359] Christopher T Seminack and Randolph A Mcbride. Geomorphic history and diagnostic features of former tidal inlets along Assateague Island, Maryland-Virginia: A life-cycle model for inlets along wave-dominated barrier islands. *Shore & Beach*, 83(3):3–24, 2015.

[360] Miles O. Hayes. Barrier Morphology as a Function of Tidal and Wave Regime. In Stephen P. Leatherman, editor, *Barrier Islands: From the Gulf of St. Lawrence to the Gulf of Mexico*, pages 1–28. Academic Press, 1979.

[361] Courtney Schupp. Assateague Island National Seashore Geologic Resources Inventory Report. Natural Resource Report NPS/NRSS/GRD/NRR—2013/708. Technical report, National Park Service, Fort Collins, Colorado, 2013.

[362] E.J. Sturdivant, S.L. Zeigler, B.T. Gutierrez, and K.M. Weber. Barrier island geomorphology and shorebird habitat metrics–Sixteen sites on the U.S. Atlantic Coast, 2013–2014: U.S. Geological Survey data release, 2019.

[363] Tim Carruthers, Kris Beckert, Bill Dennison, Jane Thomas, Tracey Saxby, Mike Williams, Tom Fisher, Jack Kumer, Courtney Schupp, Brian Sturgis, and Carl Zimmerman. Assateague Island National Seashore Natural Resource Condition Assessment. *Maryland, Virginia. Natural Resource Report NPS/ASIS/NRR—2011/405. National Park Service, Fort Collins, Colorado*, 2011.

[364] D. J. Nowacki and N. K. Ganju. Storm impacts on hydrodynamics and suspended-sediment fluxes in a microtidal back-barrier estuary. *Marine Geology*, 404(July):1–14, 2018. ISSN 00253227. doi: 10.1016/j.margeo.2018.06.016. URL https://doi.org/10.1016/j.margeo.2018.06.016.

[365] Randolph A. McBride, Michael S. Fenster, Christopher T. Seminack, Trent M. Richardson, Julie M. Sepanik, J. Thomas Hanley, Joshua A. Bundick, and Elizabeth Tedder. Holocene barrier-island geology and morphodynamics of the Maryland and Virginia open-ocean coasts: Fenwick, Assateague, Chincoteague, Wallops, Cedar, and Parramore Islands. In D.K. Brezinski, J.P. Halka, and R.A. Ortt Jr., editors, *Tripping from the Fall Line: Field Excursions for the GSA Annual Meeting, Baltimore, 2015: Geological Society of America Field Guide 40*, pages 309–423. The Geological Society of America, 2015. ISBN 9780813756400. doi: 10.1130/2015.0040(10).

[366] C Wazniak, R Jesien, M Hall, J Casey, and D Wells. A Brief History of Maryland's Coastal Bays (Updated 2014). Technical report, Maryland Department of Natural Resources, 2014. URL http://citeseerx.ist.psu.edu/viewdoc/download?doi=10.1.1.506.6394&rep=rep1&type=pdf.

[367] Norbert P. Psuty, Christopher Menke, Katherine Ames, Andrea Habeck, and Casey Jones. Shoreline Position and Coastal Topographical Change Monitoring at Assateague Island National Seashore: 2005-2020 Trend Report. Technical report, National Park Service, 2022.

[368] John S. Fisher and Donald K. Stauble. Impact of Hurricane Belle on Assateague Island washover. *Geology*, 5(12):765–768, 1977. ISSN 19432682. doi: 10.1130/0091-7613(1977)5⟨765:IOHBOA⟩2.0.CO;2.

[369] Darlene V. Wells, E. Lamere Hennessee, and James M. Hill. Shoreline Erosion as a

Source of Sediments and Nutrients Middle Coastal Bays, Maryland. Technical report, Maryland Geological Survey, 2003.

[370] National Park Service. Record of Decision: General Management Plan/Environmental Impact Statement Assateague Island National Seashore, 2021.

[371] NOAA. Relative Sea Level Trend Dataset for Station 8570283 Ocean City, Maryland, 2024.

[372] James T. Morris, James Lynch, Katherine A. Renken, Sara Stevens, Megan Tyrrell, and Holly Plaisted. Tidal and Hurricane Impacts on Saltmarshes in the Northeastern Coastal and Barrier Network: Theory and Empirical Results. *Estuaries and Coasts*, 43(7):1658–1671, 2020. ISSN 15592731. doi: 10.1007/s12237-020-00790-5.

[373] Christy Swann, Kate Brodie, and Nick Spore. Coastal Foredunes : Identifying Coastal , Aeolian , and Management Interactions Driving Morphologic State Change Coastal and Hydraulics Laboratory. Technical report, USACE, ERDC, CHL, 2015.

[374] Gary L. Ray. Thin layer placement of dredged material on coastal wetlands: A review of the technical and scientific literature. Technical report, USACE ERDC, Vicksburg, MS, 2007. URL http://oai.dtic.mil/oai/oai?verb=getRecord&metadataPrefix=html&identifier=ADA475811.

[375] B. Fox-Kemper, H. T. Hewitt, C. Xiao, G. Aoalgeirsdottir, S. S. Drijfhout, T. L. Edwards, N. R. Golledge, M. Hemer, R. E. Kopp, G. Krinner, A. Mix, D. Notz, S. Nowicki, I. S. Nurhati, L. Ruiz, J-B. Sallee, A. B. A. Slangen, and Y. Yu. Ocean, Cryosphere and Sea Level Change. In V. Masson-Delmotte, P. Zhai, A. Pirani, S. L. Connors, C. Pean, S. Berger, N. Caud, Y. Chen, L. Goldfarb, M. I. Gomis, M. Huang, K. Leitzell, E. Lonnoy, J. B. R. Matthews, T. K. Maycock, T. Waterfield, O. Yelekci,

R. Yu, and B. Zhou, editors, *Climate Change 2021: The Physical Science Basis. Contribution of Working Group I to the Sixth Assessment Report of the Intergovernmental Panel on Climate Change*, pages 1211–1362. Cambridge University Press, 2021. doi: 10.1017/9781009157896.011.

[376] R. E. Kopp, G. G. Garner, T. H. J. Hermans, S. Jha, P. Kumar, A. Reedy, A. B. A. Slangen, M. Turilli, T. L. Edwards, J. M. Gregory, G. Koubbe, A. Levermann, A. Merzky, S. Nowicki, M. D. Palmer, and C. Smith. The Framework for Assessing Changes To Sea-level (FACTS) v1.0: a platform for characterizing parametric and structural uncertainty in future global, relative, and extreme sea-level change. *Geoscientific Model Development*, 16(24):7461–7489, 2023. doi: 10.5194/gmd-16-7461-2023.

[377] G. G. Garner, T. Hermans, R. E. Kopp, A. B. A. Slangen, T. L. Edwards, A. Levermann, S. Nowikci, M. D. Palmer, C. Smith, B. Fox-Kemper, H. T. Hewitt, C. Xiao, G. Aoalgeirsdottir, S. S. Drijfhout, T. L. Edwards, N. R. Golledge, M. Hemer, R. E. Kopp, G. Krinner, A. Mix, D. Notz, S. Nowicki, I. S. Nurhati, L. Ruiz, J-B. Sallee, Y. Yu, L. Hua, T. Palmer, and B. Pearson. IPCC AR6 Sea-Level Rise Projections. Version 20210809, 2021. URL https://doi.org/10.5281/zenodo.5914709.

[378] Neil K. Ganju, Zafer Defne, and Sergio Fagherazzi. Are Elevation and Open-Water Conversion of Salt Marshes Connected? *Geophysical Research Letters*, 47(3), 2 2020. ISSN 0094-8276. doi: 10.1029/2019GL086703. URL https://agupubs.onlinelibrary.wiley.com/doi/10.1029/2019GL086703.

Appendices

Appendix A

Barrier Island Modeling Insights from Applied Global Sensitivity Analyses

Steven W.H. Hoagland[1], Jennifer L. Irish[1], Robert Weiss[2,3]

[1]Department of Civil and Environmental Engineering, Virginia Tech, Blacksburg, VA

[2]Department of Geosciences, Virginia Tech, Blacksburg, VA

[3]Academy of Integrated Science, Virginia Tech, Blacksburg, VA

Author accepted version from *Proceedings of the Coastal Sediments 2023*, pp. 2875-2882, Barrier Island Modeling Insights from Applied Global Sensitivity Analysis, Hoagland, S.W.H., Irish, J.L., Weiss, R. (2023), doi:10.1142/9789811275135_0261.

A.1 Abstract

Barrier island models that include marsh and lagoon processes are highly parameterized. To constrain model uncertainty, those desiring to use these models should seek a robust understanding of the parameter sensitivities. In this study, global sensitivity analysis was performed on a long-term barrier island model to yield insights into the modeled barrier-backbarrier system. Given that a variety of global sensitivity analysis methods exist, each one appearing to differ in its implementation, computational burden, and output, three methods (i.e., the Two-Level Full Factorial Method, Morris Method, and Sobol Method) were applied to the model for the purposes of comparison. Key influential parameters (e.g., sea level rise rate, equilibrium/critical barrier width, and reference wind speed) were consistently identified by all three sensitivity analysis methods. Despite the relatively low number of simulations required by the Morris Method, the Two-Level Method computationally outperformed the others, warranting further exploration of the Morris Method's parallelization structure.

A.2 Introduction

Barrier island models that include backbarrier (i.e., marsh and lagoon) processes are highly parameterized. To constrain model uncertainty, those desiring to use these models should seek a robust understanding of the parameter sensitivities. To gain additional insights into the modeled morphodynamics of a coupled barrier island-backbarrier system, the parameter space of a long-term barrier model published by Lorenzo-Trueba and Mariotti [1], hereafter the 'LTM17' model, was explored by means of conducting a global sensitivity analysis (GSA). However, there are a variety of GSA methods, each of which appears to differ in its implementation, computational burden, and output. Therefore, in addition to gaining

additional insights into the LTM17 model, three GSA methods were applied to the model for comparison purposes.

The three GSA methods are the Two-Level Full Factorial Method (overviewed in Saltelli et al. [23]), the Morris Method [323], and the Sobol Method [20]. Using these methods, we evaluated the influence of 20 input parameters on the LTM17 model results over a 100-year period. Each method is briefly discussed and select results from the sensitivity analyses are presented.

A.3 Coastal Barrier Island System Model

The LTM17 model, published by Lorenzo-Trueba and Mariotti [1], is a 1D idealized barrier transect model that was developed by coupling two previous models: a 2014 barrier island model from Lorenzo-Trueba and Ashton [19], hereafter the 'LTA14' model, and a 2014 marsh-lagoon model from Mariotti and Carr [18], hereafter the 'MAC14' model. The model simulates temporal changes to 10 state variables, including the transect boundaries, barrier height, and marsh and lagoon depths. These variables are modified through sediment flux calculations, which are based on the system's deviation from prescribed equilibrium states. A graphical representation of the model transect and state variables is displayed in Figure A.1.

The 20 LTM17 model input parameters shown in Table A.1 were selected for GSA. Each parameter's sensitivity range was set at plus or minus 50 percent of the base value in Table A.1, with the exceptions of tidal range (r), which has a lower limit of 0.7 meters, and sea level rise rate ($\dot{z}$), which has a defined range of 3-20 mm/yr based on global sea level rise projections through 2100 by Sweet et al. [341].

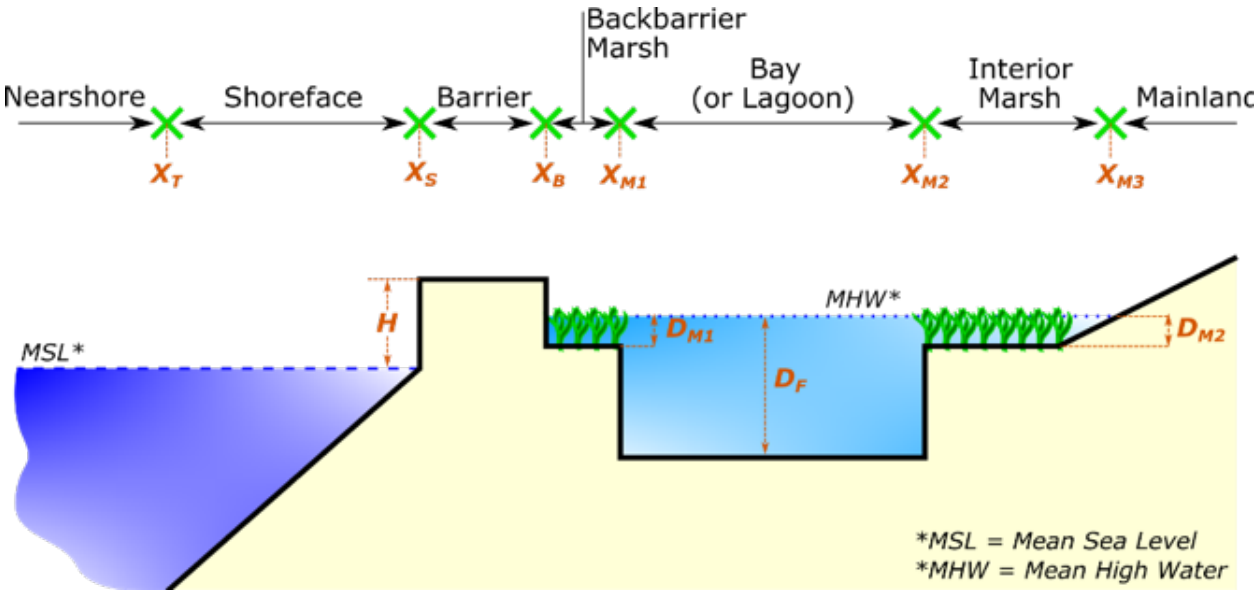

Figure A.1: LTM17 Model Transect and State Variables. *Figure reproduced and modified Lorenzo-Trueba and Mariotti (2017).*

Table A.1: LTM17 Model Input Parameters

Parameter (Symbol)	Base Value	Units
Mainland Slope (β)	$7e^{-4}$	$[m/m]$
Toe Depth (D_T)	10	$[m]$
Equil./Crit. Width (W_{cr})	175	$[m]$
Equil./Crit. Height (H_{cr})	3	$[m]$
Equil. Shoreface Slope (α_e)	$6.5e^{-3}$	$[m/m]$
Critical Marsh Width ($B_{M1,cr}$)	70	$[m]$
Marsh Profile Shape Const. (d)	10	$[m]$
Max. Annual Overwash Flux ($Q_{OW,*}$)	60	$[m^3/m/yr]$
Sea Level Rise Rate ($\dot{z}$)	5	$[mm/yr]$
Shoreface Flux Const. (K)	$2e^3$	$[m^3/m/yr]$
Tidal Range (r)	0.87	$[m]$
Wind Speed (U_{ref})	8	$[m/s]$
Sediment Settling Velocity (ω_s)	0.4	$[mm/s]$
Sediment Erodibility Constant (λ)	$1e^{-4}$	[...]
Critical Bed Shear Stress (τ_{cr})	0.1	$[Pa]$
Marsh Accretion Const. (K_a)	2	[...]
Marsh Erosion Const. (K_e)	0.16	[...]
Ocean Sediment Conc. (C_o)	30	$[mg/l]$
Peak Biomass Production (B_P)	2.5	$[kg/m^2]$
Fraction Accumulated Carbon (χ_{ref})	0.15	[...]

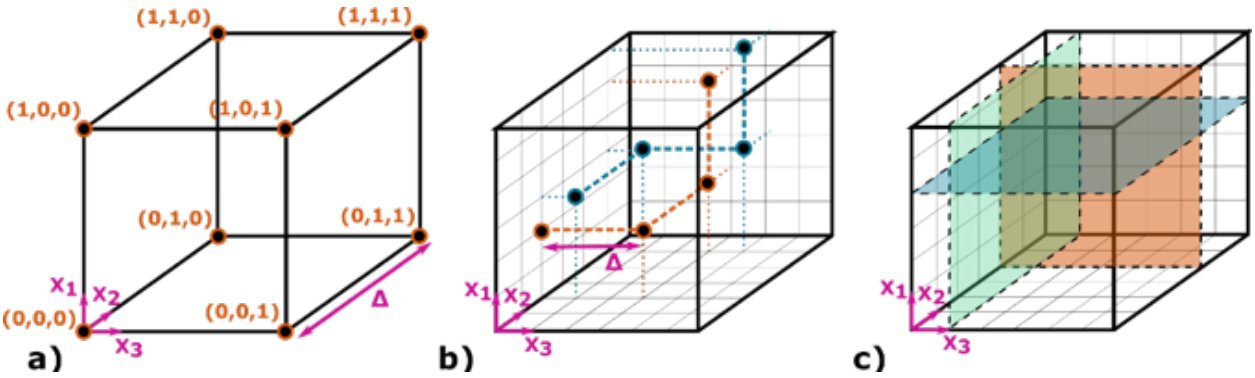

Figure A.2: Graphical representation of a) the Two-Level Full Factorial Method, b) the Morris Method, and c) the Sobol Method, for a hypothetical 3-parameter model.

A.4 Global Sensitivity Analysis Methods

Three GSA methods were integrated into the LTM17 model code: the Two-Level Full Factorial Method (hereafter the 'Two-Level' Method), the Morris Method, and the Sobol Method. These methods are graphically represented in Figure A.2 for a hypothetical model with 3 input parameters, where the cube represents the 3-dimensional parameter space, the axes represent the hypothetical input parameters (X_1, X_2, X_3), and each dot represents a single model simulation with distinct input parameter values (Note: only parameter constraints are represented in Figure A.2c).

In the Two-Level Method (Fig. A.2a), simulations were run for every extreme value combination of the input parameters (i.e., at the 'corners' of the parameter space), whereas simulations in the Morris Method (Fig. A.2b) were run from randomized sample trajectories (represented by the dashed lines) throughout the interior of the parameter space, making discrete parameter value 'jumps' according to a defined delta (Δ) value. Both methods follow the 'One-At-a-Time' (or OAT) approach, where sensitivity of a specific input parameter is represented by the average change in model results, or average of all 'elementary effects,' across all simulations. The averaged results are referred to herein as the 'average effect.'

Thus, the average effect of a parameter 'X_i' (AE_{X_i}) is calculated by Equation A.1:

$$AE_{X_i} = \frac{1}{N}\sum_{N} Y|_{X_i=B} - Y|_{X_i=A} \tag{A.1}$$

where N is either half the number of possible 2-parameter combinations (when using the Two-Level Method) or the number of user-defined trajectories (when using the Morris Method), Y is the model output, and A and B represent two distinct values for parameter X_i.

Oppositely, the Sobol Method (Fig. A.2c) follows a variance-based approach, which computes sensitivity indices based on the ratio of model output variance, constrained by fixed parameter values (the colored planes in Figure A.2c), to the total unconstrained model variance. The two indices computed in this study were the first-order Sobol index (S_i) and the kth-order Sobol index (S_{T_i}), where k represents the number of input parameters. Following the notation of Saltelli et al. [23], these index values are calculated using Equations A.2 and A.3:

$$S_i = \frac{V(E(Y|X_i))}{V(Y)} \tag{A.2}$$

$$S_{T_i} = 1 - \frac{V(E(Y|X_{\sim i}))}{V(Y)} \tag{A.3}$$

where S_i and $S_(T_i)$ are the first and kth-order index values, respectively, for the ith input parameter (X_i), V is the variance, E is the mean or expected value, and Y is the model output. The first-order index indicates the percentage of model variance accounted for by each parameter, while the kth-order index accounts for the percentage of model variance from each parameter and its interactions with other parameters. For additional details on

the methods, readers are referred to Sobol [20], Morris [323] and Saltelli et al. [23], who provides an accessible summary of all three methods.

A.5 Results and Discussion

Each GSA method that was used to evaluate the sensitivity of the LTM17 model's 20 input parameters varied in its number of simulations and computational burden. The Two-Level Method completed its 2^k (i.e., 1,048,576) simulations and sensitivity calculations in 30 minutes. The Sobol Method, which runs a user-defined number of simulations per input parameter, took 2.3 hours to run its 5.5 million simulations. The Morris Method, which was set up with 3 elementary effects per parameter range (i.e., $\Delta = 3/5$), required the greatest computational burden with a run time of 3 hours; however, this was not expected since the total number of simulations was only 210,000. This suggests that there may be a more efficient way to parallelize the Morris Method computations.

Select results from the sensitivity analyses are presented in Figure A.3, where Figures A.3a, A.3c, and A.3e show the results for change in barrier width, and Figures A.3b, A.3d, and A.3f show the results for change in backbarrier marsh width. Additionally, Figures A.3a and A.3b show the Two-Level Method results, Figures A.3c and A.3d show the Morris Method results, and Figures A.3e and A.3f show the Sobol Method results. The sensitivity indicators associated with each method are plotted on the y-axes for each input parameter on the x-axes. The background colors in each subplot of Figure A.3 identify a broad categorization for the input parameters: dark grey for parameters associated with system geometry, and white for other parameters.

Figure A.3 displays remarkable consistency between the results of the three GSA methods. Comparing the barrier width results in Figures A.3a, A.3c, and A.3e, each method consis-

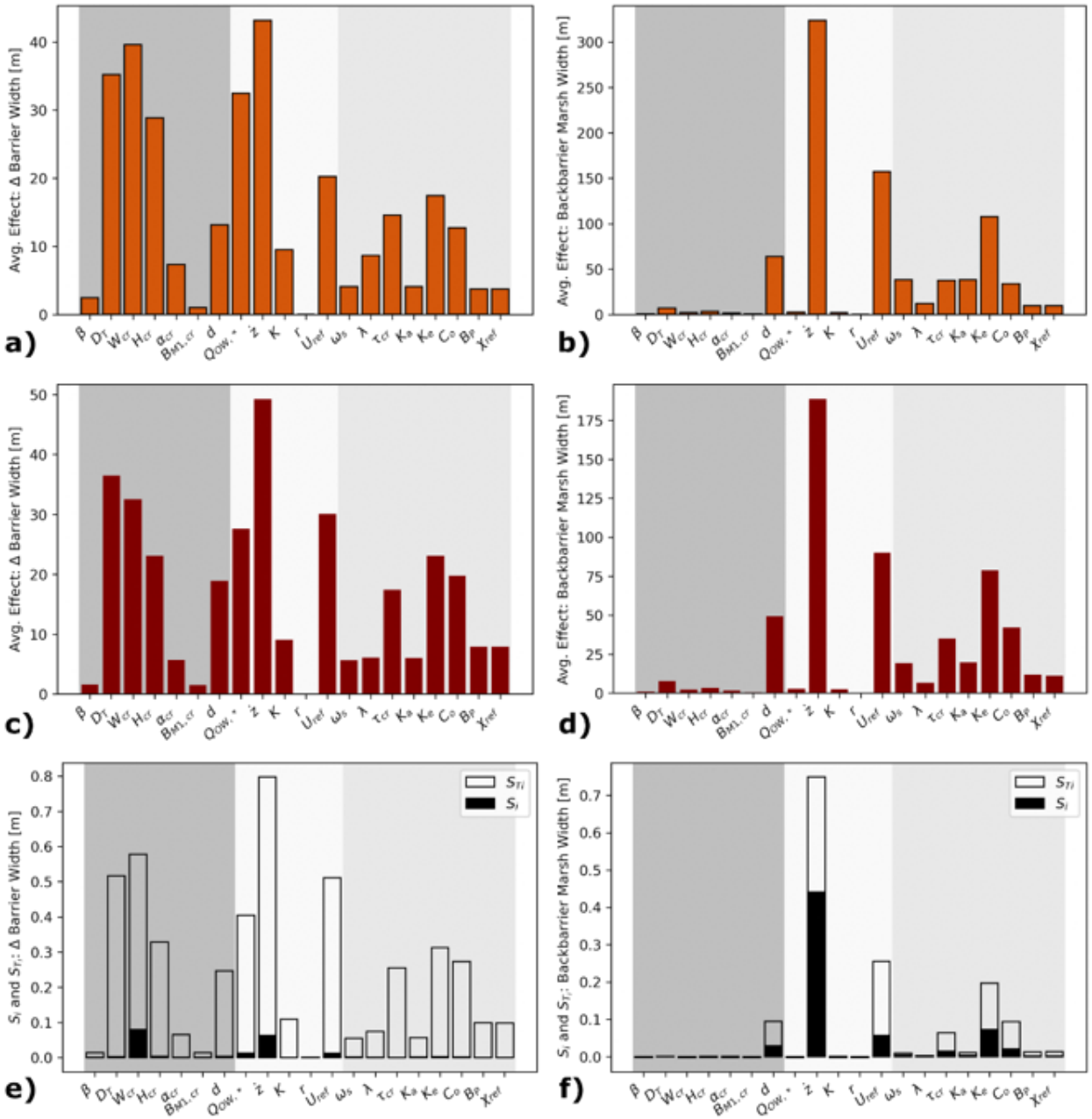

Figure A.3: Sensitivity analysis results for Barrier Width (a,c,e) and Backbarrier Marsh Width (b,d,f) for the Two-Level (a,b), Morris (c,d), and Sobol (e,f) Methods

tently identifies the most influential parameters (i.e., those with the highest sensitivity indicators) and non-influential parameters. Sea level rise rate ($\dot{z}$) and equilibrium/critical width (W_{cr}) were consistently two of the most influential parameters, while critical backbarrier marsh width ($B_{M1,cr}$) and tidal range (r) were consistently the least influential parameters. These results suggest that parameters such as $\dot{z}$ and W_{cr} are the most important parameters for modelers to understand and to constrain for future projections. The most and least influential parameters were also identified for the backbarrier marsh width results from Figures A.3b, A.3d, and A.3f. It should be noted that $\dot{z}$ and the reference wind speed (U_{ref}) were consistently influential for both the barrier and backbarrier results.

Given the consistency in results between methods, the Two-Level Method proved to be the least computationally burdensome method to identify the most sensitive parameters in this study. However, future work in optimizing the Morris Method parallelization or the Morris and Sobol Method setups may improve performance.

Comparing the barrier width and backbarrier marsh width results (e.g., Figure A.3a and A.3b) suggests parameter sensitivity can vary significantly from one set of results to the next. For example, the geometrical parameters (i.e., those with a dark grey background), most of which were associated with the original LTA14 barrier island model, have substantial influence on the barrier width results, but little to no influence on the backbarrier marsh width results. The sediment transport parameters, which were associated with the original MAC14 model, influence both the barrier width and backbarrier marsh width results. These observations also suggest that the backbarrier component of the model has more influence on the barrier results than vice versa.

A.6 Conclusion

The sensitivity analysis results from this study provide a few modeling insights. First, the most influential parameters were sea level rise rate ($\dot{z}$), equilibrium/critical barrier width (W_{cr}), and reference wind speed (U_{ref}), while the least influential parameters were critical backbarrier marsh width ($B_{M1,cr}$) and tidal range (r). Second, the relative sensitivity of input parameters was found to be highly dependent on the results of interest. Third, the Two-Level Method identified the parameter sensitivities with the least computational burden for this study. However, given the differences in the number of simulations, run time, and output of each method, there remains future work in comparing method performance and improving the parallelization of the Morris Method code. These results may be used to help identify parameter constraints and characterize model uncertainty toward more confident predictions and management decisions for coastal barrier systems.

A.7 Acknowledgements

The authors would like to thank those who have supported this work including the U.S. Army Corps of Engineers through the U.S. Coastal Research Program (under Grant No. W912HZ-20-2-0005), the National Science Foundation (under Grant Numbers 1630099 and 1735139), and the Virginia Sea Grant College Program (Project R/72155T), from the National Oceanic and Atmospheric Administration's National Sea Grant College Program, U.S. Department of Commerce under award NA18OAR4170083. Any opinions, findings, and conclusions or recommendations expressed in this material are those of the authors and do not necessarily reflect the views of these organizations. The authors also acknowledge Advanced Research Computing at Virginia Tech for providing computational resources and technical support

that have contributed to the results reported within this paper. URL: https://arc.vt.edu/

Appendix B

Supplementary Material for Chapter 3

Outline of Supplementary Material:

1. Input parameter ranges for this sensitivity study
2. All results from Simulation Set A
3. Initial and Critical Geometry Interactions from Simulation Set A
4. All results from Simulation Set C

1. Input parameter ranges for this sensitivity study

The input parameters for this sensitivity study are listed in Table B1.1 below with their value ranges highlighted in yellow. Each parameter range is compared to the value ranges from previous model publications including LTA14 (Lorenzo-Trueba & Ashton, 2014), MAC14 (Mariotti & Carr, 2014), LTM17 (Lorenzo-Trueba & Mariotti, 2017), and MLT17 (Miselis & Lorenzo-Trueba, 2017).

Table B1.1 Comparison of Ranges to Other Studies

Parameter	Symbol	Units	Range	LTA14	MAC14	LTM17	MLT17
Mainland Slope	β	[m/m]	0.0001-0.005	0.00001 – 0.005	NA	0.0001 – vertical	
Toe Depth	D_T	[m]	5 – 15	10, 15 (SI: 5 – 20)	NA	10	16
Critical Width	W_{cr}	[m]	100 – 600	300 (SI: 50 – 600)	NA	800	350 - 450
Critical Height	H_{cr}	[m]	0.5 – 4	1, 2 (SI: 0.5 – 2)	NA	2	5.9 – 6.7
Initial Width	W_0	[m]	100 – 1,000	(SI: 250 – 350)	NA	800	
Initial Height	H_0	[m]	0.5 – 4		NA	2	
Equil. Shoreface Slope	α_e	[m/m]	0.005 – 0.025	0.015, 0.02 (SI: 0.01 – 0.025)	NA	0.02	0.021 – 0.027
Critical BB Marsh Width	$B_{M1,cr}$	[m]	50 – 500	NA	NA	1,000	
Initial BB Marsh Width	$B_{M1,0}$	[m]	50 – 1,000	NA	NA	1,000	
Initial Lagoon Width	$B_{F,0}$	[m]	1,000 – 10,000	NA	1,000 – 9,000	5,000 – 30,000	
Initial Lagoon Depth	$D_{F,0}$	[m]	1 – 3	9 (Fig. 9)	NA		1.2 – 1.8
Max. Annual Overwash Flux	$Q_{OW,*}$	[m^3/m/yr]	1 – 100	5 - 100	NA	10, 100	0 - 100
SLR Rate	$\dot{z}$	[mm/yr]	3 – 20	1 – 8	0 – 15	0 - 10	4, 7, 10
Shoreface Sediment Flux Cont.	K	[m^3/m/yr]	100 – 10,000	0 – 10,000	NA	2,000	2,011
Ref. Wind Speed	U_{ref}	[m/s]	5 – 10	NA	6 (5 – 8)	10	
Tidal Range	r	[m]	0.7 – 2.8	NA	1.4 – 2.8	1.4 – 2	
Settling Velocity	ω_s	[mm/s]	0.05 – 0.5	NA	0.5	0.5	
Critical Bed Shear Stress	τ_{cr}	[Pa]	0.05 – 0.4	NA	0.1 – 0.4		
Ocean Sediment Concentration	C_o	[g/l]	0.03 – 0.2	NA	0 – 0.15	0 – 0.2	
Peak Biomass Production	B_P	[kg/m^2]	1.5 – 3.5	NA	?	2.5	

2. All Results from Simulation Set A

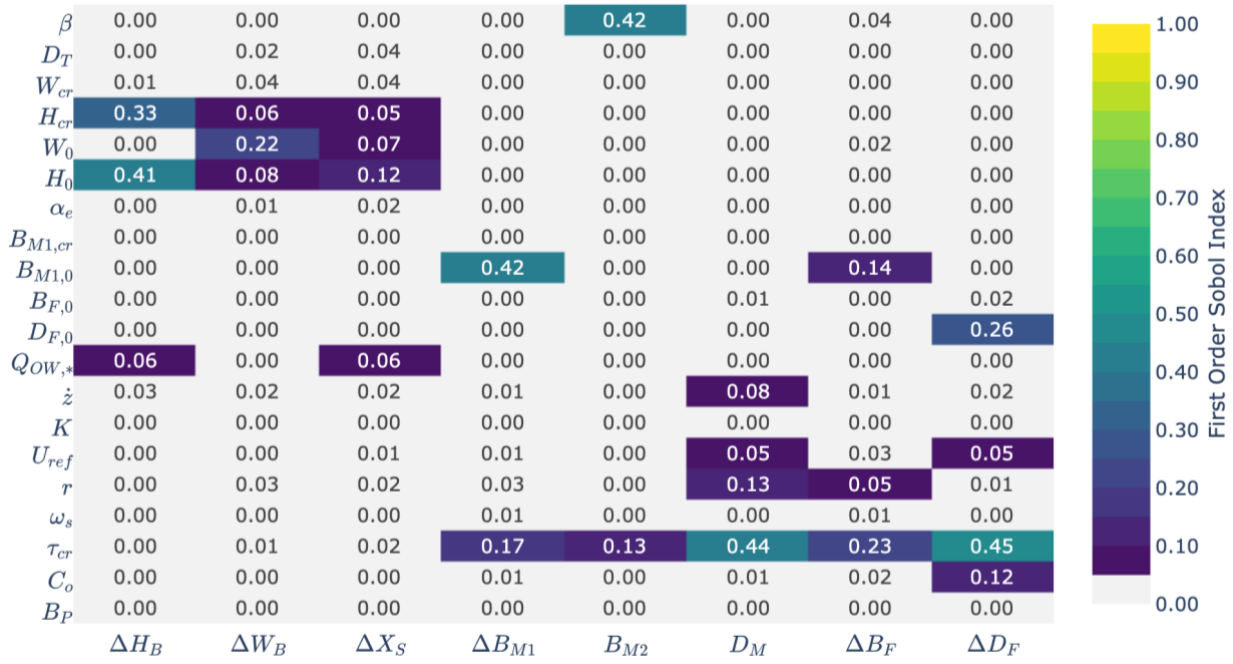

Figure B2.1. First-order Sobol Indices (Simulation Set A)

Figure B2.2. *k*th-order Sobol Indices (Simulation Set A)

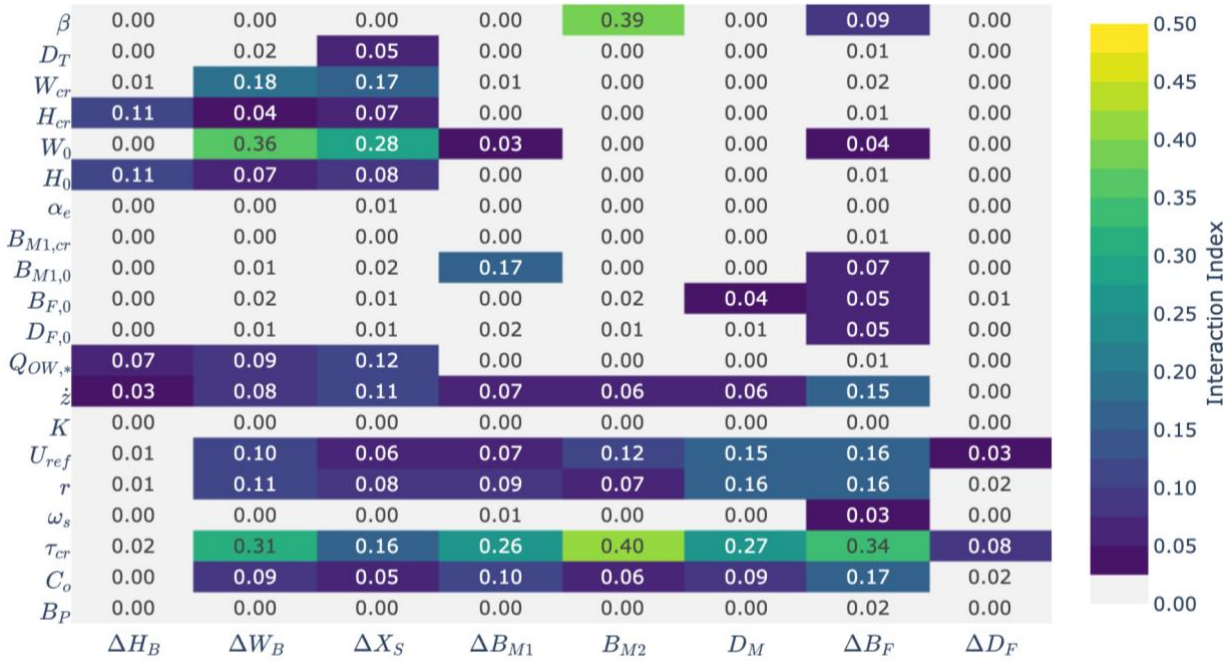

Figure B2.3. Interaction Indices (Simulation Set A)

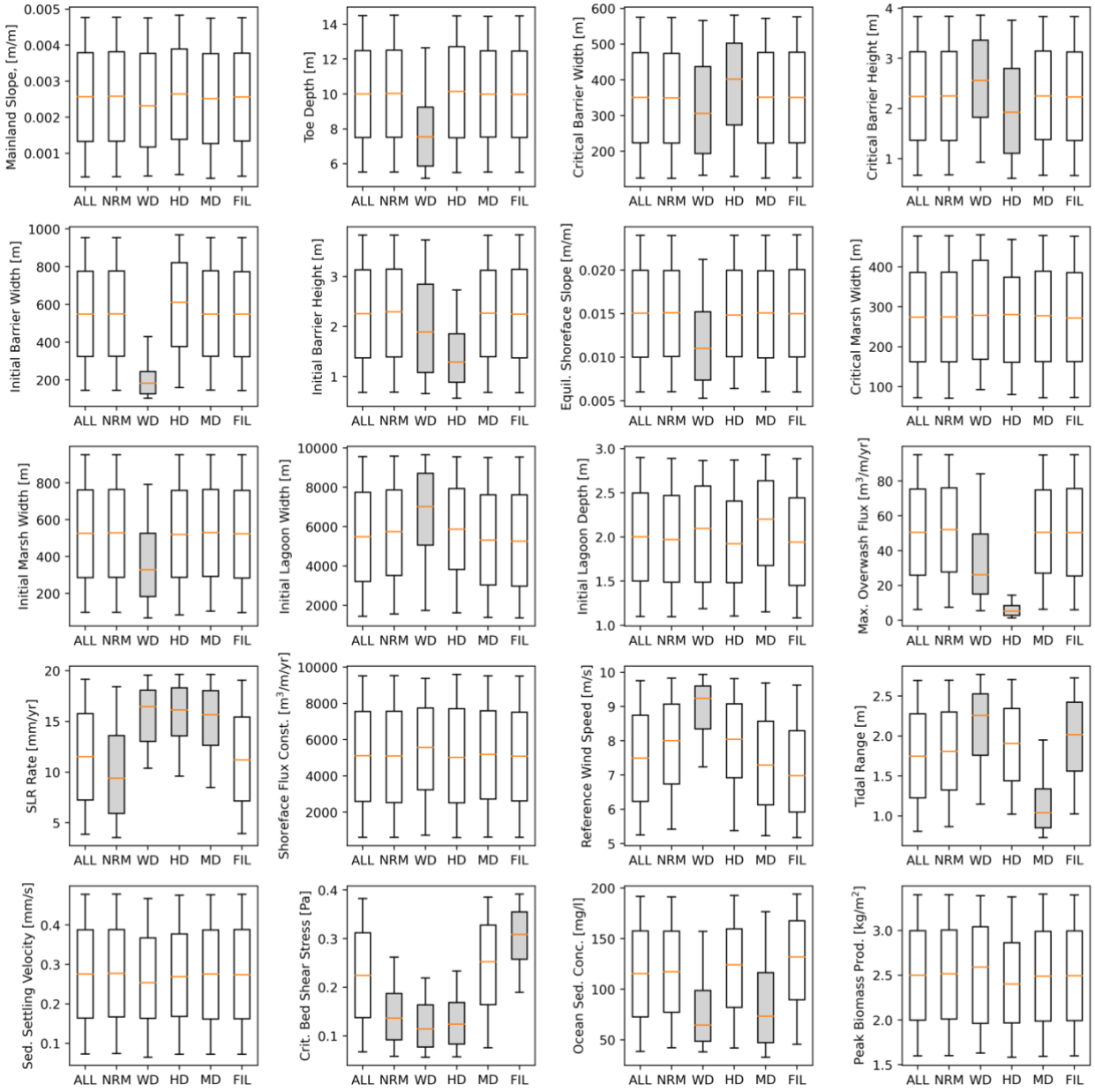

Figure B2.4. Distinctive Simulation Category Boxplots (Simulation Set A)

Table B2.1. Ninety Five Percent Confidence Intervals on Boxplot Medians for Parameters β through H_0 (Simulation Set A)

Parameter	Category	Non-Overlap	p5	Mean	p95
β	ALL		0.00237	0.00256	0.00275
β	NRM	NO	0.00240	0.00258	0.00277
β	WD	NO	0.00226	0.00237	0.00260
β	HD	NO	0.00249	0.00267	0.00285
β	MD	NO	0.00232	0.00252	0.00271
β	FILL	NO	0.00238	0.00256	0.00275
D_T	ALL		9.283	10.020	10.692
D_T	NRM	NO	9.291	10.040	10.750
D_T	WD	YES	6.757	7.487	8.156
D_T	HD	NO	9.552	10.137	10.733
D_T	MD	NO	9.263	9.986	10.662
D_T	FILL	NO	9.249	9.987	10.659
W_{cr}	ALL		326.1	350.8	374.6
W_{cr}	NRM	NO	323.2	348.2	374.3
W_{cr}	WD	YES	299.8	308.0	321.9
W_{cr}	HD	YES	380.5	403.1	431.6
W_{cr}	MD	NO	325.9	350.3	375.9
W_{cr}	FILL	NO	324.6	350.9	375.6
H_{cr}	ALL		2.062	2.239	2.411
H_{cr}	NRM	NO	2.066	2.245	2.401
H_{cr}	WD	YES	2.453	2.610	2.748
H_{cr}	HD	YES	1.826	1.919	2.009
H_{cr}	MD	NO	2.100	2.256	2.418
H_{cr}	FILL	NO	2.076	2.235	2.402
W_0	ALL		511.3	549.8	591.5
W_0	NRM	NO	512.3	550.7	589.4
W_0	WD	YES	174.8	181.5	186.9
W_0	HD	NO	582.7	612.8	646.6
W_0	MD	NO	511.6	549.4	587.0
W_0	FILL	NO	508.7	549.2	592.1
H_0	ALL		2.104	2.257	2.430
H_0	NRM	NO	2.131	2.292	2.454
H_0	WD	YES	1.702	1.903	2.042
H_0	HD	YES	1.203	1.298	1.410
H_0	MD	NO	2.108	2.269	2.424
H_0	FILL	NO	2.100	2.250	2.420

Table B2.2. Ninety Five Percent Confidence Intervals on Boxplot Medians for Parameters α_e through $Q_{OW,*}$ (Simulation Set A)

Parameter	Category	Non-Overlap	p5	Mean	p95
α_e	ALL		0.0140	0.0150	0.0161
α_e	NRM	NO	0.0140	0.0151	0.0161
α_e	WD	YES	0.0101	0.0109	0.0118
α_e	HD	NO	0.0139	0.0149	0.0158
α_e	MD	NO	0.0141	0.0151	0.0161
α_e	FILL	NO	0.0139	0.0150	0.0162
$B_{M1,cr}$	ALL		254.1	274.3	294.7
$B_{M1,cr}$	NRM	NO	253.6	273.7	292.8
$B_{M1,cr}$	WD	NO	261.0	276.5	290.1
$B_{M1,cr}$	HD	NO	256.8	278.5	296.0
$B_{M1,cr}$	MD	NO	256.8	277.5	297.1
$B_{M1,cr}$	FILL	NO	251.6	272.8	292.8
$B_{M1,0}$	ALL		487.3	525.3	563.9
$B_{M1,0}$	NRM	NO	493.0	527.2	562.4
$B_{M1,0}$	WD	YES	307.9	332.2	349.3
$B_{M1,0}$	HD	NO	487.6	519.8	552.7
$B_{M1,0}$	MD	NO	492.1	529.4	564.9
$B_{M1,0}$	FILL	NO	484.9	523.0	560.4
$B_{F,0}$	ALL		5084.6	5479.8	5864.9
$B_{F,0}$	NRM	NO	5294.9	5741.0	6166.3
$B_{F,0}$	WD	YES	6743.1	7087.4	7736.7
$B_{F,0}$	HD	NO	5533.9	5893.6	6265.6
$B_{F,0}$	MD	NO	4932.5	5331.0	5737.8
$B_{F,0}$	FILL	NO	4884.2	5251.1	5650.8
$D_{F,0}$	ALL		1.859	2.003	2.143
$D_{F,0}$	NRM	NO	1.831	1.972	2.106
$D_{F,0}$	WD	NO	1.950	2.086	2.212
$D_{F,0}$	HD	NO	1.778	1.922	2.077
$D_{F,0}$	MD	NO	2.053	2.198	2.336
$D_{F,0}$	FILL	NO	1.796	1.940	2.081
$Q_{OW,*}$	ALL		46.79	50.51	54.11
$Q_{OW,*}$	NRM	NO	48.07	52.00	55.53
$Q_{OW,*}$	WD	YES	25.23	27.28	29.66
$Q_{OW,*}$	HD	YES	5.06	5.31	5.57
$Q_{OW,*}$	MD	NO	47.31	50.40	54.04
$Q_{OW,*}$	FILL	NO	46.70	50.34	54.03

Table B2.3. Ninety Five Percent Confidence Intervals on Boxplot Medians for Parameters $\dot{z}$ through τ_{cr} (Simulation Set A)

Parameter	Category	Non-Overlap	p5	Mean	p95
$\dot{z}$	ALL		0.0107	0.0115	0.0123
$\dot{z}$	NRM	YES	0.0087	0.0094	0.0100
$\dot{z}$	WD	YES	0.0153	0.0164	0.0170
$\dot{z}$	HD	YES	0.0152	0.0162	0.0171
$\dot{z}$	MD	YES	0.0147	0.0157	0.0166
$\dot{z}$	FILL	NO	0.0105	0.0112	0.0120
K	ALL		4732.9	5103.4	5480.2
K	NRM	NO	4751.1	5099.9	5464.4
K	WD	NO	5206.9	5689.7	6428.7
K	HD	NO	4624.9	4976.7	5277.6
K	MD	NO	4852.9	5195.7	5542.6
K	FILL	NO	4695.0	5073.0	5445.7
U_{ref}	ALL		6.968	7.501	8.019
U_{ref}	NRM	NO	7.495	8.002	8.512
U_{ref}	WD	YES	8.562	9.149	9.534
U_{ref}	HD	NO	7.480	8.036	8.618
U_{ref}	MD	NO	6.745	7.300	7.840
U_{ref}	FILL	NO	6.471	6.988	7.541
r	ALL		1.626	1.743	1.868
r	NRM	NO	1.682	1.807	1.934
r	WD	YES	2.129	2.282	2.432
r	HD	NO	1.808	1.913	2.013
r	MD	YES	0.983	1.041	1.104
r	FILL	YES	1.881	2.015	2.151
ω_s	ALL		8021.7	8693.7	9316.4
ω_s	NRM	NO	8128.7	8735.1	9386.8
ω_s	WD	NO	7217.4	7857.7	8166.5
ω_s	HD	NO	8184.0	8509.6	8868.0
ω_s	MD	NO	8031.1	8692.6	9345.0
ω_s	FILL	NO	8046.8	8641.9	9268.9
τ_{cr}	ALL		0.209	0.224	0.241
τ_{cr}	NRM	YES	0.128	0.137	0.146
τ_{cr}	WD	YES	0.106	0.117	0.128
τ_{cr}	HD	YES	0.117	0.124	0.130
τ_{cr}	MD	NO	0.235	0.252	0.269
τ_{cr}	FILL	YES	0.289	0.308	0.327

Table B2.4. Ninety Five Percent Confidence Intervals on Boxplot Medians for Parameters C_o and B_P (Simulation Set A)

Parameter	Category	Non-Overlap	p5	Mean	p95
C_o	ALL		0.108	0.116	0.124
C_o	NRM	NO	0.109	0.118	0.126
C_o	WD	YES	0.062	0.064	0.069
C_o	HD	NO	0.116	0.124	0.132
C_o	MD	YES	0.068	0.073	0.078
C_o	FILL	NO	0.123	0.132	0.140
B_P	ALL		2.314	2.503	2.689
B_P	NRM	NO	2.340	2.515	2.685
B_P	WD	NO	2.433	2.585	2.782
B_P	HD	NO	2.263	2.397	2.540
B_P	MD	NO	2.311	2.487	2.672
B_P	FILL	NO	2.312	2.485	2.670

3. Initial and Critical Geometry Interactions from Simulation Set A

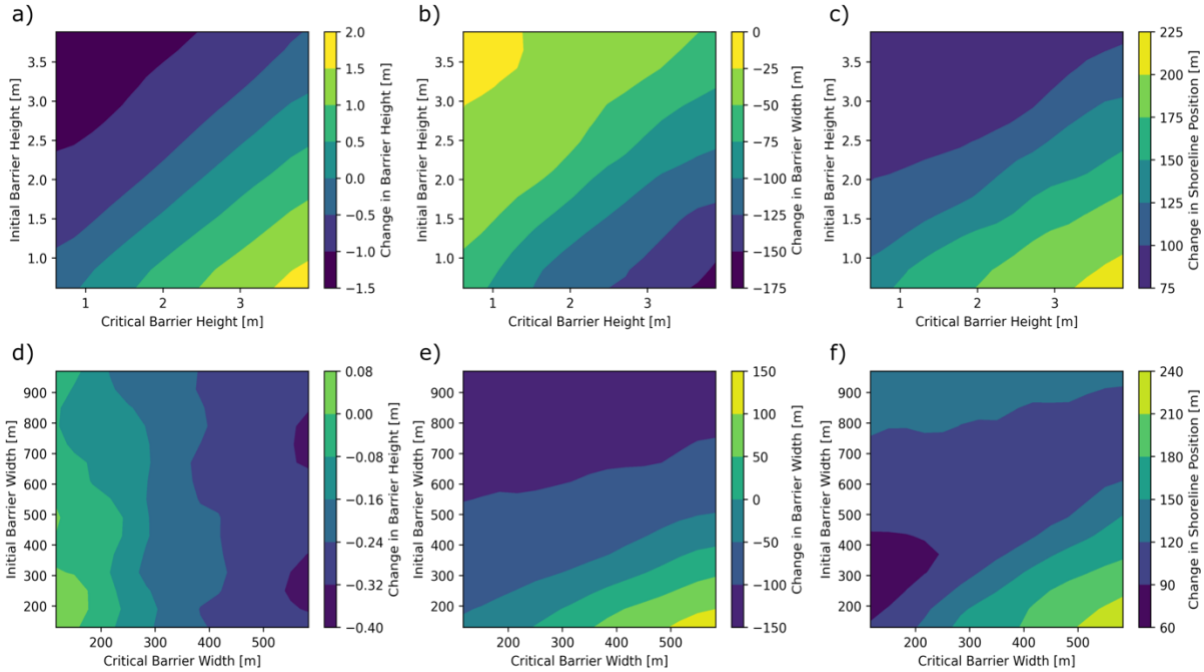

Figure B3.1. Initial and Critical Geometry Interactions (Simulation Set A)

4. All Results from Simulation Set C

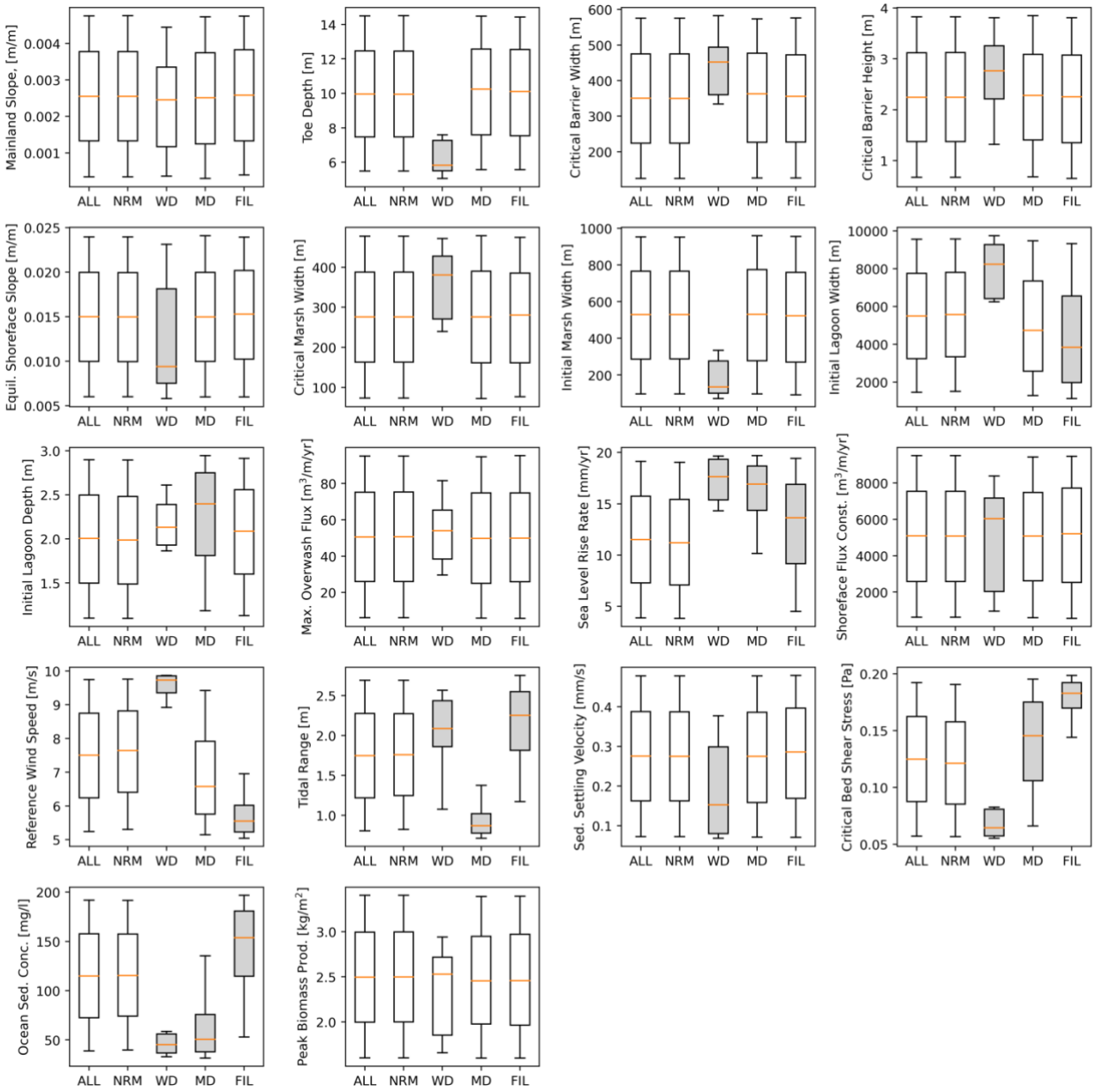

Figure B4.1. Distinctive Simulation Category Boxplots (Simulation Set C)

Table B4.1. Ninety Five Percent Confidence Intervals on Boxplot Medians for Parameters C_o and B_P (Simulation Set C)

Parameter	Category	Non-Overlap	p5	Mean	p95
β	ALL		0.00237	0.00255	0.00273
β	NRM	NO	0.00239	0.00255	0.00274
β	WD	NO	0.00239	0.00245	0.00251
β	MD	NO	0.00237	0.00253	0.00274
β	FILL	NO	0.00242	0.00258	0.00276
D_T	ALL		9.285	9.958	10.690
D_T	NRM	NO	9.311	9.975	10.660
D_T	WD	YES	5.677	5.892	6.653
D_T	MD	NO	9.468	10.203	10.879
D_T	FILL	NO	9.430	10.130	10.834
W_{cr}	ALL		327.3	350.8	374.3
W_{cr}	NRM	NO	326.1	349.9	375.4
W_{cr}	WD	YES	429.3	451.3	473.9
W_{cr}	MD	NO	334.4	361.6	387.3
W_{cr}	FILL	NO	328.2	354.6	377.2
H_{cr}	ALL		2.088	2.249	2.403
H_{cr}	NRM	NO	2.081	2.244	2.408
H_{cr}	WD	YES	2.739	2.764	2.788
H_{cr}	MD	NO	2.116	2.293	2.465
H_{cr}	FILL	NO	2.094	2.252	2.409
α_e	ALL		0.0139	0.0150	0.0161
α_e	NRM	NO	0.0139	0.0150	0.0160
α_e	WD	YES	0.0089	0.0094	0.0099
α_e	MD	NO	0.0140	0.0150	0.0161
α_e	FILL	NO	0.0142	0.0153	0.0164
$B_{M1,cr}$	ALL		255.8	276.0	297.2
$B_{M1,cr}$	NRM	NO	256.1	276.3	296.7
$B_{M1,cr}$	WD	YES	361.4	380.6	399.5
$B_{M1,cr}$	MD	NO	260.3	278.4	300.7
$B_{M1,cr}$	FILL	NO	258.9	279.6	299.2

Table B4.2. Ninety Five Percent Confidence Intervals on Boxplot Medians for Parameters C_o and B_P (Simulation Set C)

Parameter	Category	Non-Overlap	p5	Mean	p95
$B_{M1,0}$	ALL		490.8	529.3	565.9
$B_{M1,0}$	NRM	NO	490.5	527.7	565.5
$B_{M1,0}$	WD	YES	128.7	134.8	141.3
$B_{M1,0}$	MD	NO	489.6	527.7	568.1
$B_{M1,0}$	FILL	NO	481.9	523.0	564.9
$B_{F,0}$	ALL		5128.1	5505.6	5877.5
$B_{F,0}$	NRM	NO	5166.3	5573.0	5957.4
$B_{F,0}$	WD	YES	6992.0	8166.4	9088.5
$B_{F,0}$	MD	NO	4404.6	4735.4	5105.0
$B_{F,0}$	FILL	YES	3470.3	3833.0	4140.9
$D_{F,0}$	ALL		1.858	2.006	2.149
$D_{F,0}$	NRM	NO	1.834	1.984	2.125
$D_{F,0}$	WD	NO	1.980	2.135	2.308
$D_{F,0}$	MD	YES	2.203	2.382	2.514
$D_{F,0}$	FILL	NO	1.956	2.083	2.209
$Q_{OW,*}$	ALL		47.06	50.55	54.28
$Q_{OW,*}$	NRM	NO	47.14	50.75	54.52
$Q_{OW,*}$	WD	NO	51.52	53.94	56.39
$Q_{OW,*}$	MD	NO	46.85	50.16	53.66
$Q_{OW,*}$	FILL	NO	46.57	50.06	54.11
$\dot{z}$	ALL		0.0107	0.0115	0.0123
$\dot{z}$	NRM	NO	0.0104	0.0112	0.0120
$\dot{z}$	WD	YES	0.0156	0.0176	0.0193
$\dot{z}$	MD	YES	0.0160	0.0169	0.0179
$\dot{z}$	FILL	YES	0.0126	0.0136	0.0145
K	ALL		4747.9	5088.0	5432.9
K	NRM	NO	4698.3	5078.0	5421.9
K	WD	YES	5664.2	6037.2	6402.1
K	MD	NO	4693.9	5086.3	5448.0
K	FILL	NO	4829.5	5196.4	5545.8

Table B4.3. Ninety Five Percent Confidence Intervals on Boxplot Medians for Parameters C_o and B_P (Simulation Set C)

Parameter	Category	Non-Overlap	p5	Mean	p95
U_{ref}	ALL		6.980	7.512	8.014
U_{ref}	NRM	NO	7.116	7.655	8.184
U_{ref}	WD	YES	8.919	9.630	9.870
U_{ref}	MD	NO	6.154	6.614	7.126
U_{ref}	FILL	YES	5.294	5.556	5.857
r	ALL		1.617	1.747	1.876
r	NRM	NO	1.631	1.762	1.885
r	WD	YES	2.085	2.087	2.088
r	MD	YES	0.833	0.870	0.909
r	FILL	YES	2.103	2.244	2.362
ω_s	ALL		8024.1	8686.0	9323.2
ω_s	NRM	NO	8009.7	8676.9	9325.0
ω_s	WD	YES	3547.1	4836.2	6055.2
ω_s	MD	NO	8054.5	8684.6	9289.7
ω_s	FILL	NO	8342.4	8991.0	9562.8
τ_{cr}	ALL		0.116	0.125	0.134
τ_{cr}	NRM	NO	0.112	0.121	0.129
τ_{cr}	WD	YES	0.063	0.064	0.065
τ_{cr}	MD	YES	0.135	0.145	0.156
τ_{cr}	FILL	YES	0.172	0.182	0.190
C_o	ALL		0.107	0.115	0.122
C_o	NRM	NO	0.107	0.115	0.124
C_o	WD	YES	0.039	0.045	0.052
C_o	MD	YES	0.048	0.051	0.053
C_o	FILL	YES	0.145	0.154	0.162
B_P	ALL		2.315	2.500	2.683
B_P	NRM	NO	2.310	2.497	2.686
B_P	WD	NO	2.517	2.526	2.543
B_P	MD	NO	2.279	2.451	2.630
B_P	FILL	NO	2.285	2.457	2.624

Supplemental References

Lorenzo-Trueba, J., & Ashton, A. D. (2014). Rollover, drowning, and discontinuous retreat: Distrinct modes of barrier response to sea-level rise arising from a simple morphodynamic model. *Journal of Geophysical Research: Earth Surface*, 779–801. https://doi.org/10.1002/2013JF002871.Received

Lorenzo-Trueba, J., & Mariotti, G. (2017). Chasing boundaries and cascade effects in a coupled barrier-marsh-lagoon system. *Geomorphology*, *290*, 153–163. https://doi.org/10.1016/j.geomorph.2017.04.019

Mariotti, G., & Carr, J. (2014). Dual role of salt marsh retreat: Long-term and short-term resilience. *Water Resources Research*, *50*(4), 2963–2974. https://doi.org/10.1002/2013WR014676

Miselis, J. L., & Lorenzo-Trueba, J. (2017). Natural and Human-Induced Variability in Barrier-Island Response to Sea Level Rise. *Geophysical Research Letters*, *44*(23), 11,922-11,931. https://doi.org/10.1002/2017GL074811

Appendix C

Supplementary Material for Chapter 4

Supplementary Material

Manuscript Title: Comparability of global sensitivity analysis methods applied to a long-term coastal morphodynamics model

Authors: Steven W.H. Hoagland, Jennifer L. Irish, and Robert Weiss

Outline of Supplementary Material:

1. Morphodynamics model variables and initial conditions
2. Convergence of model output for uncertainty analysis
3. Ratio of factor sensitivity (RFS) and parameter ranking plots for all result variables
4. Spearman correlation convergence for all result variables
5. Morris convergence for all result variables
6. Sobol convergence for all result variables
7. VARS i50 convergence for all result variables
8. Results for 100 independent trials with 1,000-2,000 simulations for remaining result variables
9. Results for 100 independent trials with 10,000-20,000 simulations for remaining result variables

1. Morphodynamics model variables and initial conditions

Table C.1.1 – LTM17 Model Variables and Initial Conditions

Parameter	Value [units]
Maximum deficit volume per meter	Wcr*Hcr [m^2]
Maximum backbarrier depth for vegetation growth	0.7167*(tidal range)-0.0483 [m]
Marsh and mudflat densities	1000 [kg/m^3]
Initial barrier geometries (Height, Width, Shoreface Slope)	*set to equilibrium values
Tidal period	12.5 [hr]
Sediment erodibility parameter	0.0001
Shape coefficient for marsh erosion (dist)	10 [m]
Marsh progradation coefficient	2.0
Marsh erosion coefficient	0.16
Organic matter porosity	0.377
Fraction of refractory accumulated carbon	0.15
Density of organic matter	1000 [kg/m^3]
Initial lagoon width	5500 [m]
Initial backbarrier marsh width	525 [m]
Initial interior marsh width	300 [m]
Initial lagoon depth with respect to mean high water level	2 [m]
Simulation time step	0.1 [yrs]
Total simulation time	100 [yrs]

2. Convergence of model output for uncertainty analysis

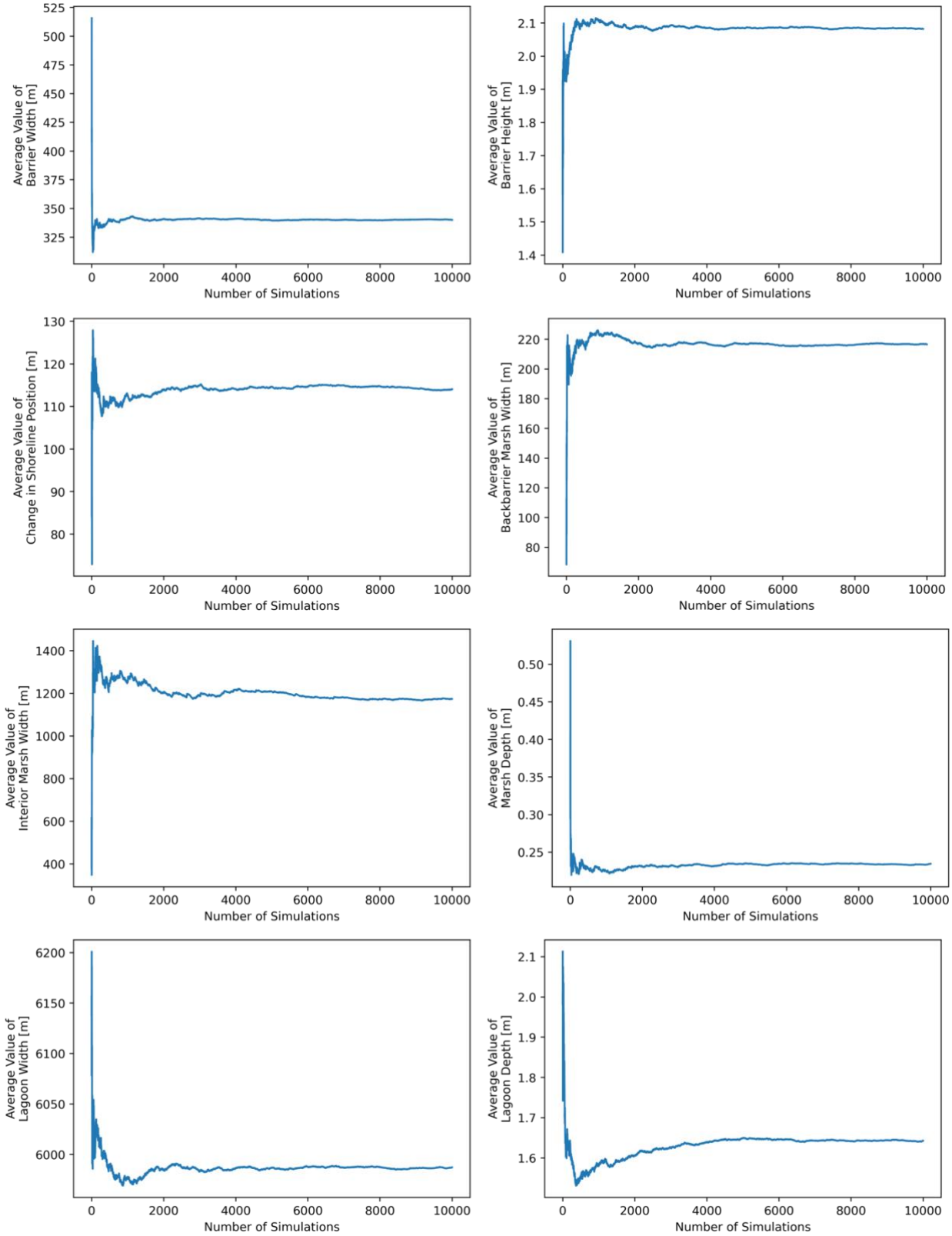

Figure C.2.1 – Convergence of Mean of Model Output for Uncertainty Analysis

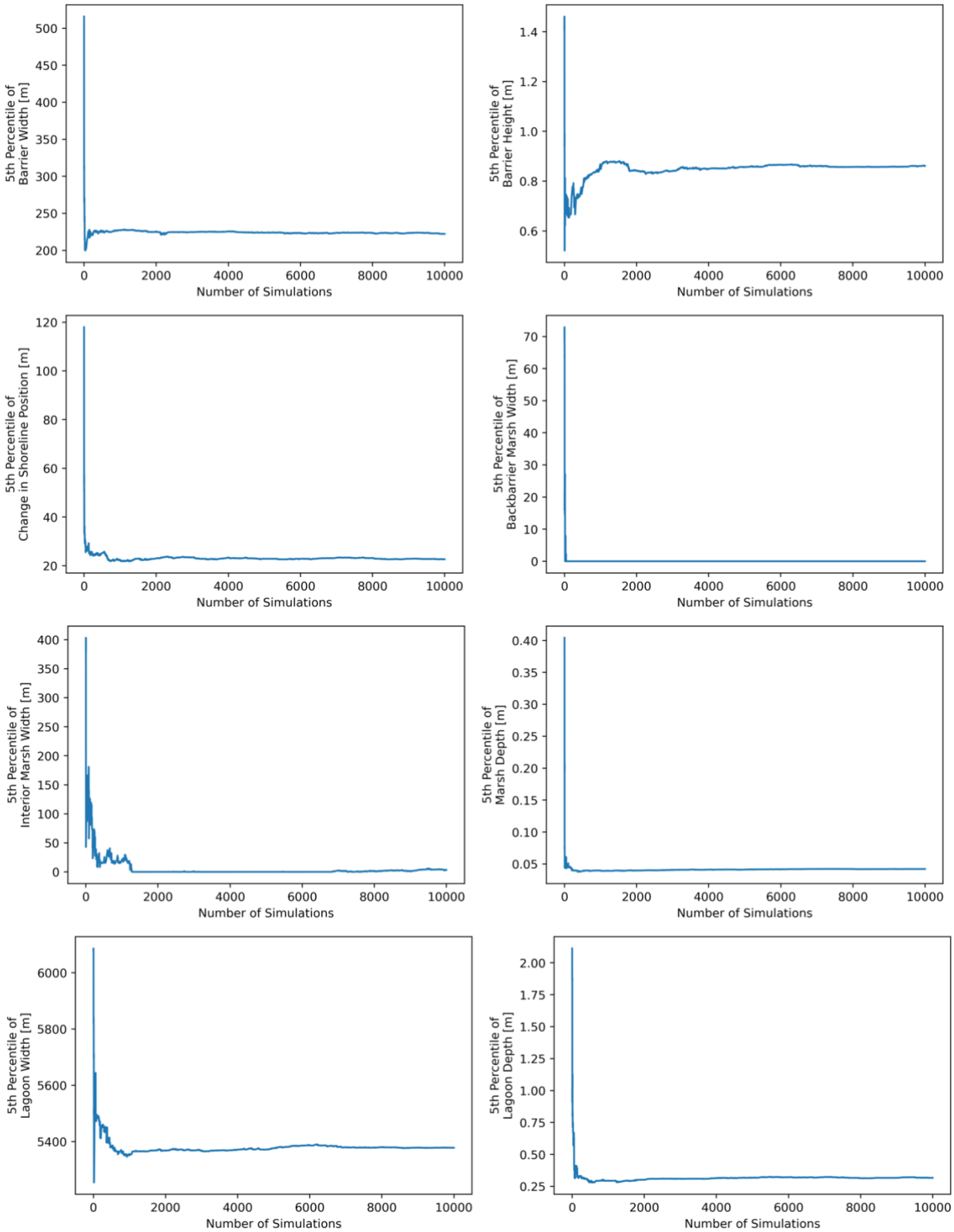

Figure C.2.2 – Convergence of 5th Percentile of Model Output for Uncertainty Analysis

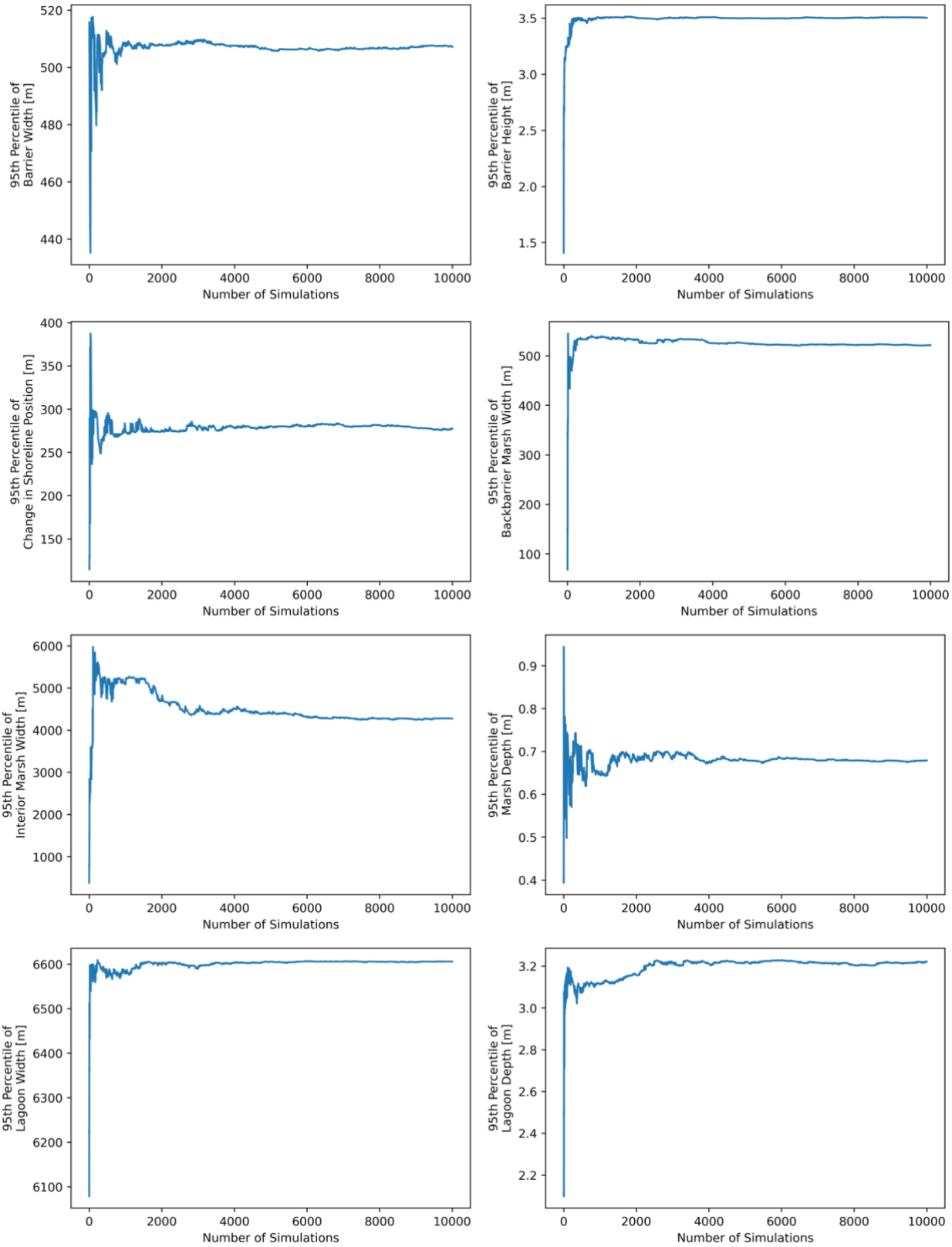

Figure C.2.3 – Convergence of 95th Percentile of Model Output for Uncertainty Analysis

3. Ratio of factor sensitivity (RFS) and parameter ranking plots for all result variables

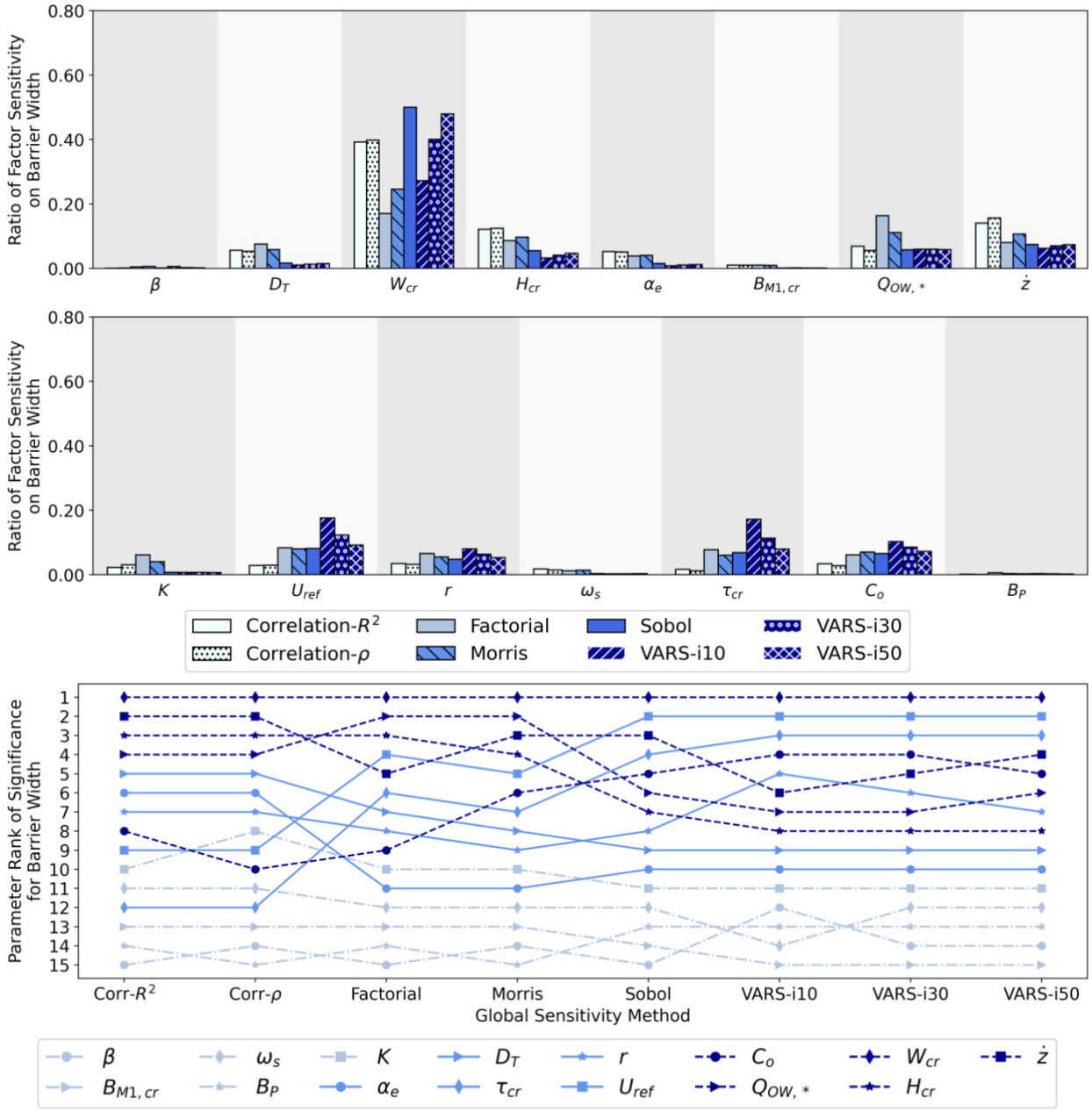

Figure C.3.1 – RFS and Parameter Ranking Results for Barrier Width

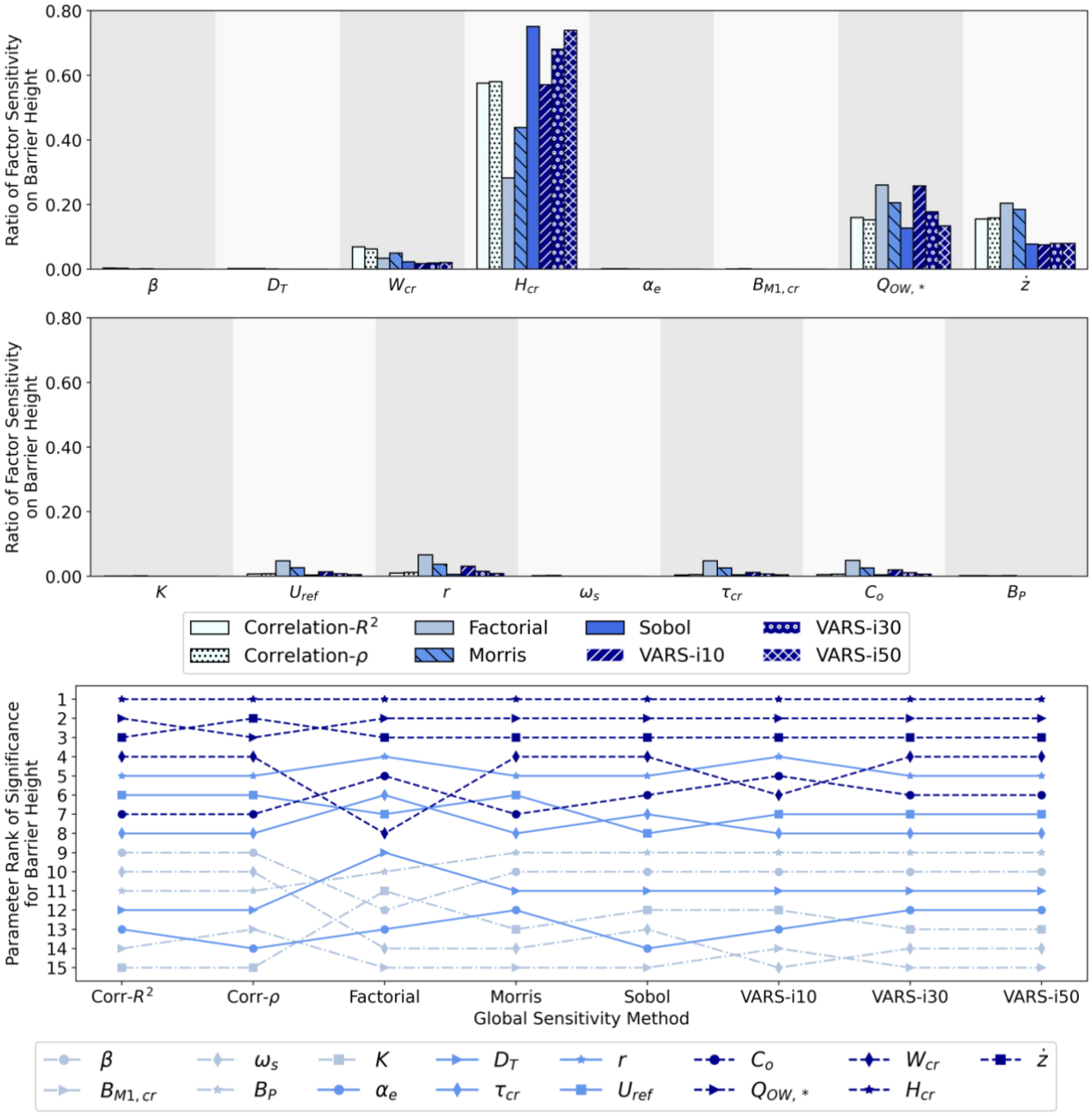

Figure C.3.2 – RFS and Parameter Ranking Results for Barrier Height

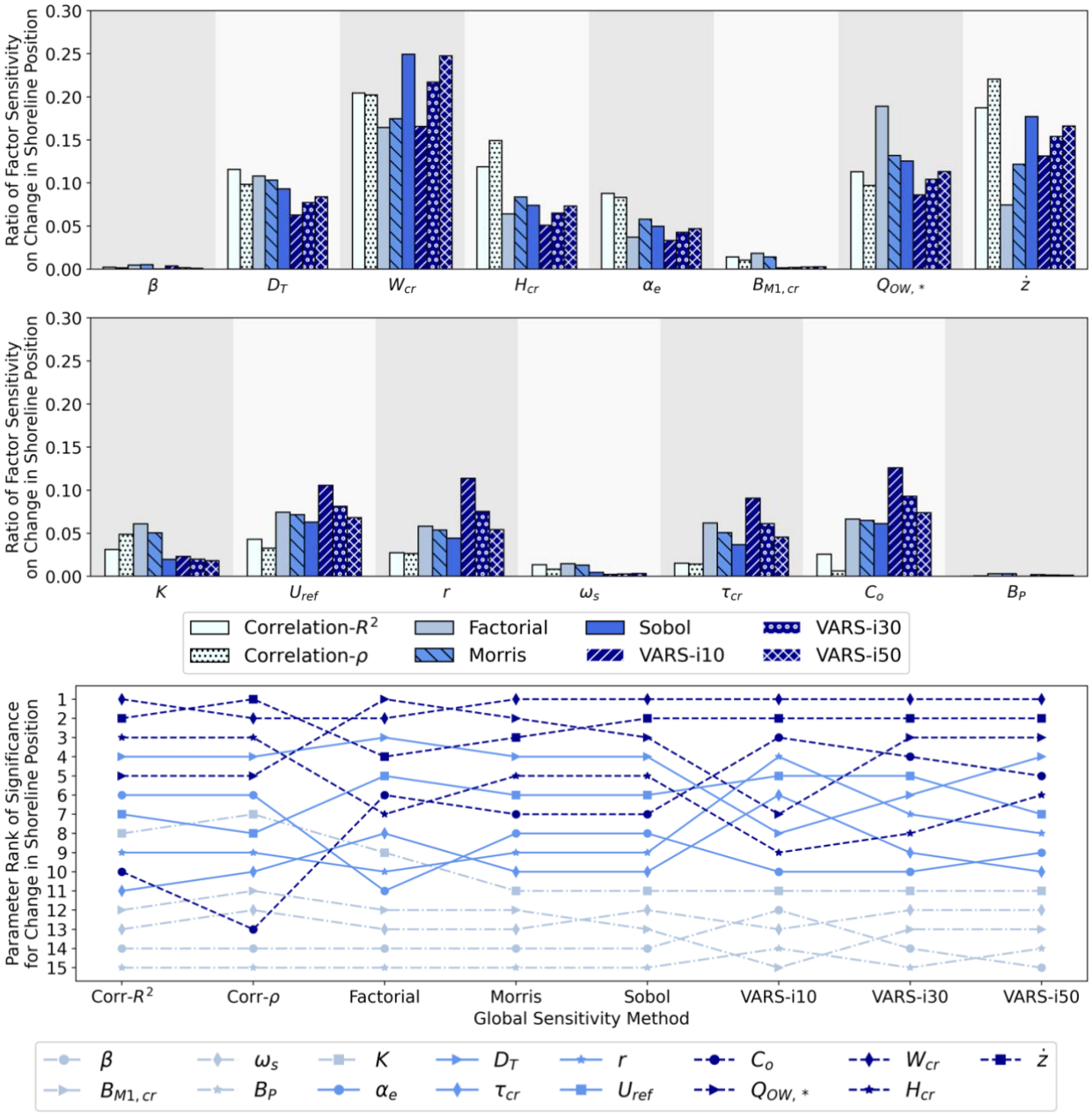

Figure C.3.3 – RFS and Parameter Ranking Results for Change in Shoreline Position

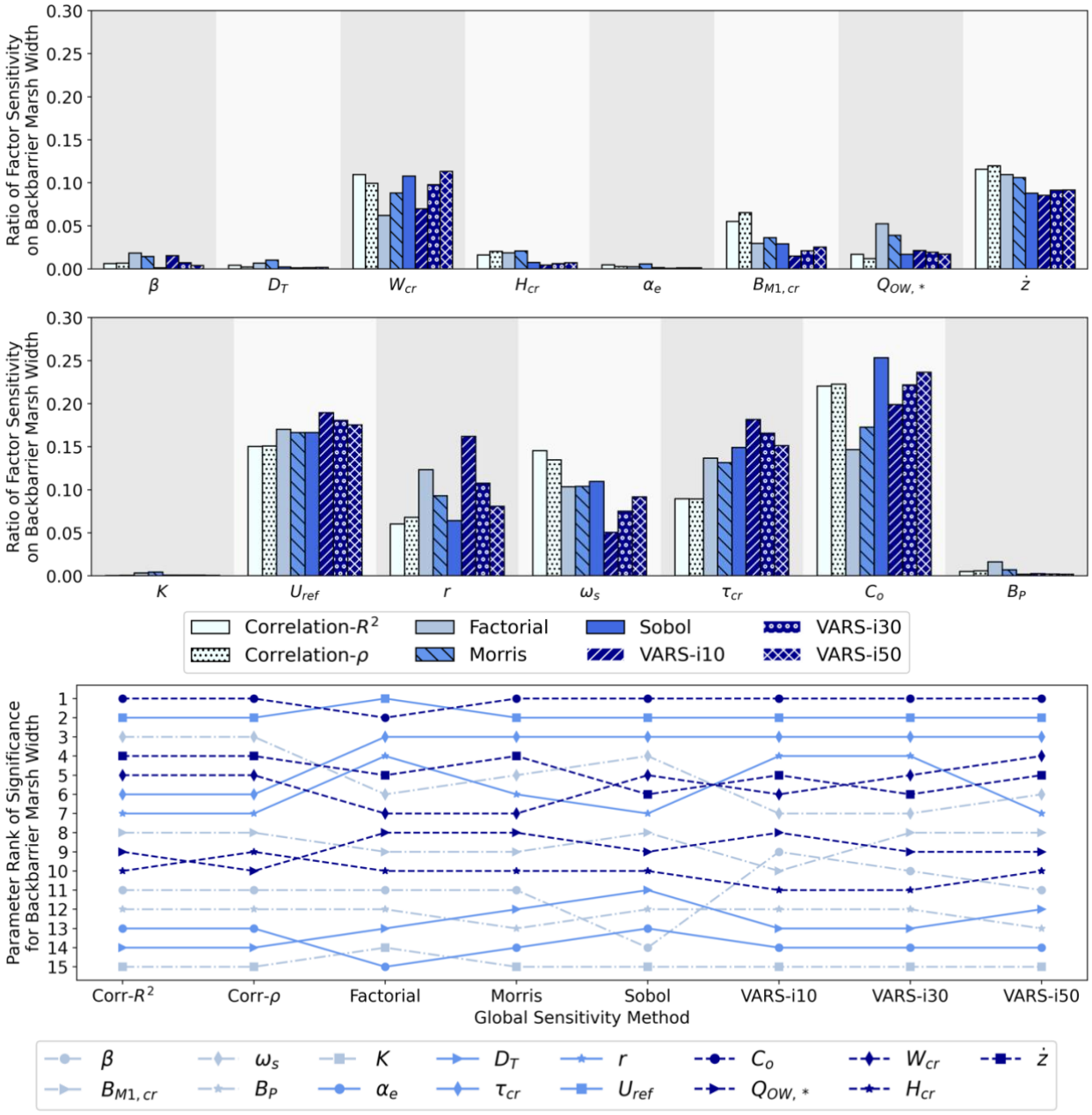

Figure C.3.4 – RFS and Parameter Ranking Results for Backbarrier Marsh Width

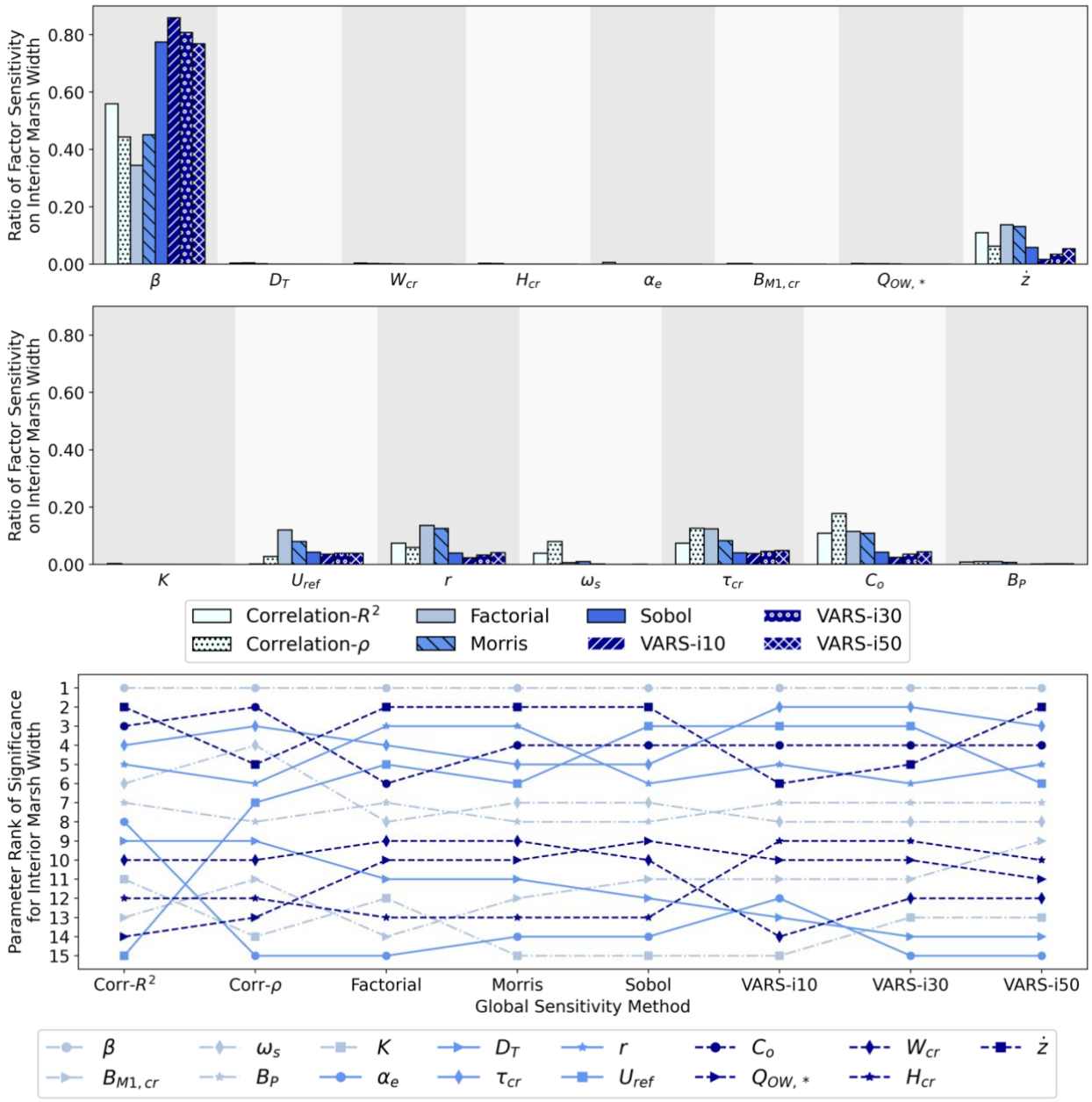

Figure C.3.5 – RFS and Parameter Ranking Results for Interior Marsh Width

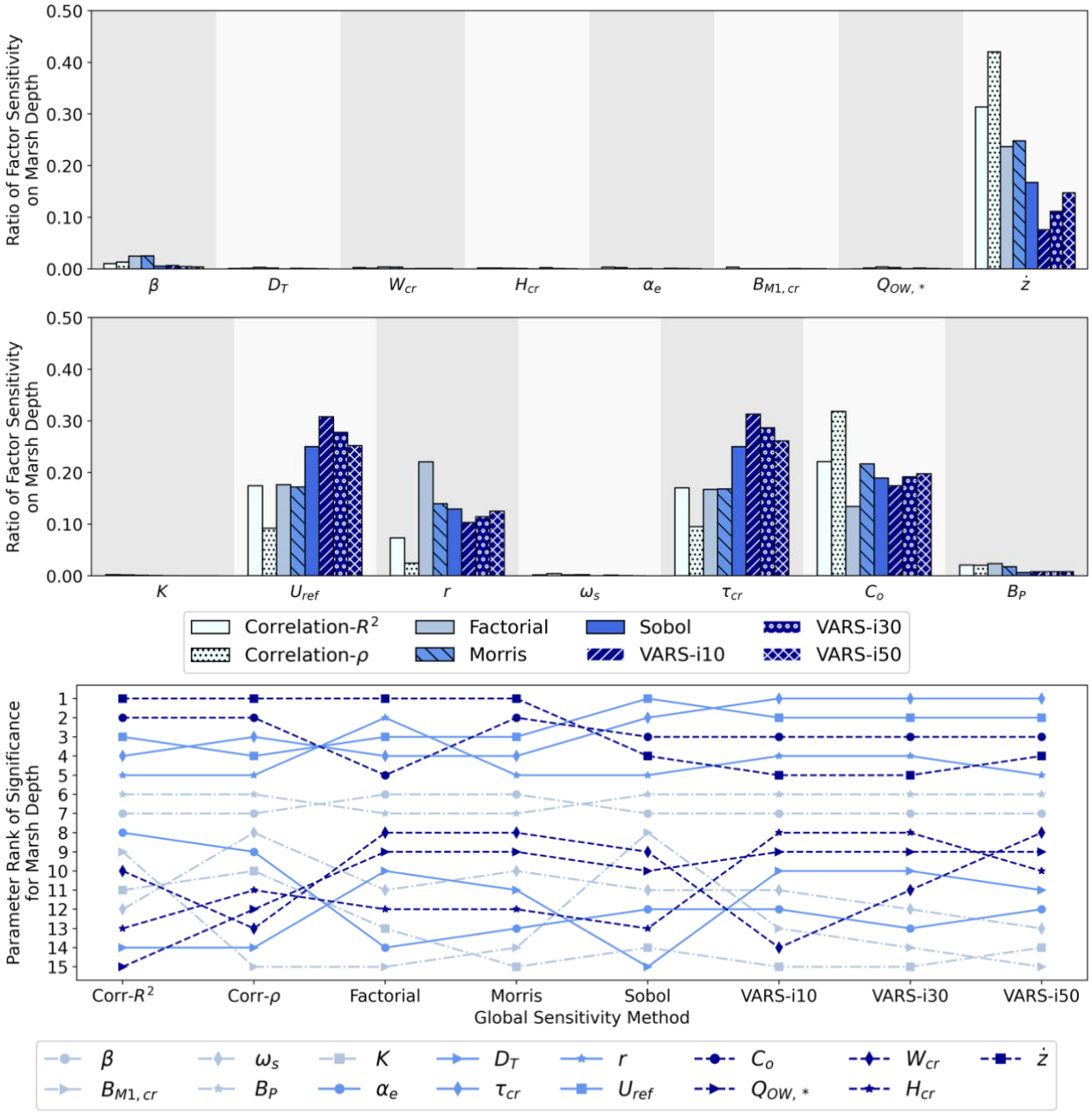

Figure C.3.6 – RFS and Parameter Ranking Results for Marsh Depth

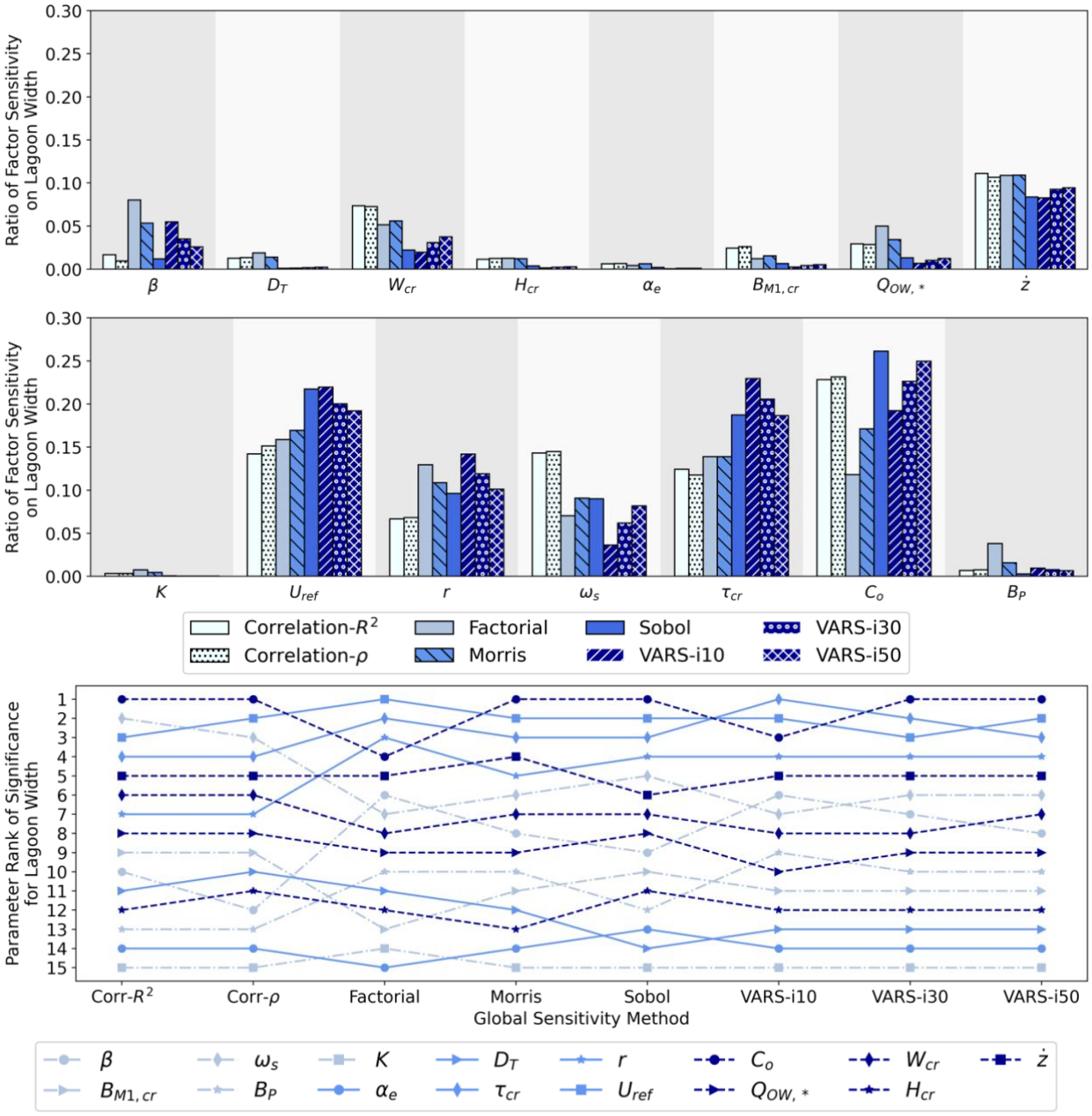

Figure C.3.7 – RFS and Parameter Ranking Results for Lagoon Width

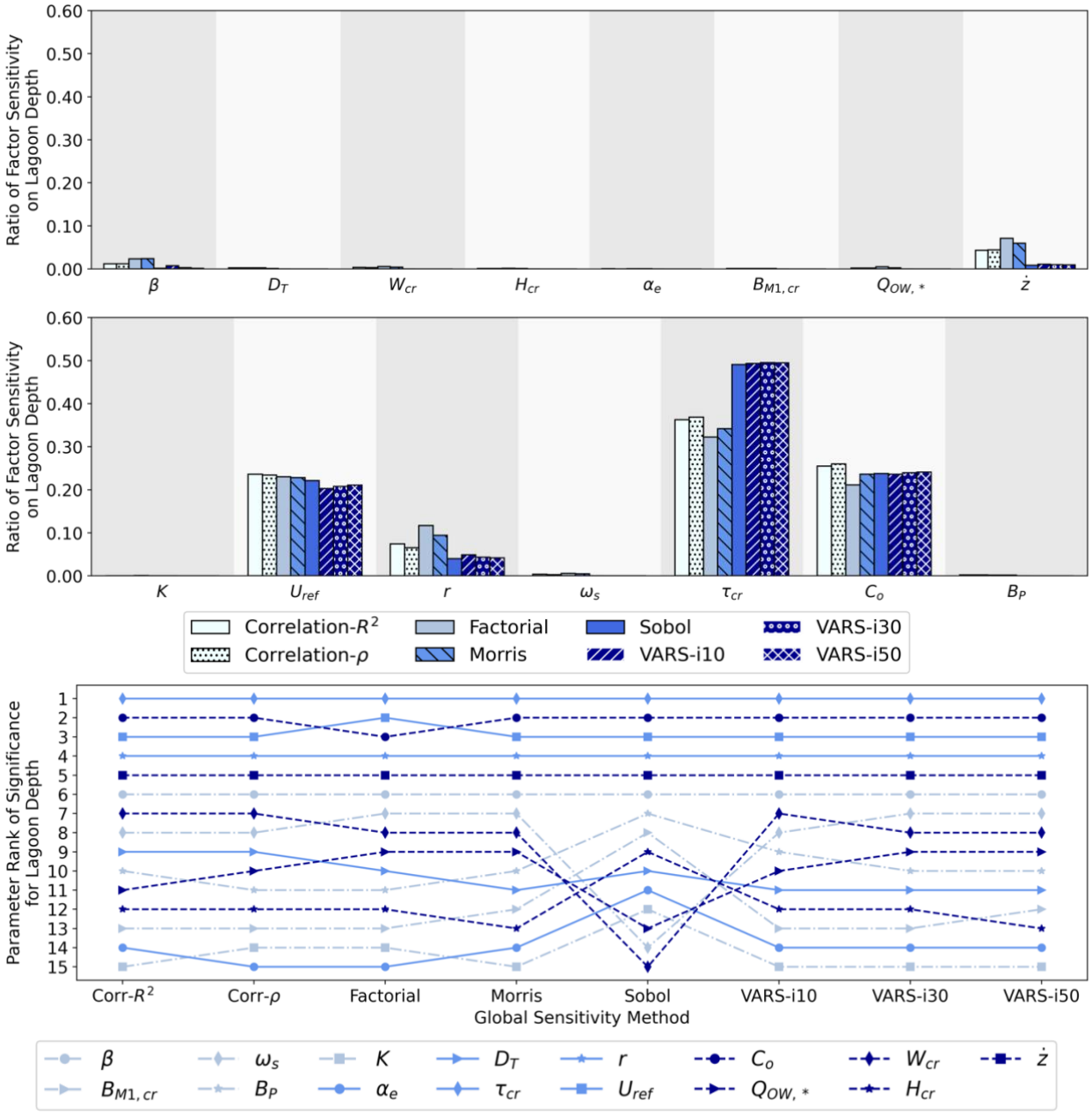

Figure C.3.8 – RFS and Parameter Ranking Results for Lagoon Depth

4. Spearman convergence results for all result variables

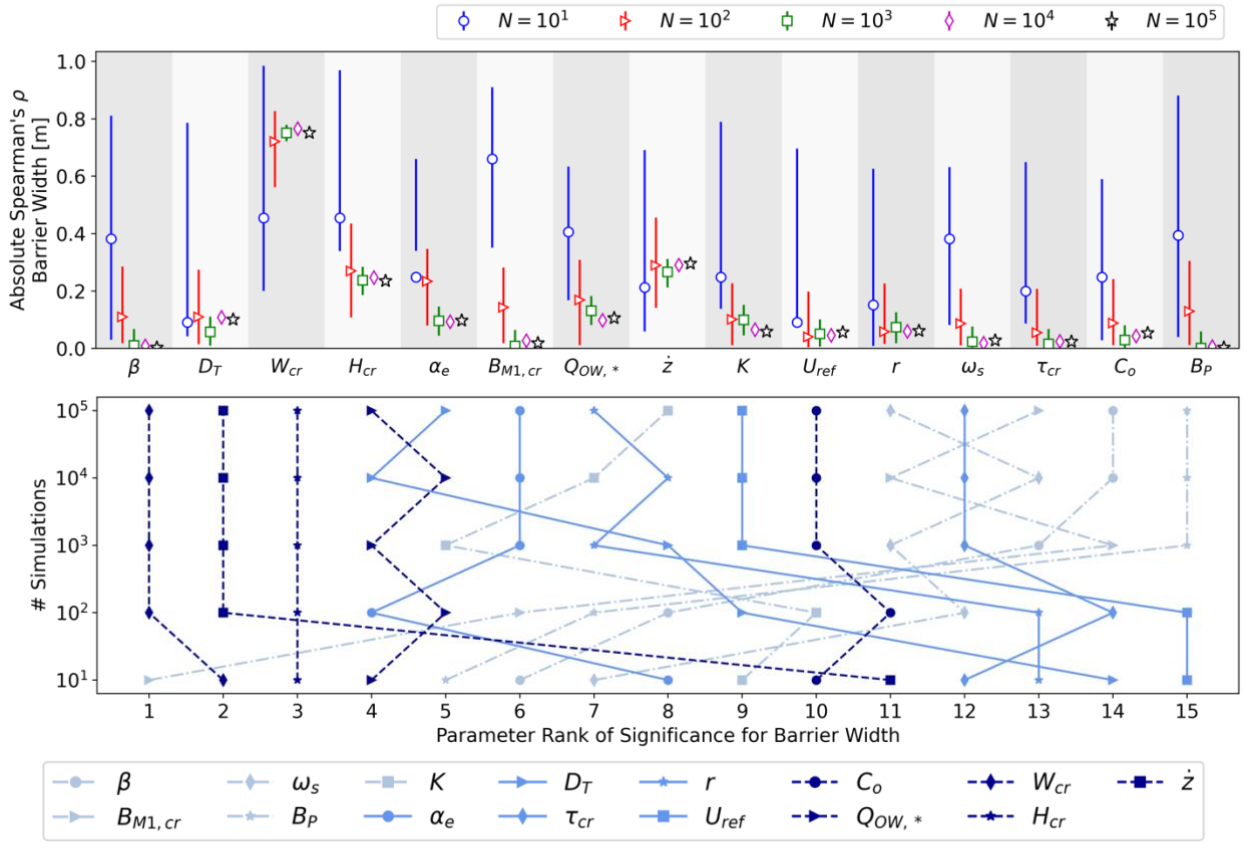

Figure C.4.1 – Spearman Correlation Convergence for Barrier Width

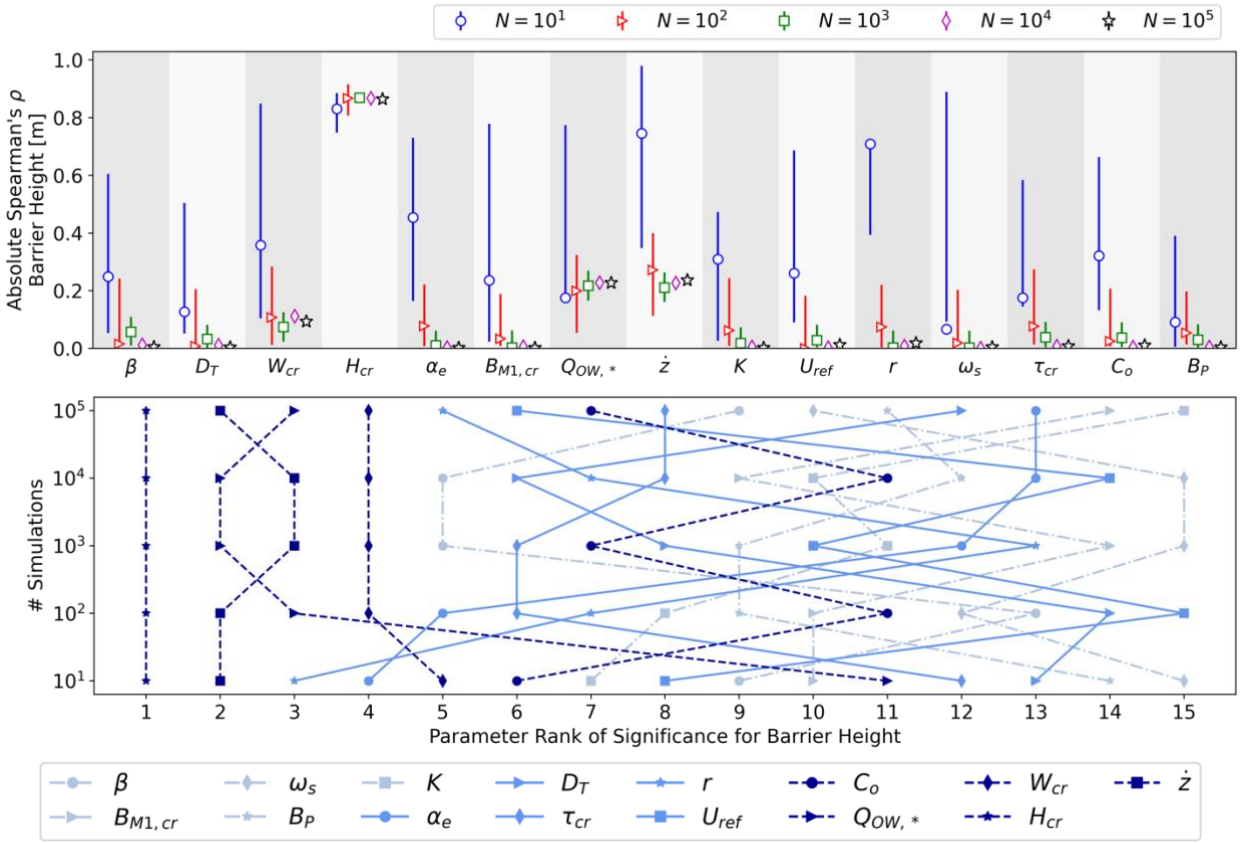

Figure C.4.2 – Spearman Correlation Convergence for Barrier Height

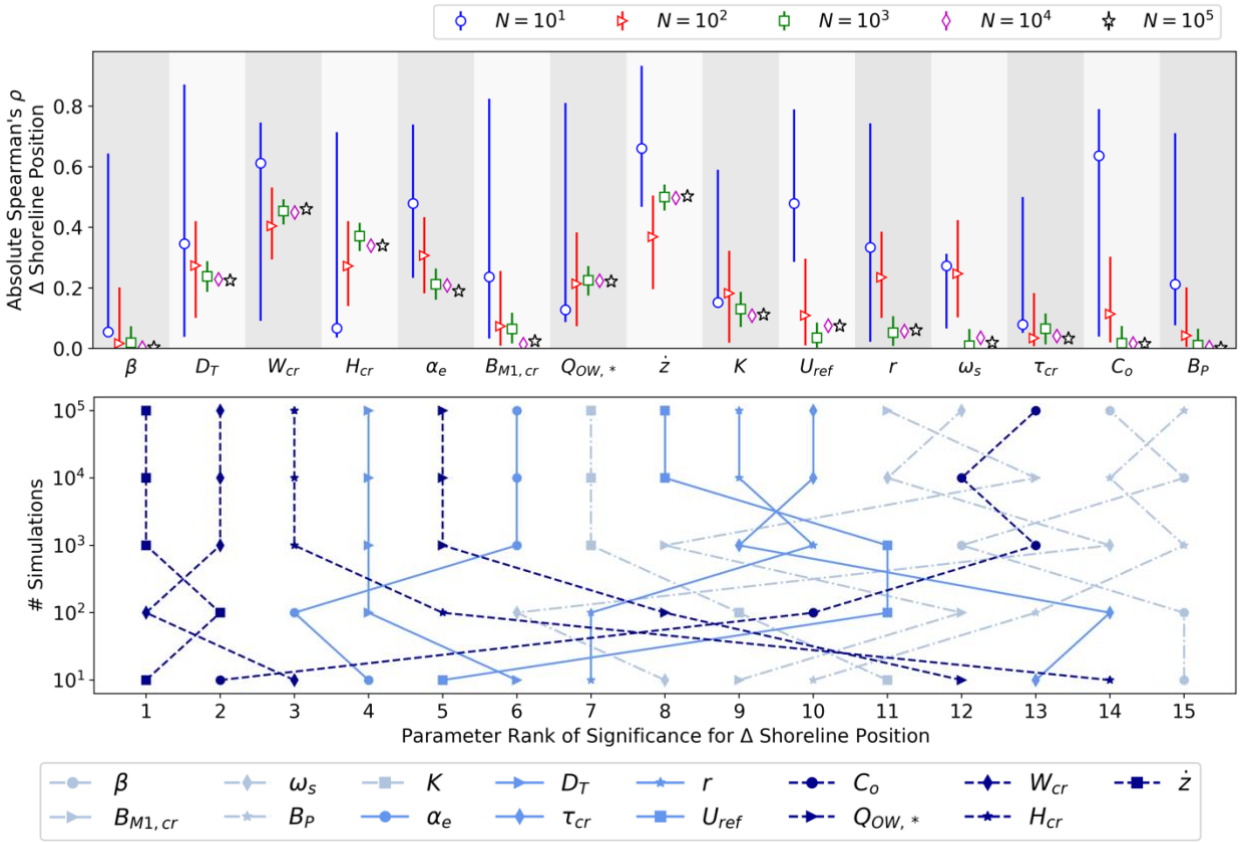

Figure C.4.3 – Spearman Correlation Convergence for Change in Shoreline Position

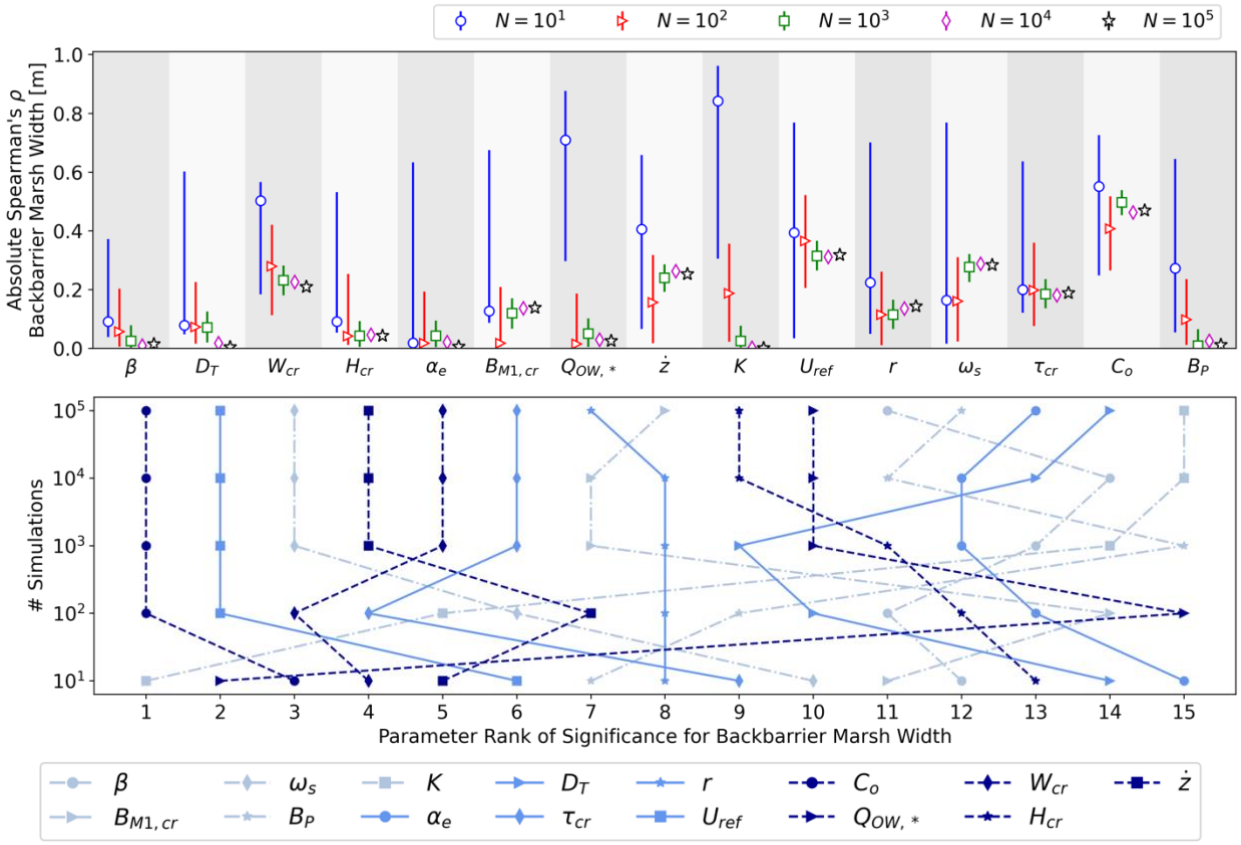

Figure C.4.4 – Spearman Correlation Convergence for Backbarrier Marsh Width

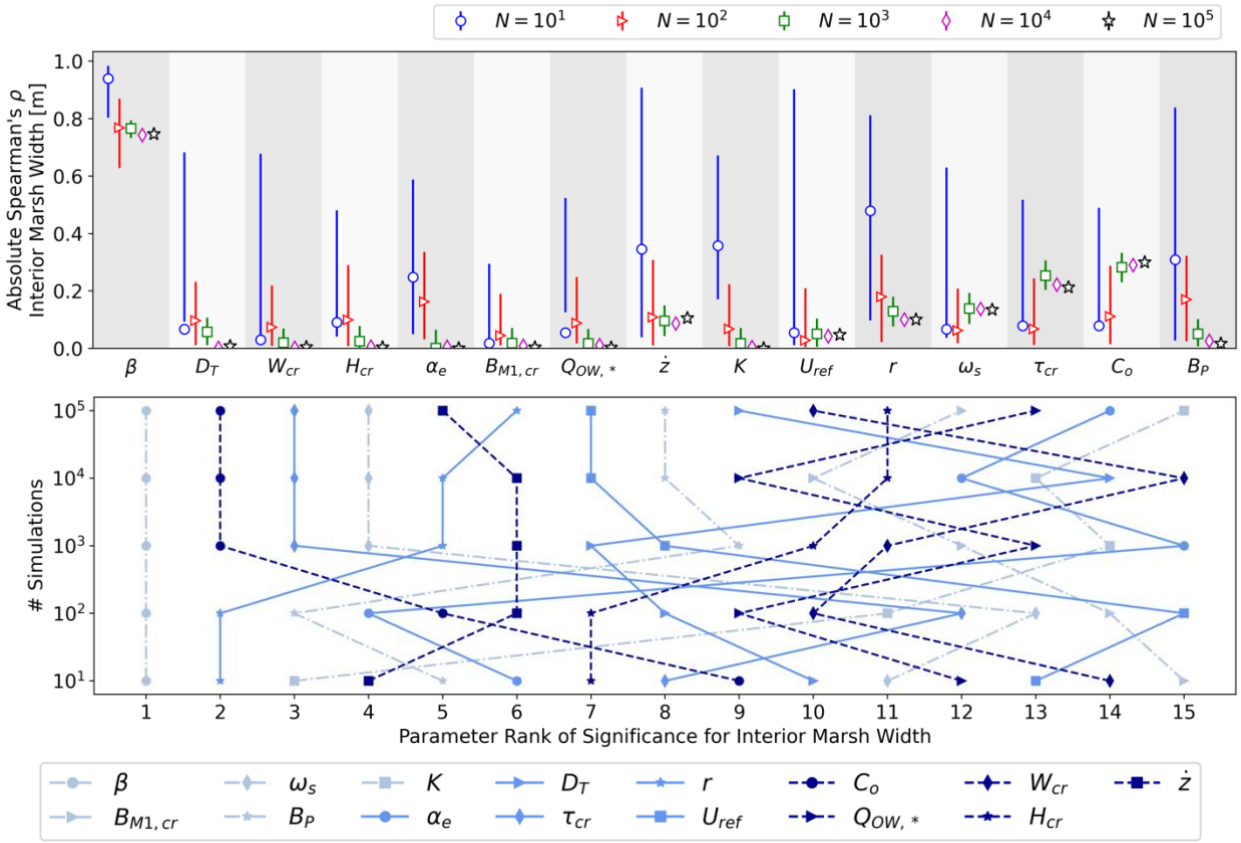

Figure C.4.5 – Spearman Correlation Convergence for Interior Marsh Width

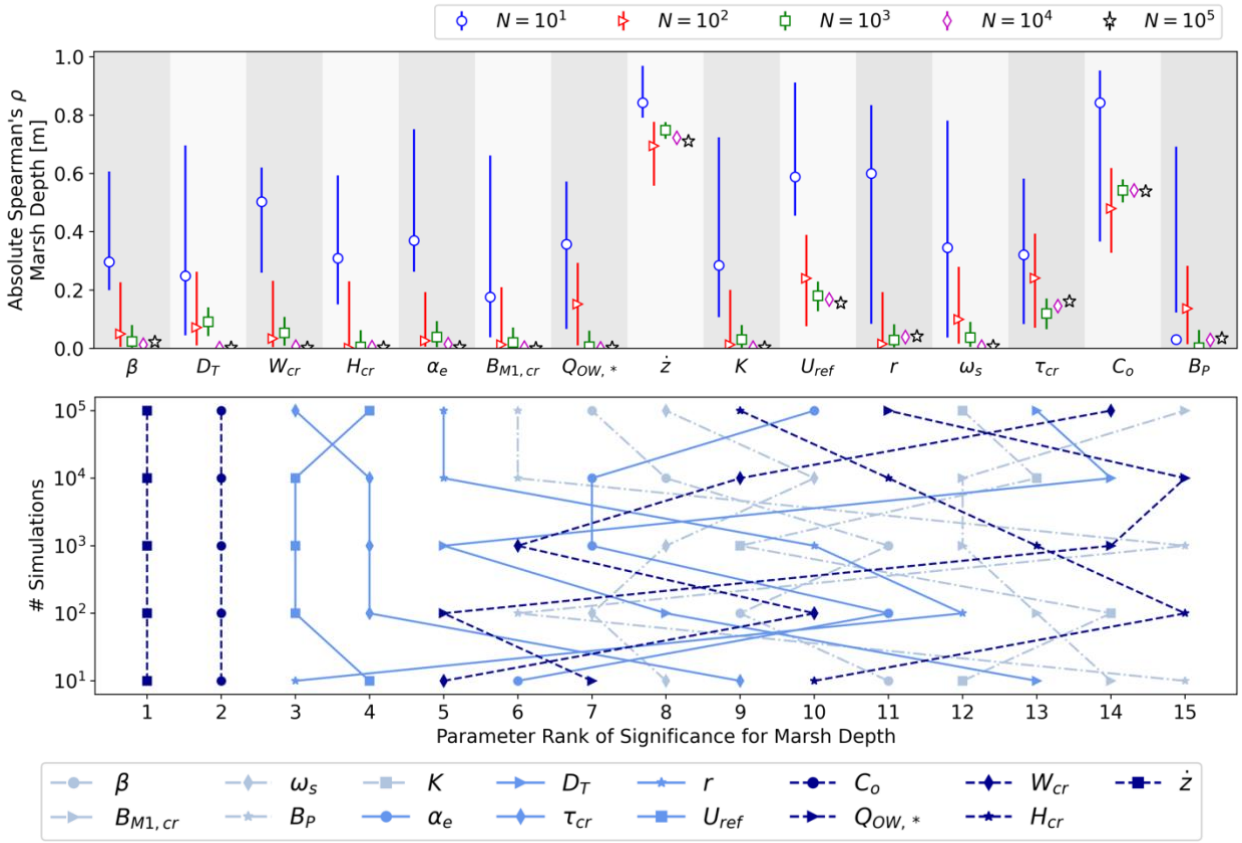

Figure C.4.6 – Spearman Correlation Convergence for Marsh Depth

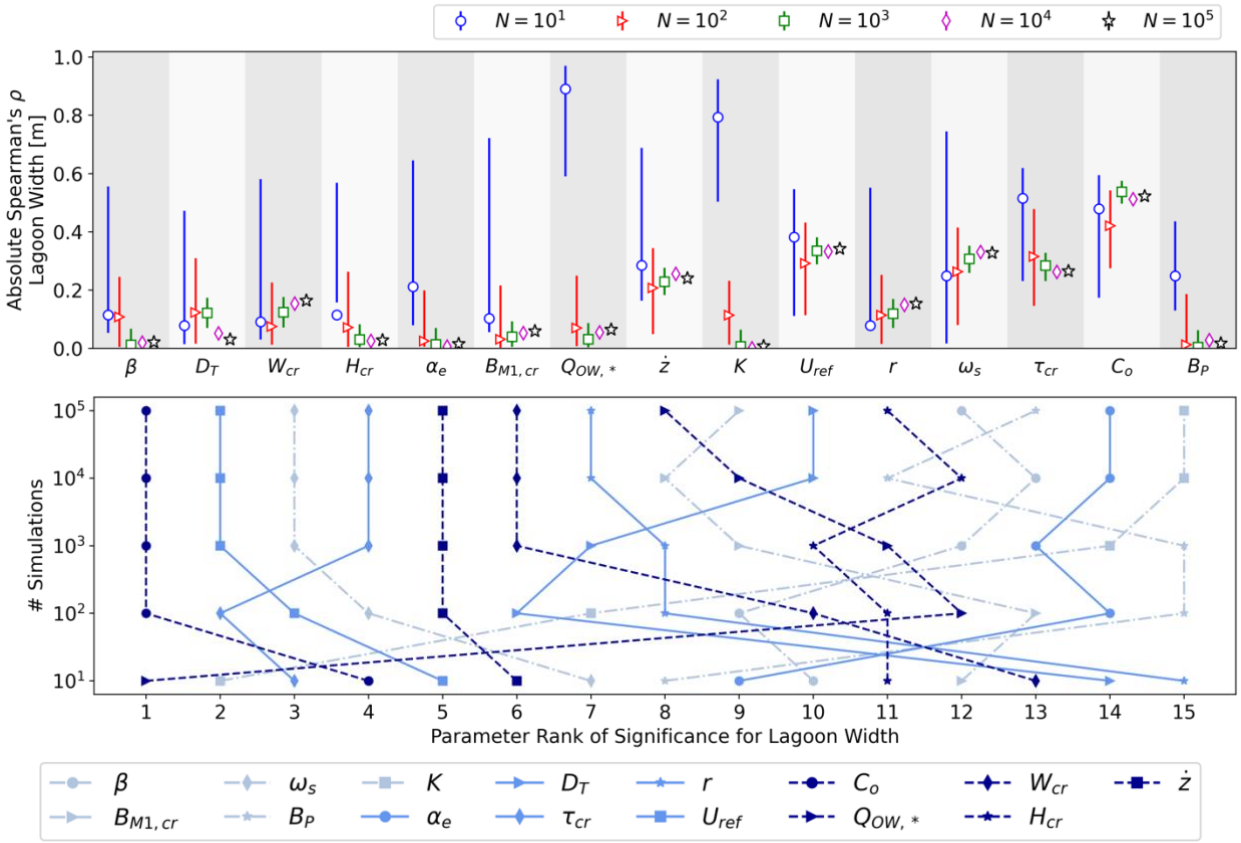

Figure C.4.7 – Spearman Correlation Convergence for Lagoon Width

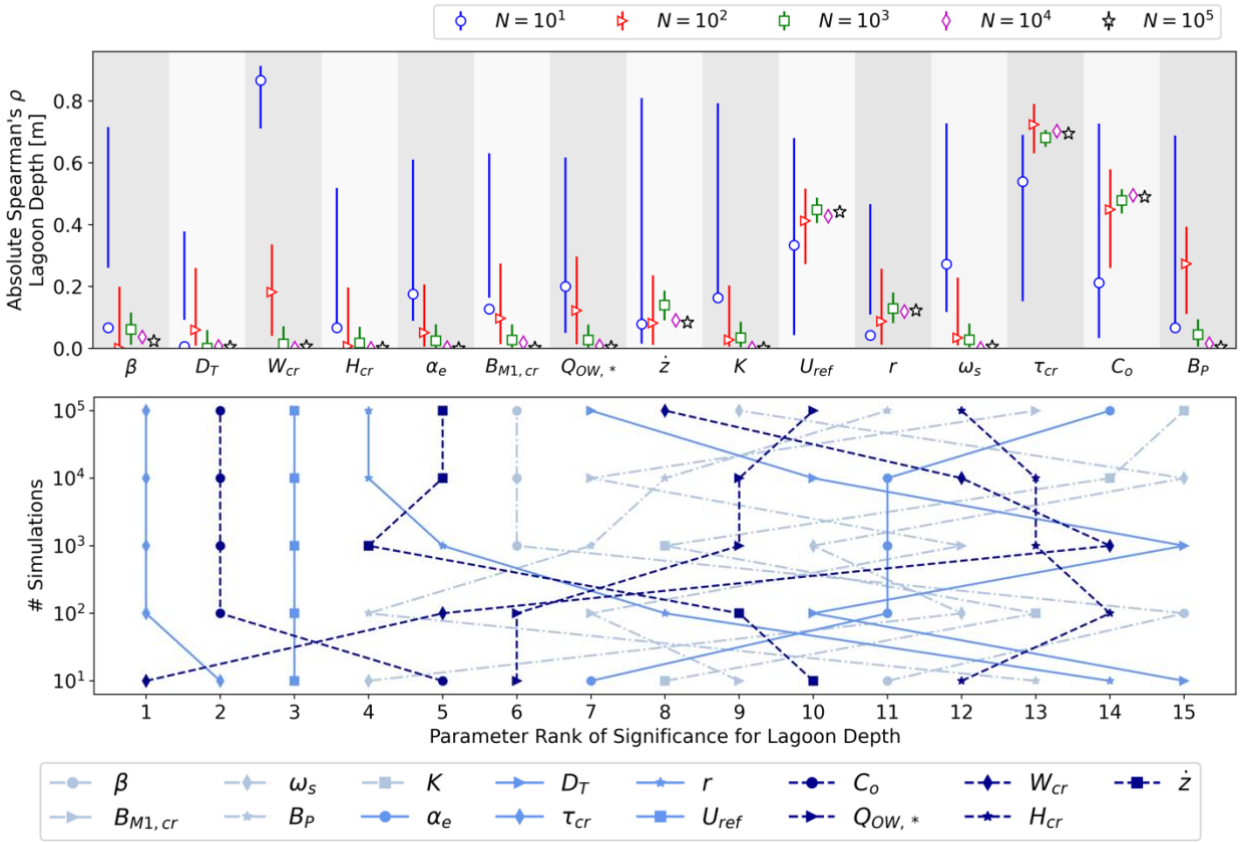

Figure C.4.8 – Spearman Correlation Convergence for Lagoon Depth

5. Morris convergence results for all result variables

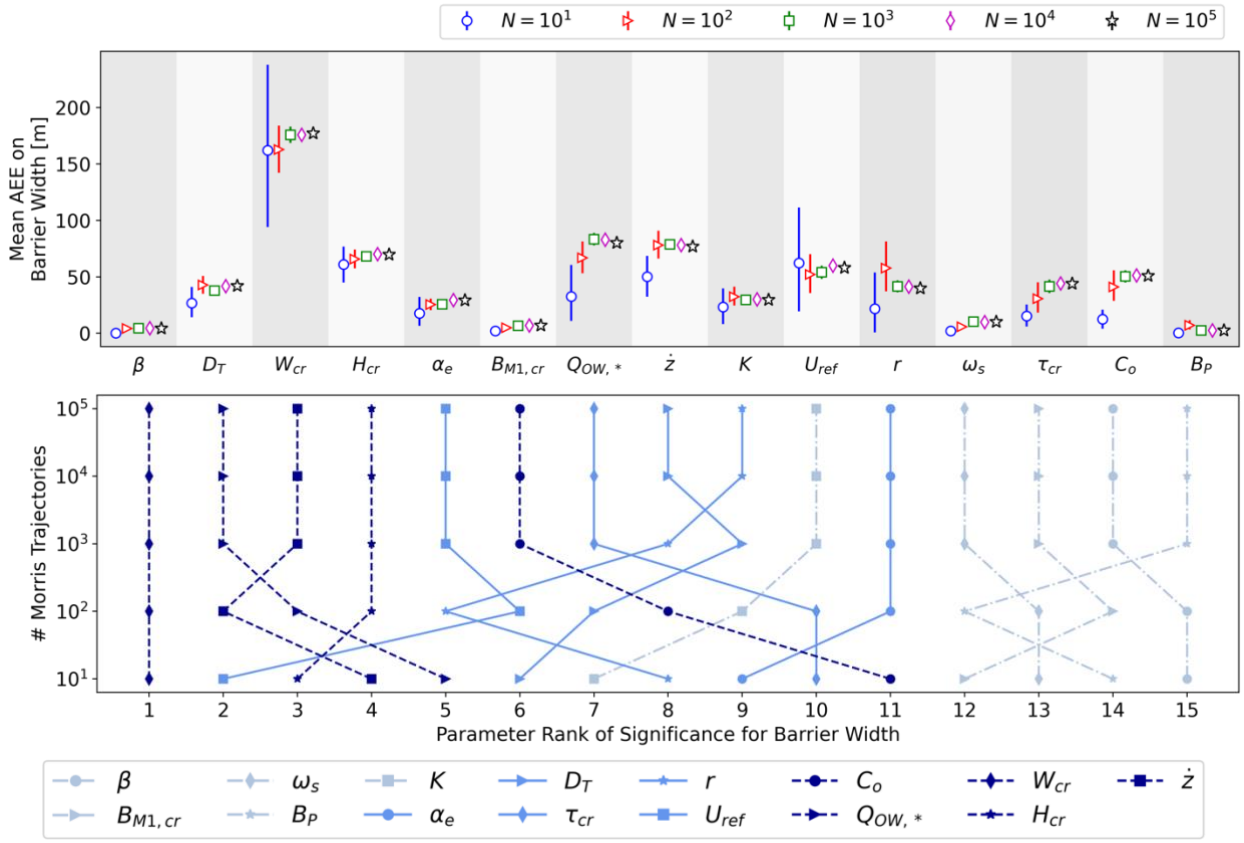

Figure C.5.1 – Morris Convergence for Barrier Width

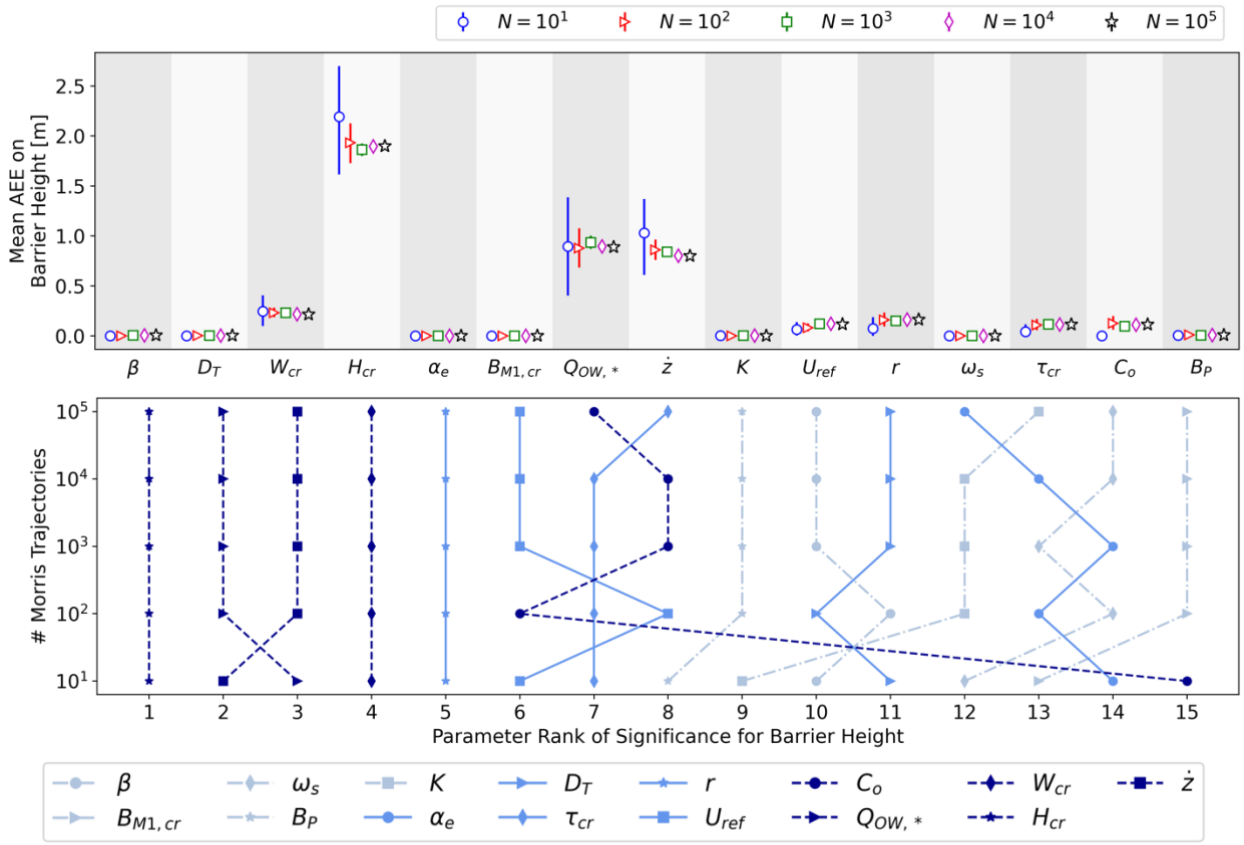

Figure C.5.2 – Morris Convergence for Barrier Height

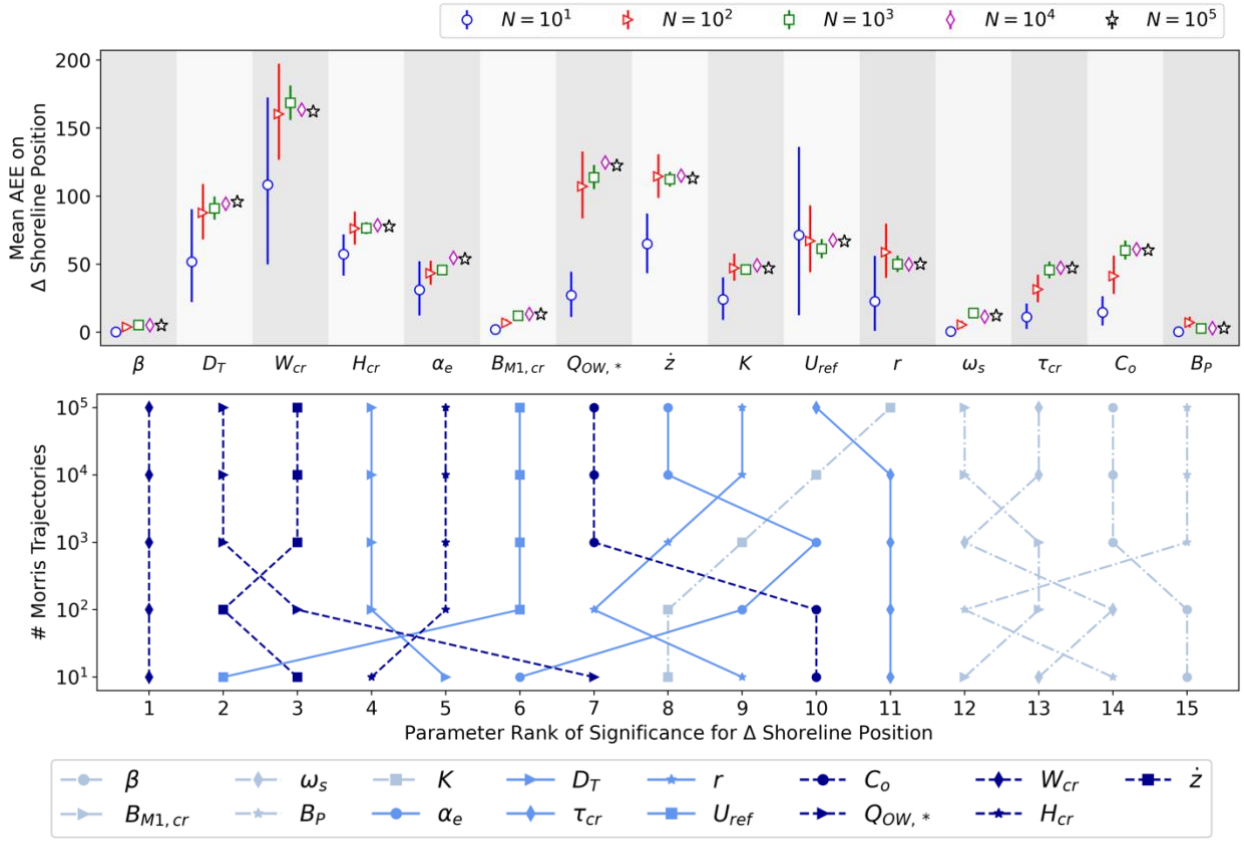

Figure C.5.3 – Morris Convergence for Change in Shoreline Position

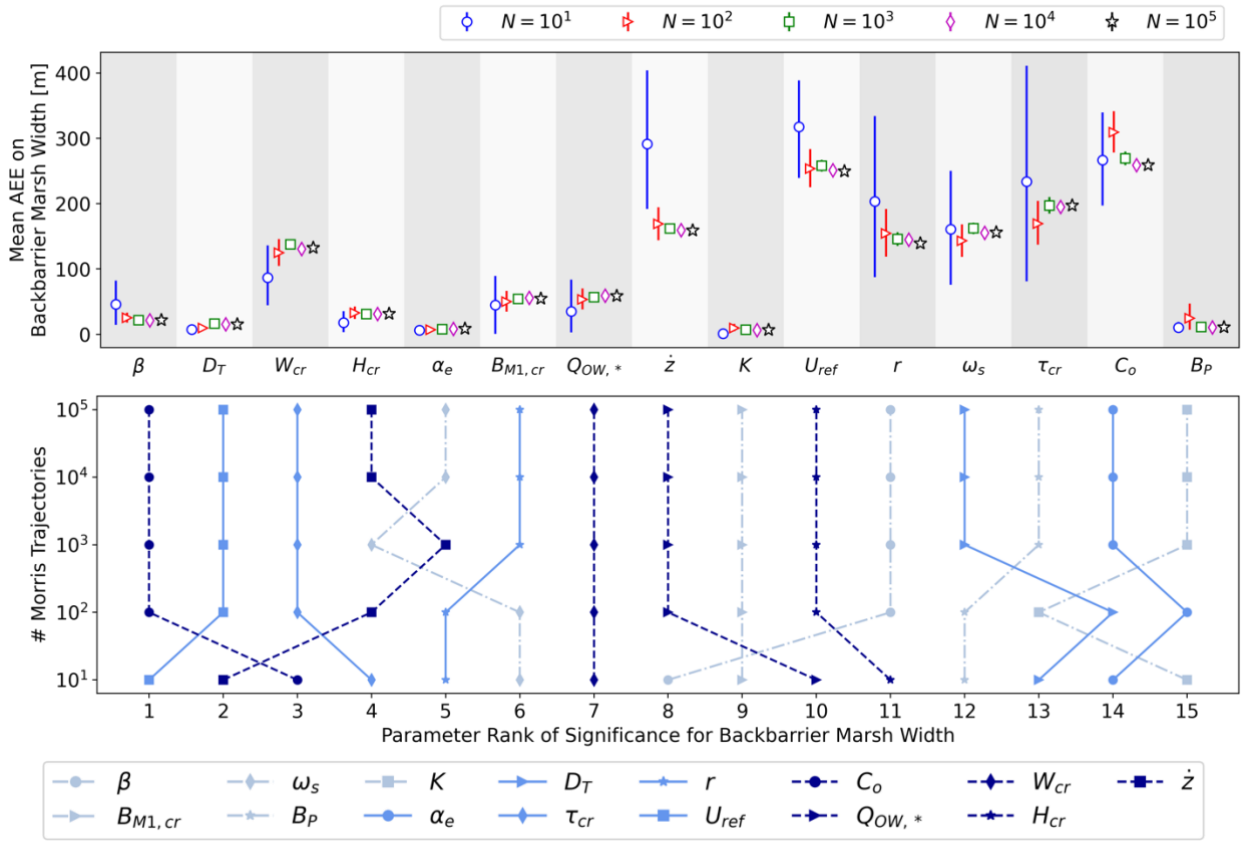

Figure C.5.4 – Morris Convergence for Backbarrier Marsh Width

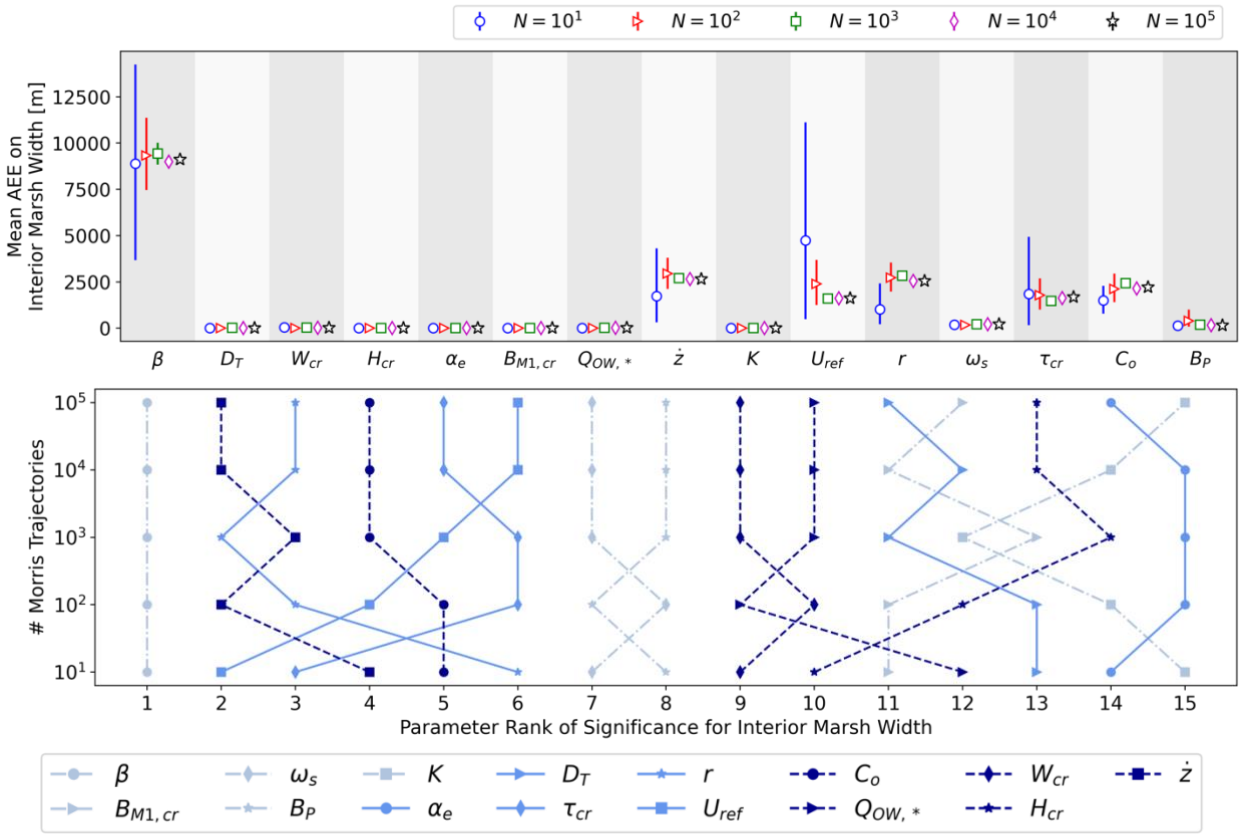

Figure C.5.5 – Morris Convergence for Interior Marsh Width

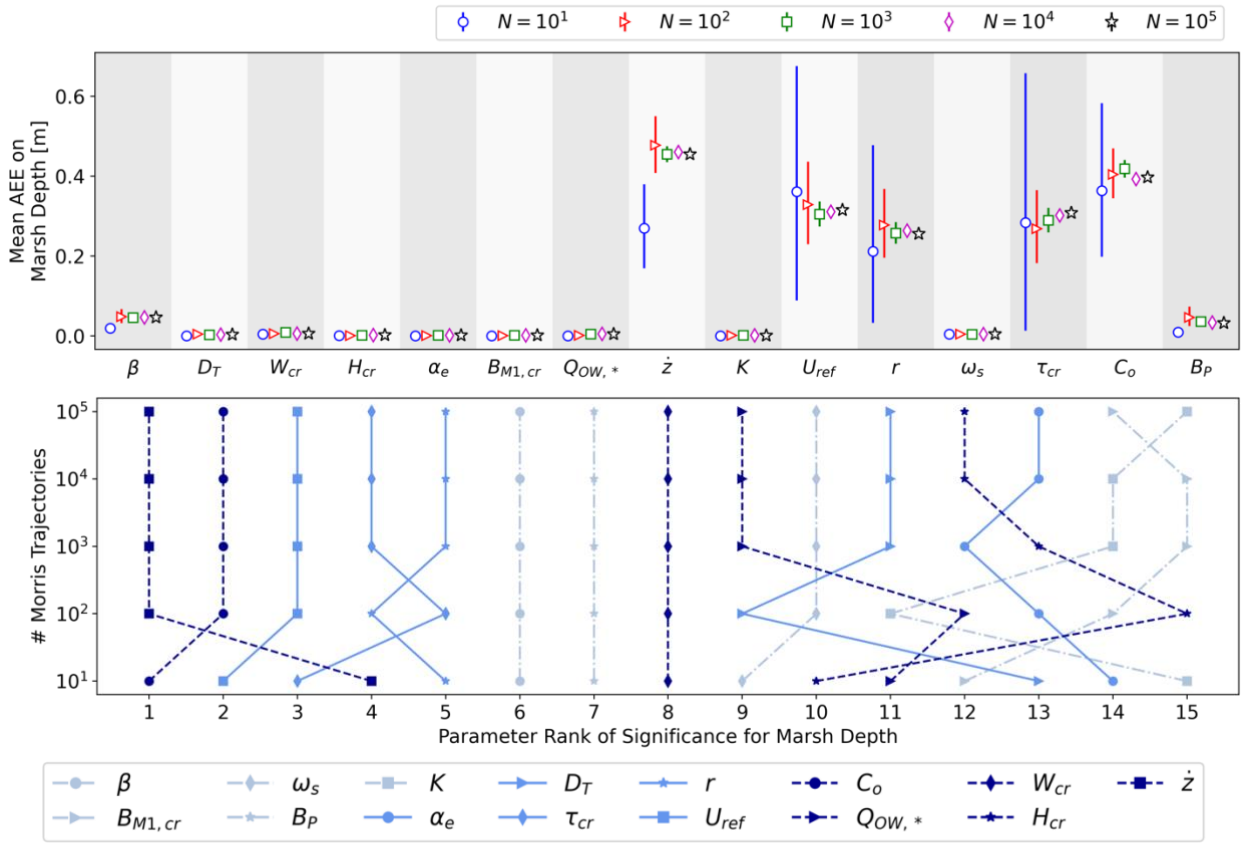

Figure C.5.6 – Morris Convergence for Marsh Depth

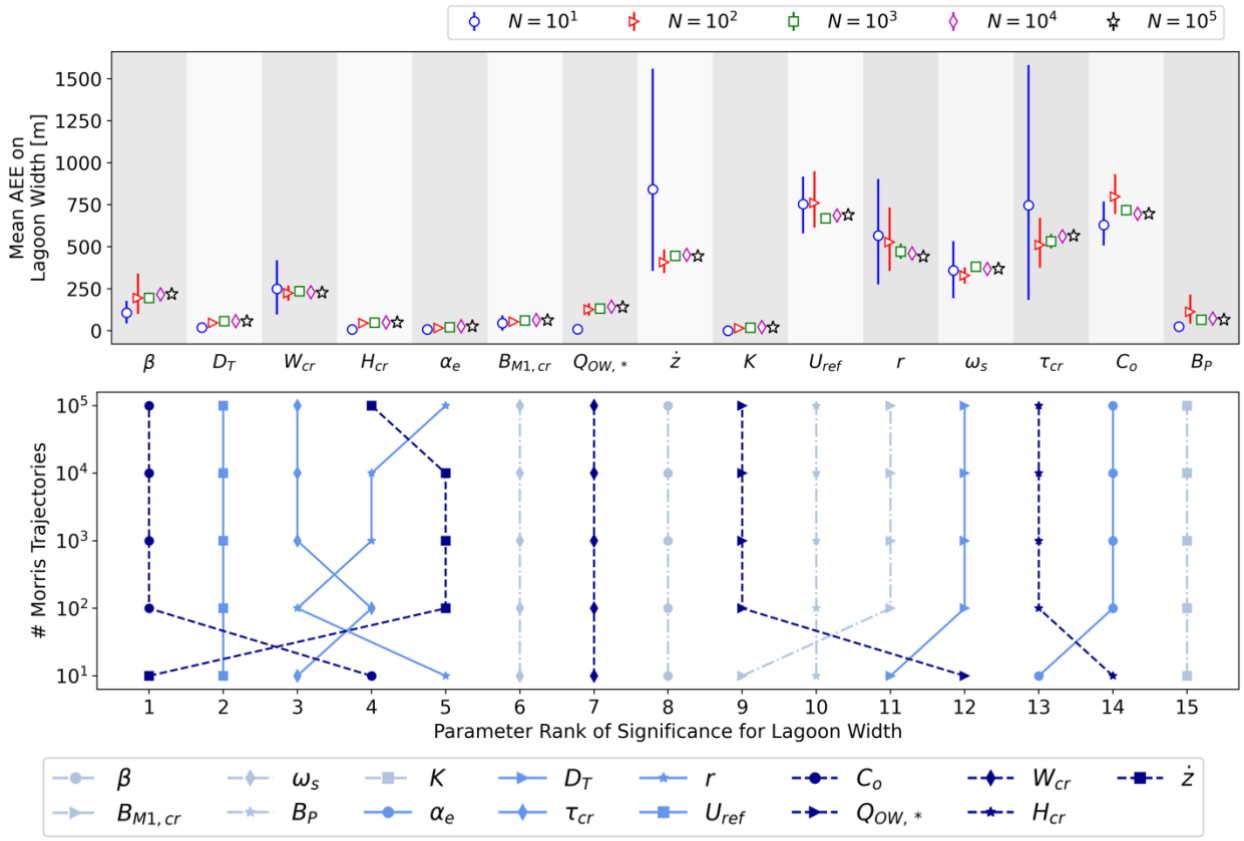

Figure C.5.7 – Morris Convergence for Lagoon Width

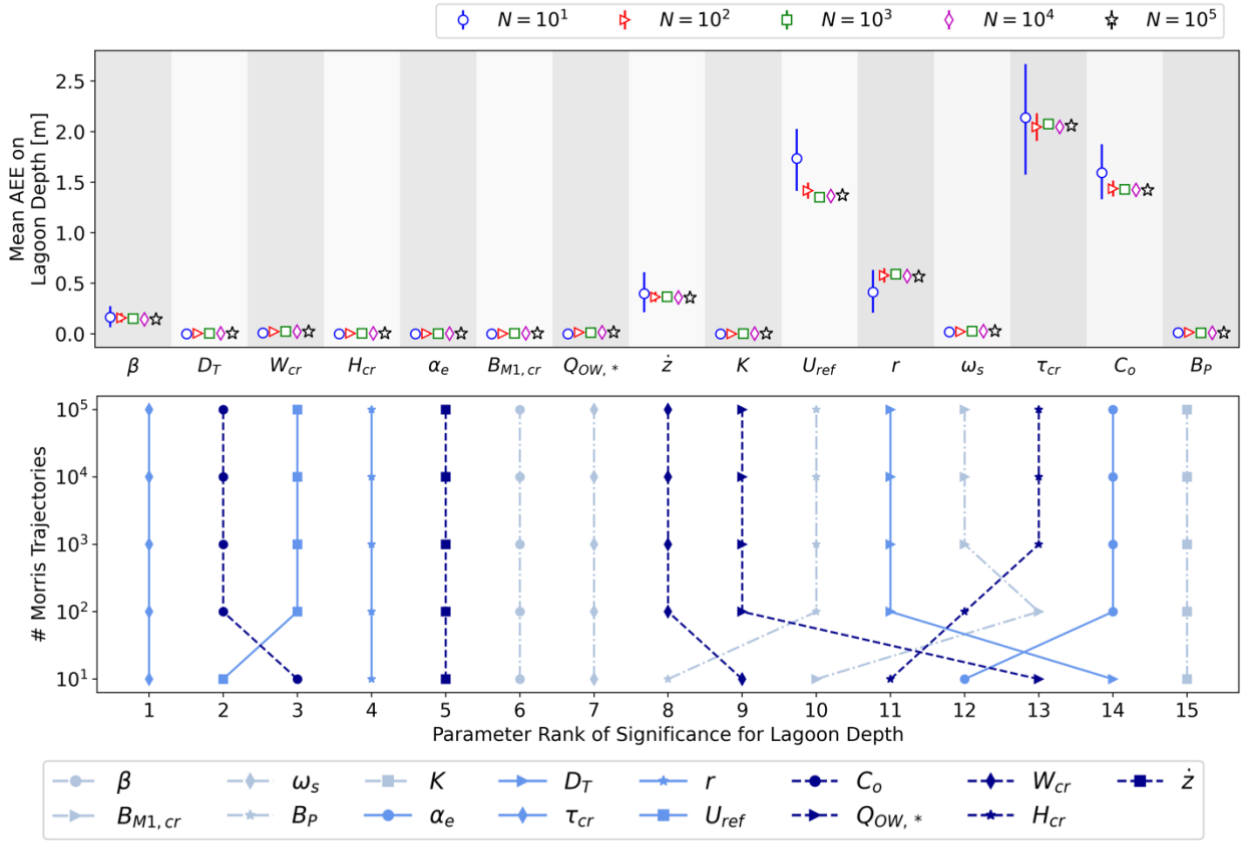

Figure C.5.8 – Morris Convergence for Lagoon Depth

6. Sobol convergence results for all result variables

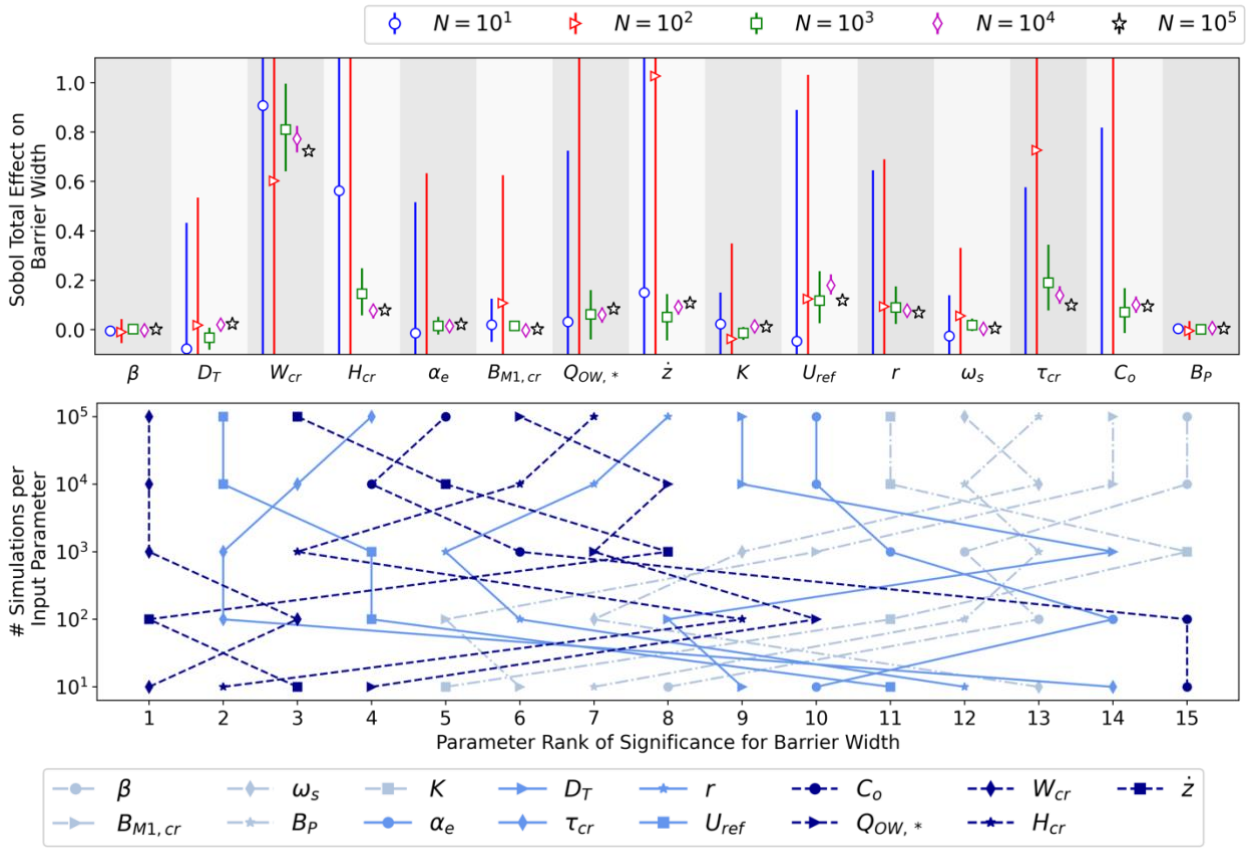

Figure C.6.1 – Sobol Convergence for Barrier Width

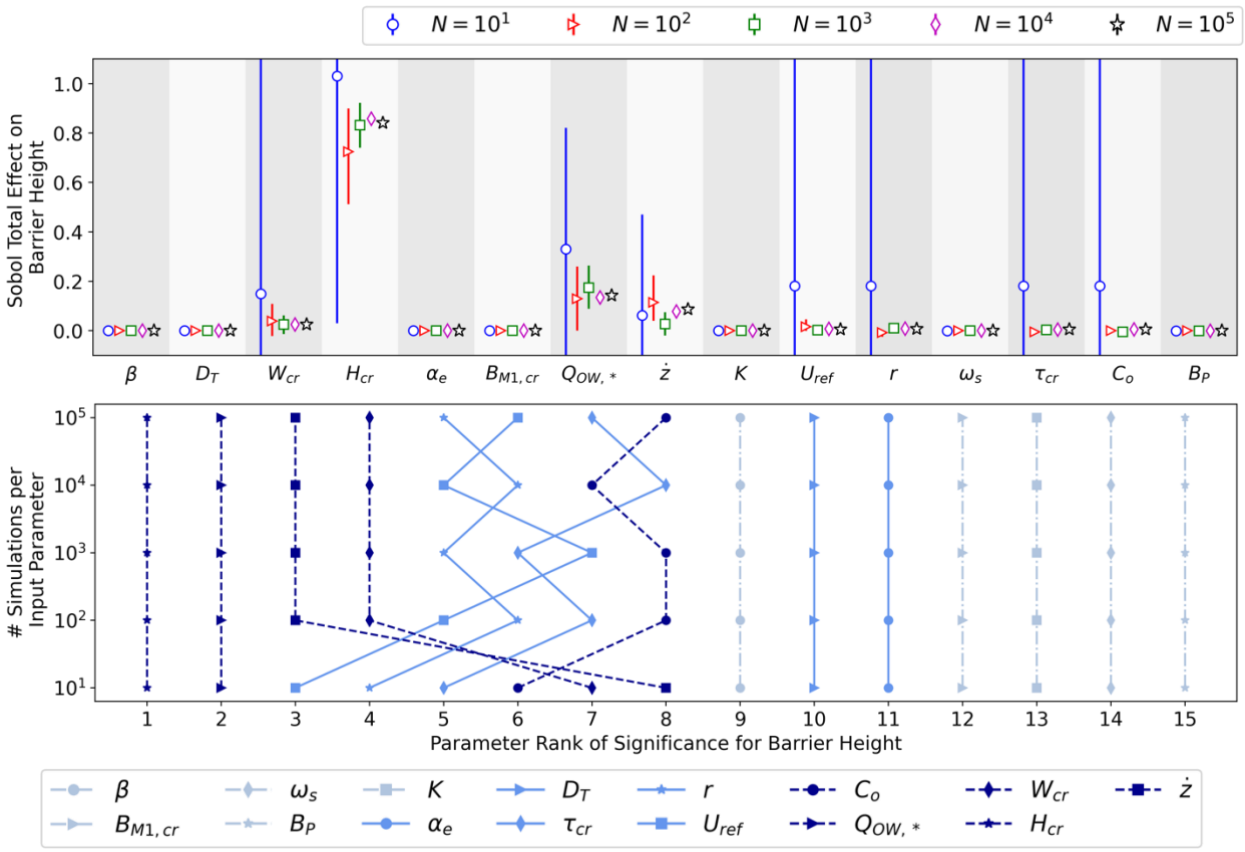

Figure C.6.2 – Sobol Convergence for Barrier Height

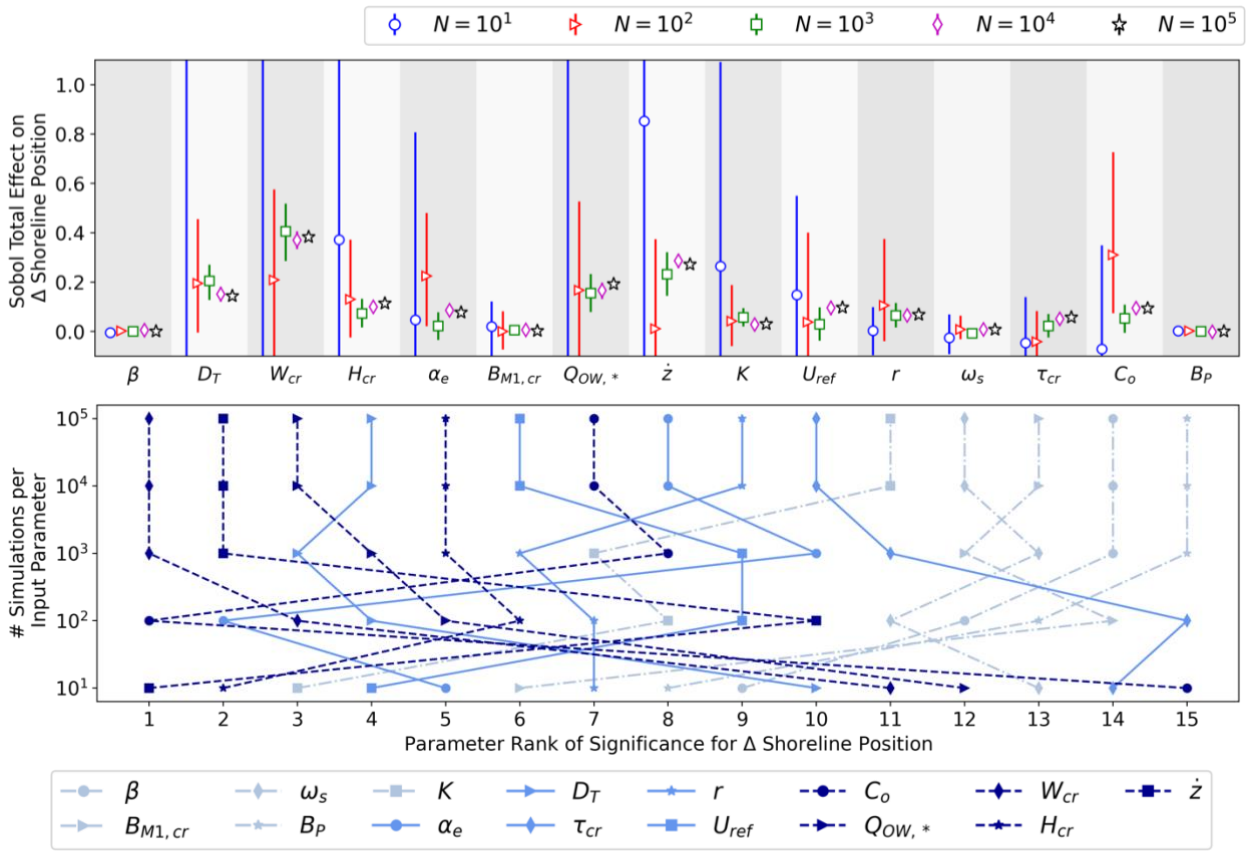

Figure C.6.3 – Sobol Convergence for Change in Shoreline Position

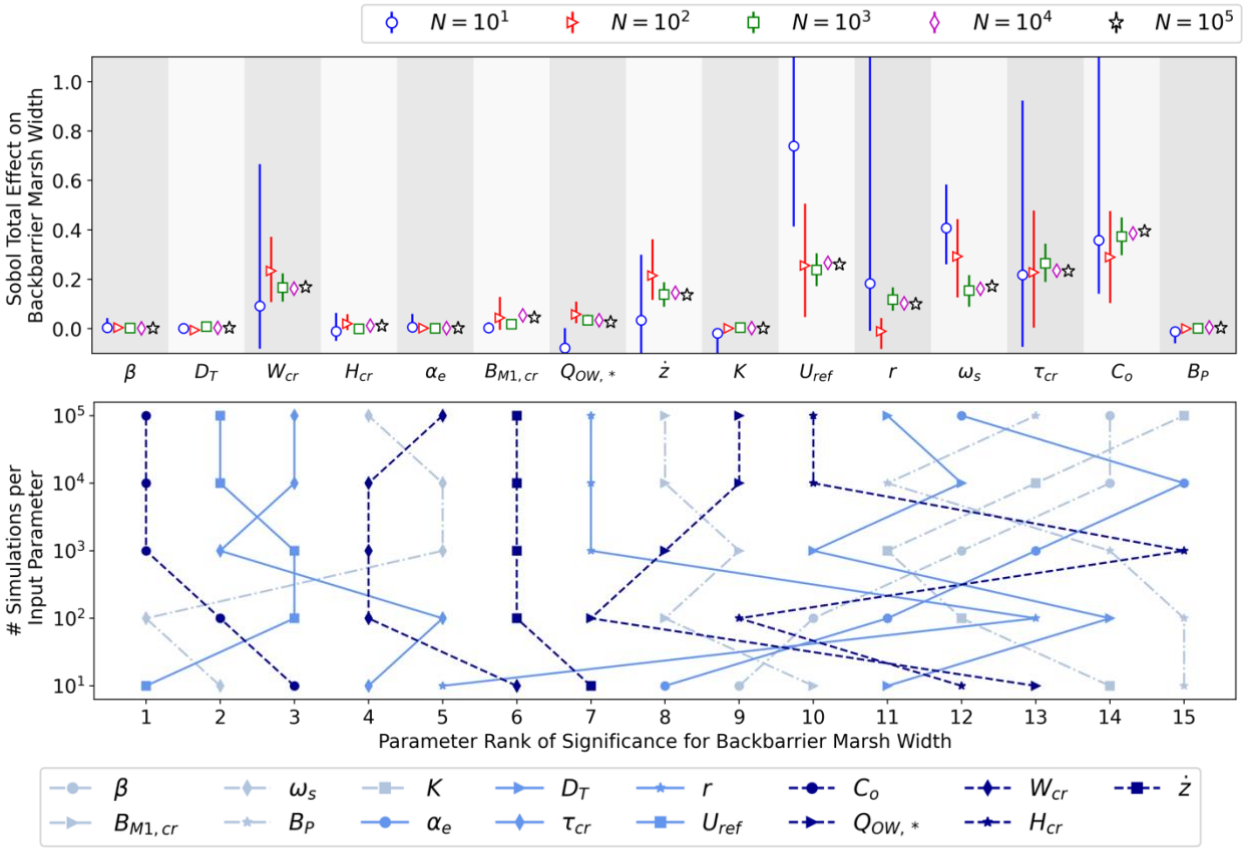

Figure C.6.4 – Sobol Convergence for Backbarrier Marsh Width

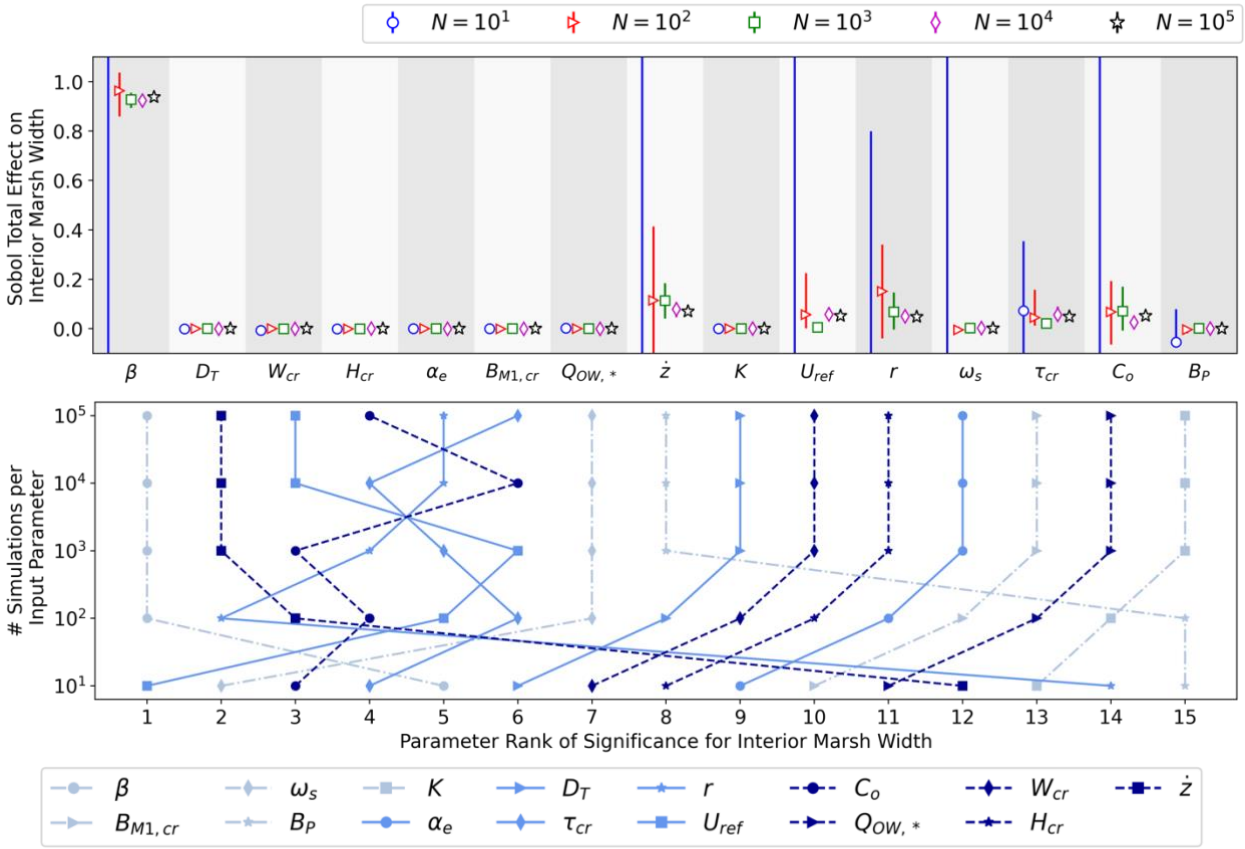

Figure C.6.5 – Sobol Convergence for Interior Marsh Width

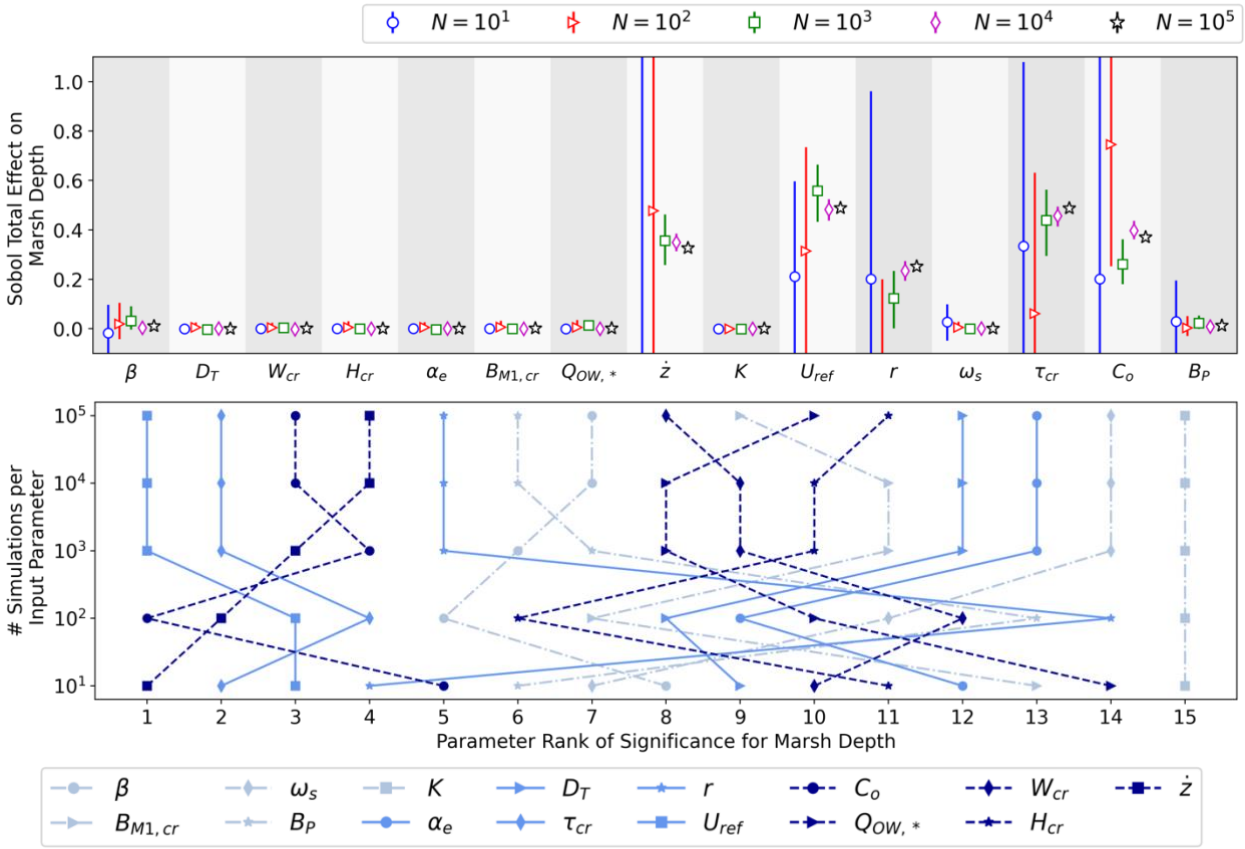

Figure C.6.6 – Sobol Convergence for Marsh Depth

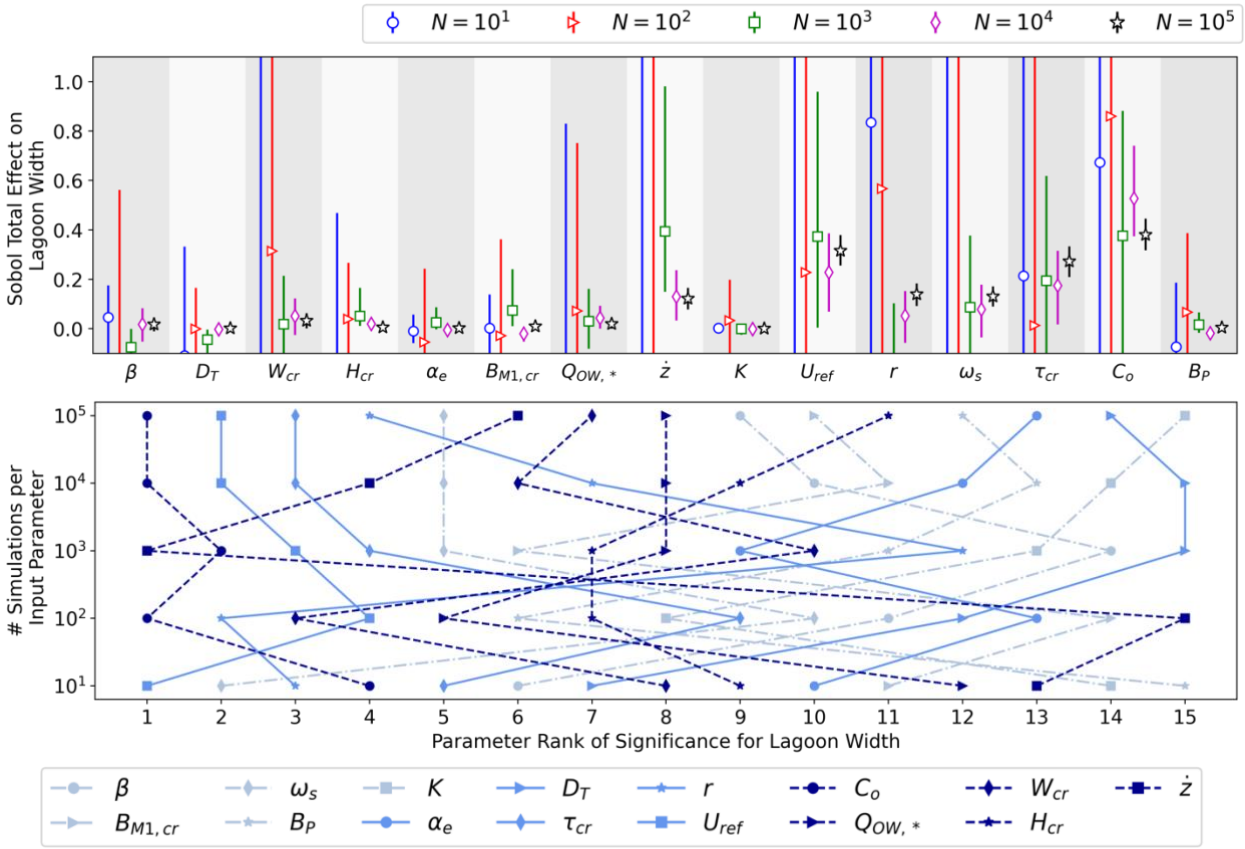

Figure C.6.7 – Sobol Convergence for Lagoon Width

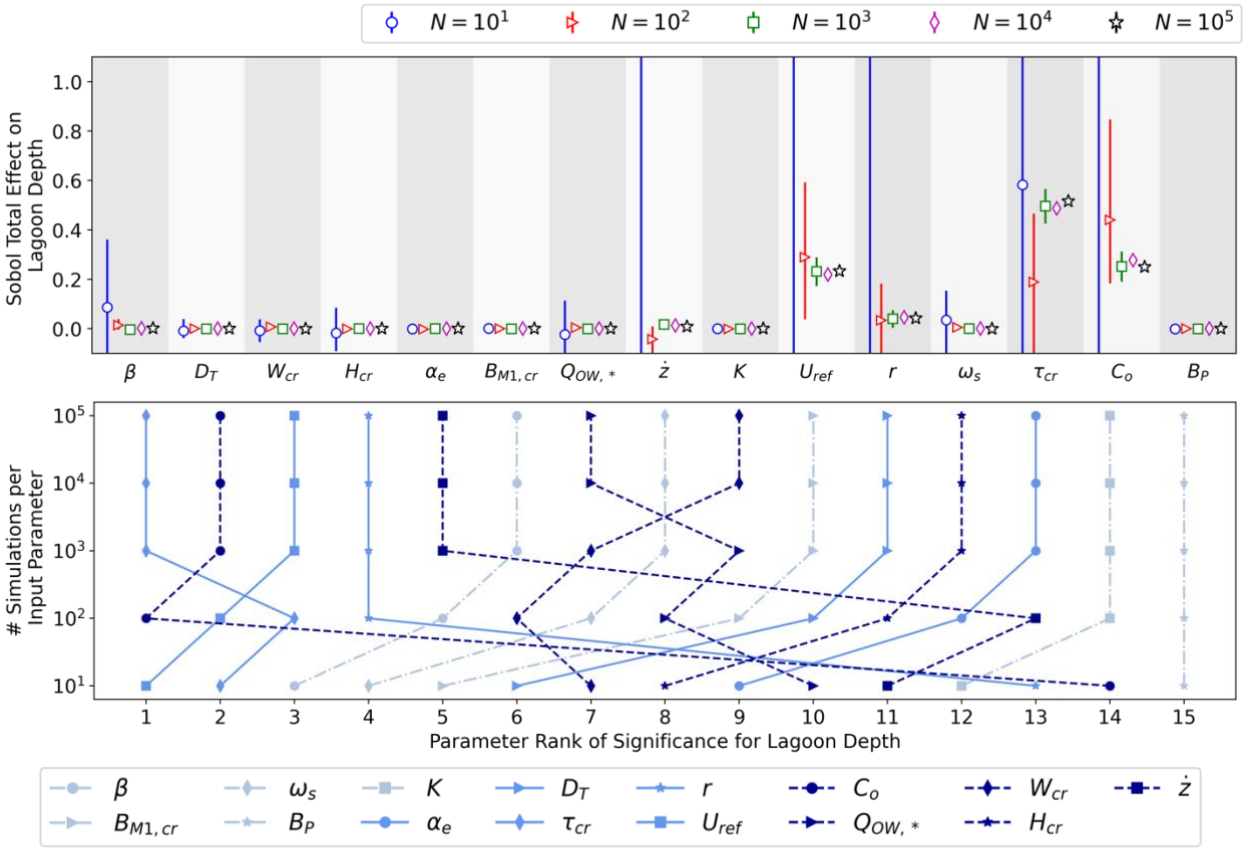

Figure C.6.8 – Sobol Convergence for Lagoon Depth

7. VARS i50 convergence results for all result variables

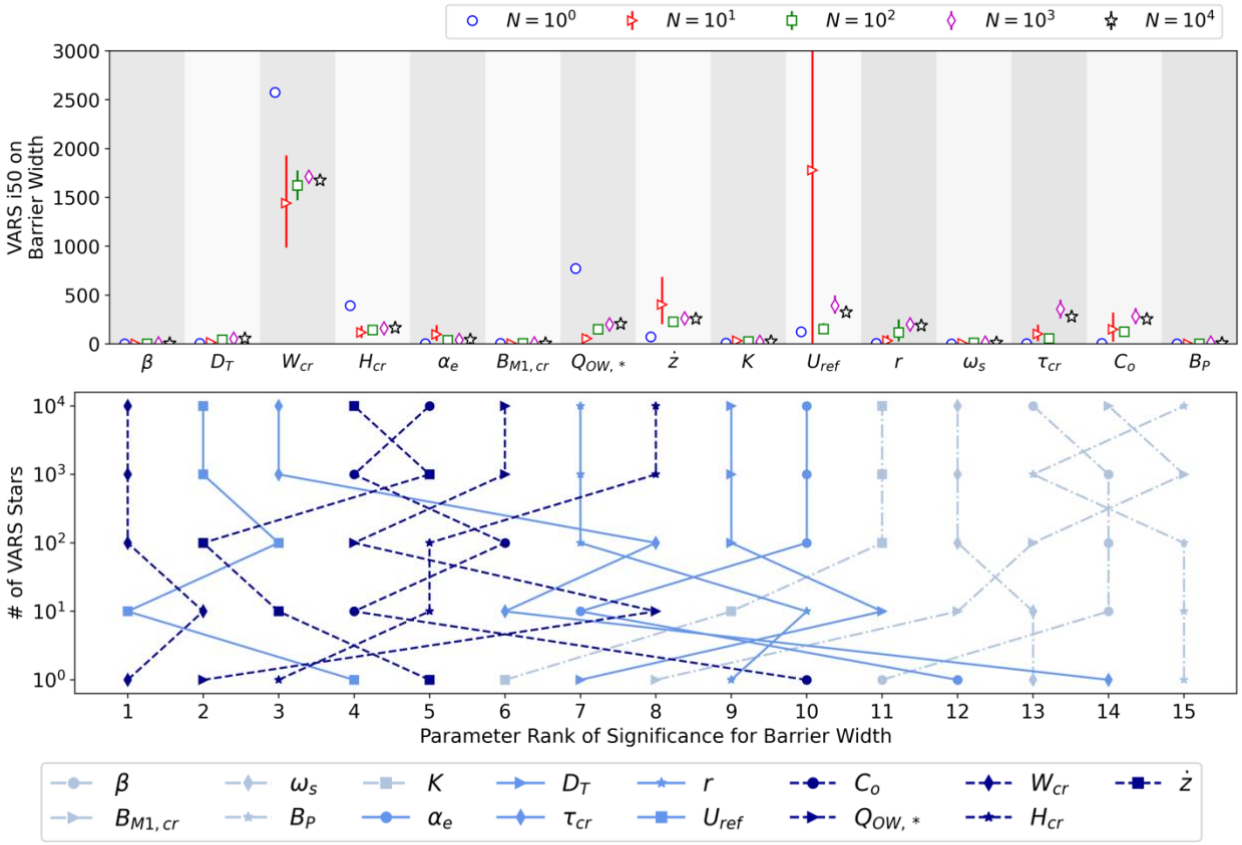

Figure C.7.1 – VARS i50 Convergence for Barrier Width

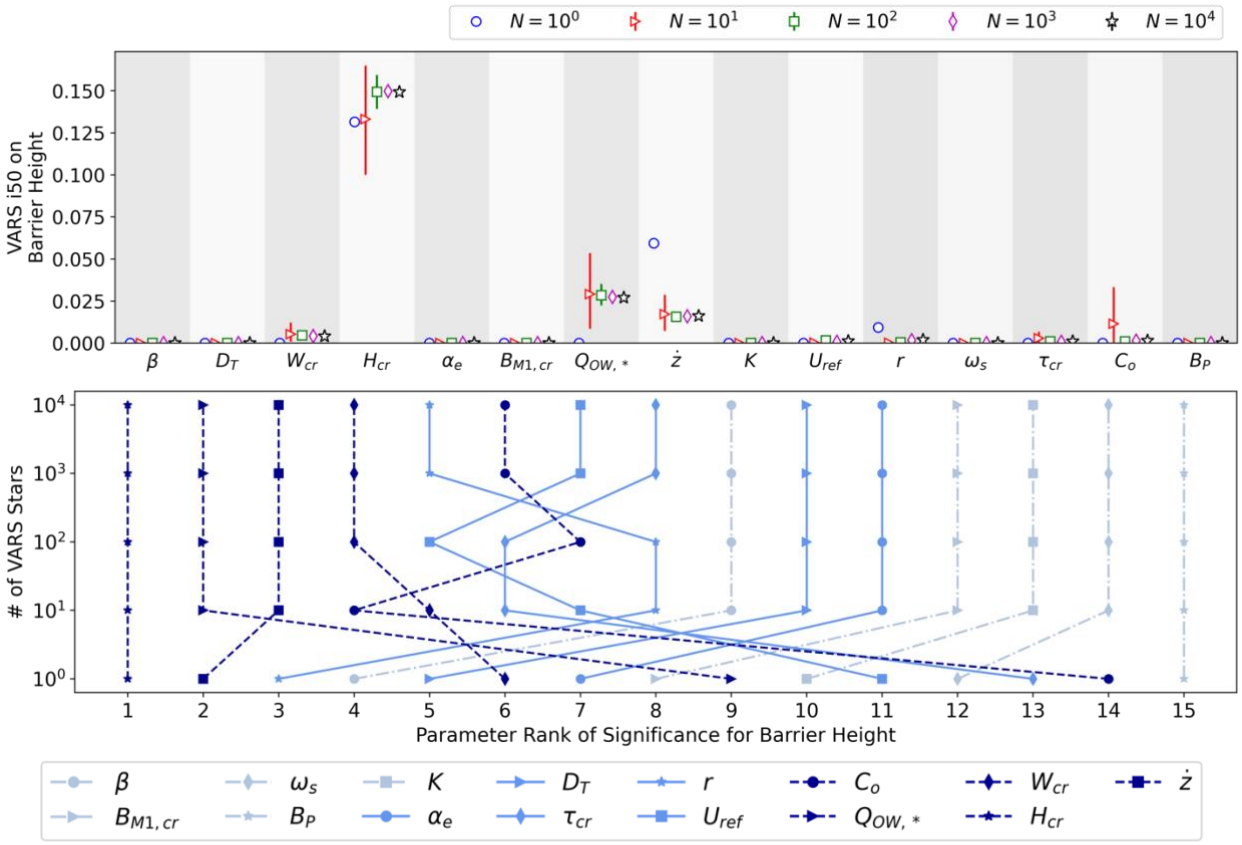

Figure C.7.2 – VARS i50 Convergence for Barrier Height

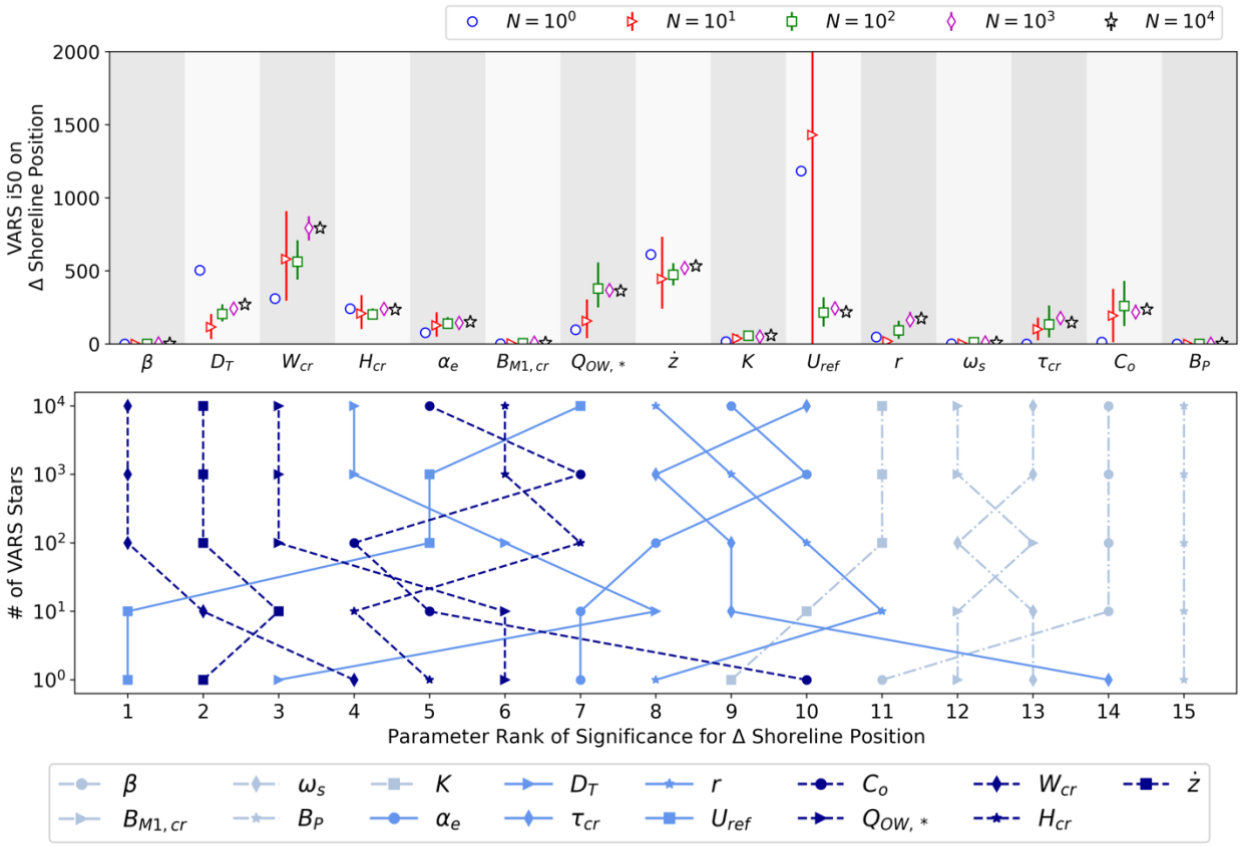

Figure C.7.3 – VARS i50 Convergence for Change in Shoreline Position

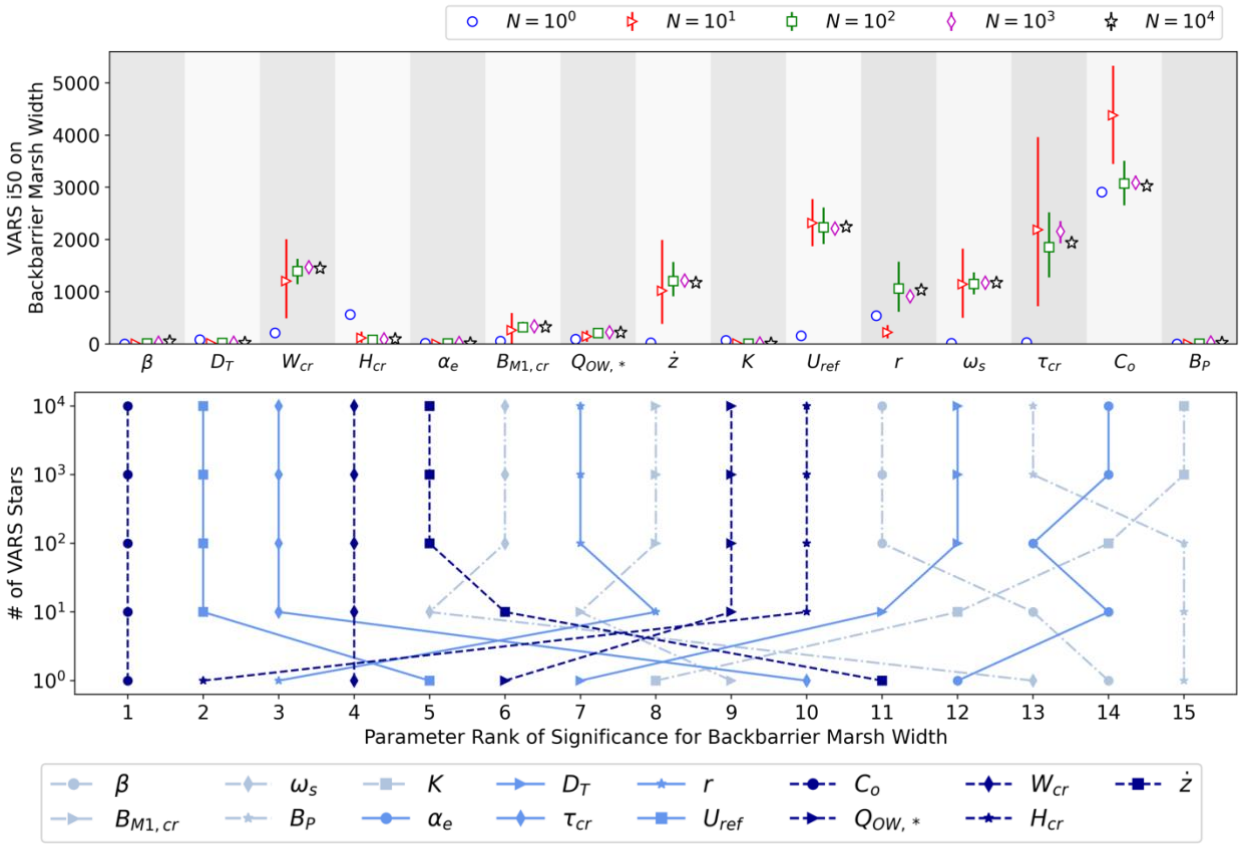

Figure C.7.4 – VARS i50 Convergence for Backbarrier Marsh Width

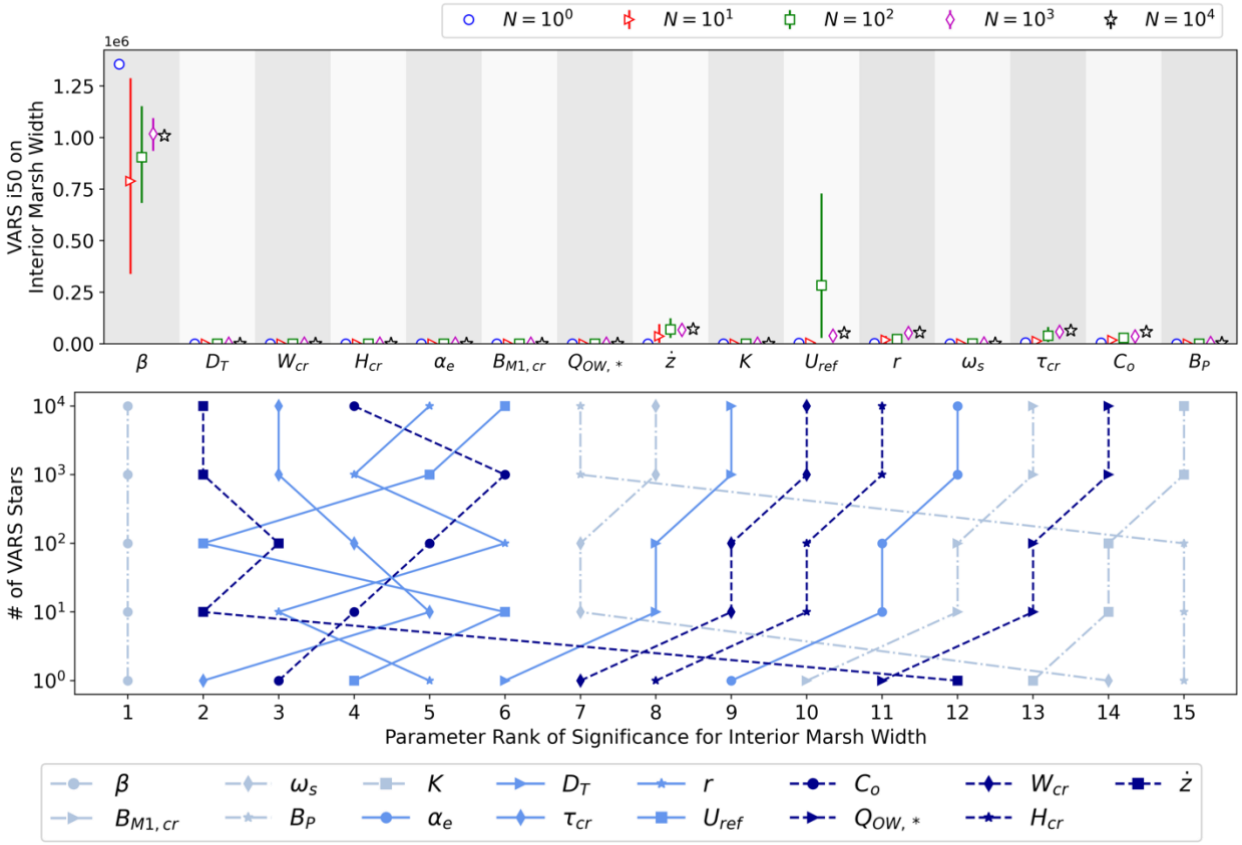

Figure C.7.5 – VARS i50 Convergence for Interior Marsh Width

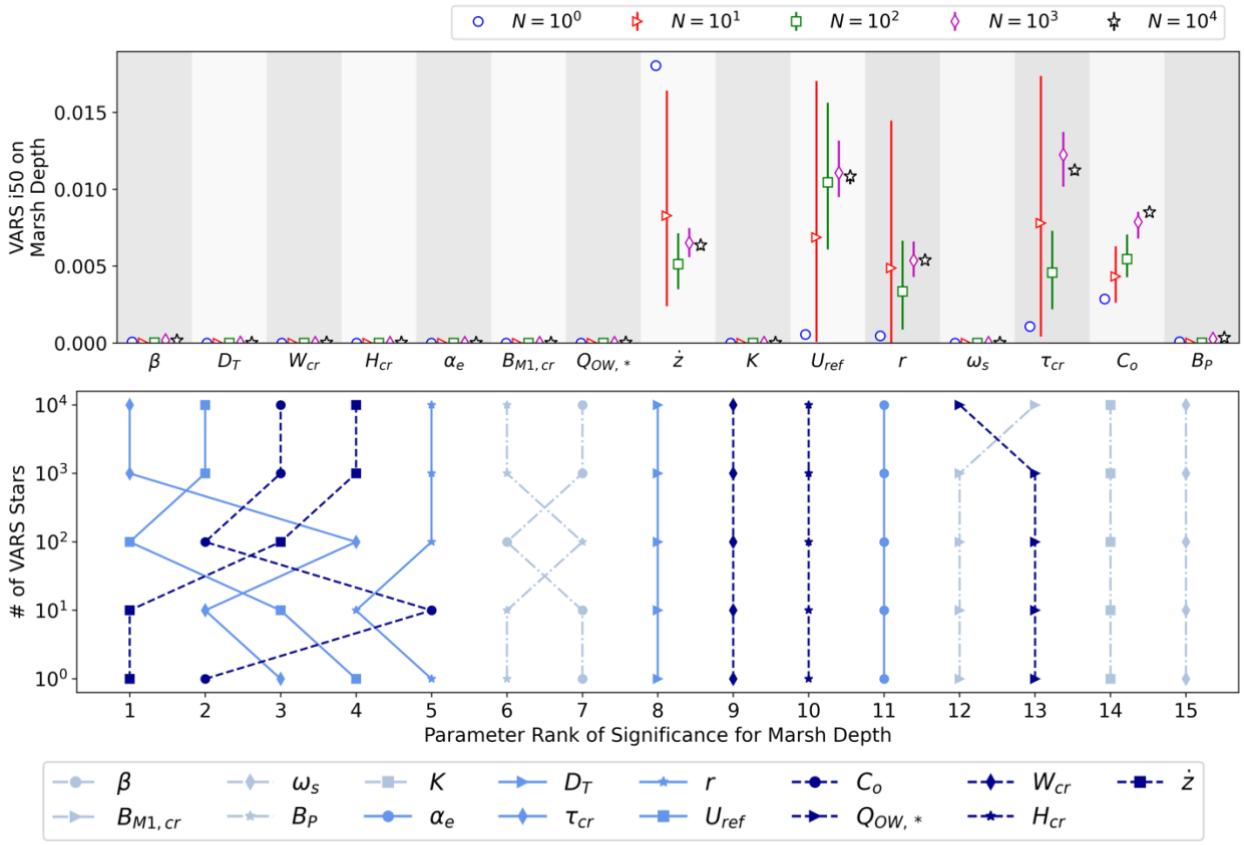

Figure C.7.6– VARS i50 Convergence for Marsh Depth

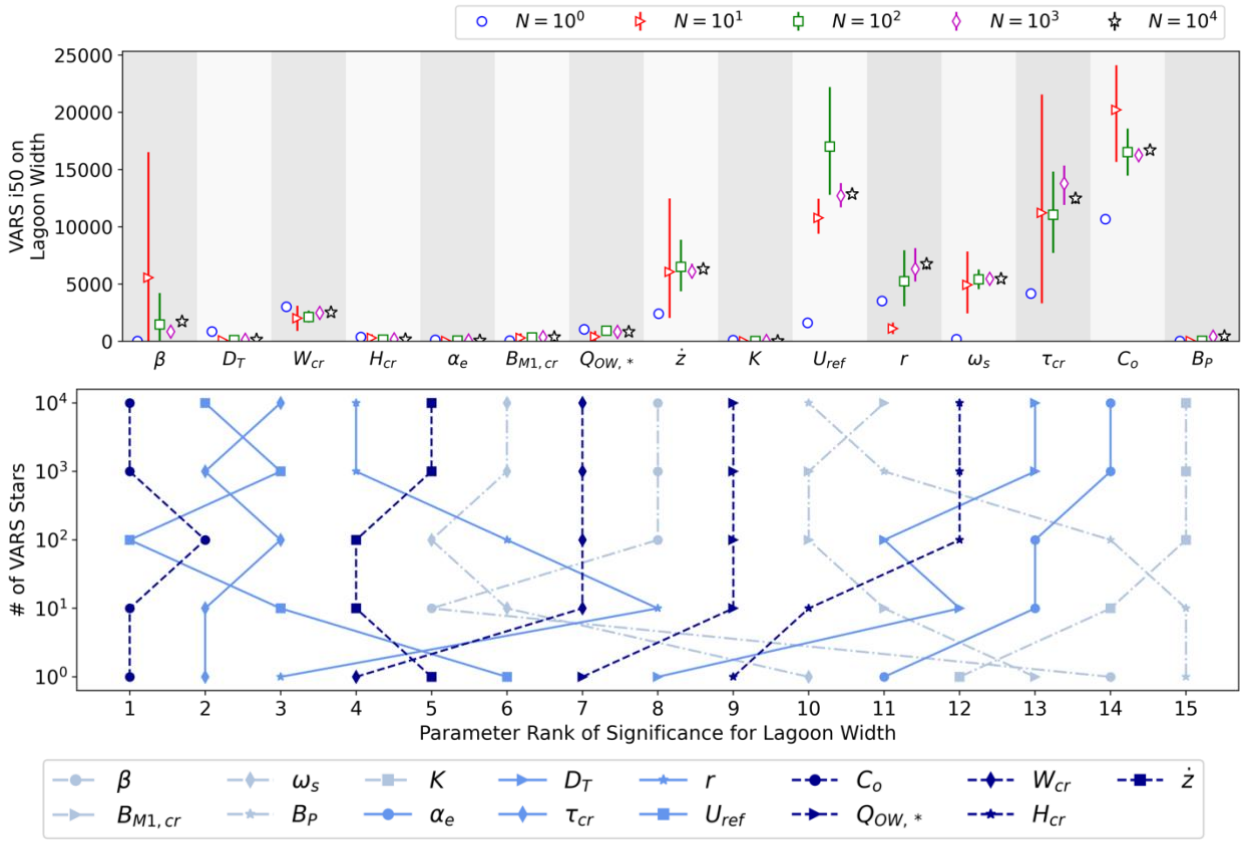

Figure C.7.7 – VARS i50 Convergence for Lagoon Width

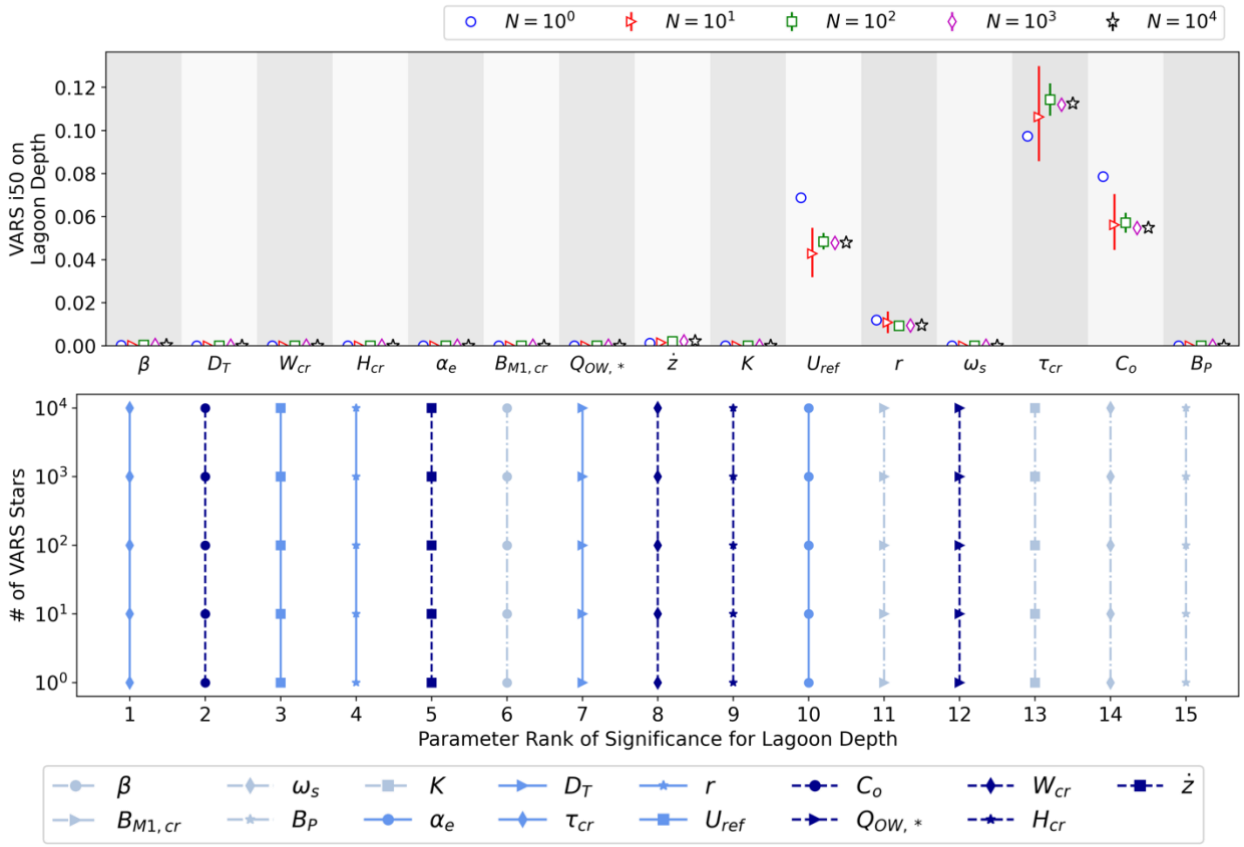

Figure C.7.8 – VARS i50 Convergence for Lagoon Depth

8. Results for 100 independent trials with 1,000-2,000 simulations for remaining result variables

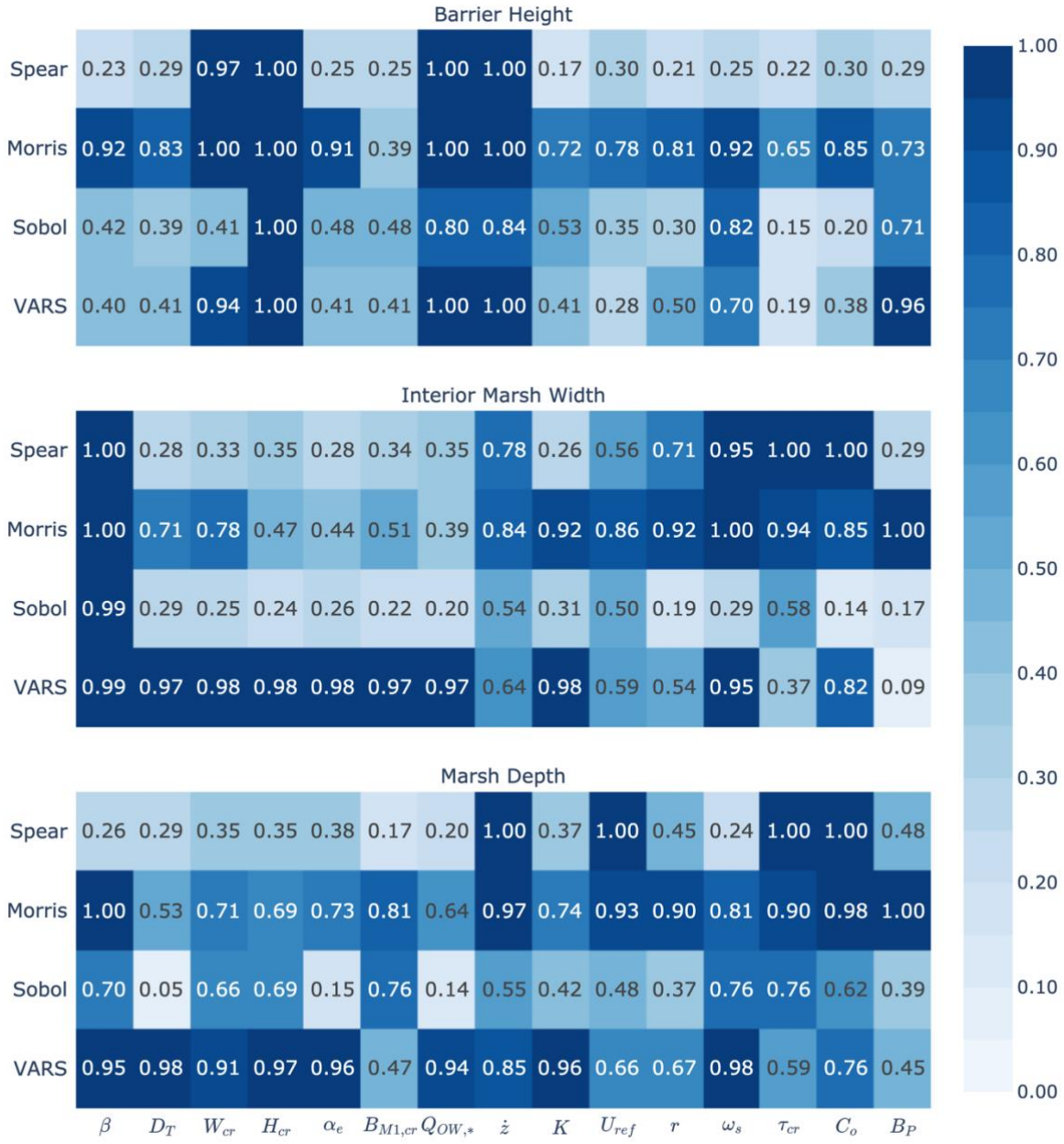

Figure C.8.1 – Probability of Parameter Ranking for 100 Independent Trials with 1-2k Simulations. Results shown for (top) Barrier Height, (middle) Interior Marsh Width, and (bottom) Marsh Depth.

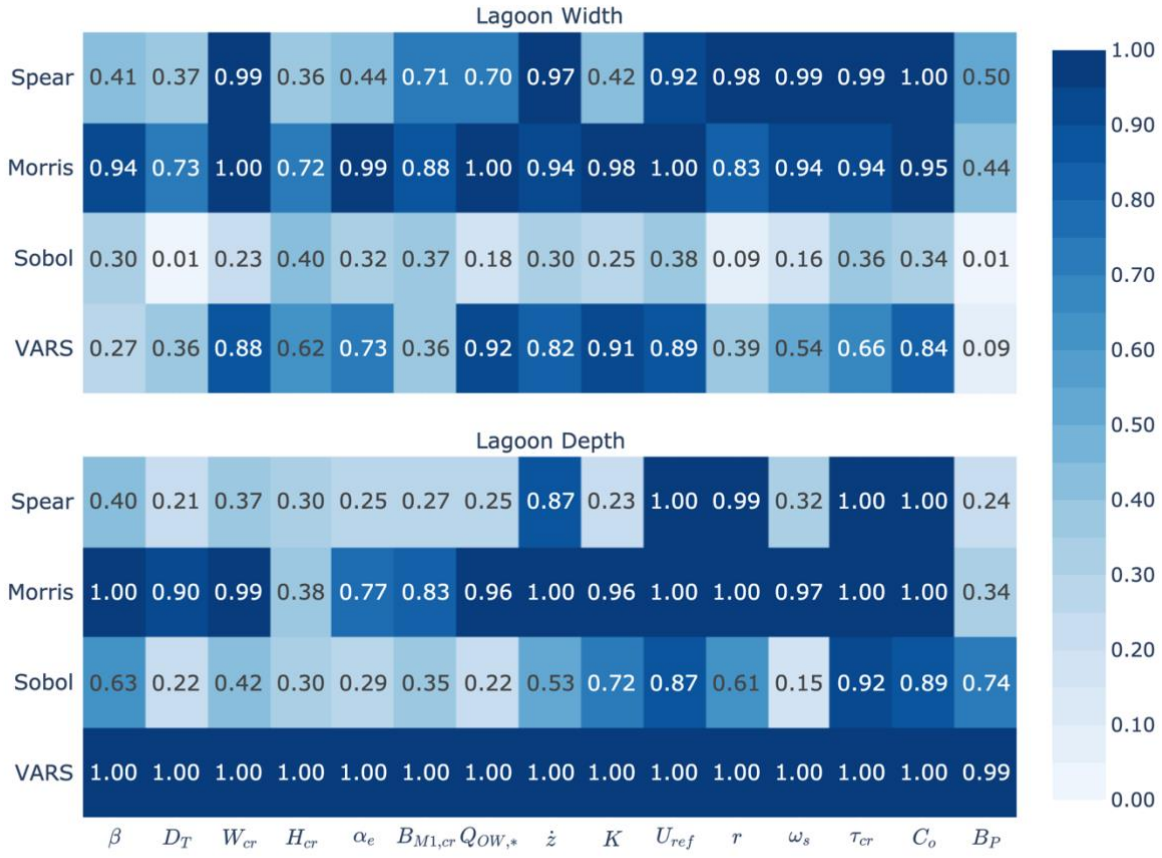

Figure C.8.2 – Probability of Parameter Ranking for 100 Independent Trials with 1-2k Simulations. Results shown for (top) Lagoon Width and (bottom) Lagoon Depth.

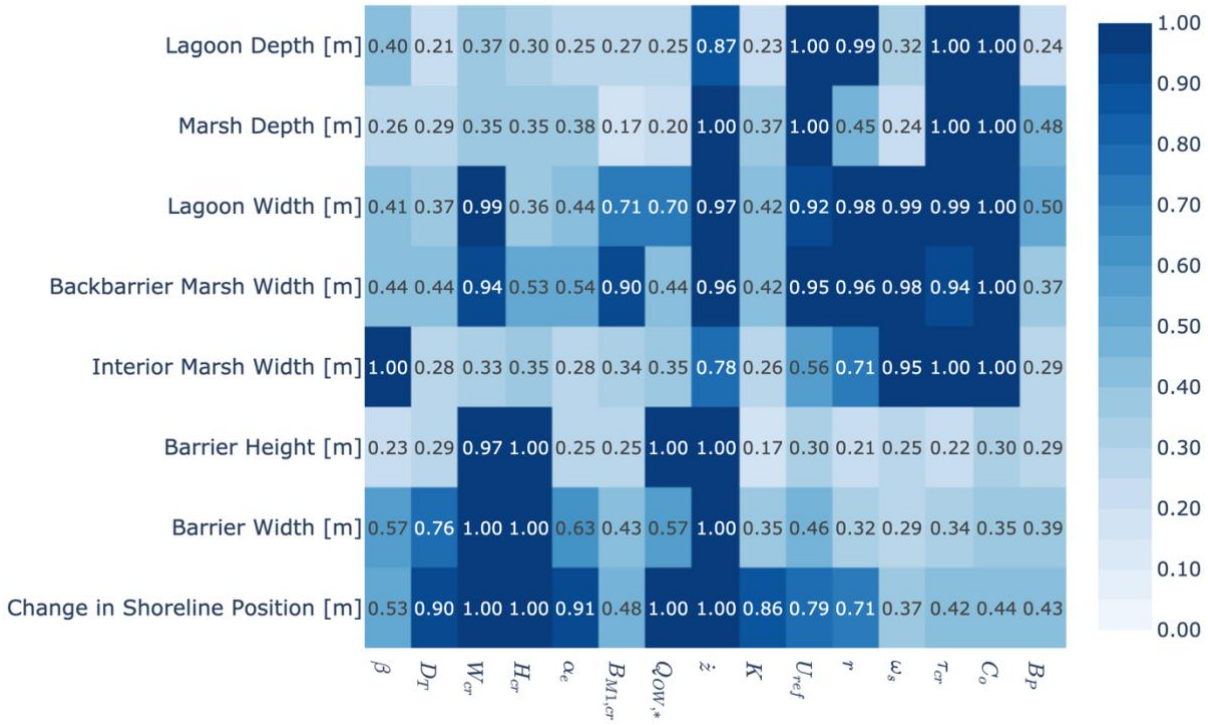

Figure C.8.3 – Probability of Parameter Ranking by Spearman Correlation for 100 Independent Trials with 1-2k Simulations.

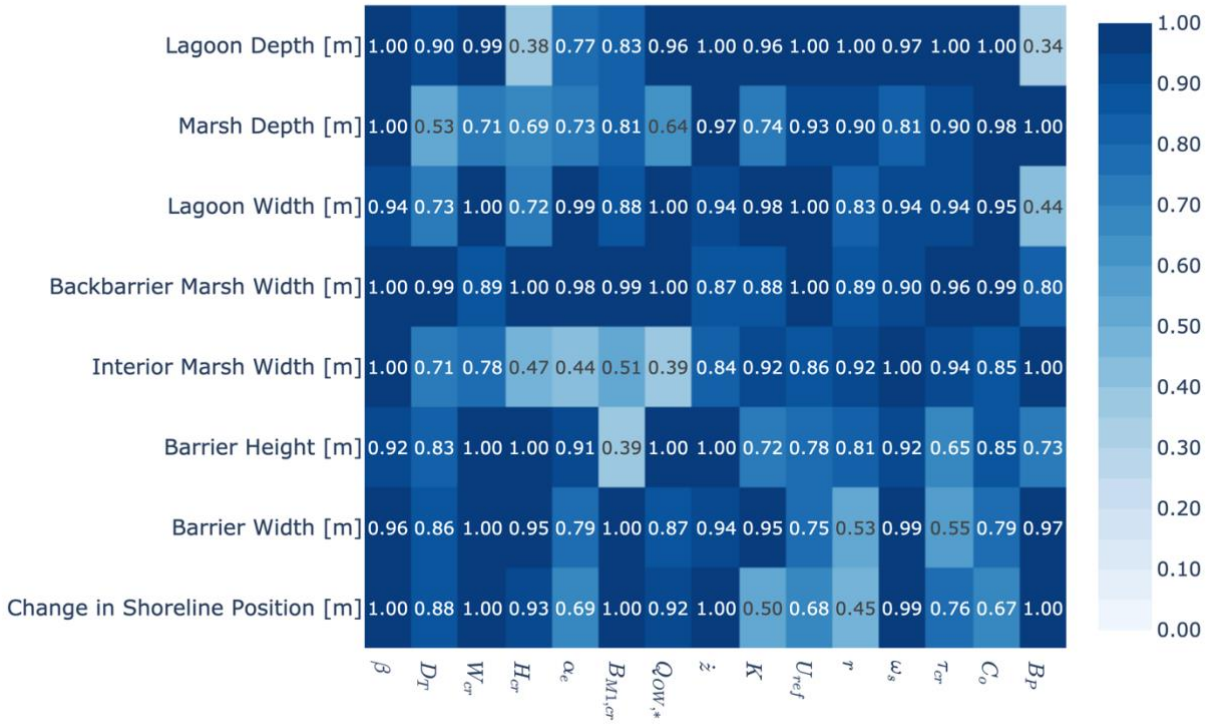

Figure C.8.4 – Probability of Parameter Ranking by Morris Method for 100 Independent Trials with 1-2k Simulations.

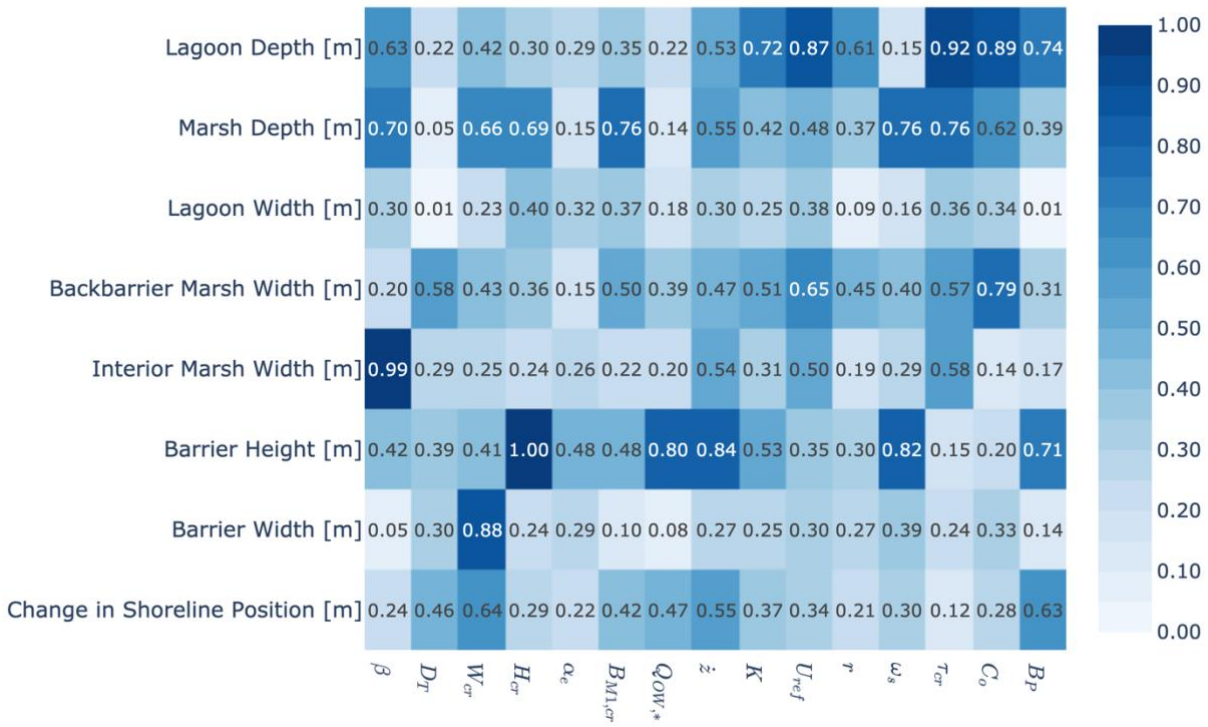

Figure C.8.5 – Probability of Parameter Ranking by Sobol Method for 100 Independent Trials with 1-2k Simulations.

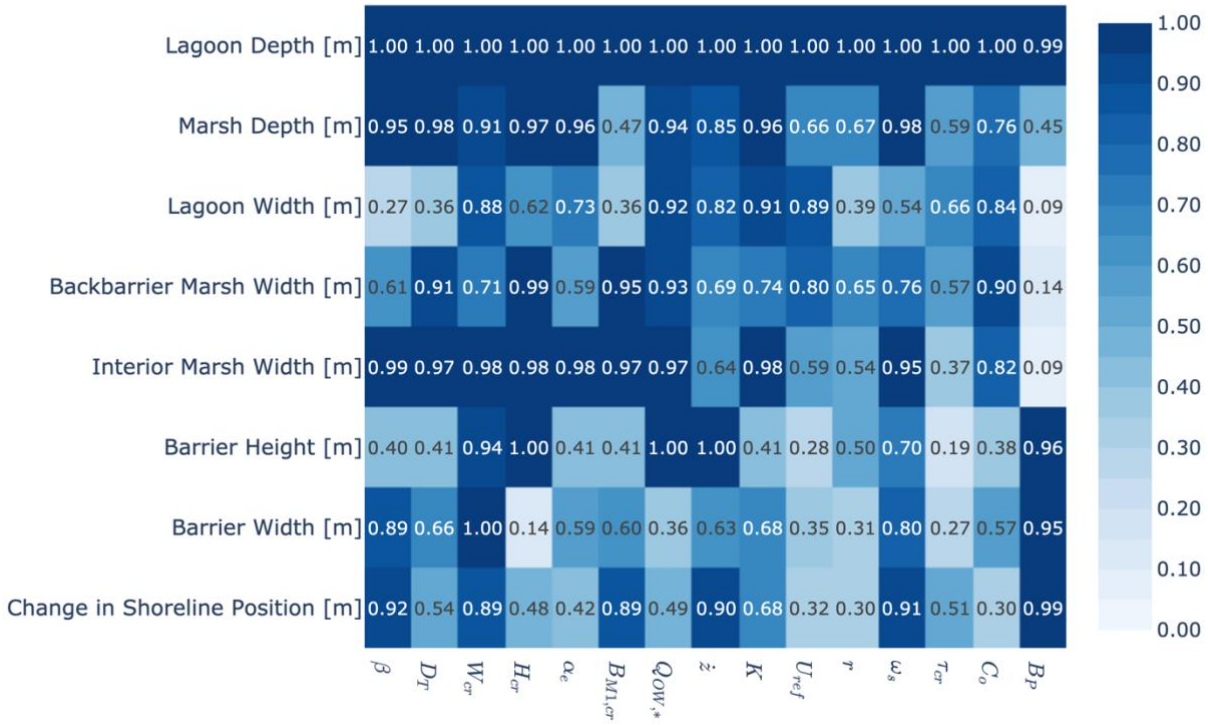

Figure C.8.6 – Probability of Parameter Ranking by VARS Method for 100 Independent Trials with 1-2k Simulations.

9. Results for 100 independent trials with 10,000-20,000 simulations for remaining result variables

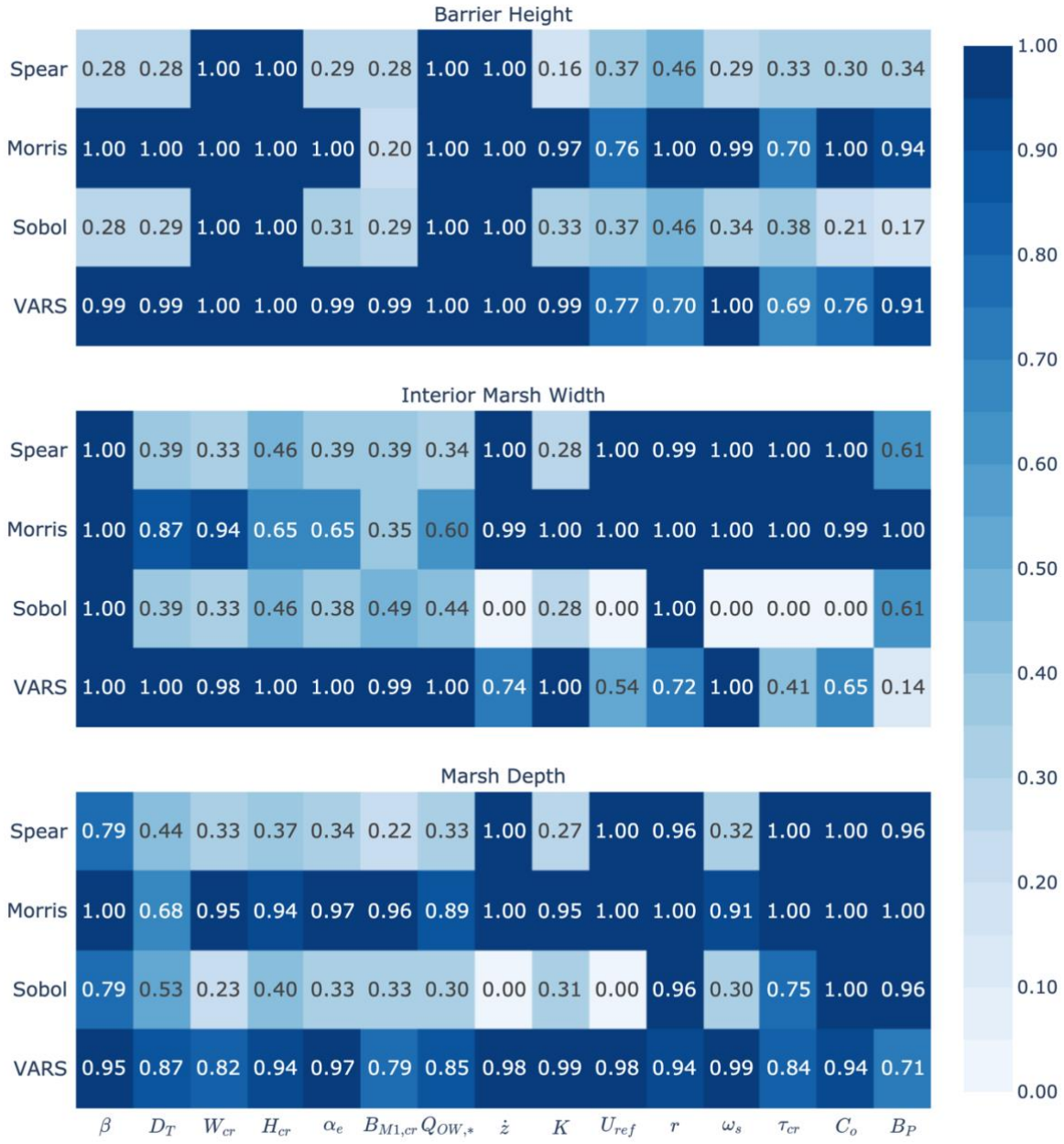

Figure C.9.1 – Probability of Parameter Ranking for 100 Independent Trials with 10-20k Simulations. Results shown for (top) Barrier Height, (middle) Interior Marsh Width, and (bottom) Marsh Depth.

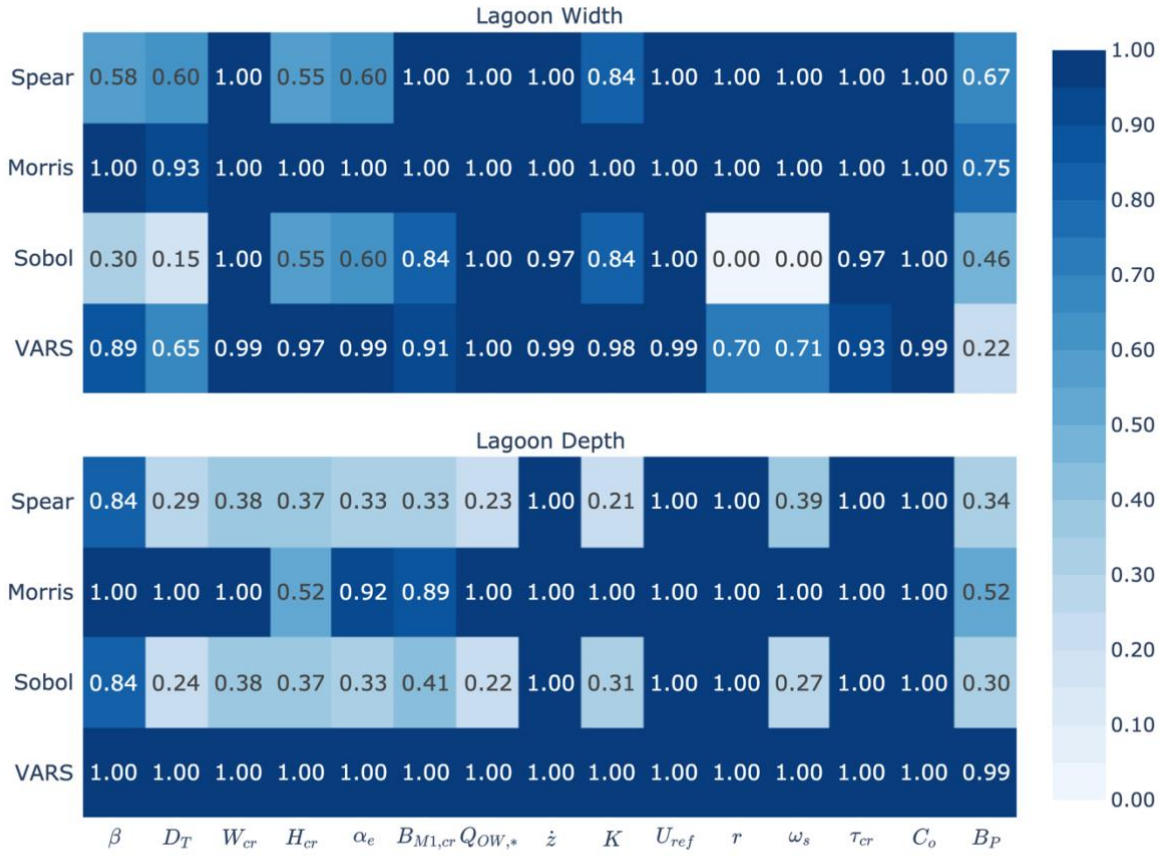

Figure C.9.2 – Probability of Parameter Ranking for 100 Independent Trials with 10-20k Simulations. Results shown for (top) Lagoon Width and (bottom) Lagoon Depth.

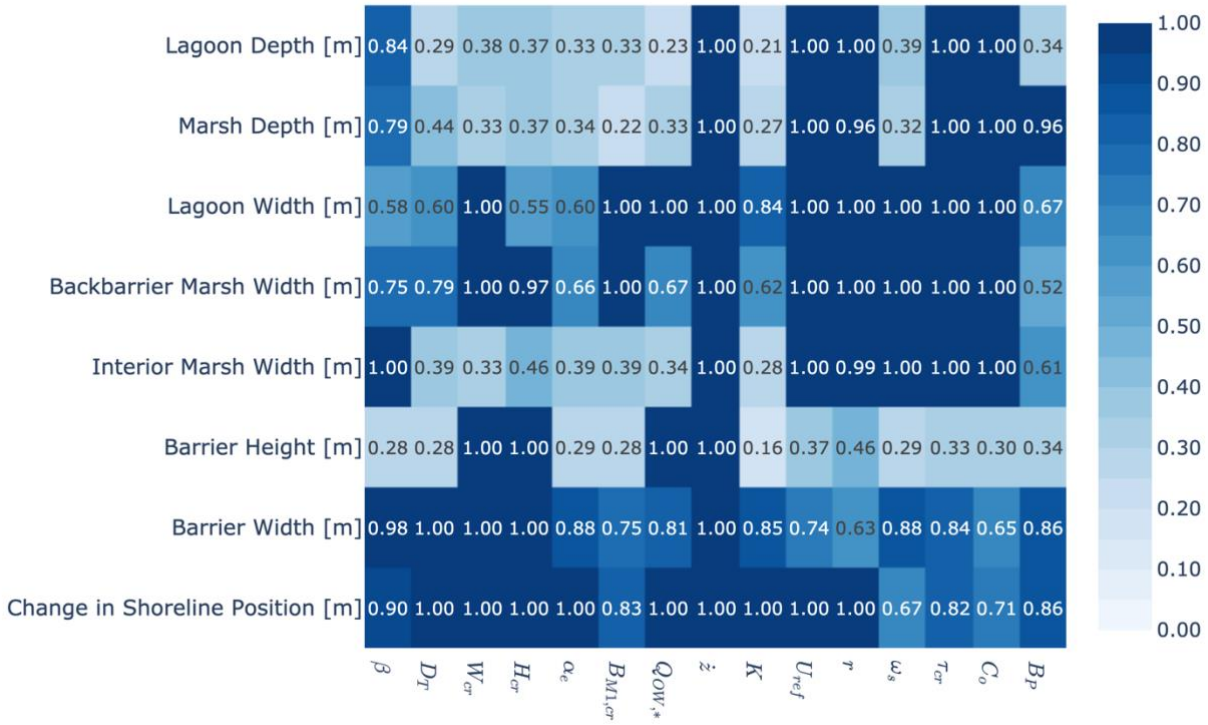

Figure C.9.3 – Probability of Parameter Ranking by Spearman Correlation for 100 Independent Trials with 10-20k Simulations.

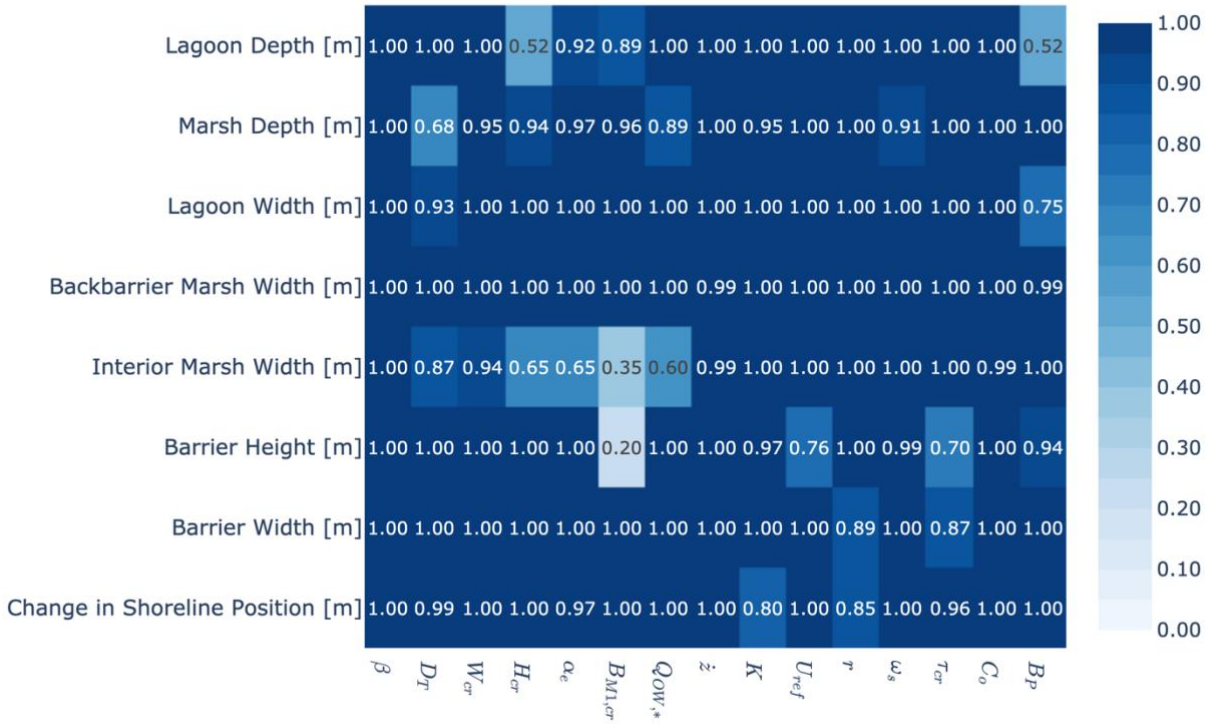

Figure C.9.4 – Probability of Parameter Ranking by Morris Method for 100 Independent Trials with 10-20k Simulations.

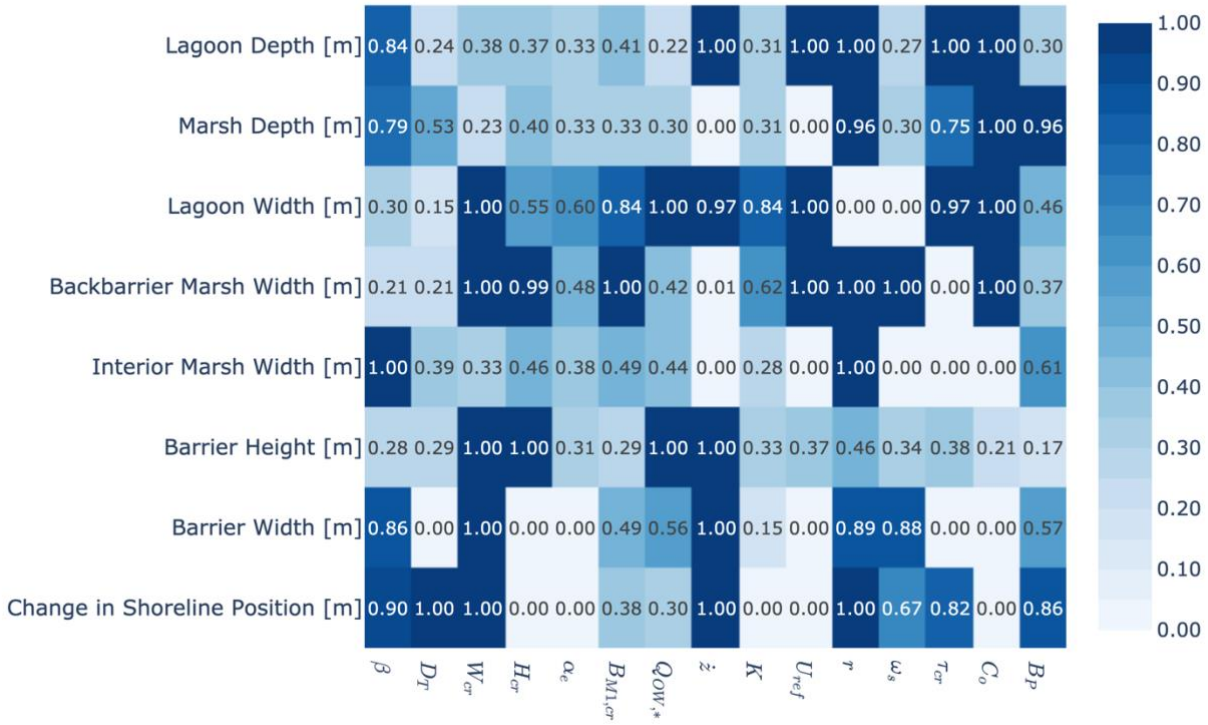

Figure C.9.5 – Probability of Parameter Ranking by Sobol Method for 100 Independent Trials with 10-20k Simulations.

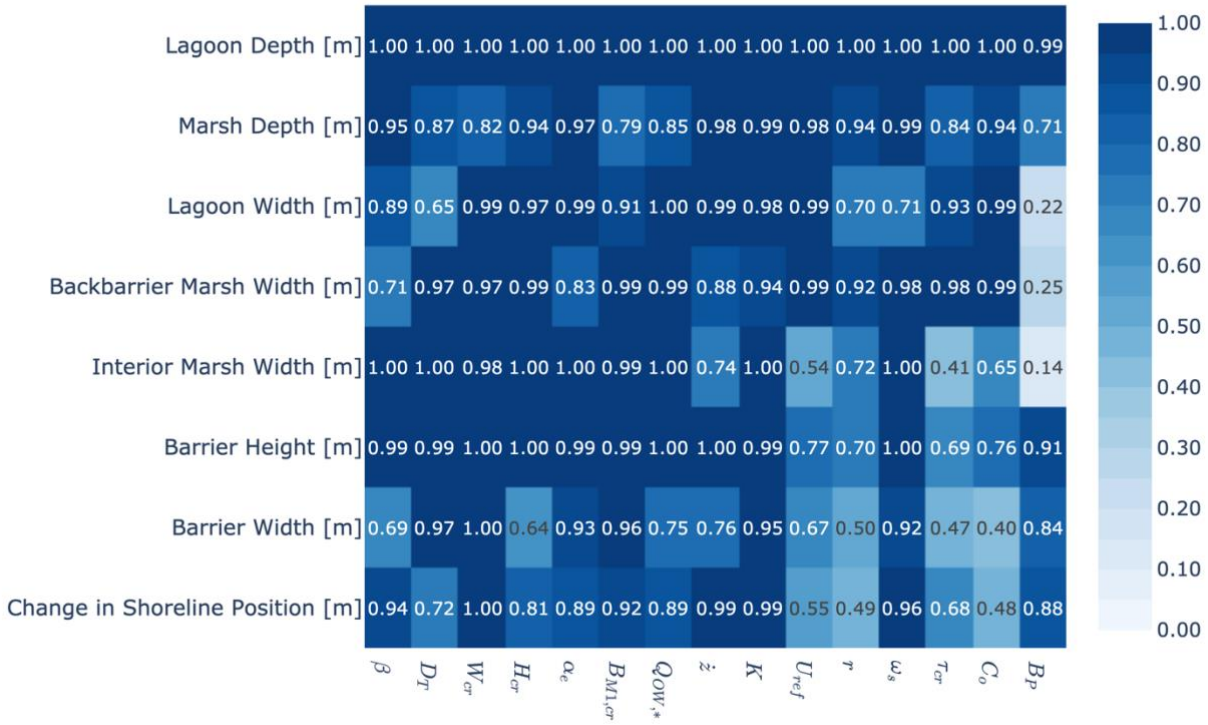

Figure C.9.6 – Probability of Parameter Ranking by VARS Method for 100 Independent Trials with 10-20k Simulations.

Appendix D

Supplementary Material for Chapter 5

Supplementary Material

Manuscript Title: Modeling Decadal Evolution of a Mid-Atlantic Barrier Island Under Sea Level Rise and Management Scenarios

Authors: Steven W.H. Hoagland, Jennifer L. Irish, Robert Weiss, and Sean Vitousek

Outline of Supplementary Material:

1. Transect parameterization

1. Transect Parameterization

Table D.1 provides a list of LTM17 model parameters, their values, and justifications for all parameters that are the same across all transects.

Table D.1. Spatially Invariant LTM17 Model Parameters

Parameter	Value [units]	Notes
Critical backbarrier marsh width	50 [m]	Used reasonable estimate based on calibrated critical barrier width of 400 m and definition; this parameter also determined to be insensitive from previous sensitivity study – see Hoagland et al. 2024
Density of organic matter	1000 [kg/m^3]	Value taken from Mariotti and Carr 2014
Equilibrium/critical height	Ho (Initial Height) [m]	Value determined from model calibration; setting Hcr equal to initial height provided best fit for shoreline change data.
Equilibrium/critical width	400 [m]	Value determined from model calibration
Equilibrium shoreface slope	0.018 [m/m]	Approximate average value from looking at CIRES, 2014 elevations extracted by transect
Mainland slope	0.0023 [m/m]	Approximate average value from looking at CIRES, 2014 elevations extracted by transect; parameter insensitive for all results but change in interior marsh width as determined by Hoagland et al. 2024
Marsh and mudflat sediment densities	1000 [kg/m^3]	Value taken from Mariotti and Carr 2014
Maximum backbarrier depth for vegetation growth	0.7167*(tidal range)-0.0483 [m]	Value taken from Mariotti and Carr 2014
Maximum deficit volume per meter	Wcr*Hcr [m^2]	Value taken from Lorenzo-Trueba and Mariotti 2017
Organic matter porosity	0.377	Value taken from Mariotti and Carr 2014
Peak Biomass	2.5 [kg/m^2]	Value taken from Mariotti and Carr 2014
Sediment settling velocity	0.5 mm/s	Value taken from Mariotti and Carr 2014
Sediment erodibility parameter	0.0001	Value taken from Mariotti and Carr 2014
Shape coefficient for marsh erosion (dist)	10 [m]	Value taken from Mariotti and Carr 2014
Shoreface flux constant	2000 [m^3/m/yr]	Value taken from Lorenzo-Trueba and Mariotti 2017
Tidal period	12.5 [hr]	Value selected based on tidal observations from NOAA's Tides and Currents data at Ocean City Inlet, MD – Station ID 8570283
Toe depth	6 [m]	Value from Schupp 2007
Reference wind speed	6 [m/s]	Value from Carruthers et al. 2011

References

Carruthers, T., Beckert, K., Dennison, B., Thomas, J., Saxby, T., Williams, M., Fisher, T., Kumer, J., Schupp, C., Sturgis, B., Zimmerman, C., 2011. Assateague Island National Seashore Natural Resource Condition Assessment. Maryland, Virginia. Natural Resource Report NPS/ASIS/NRR—2011/405. National Park Service, Fort Collins, Colorado.

CIRES, 2014. Continuously Updated Digital Elevation Model (CUDEM) - 1/9 Arc-Second Resolution Bathymetric-Topographic Tiles. URL: doi:10.25921/ds9v-ky35.553

Hoagland, S. W., Irish, J. L., & Weiss, R. (2024). Morphodynamic and modeling insights from global sensitivity analysis of a barrier island evolution model. Geomorphology, 451, 109087.

Lorenzo-Trueba, J., & Mariotti, G. (2017). Chasing boundaries and cascade effects in a coupled barrier-marsh-lagoon system. Geomorphology, 290, 153-163.

Mariotti, G., & Carr, J. (2014). Dual role of salt marsh retreat: Long-term loss and short-term resilience. Water Resources Research, 50(4), 2963-2974.

Schupp, C. A., Bass, G. P., & Grosskopf, W. G. (2007). Sand bypassing restores natural processes to Assateague Island, Maryland. In Coastal Sediments' 07 (pp. 1340-1353).